



Trinity College Dublin

Coláiste na Tríonóide, Baile Átha Cliath

The University of Dublin

BRAIN: Brain Injury in Neonates

Megan Ní Bhroin

Thesis submitted to the University of Dublin, Trinity
College for the degree of

Doctor in Philosophy

2022

Supervisors

Prof. Arun L.W. Bokde

Co-supervisor

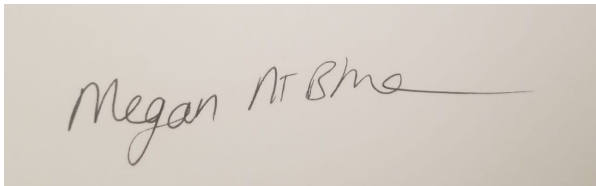
Eleanor Molloy

Declaration and Permission

I declare that this thesis has not been submitted as an exercise for a degree at this or any other university and it is entirely my own work.

I agree to deposit this thesis in the University's open access institutional repository or allow the Library to do so on my behalf, subject to Irish Copyright Legislation and Trinity College Library conditions of use and acknowledgement. I consent to the examiner retaining a copy of the thesis beyond the examining period, should they so wish.

Signed:

A rectangular box containing a handwritten signature in black ink. The signature reads "Megan McBride" in a cursive script, followed by a horizontal line extending to the right.

Summary

Despite advances in neonatal care leading to a dramatic reduction in mortality rates in recent decades, there have been comparatively modest improvements in neurodevelopmental outcomes for infants born with neonatal encephalopathy (NE), congenital heart disease (CHD), stroke, and preterm birth. The burden of the problem is significant, affecting a wide range of developmental domains including cognition, executive function, motor and language skills, and behavioural impairments. Hence, by using MRI, this PhD sought to examine the structure and function of the neonatal human brain to provide further insight into early neurodevelopment. It included three related experimental studies and one systematic review.

The first experimental study of this thesis investigated the relationship between 3 different MRI scoring systems (e.g. Barkovich, NICHD-NRN and Weeke) and neurodevelopmental outcome assessed using Bayley Scales of Infant and Toddler Development (Bayley-III) at 2 years of age in term-born infants with NE. Using multiple linear regression, we found a significant association between Barkovich, NICHD-NRN and Weeke scores and Bayley-III cognitive and motor scores. Only the Weeke scoring system was associated with Bayley-III language scores, suggesting more detailed scoring systems have higher predictive ability for outcome prediction. The second experimental study of this thesis used graph theory and network-based statistics (NBS) to assess global brain network topology and identify subnetworks of altered connectivity in infants with CHD prior to cardiac surgery. Using NBS we identified one subnetwork with reduced structural connectivity in infants with CHD involving basal ganglia, amygdala, hippocampus, cerebellum, vermis, and temporal and parieto-occipital lobe, primarily affecting core nodes and edges. The third study of this thesis involved a systematic review of resting-state

functional MRI (rs-fMRI) studies to identify deviations in brain function due to early disruptions (e.g. prematurity, neonatal insults) that were associated with motor and language outcomes in child- and adulthood. Evidence from this systematic review suggests a possible association between diaschisis and motor and language impairments in individuals after perinatal brain lesions. This result is demonstrated by altered intra- and inter-hemispheric connectivity and impaired lateralization of brain regions important for motor (primary motor cortex, parietal operculum, supplementary motor area, supramarginal gyrus, calcarine cortex, inferior parietal lobule) and language (inferior frontal gyrus, superior temporal gyrus, angular gyrus) functioning, as well as altered connectivity within and between RSNs of primary (sensorimotor, visual, auditory) and higher-order (cerebellum, frontoparietal, default-mode, salience, self-referential and attentional) functions. Finally, the fourth experimental study of this thesis assessed metastable neural dynamics using rs-fMRI data in healthy term-born infants from the developing human connectome project (HCP). We found that metastability of the thalamus and primary order networks were generally more mature than higher-order/associative networks, suggesting different developmental patterns of metastable neural dynamics between primary and higher-order functional systems. Overall, this thesis furthers our understanding of the link between the brain and behavioural changes in infants at risk of neurodevelopmental impairment and offers support for the use of neuroimaging biomarkers with the goal of improving outcomes in infants.

Acknowledgements

The work presented in this thesis would not have been possible without the generous help and support from a large number of people. Firstly, I would like to thank Prof Arun Bokde, for his time, guidance, encouragement and support throughout, and to Prof Eleanor Molloy for her expertise and advice.

I would like to acknowledge support from colleagues from the Centre for the Developing Brain and St Thomas' Hospital, especially Prof Serena Counsell and Dr Dafnis Batalle for their mentorship, enthusiasm, guidance and encouragement. Thank you also to Prof Eleanor Molloy's Laboratory for their advice, guidance and assistance.

I am so grateful to my colleagues from the Cognitive Systems lab, and to Francesca Sabilia and Therese Gilligan, for their endless support, and for all the laughs and amazing memories along the way! Thanks to Nadja Enz and Alexandra Rodrigues Martinez, who helped keep me on track and without whose help and support this dissertation would not exist. You have all been such patient loyal friends during this process and I am forever grateful. Thanks to everyone at the TCIN Lloyd building, particularly to Cian Judd who was a very fun visitor to the office over the last few months in particular.

Finally, thank you to my parents, family, and friends for all their encouragement over the years and without whose support this would not have been possible. Finally, thank you to Calum, for being so patient and encouraging and for minding me so well during the submission of this thesis!

Publications

The following publications were written during the course of the PhD:

Ní Bhroin, M., Abo Seada, S., Bonthron, A. F., Kelly, C. J., Christiaens, D., Schuh, A., Pietsch, M., Hutter, J., Tournier, J. D., Cordero-Grande, L., Rueckert, D., Hajnal, J. V., Pushparajah, K., Simpson, J., Edwards, A. D., Rutherford, M. A., Counsell, S. J., & Batalle, D. (2020). Reduced structural connectivity in cortico-striatal-thalamic network in neonates with congenital heart disease. *NeuroImage. Clinical*, *28*, 102423. doi:10.1016/j.nicl.2020.102423

Ní Bhroin, M., Molloy, E. J., & Bokde, A. (2021). Relationship between resting-state fMRI functional connectivity with motor and language outcome after perinatal brain injury - A systematic review. *European journal of paediatric neurology : EJPN : official journal of the European Paediatric Neurology Society*, *33*, 36–49. doi:10.1016/j.ejpn.2021.05.007

Ní Bhroin, M., Kelly, L., Sweetman, D., Aslam, S., O'Dea, M. I., Hurley, T., Slevin, M., Murphy, J., Byrne, A. T., Colleran, G., Molloy, E. J., & Bokde, A. (2021). Relationship Between MRI Scoring Systems and Neurodevelopmental Outcome at Two Years in Infants With Neonatal Encephalopathy. *Pediatric neurology*, *126*, 35–42. doi:10.1016/j.pediatrneurol.2021.10.005

O'Dea, M. I., Kelly, L., McKenna, E., Melo, A. M., **Ni Bhroin, M.**, Hurley, T., Byrne, A. T., Colleran, G., Vavasseur, C., El-Khuffash, A., Miletin, J., Murphy, J., Hickey, F., & Molloy, E. J. (2021). Dysregulated Monocyte and Neutrophil Functional Phenotype in Infants With Neonatal Encephalopathy Requiring Therapeutic Hypothermia. *Frontiers in pediatrics*, *8*, 598724. doi:10.3389/fped.2020.598724

Conference abstracts

1. Young Neuroscience Ireland (YNSI) conference 2018 – “Interhemispheric functional connectivity and its association with the corpus callosum using data from the developing Human Connectome (dHCP).”
2. Sixth biennial conference on Resting state and brain connectivity 2018 – “Interhemispheric functional connectivity and its association with the corpus callosum using data from the developing Human Connectome (dHCP).”
3. British Neuroscience Association (BNA) 2019 – “Graph theory application in functional brain network architecture of healthy neonates using data from the developing human connectome (dHCP)”.
4. Irish Paediatric Association (IPA) 2019 – “Graph based network analysis of resting state functional MRI in the healthy neonate brain”.
5. Organisation of Human Brain Mapping (OHBM) (June 2020) – “Reduced structural connectivity in cortico-striatal-thalamic network in neonates with congenital heart disease.”
6. Organisation of Human Brain Mapping (OHBM) (June 2020) – “Evaluation of MRI scoring systems prediction with two-year outcome in Neonatal Encephalopathy.”
7. Paediatric Academic Societies (PAS) (cancelled due to COVID) – “Evaluation of MRI scoring systems prediction with two-year outcome in Neonatal Encephalopathy.”
8. Federation of European Neuroscience Societies (FENS) (July 2020) – “The role of resting-state fMRI in assessing motor and language outcomes after perinatal brain injury – A systematic review.”

9. Young Neuroscience Ireland (YNSI) conference 2020 - “Evaluation of MRI scoring systems prediction with two-year outcome in Neonatal Encephalopathy.”

Table of contents

Chapter 1: Introduction: The developing brain and neonatal brain injury	1
1.1 Introduction	1
1.2 Normal brain development	1
1.3 Neurodevelopment	5
1.4 Neonatal and congenital conditions leading to perinatal brain injury	7
1.4.1 Neonatal Encephalopathy	7
1.4.1.1 Diagnosis	8
1.4.1.2 Therapeutic Hypothermia	9
1.4.1.3 Outcome	10
1.4.1.4 Neuroimaging	12
1.4.2 Congenital Heart Disease	14
1.4.2.1 Outcome	15
1.4.2.2 Neuroimaging	17
1.5 Thesis objective	17
Chapter 2: Materials and Methods: Magnetic Resonance Imaging (MRI) physics and analysis	19
2.1 Magnetic resonance imaging	19
2.2 Basic physics of MRI signal	19
2.2.1 Nuclear magnetic resonance	19
2.2.2 MR signal	21
2.2.3 MRI image formation	23
2.2.4 Scanning parameters	24
2.2.5 Echo planar imaging	25
2.3 Diffusion-weighted MRI	26
2.3.1 Diffusion tensor imaging	29
2.4 Spectrum formation in MRS	31
2.5 Functional MRI	33
2.5.1 Foundations of BOLD response	33
2.5.2 Resting state fMRI	34
2.5.2.1 Seed based analysis	35
2.5.2.2. Independent component analysis	35
2.5.3 Dynamic functional connectivity	37
2.6 Connectome	38
2.7 Neonatal MRI considerations	39
Chapter 3: Relationship between MRI scoring systems and neurodevelopmental outcome at 2 years in infants with Neonatal Encephalopathy	41
Abstract	41
3.1 Introduction	42
3.2 Materials and Methods	44
3.2.1 Ethical approval	44
3.2.2 Study design and patient population	44
3.2.3 MR imaging protocol	45
3.2.4 MRI scoring	45
3.2.5 Neurodevelopmental outcome	47
3.2.6 Statistical analysis	47
3.3 Results	47
3.3.1 Clinical characteristics	47
3.3.2 MRI scoring characteristics	51
3.3.3 Neurodevelopmental characteristics	55

3.3.4 Relationship between MRI score and neurodevelopmental outcome	56
3.4 Discussion	58
3.5 Conclusion	64
Chapter 4: Reduced structural connectivity in cortico-striatal-thalamic network in neonates with congenital heart disease	65
Abstract	65
4.1 Introduction	66
4.2 Materials and Methods	67
4.2.1 Participants	67
4.2.2 Data acquisition	69
4.2.3 Qualitative MRI analysis	70
4.2.4 Pre-processing and network construction	70
4.2.5 Network measures	72
4.2.6 Core and periphery partitioning and local characteristics	73
4.2.7 Network based statistics	73
4.2.8 Statistical analysis	74
4.3 Results	74
4.3.1 Clinical characteristics	74
4.3.2 Global network features	75
4.3.3 Core/Periphery partitioning and local characteristics	76
4.3.4 Subnetwork of brain regions with reduced connectivity in CHD	80
4.4 Discussion	83
4.5 Conclusion	87
Chapter 5: Relationship between resting-state fMRI functional connectivity with motor and language outcome after perinatal brain injury – A systematic review	88
Abstract	88
5.1 Introduction	89
5.2 Materials and Methods	91
5.2.1 Search strategy	91
5.2.2 Study selection	91
5.2.3 Data extraction	92
5.3 Results	93
5.3.1 Study selection	93
5.3.2 Lesion location	94
5.3.3 Neurodevelopmental assessments	94
5.3.4 ROI-based functional connectivity analysis and motor outcome	95
5.3.5 Network based analysis and motor outcome	96
5.3.6 ROI-based functional connectivity analysis and language outcome	97
5.4 Discussion	120
5.5 Limitations	126
5.6 Conclusion	126
Chapter 6: Metastable resting state neural dynamics of brain networks in the neonate brain	128
6.1 Introduction	128
6.2 Materials and methods	129

6.2.1	Participants	129
6.2.2	Data acquisition	131
6.2.3	MRI pre-processing	131
6.2.4	Functional data analysis	132
6.2.5	Defining brain functional parcels	133
6.2.6	Calculating metastability	139
6.2.7	Statistical analysis	140
6.3	Results	140
6.3.1	Demographic and clinical characteristics	141
6.3.2	Resting state networks	142
6.3.3	Metastability and synchrony within resting state networks	145
6.3.4	Effect of postmenstrual age at scan	147
6.3.5	Metastability and synchrony between resting state networks	150
6.4	Discussion	152
6.5	Conclusion	155
Chapter 7: General discussion		156
7.1	Summary of findings	156
7.2	Future Perspectives	160
7.2.1	Does the inclusion of rs-fMRI in MRI scoring systems have added prognostic benefit?	160
7.2.2	Is altered structural connectivity associated with neurodevelopmental outcome in CHD	161
7.2.3	What are the consequences of neonatal brain injury on metastability and synchrony of RSN's in the brain	161
7.3	Limitations	162
7.4	Conclusions	163
References		165
Appendix A		200
Appendix B		243

List of Figures

Figure 2.1 Alignment of protons in a magnetic field	20
Figure 2.2 Tissue magnetization and relaxation	23
Figure 2.3 Diffusion ellipsoid in an (a) isotropic and (b) anisotropic environment	27
Figure 4.1 Global graph theory characteristics in CHD and control group	76
Figure 4.2 Distribution of core/periphery nodes common in CHD and control networks	77
Figure 4.3 Average nodal efficiency of core and periphery nodes in CHD and controls	79
Figure 4.4 Illustration of NBS-derived subnetwork with reduced structural connectivity in CHD neonates compared to controls	81
Figure 5.1 Search strategy and selected articles	92
Figure 5.2 Abnormal rs-FC of brain regions associated with motor and language outcomes in individuals with a history of perinatal brain injury	114
Figure 6.1 Spatial maps of resting state networks identified by group independent component analysis in 17 term-born infants scanned at 43.5-44.5 weeks PMA	143
Figure 6.2 Resting state network metastability and synchrony	146
Figure 6.3 Relationship between postmenstrual age at scan and resting state network metastability and synchrony	149
Figure 6.4 Average metastability and synchrony interaction matrix	151

List of Tables

Table 2.1 Types of MRI modalities used and their neonatal clinical applications	40
Table 3.1 Neonatal Clinical characteristics	49
Table 3.2 MRI Scoring systems	53
Table 3.3 MRI Scoring characteristics of the infants	55
Table 3.4 Neurodevelopmental characteristics of the infants	56
Table 4.1 Demographic Characteristics of the CHD and Control Cohorts	68
Table 4.2 Characteristics and MRI findings of the infants	75
Table 4.3 List of core (n=34) and peripheral nodes (n=59) common in CHD and control networks	78
Table 4.4 Subnetwork with reduced structural connectivity in CHD neonates	82
Table 5.1 rs-fMRI studies assessing motor and language outcomes following perinatal brain injury	99
Table 5.2 Summary of relations between network topology and motor outcome	115
Table 5.3 STROBE reporting for each study	117
Table 6.1 List of ROIs belonging to each ICA network in neonates	134
Table 6.1 Demographic and clinical characteristics of the study population	141

List of Tables

Table 2.1 Types of MRI modalities used and their neonatal clinical applications	40
Table 3.1 Neonatal Clinical characteristics	49
Table 3.2 MRI Scoring systems	53
Table 3.3 MRI Scoring characteristics of the infants	55
Table 3.4 Neurodevelopmental characteristics of the infants	56
Table 4.1 Demographic Characteristics of the CHD and Control Cohorts	69
Table 4.2 Characteristics and MRI findings of the infants	75
Table 4.3 List of core (n=34) and peripheral nodes (n=59) common in CHD and control networks	79
Table 4.4 Subnetwork with reduced structural connectivity in CHD neonates	83
Table 5.1 rs-fMRI studies assessing motor and language outcomes following perinatal brain injury	100
Table 5.2 Summary of relations between network topology and motor outcome	116
Table 5.3 STROBE reporting for each study	118
Table 6.1 List of ROIs belonging to each ICA network in neonates	135
Table 6.1 Demographic and clinical characteristics of the study population	142

List of Abbreviations

AAL	Automated anatomic labelling
AD	Axial diffusivity
ADC	Apparent diffusion coefficient
ADHD	Attention deficit hyperactivity disorder
ADP	Adenosine diphosphate
ATP	Adenosine triphosphate
BGT	Basal ganglia/thalamic
BOLD	Blood oxygen level dependant
Cho	Choline
CHD	Congenital heart disease
CP	Cerebral palsy
CST	Corticospinal tract
CSVT	Cerebral sinovenous thrombosis
DGM	Deep grey matter
dHCP	Developing Human Connectome Project
DMN	Default Mode Network
DWI	Diffusion-weighted imaging
EEG	Electroencephalogram
EPI	Echo planar imaging
FA	Fractional anisotropy
FC	Functional connectivity
fMRI	Functional magnetic resonance imaging
FWHM	Full width half maximum
GA	Gestational age
GMFCS	Gross motor function classification system
¹ H-MRS	Proton magnetic resonance imaging
ICA	Independent component analysis
IQ	Intelligence quotient
IUGR	Intrauterine growth restriction
IVH	Intraventricular haemorrhage
MD	Mean diffusivity
MNI	Montreal Neurological Institute
MOOSE	Meta-analysis of Observational Studies in Epidemiology
MRI	Magnetic resonance imaging
MRS	Magnetic resonance spectroscopy
NAA	N-acetylaspartate
NE	Neonatal encephalopathy
PLIC	Posterior limb internal capsule
PMA	Postmenstrual age
PRISMA	Preferred reporting items for systematic reviews and meta-analyses
PVL	Periventricular leukomalacia

PWML	Punctate white matter lesions
RD	Radial diffusivity
RF	Radio frequency
Rs-FC	Resting state functional connectivity
rs-fMRI	Resting state functional MRI
ROI	Region of interest
SDH	Subdural haemorrhage
SMA	Supplementary motor area
SNR	Signal to noise ratio
TE	Echo time
TEA	Term equivalent age
TR	Repetition time
WM	White matter
WMI	White matter injury
WS	Watershed

Chapter 1: The developing brain and neonatal brain injury

1.1 Introduction

Brain injuries during the perinatal period are a leading cause of death and disability in young children. Recent advances in perinatal medicine and neonatal intensive care have led to higher survival rates for these children, however, the rate of disability in later life remains high. Perinatal brain injury is a major cause of neurodevelopmental impairments and neurological deficits such as cerebral palsy, autism and intellectual disability, leading to major burdens for the infant, family and society. Therefore, current research efforts are directed on understanding the consequences of injury for brain functioning in later life.

Brain maturation occurs at different stages, establishing critical periods for development of specific functions with various pre- and postnatal events that affect neural systems related to various functions (e.g. sensory, motor, cognitive) increasing the risk for impairments later in life. This chapter will therefore discuss brain development, neurodevelopment, and congenital and neonatal conditions that affect brain development.

1.2 Normal brain development

The perinatal period is characterized by rapid and highly programmed sequence of events during which the fetus is prepared to adapt for life outside of the womb (Kostovic et al., 2019). Sequential development of the major transient laminar zones takes place during gestation, with the brain reorganising into permanent cortical pathways beginning from the centre to the periphery: the proliferative zones (ventricular and subventricular zones), the intermediate zone (fetal white matter), the subplate, the cortical plate (future cortex), and the marginal zone. These zones change due to neuronal proliferation and migration, which are predominant in the first trimester of pregnancy; and axonal and dendrite growth which occur during the second and third trimester of pregnancy. Cellular proliferation occurs

initially around 2 months gestation and is associated with radial glia and neuronal proliferation, with a peak period between 3-4 months. This is followed by glial multiplication which begins around 5 months gestation and continues beyond the first year of life (Dobbing & Sands et al., 1973).

Neurons and glia originate in ventricular and subventricular zones (Samuelson et al., 2003) and during the neuronal migration phase, millions of neurons migrate from their site of origin to their target location in the cortical plate via the subplate, with a peak in this process occurring between 12 and 20 weeks of gestation (de Graaf-Peters & Hadders-Algra, 2006). By around the 20th week of gestation the laminar zones are (from ventricular zone to pial surface), the ventricular zone, subventricular zone, intermediate zone, subplate and the cortical plate (Kostovic & Jovanov-Milosevic, 2006). The subplate comprises migratory neurons, axons, and glial cells (Kostovic & Judas, 2010) and is the thickest laminar zone. Afferent fibres wait within the subplate zone before penetrating the cortical plate, with central and periventricular regions containing crossing callosal, association, corticofugal and thalamocortical fibres (Judas et al., 2005). By around the 25th week of gestation, thalamocortical afferent neurons have passed through the posterior limb internal capsule (PLIC), periventricular crossroads and intermediate zone before approaching their target in the subplate where they wait before entering the cortical plate (Kostovic & Jovanov-Milosevic, 2006). Between 24-32 weeks of gestation, thalamocortical afferent neurons reach their target in the cortical plate. The ventricular and subventricular zone reduce substantially after 25 weeks of gestation (Vasung et al., 2016), and after 31 weeks of gestation the subplate disappears (de Graaf-Peters & Hadders-Algra, 2006) and by term age the laminar zones have also disappeared. The cortex begins to differentiate into the six layers of the cortex by around 31-34 weeks of gestation.

Synapses appear in the cortical plate between 26 and 28 weeks of gestation (Kostovic and Judas, 2010). Dendritic arborization and synaptogenesis accelerate in the third trimester to produce a thickening of the developing cortex with ~40 000 new synapses formed every second (Huttenlocher & Dabholkar, 1997), coinciding with the appearance of primary sulci and gyri (Garel et al, 2001; Huisman et al, 2002; Kostovic et al., 2014). The timing of synaptogenesis differs across the cortical layers, occurring earlier in deeper layers than in superficial layers (Huttenlocher, 1990). Synaptogenesis occurs earliest in primary motor areas (Huttenlocher, 1984, 1990; Huttenlocher & Dabholkar, 1997) and begins in the visual cortex between 3-4 months of age with its peak period between 4-12 months (Bourgeois, 1997; Bourgeois & Rakic, 1993; Huttenlocher, 1990; Huttenlocher et al, 1982a, 1982b; Michel & Garey, 1984). Synaptogenesis of the prefrontal cortex occurs around the same time as the visual cortex, reaching its peak period at around 8 months of age (Huttenlocher & Dabholkar, 1997; Kostovic et al, 1995).

After synapse formation by proliferation and migration, programmed cell death, or apoptosis occurs (Huttenlocher et al. 1982a) (i.e. elimination of aberrant or incorrect neuronal populations) (Cowan et al. 1984). A second regressive event in which the selective pruning of synapses also occurs (Volpe, 2008). Neural connectivity is nearly twice as high as the adult brain by the end of the first year of life due to the overproduction of connections between neurons due to synaptogenesis (Innocenti & Price, 2005). Synaptic pruning of redundant connections allows only connections that are functionally relevant to be maintained, resulting in the elimination of almost 50% of synapses by adolescence (Huttenlocher et al., 1997). Synaptic pruning improves the efficiency of neurotransmission and begins in late gestation period and becomes increasingly active postnatally. Synaptic pruning occurs at different timepoints across brain regions, with sensory and motor

cortices undergoing considerable pruning after birth, followed by association cortices and corpus callosum, and later by regions involved in higher cognitive functions (Levitt, 2003).

The process of myelination (i.e. wrapping of mature oligodendrocytes around axons) stabilizes functionally relevant connections and improves the efficiency of information transmission in the brain by accelerating axonal conduction. This process begins in the second trimester of pregnancy and peaks during the first postnatal year (Jakovcevski & Zecevic, 2005; Brody et al., 1987; Kinney et al., 1994; Huppi et al., 1998). The myelination process follows a heterogeneous spatiotemporal pattern, but generally relies on a caudorostral gradient, progressing from centre to the periphery, and occurring in sensory pathways first, followed by motor pathways and then associative pathways. At birth, the rostral brain stem, cerebellar peduncles and PLIC are myelinated, and between 36-40 weeks myelination of the corticospinal tracts (CST) and pre- and post-central gyri can be identified. The splenium of the corpus callosum and the optic radiations begin myelinating at around 6 and 8 weeks, respectively, followed by myelination of the occipital and parietal lobes, and finally advancing towards the frontal and temporal lobes between 8-12 months (Brody et al., 1987; Barkovich et al., 1988; Kinney et al., 1988; Paus et al., 2001; Yakovlev & Lecours, 1967; Counsell et al., 2002).

The developmental processes described above establish the fundamental organization for the initial functioning of the brain. A variety of neurodevelopmental disorders stem from early disturbances in these complex mechanisms during the pre- and perinatal period.

1.3 Neurodevelopment

The rapid development of the brain underlies the behavioural abilities of the child.

Neurodevelopmental skill attainment is similar among healthy children developing across particular timepoints and is also sequential (Oudgenoeg-Paz et al., 2012; Hongwanishkul et al., 2005; Carlson & Beck, 2009). During the first few years of life, early behavioural development is characterised by advances in gross and fine-motor abilities, language abilities, and an ability to solve increasingly complex problems. Neurodevelopmental disorders arise when a child has not reached the neurodevelopmental skills expected of them compared to other children of the same age. This section will therefore focus on some of the key behavioural milestones a child reaches from birth to 2 years.

At birth, infants show a preference for human faces and voices compared to shapes and silence (Sheridan, 2008), and give preferential orientation to the sights, sounds and smells of their caregivers (DeCasper & Fifer, 1980; Bushnell et al., 1989; Bushnell, 2001; Johnson et al., 1991). Newborns also preferentially orientate towards faces with eyes open or directed gaze, compared with closed eyes or averted gaze (Batki et al., 2000; Farroni et al., 2002). Newborns can imitate facial gestures (Sheridan, 2008) and cry in response to another newborn crying (Geangu et al., 2010). Newborns also have a flexed posture (Piper & Darrah, 1994) and display the moro reflex, which is an involuntary motor response to a sudden loss of support involving rapid and symmetrical abduction and adduction of both extremities.

Around 2 months of life, infants begin to develop social behaviour by responding to social cues in their environment through smiling (Emde & Harmon, 1972) and gaze following abilities (Farroni et al., 2004). Infants also start to repeat non-crying sounds such as cooing

and gurgling, and some infants begin to vocalize vowel-like sounds like “ah-ah” or “ooh-ooh” (Oller, 1978). By around 3 months of age, verbal communication is combined with smiling, and eye contact becomes integrated with hand gestures (Sheridan, 2008).

Visual attention to their environment begins to develop by about 9 months of age (Sheridan, 2008), and infants are also able to respond to their name (Fenson et al., 1993) and recognise familiar words from everyday life (Bergelson & Swingley, 2012). Infants also begin to clap their hands at around 9 months of age and take part in social games such as peek-a-boo (Hodapp et al., 1984) and vocalize with others by babbling loudly and repetitively (Sheridan, 2008). As they reach 12 months of age, infants can babble using most vowels and many consonants (Sheridan, 2008), recognise familiar faces and objects and successfully localize sounds from many directions (Corkum & Moore, 1998; Gredebäck et al., 2008). Infants also begin to improve their skill co-ordination and increasingly demonstrate gesture use (Bates & Dick, 2002).

At 1 month of age, infants bodily movements appear jerky or jittery, their hands are clenched with their thumb turned in and bent across the palm, and they are able to open their hands to grasp objects (Sheridan, 2008). By 3 months of age, most babies begin to unclench their hands, and move their body in a less jerky and more continuous manner. Infants are able to lie on their front in the prone position and lift their head and upper chest above the plane of their body. By 4 months of age, infants are able to hold their head up if pulled into a sitting position, with head lag uncommon by 6 months (Bly, 1994). The development of gross motor skills continues with infants displaying crawling behaviour by 7-9 months, walk with one or both hands held and some will be able to walk without support by 12 months.

From the age of 15 months toddlers begin to engage in functional play (Sheridan, 2008), and symbolic play activities such as role-play, make-believe, and pretend play by 2 years. Toddlers learn by observation as they develop the capabilities to imitate a range of behaviours in the second year of life (Barr & Hayne, 2003) and acquire a comprehensive vocabulary through imitation (Masur, 1995), with their first words emerging in the first year of life. By about 18 months of age they are able to produce between six and twenty words, and by 2 years, they learn how to build simple sentences (Fenson et al., 1994). The development of auditory comprehension develops at a faster pace than spoken language, with toddlers showing the ability to understand more words than they are able to produce (Fenson et al., 1994).

1.4 Neonatal and congenital conditions leading to perinatal brain injury

The perinatal period is particularly sensitive to a variety of insults representing the highest risk for brain injury during the lifespan. Neonatal and congenital conditions impacting brain development include neonatal encephalopathy (NE), and congenital heart disease (CHD). Common among these conditions is the increased risk of neurodevelopmental impairments creating the need for early and ongoing interventions (Gaynor et al., 2015; Natarajan et al., 2016).

1.4.1 Neonatal encephalopathy

NE is a heterogenous syndrome characterized by abnormal neurological function including seizures, an altered state of consciousness, depression of tone and reflexes and difficulty in maintaining normal respiration developing before, during or after birth and affecting mainly term infants (Volpe, 2012). The incidence of NE is estimated to be 1-8 per 1000 live births worldwide (Lee & Glass, 2021). NE was previously thought to occur due to a

hypoxic-ischaemic insult (Ferriero, 2004), and the terminology of NE and hypoxic-ischaemic encephalopathy (HIE) has been the subject of much debate (Chalak et al., 2019; Nelson et al., 2012; Badawi et al., 1998; Volpe, 2012; Molloy & Bearer, 2018; Dammann et al., 2011). This is due to the fact that the term HIE is often misused as it is difficult to prove when hypoxia ischemia is the cause of NE (Badawi et al., 1998). NE is the preferred term to describe the clinical syndrome of neurological dysfunction in the newborn period as it does not imply a specific underlying aetiology or pathophysiology. Therefore it is important to exclude a variety of causes including perinatal infections, placental abnormalities, metabolic disorders, coagulopathies and neonatal vascular stroke as other possible causes of NE (Aslam et al., 2019). The cause of NE is unknown in more than half of the infants (Nelson et al., 2021).

1.4.1.1 Diagnosis

The diagnosis of NE depends on information gained from neonatal clinical history, neurological examination, certain metabolic parameters, electroencephalogram (EEG) and neuroimaging evaluations (Volpe, 2008). Various clinical signs of NE include low Apgar scores, low cord pH, seizures, and encephalopathy. Neonatal neurological assessments to diagnose NE rely on standardised scoring systems that are correlated with clinical outcome. The Sarnat system grades infants with NE as mild (NE I), moderate (NE II), or severe (NE III). The grading is based on the response of infants to handling, level of consciousness, changes in tone or reflexes, presence of seizures and the duration of the symptoms within seven days after birth (Sarnat & Sarnat, 1976). Infants with mild NE demonstrate hyperalertness, uninhibited moro and stretch reflexes, sympathetic effects, and a normal EEG. Infants with moderate NE are characterized by reduced level of

alertness or consciousness, hypotonia (i.e. low muscle tone), strong distal flexion, and multifocal seizures. Infants with severe NE are stuporous and flaccid, brain stem and autonomic functions are suppressed, and display abnormal EEG patterns.

1.4.1.2 Therapeutic Hypothermia

Although cerebral brain damage occurs during the hypoxic-ischaemic phase, neuronal cell death continues to evolve for hours after resuscitation providing the potential to initiate treatments that may reduce brain injury (Gunn & Bennet 2008). Therapeutic hypothermia started within 6 hours after birth has been shown to improve prognosis for infants with moderate to severe NE (Jacobs et al., 2013). Therapeutic hypothermia has been shown to be neuroprotective and reduce the rate of death or disability at 18 months for infants with moderate or severe NE (Shankaran et al., 2005; Gluckman et al., 2005; Azzopardi et al., 2009; Jacobs et al., 2013). There has also been reports of less severe cerebral palsy outcomes (Jary et al., 2015) and increased frequency of survival for infants with an intelligence quotient (IQ) score of 85 or higher (Azzopardi et al., 2014) after therapeutic hypothermia. There are adverse effects associated with therapeutic hypothermia, including sinus bradycardia, thrombocytopenia and subcutaneous fat necrosis (Strohm et al. 2011); however, the benefits of treatment outweigh these short-term risks. Therapeutic hypothermia is the gold standard of care for term infants with moderate and severe NE and is achieved using selective head (Gluckmann et al. 2005; Gunn & Gluckman, 2007) or whole body cooling (Shankaran et al. 2005; Azzopardi et al. 2010; Jacobs et al. 2011). Selective head cooling provides cooling to the head while the rest of the body is actively warmed, whereas whole body cooling also reduces the body temperature (Tolley et al. 2005). Despite the reduction of severe disabilities following hypothermic neuroprotection,

nearly half of the infants continue to suffer long-term disability from brain injury, which suggests that brain development remains affected by NE. As therapeutic hypothermia is only partially protective for NE, safe and effective adjunct therapies are needed with melatonin and erythropoietin showing promise (Welin et al., 2007; Pandi-Perumal et al., 2006; Zhu et al., 2009; Elmahdy et al., 2010).

1.4.1.3 Outcome

Up to 20% of infants affected with NE die in the neonatal period (Jacobs et al., 2013). Epilepsy, motor and feeding problems often precedes death in these children (Martinez-Biarge et al., 2010). Survivors of NE are at risk of developing epilepsy, feeding, cognitive, behavioural, fine and gross motor problems and may have cognitive difficulties at school age (Gonzalez & Miller 2006). Long-term neurodevelopmental sequelae of NE includes impaired mental and motor development, vision and hearing impairments, epilepsy, and cerebral palsy. In the absence of cerebral palsy or major disability, children with NE have been found to have cognitive impairments, and difficulties in executive functions, behaviour, and social competence (Robertson & Finer 1985; Gonzalez et al., 2006, van Handel et al., 2012). Internalizing behaviours such as depression and anxiety, and externalizing behaviours such as attention deficit hyperactivity disorder (ADHD) and aggression have also been observed in children with NE (Marlow et al., 2005, Edmonds et al., 2020; Moster et al. 2002). The severity of neurodevelopmental outcome has been associated with the severity of NE (Miller et al., 2005; de Vries et al., 2010). Pin et al. (2008) conducted a meta-analysis and reported that the risk of adverse outcomes such as death, cerebral palsy and severe cognitive impairment were rare in children with mild NE,

more common in children with moderate NE and consistently present in children with severe NE.

Children with severe NE may develop cerebral palsy (CP), mental retardation, epilepsy, cognitive, visual and auditory impairment and show cognitive deficits (Robertson & Finer, 1993; van Handel et al. 2007).

Children with moderate NE are a heterogeneous group with respect to neurodevelopmental outcome (van Handel et al., 2007) demonstrating delays in reading, spelling and arithmetic (Robertson et al., 1988) and deficits in language, narrative memory, sentence repetition and sensorimotor domains (Marlow et al., 2005). Children with moderate NE demonstrate general intellectual abilities that are generally below children with mild NE as well as healthy controls. They may develop cognitive deficits, such as memory problems, visual-motor or visual-perceptive dysfunction (Robertson et al. 1989; Maneru et al. 2001; Dixon et al. 2002; Marlow et al. 2005). Reduced IQ, executive function scores and memory in 7-year-old children with moderate NE compared to children with less severe NE has also been observed (Marlow et al., 2005). Additionally, one third of children with a history of moderate NE will have delayed motor development at 1 year (Van Schie et al., 2007).

Mild to moderate NE may also show more problematic behaviour, attention problems and hyperactivity (Robertson et al. 1988; Marlow et al. 2005; van Handel et al. 2010).

Children with mild NE were expected to have a good prognosis with outcomes reported to be very similar to healthy controls (Robertson & Finer, 1985; Finer et al., 1983) and therapeutic hypothermia was thought to be unnecessary for these infants. However, recent evidence has identified brain injury, seizures, and neurodevelopmental impairments including cognitive impairment, cerebral palsy or sensorineural deficits in these infants (Murray et al., 2016; Lodygensky et al., 2018; Conway et al., 2018; DuPont et al., 2013;

van Handel et al., 2010; 2012; van Kooij et al., 2010; Walsh et al., 2017; Finder et al., 2020). Some mildly affected neonates are now being treated with therapeutic hypothermia following its success among neonates with more severe NE despite lack of sufficient evidence of benefit of treatment of therapeutic hypothermia for these infants (Chalak et al., 2018; Massaro et al., 2015; Oliveira et al., 2018).

1.4.1.4 Neuroimaging

Neuroimaging offers the potential to assess brain injury non-invasively in infants with NE. Most infants with normal MRI do not display motor or cognitive impairments (Miller et al., 2005), whereas the risk of an abnormal neurodevelopmental outcome is higher with increasing severity of brain injury (Barkovich et al., 1998). Injury to subcortical structures including basal ganglia, thalamus (BGT), corticospinal tracts, periorolandic cortex and brainstem has been linked to acute hypoxic ischaemia, and infants with this type of injury show hypotonia, dyskinetic cerebral palsy, hemiplegia, impaired cognitive outcomes and epilepsy (Martinez-Biarge et al., 2011; Martinez-Biarge et al., 2010; Barkovich et al., 1998; de Vries & Groenedaal, 2010; Shankaran et al., 2005). Infants with severe basal ganglia and/or thalamic injury that extends to the brainstem have high disability and mortality rates (Martinez-Biarge et al., 2011) and damage to the PLIC has been linked to severe motor deficits such as cerebral palsy (Rutherford et al., 1998; Martinez-Biarge et al., 2011; Barnett et al., 2002). The type of cerebral palsy depends on the site of brain injury with dyskinetic or quadriplegia associated with BGT injury and lesions in the periorolandic regions (van Handel et al., 2007). Infants with basal ganglia injury may also experience impairments across other domains, including speech/language development, feeding, cognition and vision, as well as seizures (Martinez-Biarge et al., 2010).

Sub-acute or chronic hypoxic ischaemia has been linked to injury involving white matter and overlying cerebral cortex in watershed vascular zones resulting in a 'watershed-predominant' pattern (Miller et al., 2005). These infants have cognitive impairments (Miller et al., 2005; Rutherford et al., 1998; Harteman et al., 2013) and clinical neurological presentations may show mild or delayed proximal extremity weakness (Izbudak & Grant, 2011). Moderate white matter abnormalities have been associated with a reasonably good outcome, whereas severe white matter infarction leads to seizures and cognitive, communication, behavioural and visual problems (Mercuri et al. 2000; Cowan et al. 2003; Martinez-Biarge et al. 2012). The risk for epilepsy and seizure burden is associated with location and severity of cortical injury (Glass et al., 2014) and cognitive and memory problems may not be apparent until school age (Gonzalez et al. 2006; de Vries & Jongmans, 2010). This pattern of injury has also been associated with poorer verbal IQ at four years of age (Steinman et al., 2009) and spastic diplegia (van Handel et al., 2007).

Most studies assessing the relationship between MRI pattern of injury and outcome have been carried out prior to the introduction of therapeutic hypothermia. Recent studies have found that the relationship between pattern of injury and outcome are still present in infants who receive therapeutic hypothermia (Al Amrani et al., 2018; Shankaran et al., 2015; Cheong et al., 2012; Rutherford et al., 2010; Trivedi et al., 2017). Moreover, the efficacy of MRI for predicting neurodevelopmental outcome between 18-24 months of age has been previously demonstrated (Thayyil et al., 2010; Sanchez Fernandez et al., 2017; Ouwehand et al., 2020) with similar efficacy shown in cooled and uncooled infants (Rutherford et al., 2010; Sanchez Fernandez et al., 2017; Shankaran et al., 2012). Injury to the basal ganglia/thalamus shows higher predictive values for adverse outcomes at 2 years of age compared with other injury patterns regardless of treatment with hypothermia

(Cheong et al., 2012). Notably, the efficacy of MRI for predicting neurodevelopment outcome has been found to continue into later childhood for children treated with therapeutic hypothermia and children that were not treated with therapeutic hypothermia (Barnett et al., 2002; Shankaran et al., 2015; Pappas et al., 2015; van Schie et al., 2015).

1.4.2 Congenital heart disease

Congenital heart disease (CHD) is the most common congenital disorder, with an estimated incidence of 6–8 per 1000 live births (van der Bom et al., 2011). CHD occurs as a result of structural abnormalities of the heart structure. The underlying causes of CHD are still unclear, with most cases of CHD multifactorial and caused by both genetic and environmental factors (van der Bom et al., 2011; Zaidi et al., 2017). The earliest identified genetic causes of CHD were aneuploidies (i.e. numerical chromosome abnormalities (Gelb et al., 2014). Other risk factors of CHD include certain in utero infections such as rubella or influenza, alcohol or drug use, parents being closely related or with a congenital heart defect, and maternal obesity or diabetes (Mendis et al., 2011). There are two types of CHD depending on whether the structural heart defect reduces the amount of oxygen in the body (i.e. cyanotic), or not (i.e. acyanotic). The most common defects may involve the interior walls of the heart, the heart valves, or the large blood vessels leading to and from the heart. The most common cyanotic lesions are tetralogy of fallot, tricuspid atresia, and transposition of the great arteries, and the most common acyanotic lesions are ventricular septal defect, atrial septal defect, atrioventricular canal, pulmonary stenosis, patent ductus arteriosus, aortic stenosis and coarctation of the aorta.

1.4.2.1 Outcome

Recent advances in surgical procedures and perioperative care have led to a significant decrease in mortality rates and most children born with CHD now survive to adulthood (Wren & O'Sullivan, 2001). As mortality rates have declined, research efforts have shifted to understanding and improving neurodevelopmental outcomes and quality of life for survivors. CHD affects neurodevelopment across the lifespan, with developmental delays in infancy including hypotonia and delays affecting language, social skills and feeding (Limperopoulos et al., 1999). Impairments become apparent as children reach school age due to increasing cognitive demands (Cassidy et al., 2015; Schaefer et al., 2013).

Neurodevelopmental impairments affect a wide range of developmental domains, including deficits in cognition, neuromotor functions, executive function, attention and hyperactivity, memory, social interaction, language and communication skills, and emotional and behavioural maladjustment (Limperopoulos et al., 2002; Latal et al., 2016; Andropoulos et al., 2014; Gunn et al., 2016; Bellinger et al., 2015; Kasmi et al., 2017), that can persist throughout childhood (Verrall et al., 2018; Gaynor et al., 2015; Hansen et al., 2012) and into adult life (Bellinger et al., 1999; 2003) presenting a burden to society (Peyvandi et al., 2019). Some children with CHD have minimal to no impairment, but the risk for more severe neurodevelopmental sequelae is more prevalent and severe with increasing complexity of CHD (Mahle et al., 2001; Cassidy et al., 2015). For example, children with milder forms of CHD have fewer impairments, whereas children with more severe forms of CHD have a higher incidence of impairments. The aetiology of neurodevelopmental impairment in CHD remains poorly understood. Risk factors are multifactorial and interrelated and include genetic and epigenetic factors, prematurity, socioeconomic factors, abnormal fetal brain flow and hypoxia-hyperoxia damage,

perioperative and postoperative factors (Marelli et al., 2016; Wernovsky et al., 2006; Bellinger et al., 2011).

Studies have shown that children with complex CHD are at increased risk of impaired intelligence (Schaefer et al., 2013) and academic achievement (Bellinger et al., 2003; Hovels-Gurich et al., 2006). Impairments in executive functioning have also been reported in children (Bellinger et al., 2003), adolescents (Schaefer et al., 2013), and adults (Tyagi et al., 2017). Attentional deficits have also been identified in children (Bellinger et al., 2003; Hovels-Gurich et al., 2007) and adults (Tyagi et al., 2017) and deficits in working memory has been found in adolescents (Schaefer et al., 2013) and adults (Ilardi et al., 2017).

Motor development is also affected in children after CHD with gross (Bellinger et al., 2003; Hovels-Gurich et al., 2006; Limperopoulos et al., 2002) or fine (Hovels-Gurich et al., 2006; Bellinger et al., 2003; Limperopoulos et al., 2002) motor impairments observed. Impaired motor functioning in adolescents (Schaefer et al., 2013) and adults with CHD (Tyagi et al., 2017) has been observed.

Children with complex CHD are also at risk of language delays (Bellinger et al., 2003; Hovels-Gurich et al., 2006; Bellinger et al., 2003), and adolescents have delays in reading (Bellinger et al., 2011).

Visual skills are also impaired in children (Bellinger et al., 2003), adolescents (Schaefer et al., 2013) and adults (Ilardi et al., 2017), and they also exhibit psychosocial maladjustment (internalizing and externalizing problems) (Bellinger et al., 2011; Hövels-Gürich et al., 2007).

1.4.2.2 Neuroimaging

Neurodevelopmental disabilities in CHD were assumed to be the result of hypoxic ischaemic injury or brain embolism associated with intraoperative events. However, it has become clear that neurological insult in CHD begins before surgery, with altered neurological state in the newborn period (Limperopoulos et al., 1999), reduced birth weight and head circumference (Matthiesen et al., 2016), and altered brain growth in the third trimester (Clouchoux et al., 2013; Limperopoulos et al., 2010). Some types of CHD reduce the amount of blood reaching the brain or oxygen content of the blood which may lead to delayed brain maturation in the fetal period (Miller et al., 2007) increasing the risk of brain injury and subsequent abnormal neurodevelopmental outcomes. The white matter is particularly vulnerable to injury in CHD (Hovels-Gurich et al., 2016; Beca et al., 2013; Claessens et al., 2018) because blood vessels in the white matter have a lower vasodilatory response compared to the rest of the brain. White matter injury (WMI) including punctate white matter lesions and periventricular leukomalacia, focal infarctions of the grey matter, and stroke are the most common injuries (Mulkey et al., 2014; Miller et al., 2004; McQuillen et al., 2007; Beca et al., 2013; Mahle et al., 2002; Mebius et al., 2017). Surgical procedures and the postoperative period pose an additional risk to the brain (Beca et al., 2013), with ischaemia and reperfusion injury, inflammatory and immune responses, altered cerebral blood flow regulation, hypothermia, and reduced cardiac output, all potentially contributing to brain injury (Burkhardt et al., 2015).

1.5 Thesis objective

Conditions that lead to brain injury around the time of birth are leading causes of neonatal mortality and life-long morbidities. Improving neurodevelopmental outcome has become one of the greatest remaining challenges for infants with neonatal brain injury. Therefore

the aim of this thesis was to investigate early neuroimaging biomarkers of neurodevelopmental outcome after neonatal brain injury. The outline of this thesis includes: Chapter 2 which introduces the fundamentals of MRI, structural MRI, diffusion-weighted imaging, magnetic resonance imaging, resting-state fMRI, the challenges that are involved in scanning a vulnerable newborn population, and introduces methods of MR image analysis that are discussed in this thesis. In Chapter 3, the predictive ability of three previously validated magnetic resonance imaging (MRI) scoring systems (Barkovich, NICHD NRN and Weeke scores) for neurodevelopmental outcome at 2 years in infants with NE are compared. In Chapter 4, diffusion MRI was used to investigate alterations in structural connectivity in infants with CHD prior to cardiac surgery compared to healthy age-matched controls using graph theoretical analyses and network-based statistics (NBS). In Chapter 5, a systematic review was conducted to identify patterns of altered brain function, quantified using functional connectivity (FC) changes in resting-state fMRI (rs-fMRI) data, that were associated with motor and language outcomes in individuals with a history of perinatal brain injury. In Chapter 6, resting-state fMRI from a large cohort of healthy neonates (n=164) from the developing human connectome project (dHCP) was used to estimate the metastable neural dynamics of fMRI BOLD signal in resting state networks in order to understand metastable dynamics of the infant brain. Chapter 7 provides a summary of the work presented in this thesis, its limitations, and examines potential avenues for future study.

Chapter 2: Materials and Methods: Magnetic Resonance Imaging (MRI) physics and analysis

2.1 Magnetic Resonance Imaging (MRI)

The studies included in this thesis have been conducted using different modalities of magnetic resonance (MR), including structural imaging, diffusion imaging, spectroscopy and functional imaging. Magnetic resonance imaging (MRI) is a non-invasive, non-ionising imaging technique increasingly being used by clinicians for the evaluation of the neonate brain. Its use in the neonatal population provides a unique opportunity to study the structure and function of the brain in vivo, advancing our understanding of typical and atypical neurodevelopment. This chapter will discuss the principles of MRI and its signal properties, the imaging modalities used to evaluate the brain, and discuss the challenges related to imaging the neonate brain.

2.2 Basic physics of MRI signal

2.2.1 Nuclear magnetic resonance (NMR)

MRI is based upon the principle of nuclear magnetic resonance (NMR) co-discovered by Purcell and Bloch in the 1940s (Bloch, 1946; Purcell et al., 1946). Purcell and Bloch both independently observed that certain atomic nuclei could absorb radiofrequency (RF) energy in the presence of an external magnetic field when exposed to RF of a specific resonance frequency. NMR is based upon the concept of “spin” and associated angular momentum and magnetic moment. Hydrogen nuclei comprises a single proton (^1H) with a corresponding positive charge, and is the most commonly imaged nucleus in MRI due to its abundance in the human body. Protons have an intrinsic angular momentum, J , resulting from the spinning motion of hydrogen atomic nuclei due to their odd number of protons. The single proton of the hydrogen atom spins around its axis producing an

electrical current similar to a bar magnet, and is said to have a magnetic moment μ . The magnetic moment, μ , is given by $\mu = \gamma J$, where γ is the gyromagnetic ratio. Without an external magnetic field, protons spin randomly with no net magnetisation, however, in the presence of an external magnetic field, protons align themselves parallel (spin-up) or anti-parallel (spin-down) with the magnetic field (Figure 2.1).

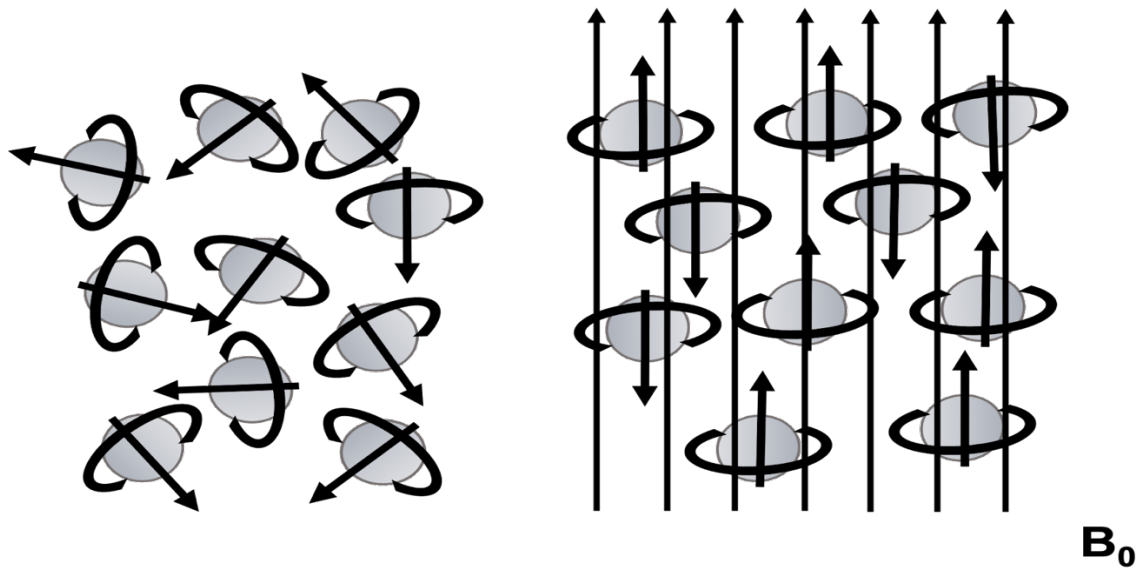


Figure 2.1 Alignment of protons in a magnetic field. On the left, shows hydrogen nuclei randomly orientated in the absence of an external magnetic field. On the right, hydrogen nuclei align themselves parallel or anti-parallel to the field when there is an external field present

High energy protons oppose the magnetic field and are anti-parallel to it (spin down), whereas, low energy protons align parallel with the magnetic field (spin up). At thermal equilibrium, hydrogen protons move between the two energy states, with a greater number of protons aligned in the direction parallel to the magnetic field leading to a net magnetisation in the direction parallel to the external magnetic field, B_0 , (z-axis) referred to as the longitudinal magnetisation.

Another aspect of net magnetisation is the precession of protons around the direction of an applied magnetic field, similar to a spinning top. When protons precess together, they are

in phase, whereas when protons precess separately, they are out-of phase. Protons regularly precess out of phase apart from when they are made to precess in phase. Protons that precess in phase give rise to a net magnetisation perpendicular to the magnetic field, known as transverse magnetisation. The precessional frequency is called the Larmor frequency and is proportional to the strength of the magnetic field, B_0 , measured in Tesla.

Larmor equation: $\omega_0 = \gamma \beta_0$, where ω_0 = Larmor frequency (MHz), γ = gyromagnetic ratio (MHz/T), and β_0 = magnetic field strength (T).

The gyromagnetic ratio determines the precessional frequency of the nucleus and is different for different NMR active atomic molecules. The ratio for hydrogen is 42.57MHz/T. In a 1.5T MRI system, protons precess at approximately 64MHz, and in a 3T MRI system protons precess at approximately 128MHz.

2.2.2 MR signal

First, employing a RF pulse equal to the Larmor frequency (x-y axis) of the hydrogen nucleus, leads to excitation of protons from low to high energy states, decreasing longitudinal magnetisation. Second, protons become synchronised and precess in phase, leading to transverse magnetisation. The angle to which the net magnetisation vector realigns to is called the flip angle, and its magnitude depends on the amplitude and duration of the applied RF pulse, which is normally 90° . The sum of transverse and longitudinal magnetization gives the net magnetic vector. The changing magnetic moment of the net magnetic vector results in free induction decay (FID). The FID signal declines as protons flip back to their low energy states and realign parallel to the external magnetic field or z-axis, and results in protons releasing their absorbed energy back into the

surrounding tissue or lattice (i.e. the environment surrounding the nucleus) in a process known as T1 longitudinal relaxation (or spin-lattice relaxation). T1 is defined as the time taken for longitudinal relaxation to return to approximately 63% of its value, prior to the application of the RF pulse (Figure 2.2). T1 relaxation time differs depending on tissue composition and structure. For example, fat has a fast T1 relaxation time because carbon bonds in fat resonate close to the Larmor frequency, whereas, water moves rapidly and does not move into lower energy state quickly so T1 relaxation time is slower.

As protons relax back to their low energy states, protons that were in phase start to dephase out of the Larmor frequency in the transverse plane (x-y axis) in a process known as T2 transverse relaxation (or spin-spin relaxation) resulting in a reduction in transverse magnetization. T2 is the time taken for transverse magnetisation to fall to approximately 37% of its original value after RF pulse application, corresponding to the 63% of transverse magnetisation that will be lost (Figure 2.2). The spins dephase much quicker than T2 because of inhomogeneities in the magnetic field (B_0), with the combination of T2 relaxation and field inhomogeneity termed T2*. Bigger variations in local magnetic fields occur if a substance is impure, causing greater differences in precession frequencies and leads to protons precessing out of phase faster (i.e. shorter T2). Fat for example demonstrates a short T2, whereas smaller and homogenous molecules seen in water result in smaller net differences in internal magnetic fields, resulting in a longer measured T2.

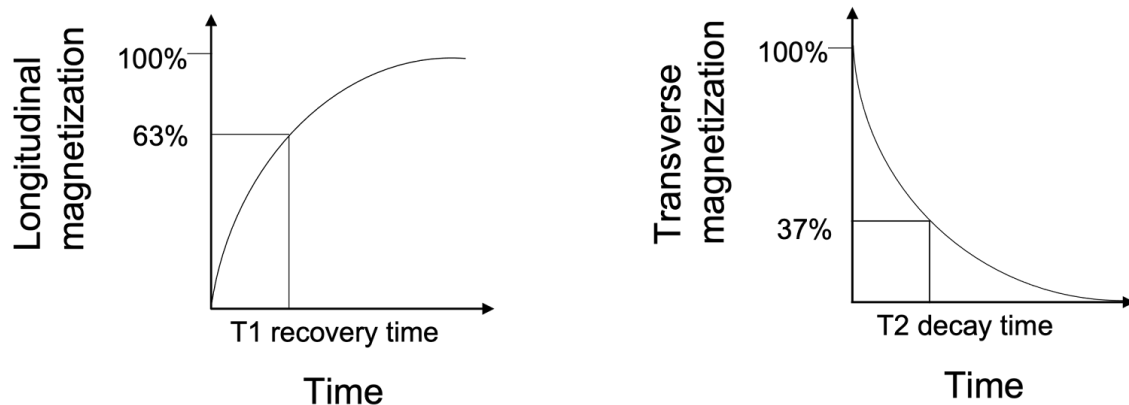


Figure 2.2 Tissue magnetization and relaxation. On the left shows T1 recovery time which is defined as a gain of 63% of the longitudinal net magnetisation vector (i.e. recover 63% of its maximum value). On the right, shows T2 decay which is defined as the time it takes for the transverse magnetisation to decay to 37% of its value (i.e. loses 63% of its maximum signal).

2.2.3 MRI image formation

Producing an MRI image involves the combination of: application of RF pulse to flip net magnetisation, various time delays to obtain the required contrast, and gradient pulses to encode the MRI signal spatially. Gradients are small spatially linear magnetic fields applied in addition to, and superimposed upon, the static magnetic field in order to convey spatial information. Three sets of orthogonal physical gradients are used, x, y and z, otherwise known as frequency encoding, phase encoding and slice selection. A frequency encoding gradient, G_x , also known as the readout gradient, is applied in the x-direction, allowing spatial reconciliation of spins precessing at any one of the frequencies in the gradient. An additional gradient, G_y gradient, or phase encoding, is applied in a stepwise manner in the y-axis permanently altering the phase of precessing spins. Both these gradients combined, allows the position of the signal to be encoded in a 2 dimensional plane. To build a 3 dimensional image, the gradient, G_z in the z-direction selectively excites spins at certain locations, where its oscillatory activity corresponds to the resonant frequency of the spins. The MR signal is first encoded in an intermediate form, known as

the k-space, which places frequency along the horizontal axis, and phase along the vertical axis. This is then decomposed by applying a Fourier transformation, reconstructing the k-space data into a matrix of pixels, with each pixel allocated to a specific spatial location and a particular shade on the grey-scale corresponding to the amplitude of the frequencies of that spatial location.

2.2.4 Scanning parameters

The tissue contrast (i.e. change in brightness between greyscale shades) in MRI is determined by intrinsic and extrinsic properties. Intrinsic properties, are tissue-specific parameters and are dependent on relaxation constants, T1 recovery (longitudinal relaxation), T2 decay (transverse relaxation), and different proton densities (PD) of the tissues. T1 recovery determines the rate at which excited protons return to equilibrium, T2 decay is determines the rate at which excited protons go out of phase with each other, and PD depends on the density of hydrogen nuclei at a particular location. Depending on the MRI acquisition technique (pulse sequence) and extrinsic properties such as sequence parameters including repetition time (TR), echo time (TE), or flip angle, different types of structural images can be obtained in order to gain the greatest contrast between tissue types, with the resulting image reflecting one of the tissue-specific parameters much stronger than the others. For example, a T1-weighted image has a very short TE, and TR and emphasises the T1 characteristics of tissue, i.e. tissues with long T1 appear darker than those with shorter T1. Whereas, a T2-weighted image has very long TE and TR, and shows differences in T2, with tissues with a long T2 such as fluids being much brighter than those with shorter T2. While a PD-weighted image has a long TR and short TE, where tissues with high proton density have a large component of transverse magnetisation

and thus a high signal, while tissues with low proton density have a small component of transverse magnetisation and a low signal.

In prenatal and postnatal periods when there is still limited myelination, T₂- weighted images provide better tissue contrast and signal to noise ratio (SNR) compared to T₁- weighted images. In neonates and infants during the first 6–8 postnatal months, T_{2w} images are generally preferred for the delineation and segmentation of GM and immature WM, whereas T_{1w} images are used to identify the myelinated WM. Neonates have different water and fat content compared with adults, therefore different signal intensities can be observed in T₁ and T₂ weighted imaging. For example from 0-6 months, known as the infantile period, there is a reversal of normal adult contrasts with T₁-weighted images having lower contrast in WM intensity than GM intensity and T₂-weighted images having higher WM intensity than GM intensity. Thereafter, from 8-12 months, known as isointense pattern, there is poor contrast between GM and WM. Then >12 months, the early adult pattern shows T₁-weighted images having higher contrast in WM intensity than GM intensity and T₂-weighted images having lower WM intensity than GM intensity

2.2.5 Echo Planar Imaging (EPI)

MRI techniques such as diffusion weighted imaging (DWI) and functional magnetic resonance imaging (fMRI) rely on echo planar imaging (EPI) for spatial encoding of the MRI image. EPI is one of the fastest techniques for acquiring the entire k-space data after a single RF pulse (single shot EPI), or a small number of RF-pulses (multi-shot EPI), whereby a 2-D image can be obtained in less than a second, using rephasing magnetic gradients. This is in contrast to the traditional method of filling up k-space line-by-line with multiple excitations.

However, the trade-off of increased speed of image collection using EPI, is that it uses bigger voxel sizes (low spatial resolution). Moreover, tissue contrast is inevitably poorer compared with structural imaging (focuses on T2* effects) and geometric distortions and susceptibility artefacts are introduced. Despite these limitations, the ability of EPI to capture rapidly changing processes such as the diffusion of water molecules in DWI and blood oxygenation in BOLD has led to its wide spread use as a research and clinical tool. Recently developed multiband EPI approaches have enabled the acquisition of fMRI and DWI to acquire multiple slices at the time it would take to obtain a single slice in a standard EPI sequence, with the multi-band factor controlling the amount of speed-up that is obtained.

2.3 Diffusion-weighted MRI (DWI)

Diffusion-weighted MRI (DWI) quantifies tissue microstructure by measuring the displacement of water molecules in tissue over time. Diffusion represents the constant motion of water molecules in fluid due to their thermal energy. In a homogenous fluid without restrictions, molecules move randomly, changing direction as they collide with other molecules. This is known as Brownian motion, and was named after the botanist Robert Brown who observed the constant movement of pollen grains suspended in water under a microscope (Brown, 1828). The theory of Brownian motion was elaborated independently by Albert Einstein and Marian Smoluchowski (Einstein, 1905; von Smoluchowski, 1906) when they observed that the mean displacement of freely-diffusing particles is dependent on both the time taken to diffuse, and the diffusion coefficient (or diffusivity) of the medium

$$\lambda = \sqrt{6Dt}$$

where λ is the root mean square displacement of a molecule in three dimensions over

time interval t , and D is the diffusion coefficient of the medium. In the case of water at body temperature, D is approximately $2.5 \mu\text{m}^2/\text{ms}$.

This ‘free’ diffusion process can be described as a Gaussian function since the probability of a molecule reaching any given point after a specific time is equal in all directions over a given time. Within a homogeneous medium (e.g. water), displacement due to diffusion can be described as isotropic. For example, in cerebrospinal fluid, diffusion is unrestricted and is isotropic. Diffusion in white matter, which mostly consists of axonal fibers pointing in a specific direction occurs preferentially along the axonal fibres, results in anisotropic diffusion. While in the grey matter, which mostly consists of dendrites with a randomly oriented microstructure, diffusion may seem to be isotropic, but is in fact anisotropic. The appearance of isotropy is due to limitations in the diffusion-weighted imaging sequences. This diffusional anisotropy of water molecules within the brain was first demonstrated by Moseley et al. (Moseley et al., 1990) in the cat brain.

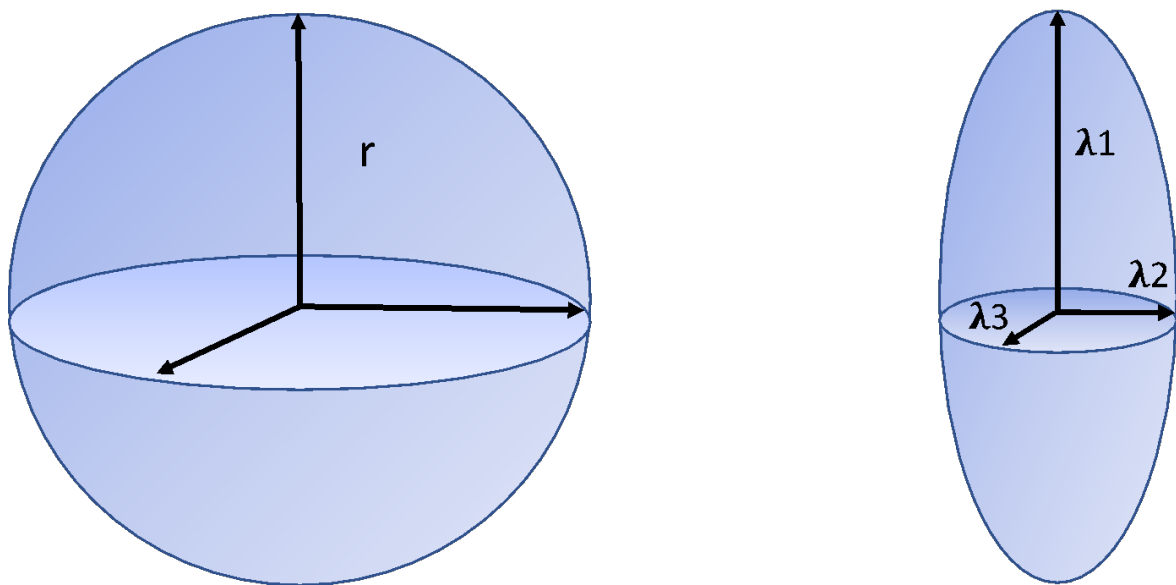


Figure 2.3. Diffusion ellipsoid in an isotropic and anisotropic environment. On the left shows a free medium (homogenous) in which water molecules diffuse freely in all directions, known as isotropic diffusion, e.g. cerebrospinal fluid ventricles. The right shows a restricted medium (heterogenous), in which motion of water molecules is limited in the direction of the hindrance, known as anisotropic diffusion, e.g. white matter bundles, where water molecules diffuse more in in one direction (λ_1), over others (λ_2 and λ_3).

To measure the diffusion of water molecules the pulsed field gradient spin-echo sequence is generally used (Stejskal and Tanner, 1965) whereby two symmetric diffusion-sensitizing gradients are applied either side of the 180° RF pulse. The first diffusion gradient dephases the magnetization of static and moving spins, introducing a phase shift to the spins. The second diffusion gradient will reverse the changes made by the first gradient and rephase static (i.e. undergoing no diffusion) spins leading to no phase shift. If however, the spins are moving (i.e. diffusing) the second gradient will not be able to completely undo the changes induced by the first gradient, resulting in a non-zero net phase difference. A non-zero net phase difference leads to signal attenuation with stronger signal attenuation occurring in tissues with fast diffusion compared to tissues with slow diffusion. Stronger signal attenuation can be seen in fluid-filled structures such as the ventricles and CSF, whereas lower signal attenuation, can be seen in grey or white matter. The amount of signal attenuation caused by diffusion can be enhanced by increasing the strength and duration of the diffusion-encoding gradients which are characterized by the b value [s/mm²] that is defined by the Stejskal-Tanner equation:

$$b = \gamma^2 G^2 \delta^2 (\Delta - \delta/3)$$

where γ is the gyromagnetic ratio, G, the amplitude of the two diffusion gradient pulses, δ , the duration of the pulses, and Δ the time between the two pulses.

The difference in measured diffusion signal between CSF and white matter bundles is not due to differences in the diffusivity of water, but is due to the effect of various cellular barriers restricting water displacement and, consequently, reducing signal attenuation. Apparent diffusion coefficient (ADC) is a widely used parameter derived from DWI, representing the level of restriction to motion of water molecules due to cellular barriers.

In infants with NE, significantly lower ADC values can be found in the PLIC, corona radiata, posterior-frontal and parietal white matter within 12 days of birth when compared with healthy control infants born at term (Wolf et al., 2001). Additionally, ADC values in the PLIC and BGT are associated with neurodevelopmental outcomes at 1 and 2 years of age (Hunt et al., 2004; Vermeulen et al. 2008; Twomey et al., 2010). However, ADC values are likely to underestimate the extent of injury within the BGT as visualized on later conventional MRI (Rutherford et al., 2004). Additionally, the evaluation of ADC is limited due to pseudonormalisation. ADC values decrease to a minimum at approximately 2-3 days of postnatal age and then increase reaching normal values (i.e. pseudonormalisation) on approximately the seventh postnatal day, and increasing further after about 2 weeks. Therefore, postnatal age at scanning must be taken into account when evaluating ADC values (McKinstry et al., 2002). In infants with NE without therapeutic hypothermia, pseudonormalisation tends to occur around 8-10 days of postnatal age (McKinstry et al. 2002; Rutherford et al. 2004; Boichot et al. 2006; Winter et al. 2007), whereas in infants with NE who underwent therapeutic hypothermia pseudonormalisation has been shown to occur at approximately 12 days (Bednarek et al., 2012).

2.3.1 Diffusion tensor imaging (DTI)

The introduction of the diffusion tensor model (DTI) enabled a rotationally invariant description of the shape of water diffusion/estimates of tissue diffusivity. The apparent diffusion tensor (equivalent to a three-dimensional ADC) is a 3×3 matrix,

$$tensor\ D = \begin{bmatrix} D_{xx} & D_{xy} & D_{xz} \\ D_{xy} & D_{yy} & D_{yz} \\ D_{xz} & D_{yz} & D_{zz} \end{bmatrix}$$

whereby the diagonal elements D_{xx} , D_{yy} , and D_{zz} represent the diffusivities along the x, y and z axis, and the off-diagonal elements describe the correlation between them. Tensors

are represented by ellipsoids characterised by three eigenvalues ($\lambda_1, \lambda_2, \lambda_3$) and corresponding eigenvectors ($\varepsilon_1, \varepsilon_2, \varepsilon_3$). Eigenvalues provide the magnitude of diffusion, describing the shape and size of the tensor, and eigenvectors describe the orientation of the tensor. The sum of the eigenvalues is known as the trace, and their average is mean diffusivity (MD) or ADC. The first eigenvalue (λ_1) represents parallel or axial diffusivity (AD), and the average of the second and third eigenvalues (λ_2, λ_3) gives the perpendicular or radial diffusivity (RD). Fractional anisotropy is calculated based on the three eigenvalues ($\lambda_1, \lambda_2, \lambda_3$), with an FA value of 0 indicating that diffusion is isotropic and an FA value of 1 indicating that diffusion is anisotropic. AD is thought to reflect axonal degeneration; RD is thought to represent myelination of axons; and FA is thought to reflect white matter microstructure in terms of myelination, axonal organisation and fiber density (Song et al., 2002). Consistent with the decrease in water content, a pattern of decreasing MD, AD, and RD and increasing FA can be observed in the cerebral white matter in preterm (Kersbergen et al., 2014) and term infants (Dubois et al., 2006; Oishi et al., 2011), occurring first in the sensorimotor cortex followed by the occipital, temporal, and frontal regions (Gupta et al., 2005; Ball et al., 2013). In the neonate brain, high FA (e.g. 0.35-0.50) is representative of well-developed white matter tracts (Dubois et al., 2014). Moreover, in the posterior limbs of the internal capsule (PLIC), high anisotropy and lower diffusivity can be observed due to early myelination of this region, whereas associative white-matter bundles usually show high diffusivity up to term-equivalent age (Hüppi et al., 1998).

A recent systematic review described decreased levels of FA in NE infants compared with healthy controls, which was associated with the severity of NE, and severity of outcomes (Dibble et al., 2020). It has also been shown that infants with NE that were not treated with

therapeutic hypothermia demonstrate significantly lower FA compared with infants that were treated with therapeutic hypothermia (Porter et al., 2010). Moreover, FA values in the PLIC and CC have been associated with adverse outcomes (Tusor et al., 2012; Massaro et al., 2015a; Massaro et al., 2015b; Ancora et al., 2013; Al Amrani et al., 2017). In newborns with CHD, lower white matter FA compared with healthy controls has been observed (Dimitropoulos et al., 2013; Miller et al., 2007; Mulkey et al., 2014; Sethi et al., 2013) and persists into adolescence (Rivkin et al., 2013).

A major limitation of DTI is that it is only able to depict a single fibre population within a voxel and is therefore not capable of directly resolving crossing fibers. The use of more advanced analysis approaches enable microstructure to be studied with greater specificity require high angular resolution diffusion imaging (HARDI) (Tuch et al., 2002). HARDI acquisition is characterised by high b-values and high numbers of uniformly distributed gradients, and enables the use of more advanced models than the diffusion tensor, which can better-delineate crossing fibres. The HARDI based methodological technique constrained spherical deconvolution (CSD) was developed to overcome issues in DTI due to voxels containing multiple fiber orientations (Tournier et al., 2007).

2.4 Spectrum formation in MRS

Magnetic resonance spectroscopy (MRS) measures the concentration of particular metabolites and changes in their levels. However, instead of producing an image, MRS produces a chemical spectrum that provides information on the cellular biochemistry underlying processes such as proliferation, differentiation, migration, and myelination. Most MRS studies use proton MRS (^1H -MRS) as the hydrogen nucleus provides greater sensitivity and allows for more accurate regional measurements (Azzopardi & Edwards 2010). ^1H -MRS relies on the fact hydrogen nuclei resonate at different frequencies

depending on the type of tissue and type of molecules surrounding them. The difference in frequency can then be used to identify the occurrence of metabolites within certain tissues. Given the small concentration of these molecules, the signal-to-noise ratio (SNR) is optimised using a single, large voxel, which results in low spatial resolution.

As opposed to DWI, ¹H-MRS results are not influenced by postnatal age at scanning in the first 30 days after birth. In the neonate brain, prominent signal peaks related to the presence of N-acetylaspartate (NAA), choline, creatine and lactate (Lac) can be identified. NAA, a marker of neural integrity, is thought to be involved in processes such as migration, synaptogenesis, myelination, energy regulation, cellular signalling, mitochondrial function, protein synthesis (Baslow, 2000). NAA increases with advancing cerebral maturity, and decreases with cerebral injury (Barkovich et al., 1999).

Additionally, lac, a marker of anaerobic metabolism, provides an indication of accelerated cell growth (Barkovich et al., 1999). Lac is limited in the healthy newborn brain (Barkovich, 2000), whereas in injured newborns with NE, a large quantity of lactate is typically present (Barkovich et al., 2006). Creatine is a marker of brain energy metabolism and decreases with major neuronal cell death, and choline is associated with membrane turnover increases in cell division and membrane breakdown. Changes in metabolite ratios (i.e. the signal amplitude of one metabolite versus another) are generally calculated in voxels positioned in the basal ganglia and thalamus and are predictive of neurodevelopmental outcomes. A meta-analysis demonstrated that Lac/NAA and Lac/Creatine ratios demonstrated high sensitivity and specificity for abnormal outcome, and were more accurate than conventional MRI and DWI in infants with NE (Thayyil et al., 2010). In fetuses with CHD, lower NAA/Choline ratio has been observed during the third trimester (Limperopoulos et al., 2010), and increased lactate/Choline and lower

NAA/Choline ratio in the basal ganglia and thalamus has been observed in newborn infants with CHD prior to surgery (Miller et al., 2007). Lower NAA/Choline ratio has also been observed in preterm infants and has been shown to be predictive of poorer motor outcomes (Kendall et al., 2014).

2.5 Functional MRI

2.5.1 Foundations of BOLD response

Functional magnetic resonance imaging (fMRI) measures the changes in blood flow and oxygenation that occur in response to neural activity, whereby more oxygen is consumed in an active brain area, leading to increased blood flow. The increase in blood flow exceeds the oxygen requirement and results in an increase in oxygenated Hb relative to deoxygenated Hb in active brain areas. This reduction in deoxygenated Hb leads to a reduced magnetic susceptibility and an increased MR signal, known as the BOLD response. The BOLD response can be quantified by the T2* relaxation time, where the increase in MR signal from the increased oxygenated Hb provides the contrast with the surrounding tissues (Ogawa et al., 1990)

The BOLD response to neural activity is generally modelled using a hemodynamic response function (HRF), which is characterised by a small amplitude ‘initial dip’, a large amplitude positive peak, and a negative undershoot during which the signal falls beneath baseline (Buxton et al., 2004). It is thought that the initial dip of the HRF reflects an early increase in deoxygenated Hb, and the large amplitude positive peak represents functional hyperemia (i.e. increased perfusion of oxygen in activated brain tissue). In term-born neonates, the HRF is characterised by a longer time to positive peak amplitude, a smaller positive peak amplitude and a deeper negative undershoot period relative to the adult HRF (Arichi et al., 2012). The BOLD response is a much slower response than that of the

neuronal changes themselves, taking around 6 seconds to reach a peak after the onset of a stimulus and around 20 seconds to return to the baseline. The first study to assess increased blood flow as a measure of increased neuronal activity using fMRI was in 1991, which demonstrated activation of the visual cortex (Belliveau et al., 1991).

2.5.2 Resting state fMRI

Resting-state fMRI (rsfMRI) involves collecting functional imaging data from participants at rest and not engaging in a cognitive task. During a rsfMRI scanning session, subjects typically fixate on a cross hair or with their eyes closed. In the case of infants or toddlers, subjects are asleep or their eyes are opened during passive movie watching or story listening. Resting-state functional connectivity (rs-FC) measures spontaneous, high amplitude, low-frequency ($<0.1\text{Hz}$) synchronized fluctuations in the BOLD signal to determine tightly coupled resting state networks (RSNs). Many rs-fMRI studies in adults have identified the presence of correlated rs-FC signal in distributed but functionally related brain regions, beginning with somatomotor (Biswal et al., 1995), visual (Lowe et al., 1998), auditory (Cordes et al., 2001), and default mode networks (Fox et al., 2005; Greicius et al., 2003). The rs-fMRI BOLD signal has been found to be present during light sleep (Larson-Prior et al., 2009) and under anaesthesia (Kiviniemi et al., 2000), and is similar across scanners and subjects (Biswal et al., 2010). A rsfMRI scanning session length of 7–10 minutes appears to be adequate for analyses (Van Dijk et al., 2010). However, rs-fMRI analysis is challenging due to the massive amount of data that is acquired as well as the need for sophisticated analysis.

Before analysing rs-fMRI data, important pre-processing steps are required such as realignment, removal of potential confounding artifacts (e.g., head motion, CSF signal),

removal of the first 10-20 time points, slice timing, data normalization, band-pass filtering, and smoothing.

2.5.2.1 Seed based analysis

Seed-based functional connectivity identifies brain regions with correlated brain activity by computing the correlation of a seed time series with the rest of the brain. The coupling of activation between different brain regions is interpreted as brain regions being functionally connected. Seed analysis requires a priori determination of the seeds, often based on a hypothesis or prior results, making it vulnerable to bias. Moreover, seed based analytic methods provide only one measure of connectivity between brain regions. In contrast, independent component analysis (ICA) based methods provide measures of connectivity including total connectivity, and within- and between-network connectivity.

2.5.2.2. Independent component analysis

Independent Component Analysis (ICA) has several advantageous properties when compared with seed based analysis. Most notably, it is model-free and multivariate, thus switching the focus from evaluating the connectivity between single brain regions to evaluating connectivity in terms of resting state networks (RSNs) that simultaneously engage in oscillatory activity. ICA is performed without a priori assumptions, except for the selection of the number of independent components to identify. However, the interpretation of results is complicated due by the fact that synchrony within RSNs may be non-neural in origin (i.e. respiration or cardiac cycle). Additionally, a single RSN could be broken into subnetworks depending on the number of defined independent components. Finally, using ICA requires manual or automated methods to identify specific networks.

A number of RSNs have been identified, that are involved in primary order functions such as somatomotor, auditory or visual processing, and higher-order functions such as self-referential processing (default mode network) (Raichle et al., 2001), goal directed behaviour (central executive network) (Corbetta et al., 2002), information processing related to behaviourally relevant stimuli (salience network) (Seeley et al., 2007), language processing and working memory (frontoparietal network) and emotion and memory (limbic network) (Papez et al., 1995). In adults, primary order RSNs have been found to be localized and mainly containing homologous brain regions, whereas higher-order RSNs, have been found to comprise multiple brain regions spatially distributed across the brain (Damoiseaux et al., 2006; Fox et al., 2005; Raichle et al., 2001; Smith et al., 2009). Studies assessing the functional organization of the developing infant brain (Fransson et al. 2007; Gao et al. 2009b, 2011, 2013; Smyser et al. 2010; Doria et al. 2011; Alcauter et al. 2015; Fitzgibbon et al., 2020; Eyre et al., 2021) have revealed primary order RSNs develop first, followed by higher order networks (Eyre et al., 2021; Gao et al., 2015) with the developmental trajectories of RSNs and displaying remarkable similarities with neurodevelopmental milestones.

In infants with NE treated with therapeutic hypothermia, a number of RSNs have been identified including the primary order auditory, somatomotor and visual networks, and higher-order default mode networks. However, compared to age matched controls, these RSNs were found to be more unilateral and/or localized with reduced interhemispheric and long-range intrahemispheric connections (Tusor, 2014). Additionally, infants with an unfavourable outcome had significantly lower functional connectivity scores within auditory and motor networks compared to infants a favourable outcome.

2.5.3 Dynamic functional connectivity

Functional connectivity analyses are calculated based on the assumption that connectivity is static across the entire rs-fMRI time series, failing to establish a link between the dynamics of coordinated brain activity over time. Recent research efforts are directed on understanding dynamic functional connectivity (i.e. the way in which functional network connectivity changes over scanning time) and shed light on how functional organization evolves over time. Dynamic functional connectivity provides information on the spatiotemporal organization of resting brain activity giving insights into early brain functional development that cannot be completely captured by static connectivity approaches and may help deepen our understanding of how early disruptions affect the brain.

Studies have shown an association between decreased resting state metastability and decreased cognition in traumatic brain injury (Hellyer et al., 2015), and disrupted dynamic functional connectivity within the default-mode network (Du et al., 2016) and between the default-mode network and other RSNs in schizophrenia patients (Rashid et al., 2014; Su et al., 2016). Additionally, dynamic connectivity patterns have been able to identify autism patients better than standard static approaches (Price et al., 2014).

There are few dynamic functional connectivity studies in neonates, however the ability to assess dynamic functional connectivity in neonates has been previously described (Batalle et al., 2016). In addition, a previous study by Wen et al. (2020) assessed how the temporal variability of the functional architecture develops in the first 2 years of age, showing that dynamic functional connectivity of the whole brain increases with age, and higher-order RSNs display increased within and between FC dynamics, whereas primary order RSNs

show reduced within and between FC dynamics with age. Additionally, Huang et al. (2020) showed that sensorimotor areas were the most temporally dynamic in the neonate brain and visual and primary auditory areas had lower dynamic connectivity in neonates compared with adults.

2.6 Connectome

Recent studies have attempted to provide a more complete description of the brain's complex network of structural and functional connectivity by assembling the connectome (Sporns et al., 2005). Graph theoretical network based approaches are represented by 'nodes' (e.g. brain regions) connected by 'edges' (e.g. connectivity) that are typically calculated using diffusion or functional MRI. The advantage of this approach is the reduced dimensionality of brain connectivity to represent key characteristics of network infrastructure and organisation (Rubinov & Sporns, 2009) including infrastructure (e.g. network density and average strength), integration (e.g. global efficiency or characteristic path length) and segregation (e.g. local efficiency or average clustering coefficient). During development, graph theoretical network based models using diffusion MRI have shown an increase in both integration and segregation (Brown et al., 2014; van den Heuvel et al., 2015) and is thought to be associated with myelination and pruning (Dennis and Thompson, 2013b; Tymofiyeva et al., 2014). Other findings in early development include small-world characteristics (van den Heuvel et al., 2015; Tymofiyeva et al., 2012) showing high segregation and integration properties, and a 'rich club' of regions (van den Heuvel & Sporns, 2011) which are regions that are highly connected to each other (Ball et al., 2014). In studies considering graph theoretical parameters of functional brain networks the emergence of cortical functional hubs and small-world characteristics has been identified

in the neonatal brain (Gao et al., 2011). These findings are consistent with adult findings implying early establishment of these network topological features.

Studies assessing structural brain networks in infants with NE have demonstrated correlations between network strength, local efficiency, global efficiency, clustering coefficient and characteristic path length with cognitive outcomes, and found NBS-derived subnetworks associated with cognition, involving the precuneus, thalamus, and left superior parietal gyrus and inferior temporal gyrus (Spencer et al., 2020). Moreover, reduced integration and segregation has been associated with impaired motor outcomes at 6 months in infants with NE (Tymofiyeva et al., 2012). For studies assessing functional network topology, infants with severe NE exhibited decreased local efficiency, clustering coefficient, and reduced nodal efficiency in left supramarginal gyrus, bilateral superior temporal gyrus, and right middle temporal gyrus when compared with infants with mild NE (Li et al., 2019). While in neonates with CHD, one study found that hub or rich-club nodes had reduced FC in the presence of an intact overall global network topology when compared to the healthy term controls (De Asis-Cruz et al., 2018).

2.7 Neonatal MRI considerations

MRI scanning in neonates has a number of challenges related to both the acquisition and analysis of MRI data. The average brain volume is between 200-600 millilitres in the neonate brain, whereas in adults, the average brain volume is greater than 1 litre (Makropoulos et al., 2016). Therefore, a higher spatial resolution is required for describing the smaller structures seen in the neonate brain. Motion is another challenge in neonatal MRI scanning, mainly due to the fact that infants are unable to follow instructions to lie still, and the noisy machine and unfamiliar environment which can make it difficult to

sleep. A number of different approaches are used to address motion such as the use of short acquisition sequences, motion-tolerant acquisition and reconstruction approaches (Cordero-Grande et al., 2018), and hearing protections using dedicated earmuffs. Since the heart rate and respiratory frequency of newborns is 2-3 times higher (Triantafyllou et al., 2010), MRI scanning requires particular adaptation of cardiac and flow MRI. Due to the higher water content and immature myelination of the white matter there is inversion of MRI contrast when compared with adult MRI scans, requiring careful optimisation of MR sequences. Moreover, the use of dedicated coils are needed, adapted and optimized to the head size of newborns, as well as to enhance the SNR ratio in images (Hughes et al., 2017). Targeted post-processing methods of MRI images are also required to improve signal and contrast characteristics of newborn images. However, despite these challenges, MRI approaches can be used to provide a better understanding of altered development of the structural and functional brain network following early injury and the associated neurodevelopmental consequences.

Table 2.1 Summary of the types of MRI modalities used in this thesis and their neonatal clinical applications

MRI modality	Description	Neonatal clinical applications
Structural (T1, T2)	Provides information on the shape, size and integrity of tissues.	Assess anatomical development, and identify and assess the severity, extent and location of injury
DWI	Measures the motion of water diffusion across tissue.	Assess severity, location and extent of injury, describe white matter tracts and quantify measures of tissue microstructure.
Spectroscopy	Measures chemical concentrations of biochemical compounds in the brain.	Assess metabolite changes in regions of injury, and as a biomarker of outcome.
Resting state fMRI	Measures blood flow and metabolic activity changes that accompanies neural activity changes.	Assess organisation of brain into networks that support behaviours, and characterise injury severity in functional networks.

Chapter 3: Relationship Between MRI scoring systems and Neurodevelopmental Outcome at 2 years in infants with Neonatal Encephalopathy

Abstract: Magnetic resonance imaging (MRI) scoring systems are used in the neonatal period to predict outcome in infants with neonatal encephalopathy (NE). Our aim was to assess the relationship between 3 MRI scores and neurodevelopmental outcome assessed using Bayley Scales of Infant and Toddler Development, third edition (Bayley-III) at 2 years in infants with NE. Term-born neonates with evidence of perinatal asphyxia born between 2011 to 2015 were retrospectively reviewed. MRI scanning was performed within the first two weeks of life and scored using Barkovich, NICHD NRN and Weeke systems by a single assessor blinded to the infant's clinical course. Neurodevelopmental outcome was assessed using composite scores on the Bayley-III at 2 years. Multiple linear regression analyses were used to assess the association between MRI scores and Bayley-III composite scores, with postmenstrual age at scan and sex included as covariates. Of the 135 recruited infants, 90 infants underwent MRI and of these 66 returned for follow-up. MRI abnormalities were detected with the highest frequency using the Weeke score (Barkovich 40%, NICHD NRN 50%, Weeke 77%). The inter-rater agreement was good for the Barkovich score, and excellent for NICHD NRN and Weeke scores. There was a significant association between Barkovich, NICHD NRN and Weeke scores and Bayley-III cognitive and motor scores. Only the Weeke score was associated with Bayley-III language scores. Our findings confirm the predictive value of existing MRI scoring systems for cognitive and motor outcome, and suggest that more detailed scoring systems have predictive value for language outcome.

This chapter is based upon: Ní Bhroin M.....Molloy EJ, Bokde ALW. Relationship between MRI scoring systems and neurodevelopmental outcome at 2 years in infants with Neonatal hypoxic-ischaemic encephalopathy. *Pediatr Neurol.* 2021;126:35-42

3.1 Introduction

Neonatal encephalopathy (NE) affects around 1 to 9 per 1,000 live births worldwide and is an important cause of neurodevelopmental abnormalities including intellectual impairment, blindness and deafness, and cerebral palsy (Lee et al., 2013; Jacobs et al., 2013). Therapeutic hypothermia (TH), which involves cooling the infant's core temperature between 33°C to 34°C for 72 hours within the first 6 hours of life, is the only proven effective neuroprotective therapy available. Randomized controlled trials (RCT) of TH have demonstrated reduced risk of mortality and neurodevelopmental disability for infants with moderate to severe NE (Shankaran et al., 2002, 2005; Azzopardi et al., 2009; Zhou et al., 2010), however, the incidence of death or moderate/severe disability still remains high (Jacobs et al., 2011).

Early prediction of outcome remains challenging but essential to accurately counsel parents and determine the appropriate level of care. The most accurate 2-year neurological prognosis is predicted based on integration of neuroimaging, (amplitude-integrated) electro-encephalography (aEEG) and clinical neurologic examination (Bonifacio et al., 2015). Magnetic resonance imaging (MRI) is the gold standard in neuroimaging for evaluating the severity, extent and location of brain injury. MRI findings in this population have shown parasagittal watershed (WS) infarcts between intravascular boundary zones with the cortex and subcortical white matter also involved; and injury to basal ganglia, thalami, putamen, hippocampi, brainstem, corticospinal tracts, and sensorimotor cortex (Bano et al., 2017). Basal ganglia and thalamus injury, and abnormal signal intensity in the posterior limb of the internal capsule (PLIC) have been associated with poor neuromotor outcomes such as dyskinetic cerebral palsy and hemiplegia, impaired cognitive outcome and epilepsy (Barkovich et al., 1998; Rutherford et al., 1998; de Vries et al., 2010; Miller

et al., 2005; Martinez-Biarge et al., 2011; Shankaran et al., 2015). Cortical WS injuries have been related to verbal cognitive outcomes (Steinman et al., 2009) with clinical neurological presentations at birth mild or delayed (Izbudak et al., 2011). Despite studies showing a reduction in deep grey matter and cortical injury on MRI in infants treated with TH, the accuracy of MRI to predict outcome is not altered by TH (Rutherford et al., 2010).

Several MRI scoring systems which are used to quantify brain injury severity have been developed to standardize the classification of MRI findings in infants with NE. The Barkovich (Barkovich et al., 1998) and NICHD NRN (Shankaran et al., 2012) scoring systems use conventional MRI (T1- and T2-weighted sequences) to assess patterns of injury involving basal ganglia/thalamus (BGT) and WS areas, with an assessment of PLIC abnormalities also included in the NICHD NRN score. Diffusion weighted imaging (DWI) can show restricted diffusion in ischaemic brain regions earlier than conventional MRI (Rutherford et al., 2005) and proton magnetic resonance spectroscopy (¹H-MRS) has been shown to be the most accurate MR biomarker for predicting outcome (Thayyil et al., 2010). The MRI score described by Weeke et al. includes DWI and ¹H-MRS in describing brain abnormalities of the deep grey matter, white matter, cerebellum, and intracranial haemorrhages. The Barkovich score has been shown to predict adverse outcomes at 2 years (Al Amrani et al., 2018) and the NICHD NRN score predicted death or disability at 18-22 months (Shankaran et al., 2012) and 6-7 years (Shankaran et al., 2015).

Additionally, the Weeke score was found to have high predictive value for outcome at 2 years and at school age (Machie et al., 2021). The use of more detailed scoring systems such as the Weeke score has been previously shown to increase the ability to assess MRI abnormalities compared with Barkovich and NICHD NRN scores (Machie et al., 2021), however, it is not known how this relates to outcome. Here, we aimed to assess the

relationship between Barkovich, NICHD NRN and Weeke MRI scores and neurodevelopmental outcome assessed using Bayley Scales of Infant and Toddler Development, third edition (Bayley-III) at 2 years of age in infants with NE.

3.2. Materials and methods

3.2.1 Ethical approval

Approval was granted by the Ethics Committee at National Maternity Hospital and Children's Hospital Ireland at Temple Street. Parental consent was obtained for voluntary participation.

3.2.2 Study design and patient population

This retrospective cohort study enrolled infants with perinatal asphyxia admitted to the neonatal intensive care unit (NICU) at National Maternity Hospital from February 2011 to June 2015. Infants were included according to the criteria of Huang et al. (1999). Infants underwent a standardized neurological examination using the Sarnat classification which grades the degree of encephalopathy as; infants requiring resuscitation only with no neurological signs of encephalopathy, mild, moderate, or severe (Sarnat & Sarnat, 1976). Infants with congenital abnormalities, evidence of maternal substance abuse, culture-positive sepsis or with MRI performed at more than 14 days of life were excluded. Patient and clinical characteristics were obtained from electronic health records of enrolled patients. TH was administered in accordance with the TOBY (Total Body Hypothermia for Neonatal Encephalopathy) criteria (O'Hare et al., 2017) and infants were treated for 72 hours duration.

3.2.3 MR imaging protocol

Infants underwent MRI on a 1.5T MR Scanner (GE Signa HDx) situated in the NICU at Children's Hospital Ireland at Temple Street. MRI of the brain was obtained before fourteen days of life. MR consisted of harmonized protocols including T1- and T2-weighted sequences, DWI, apparent diffusion coefficient (ADC) mapping, and single-voxel ¹H-MRS in the basal ganglia.

3.2.4 MRI scoring

MRI scans were scored according to Barkovich (Barkovich et al., 1998), NICHD NRN (Shankaran et al., 2012) and Weeke (Weeke et al., 2018) scoring systems by a single assessor (M.Ní.B) blinded to the infant's clinical course.

Barkovich score: T1- and T2-weighted images were used to score infants using the combined Barkovich BG/W score. The BG/W score grades severity of injury from 0 to 4, with a score of 0 indicating normal MRI; a score of 1 representing abnormal signal intensity in basal ganglia of thalamus, a score of 2 representing abnormal signal in the cortex, a score of 3 representing abnormal signal in both the basal ganglia/thalamus and the cortex, and a score of 4 representing abnormal signal intensity in the entire cortex and basal nuclei (Barkovich et al., 1998).

NICHD NRN score: T1- and T2-weighted images were also used for the NICHD NRN score in describing brain injury patterns as: 0, normal; 1A, minimal cerebral lesions; 1B, more extensive cerebral lesions; 2A, any BGT, anterior limb internal capsule (ALIC) or PLIC, or WS infarction without any other cerebral lesions; 2B, 2A with cerebral lesions; 3, cerebral hemispheric devastation (Shankaran et al., 2012).

Weeke score: For the Weeke score (Weeke et al., 2018), T1- and T2-weighted imaging, DWI including ADC, and ¹H-MRS were used in evaluating deep grey matter (DGM), cerebral white matter/cortex (WM), and cerebellar abnormalities (Weeke et al., 2018). Each item is scored based on whether the injury is focal (score of 1), or extensive (score of 2) and if unilateral (score of 1) or bilateral (score of 2). Intraventricular haemorrhage (IVH), subdural haemorrhage (SDH) and cerebral sinovenous thrombosis (CSVST) were also recorded and included in the additional subscore. The total score (total max score 57) was calculated by adding the 4 subscores (DGM + WM + cerebellum + additional) with increasing scores reflecting greater involvement of brain injury.

The study assessor (M.Ní.B) underwent intensive training before applying each score. The intensive training comprised training by experienced paediatric neuroradiologists (A.T.B and G.C) on the 3 MRI scores, and the sequences used to evaluate them. The MRIs used for the training were from a cohort of patients with NE and with known brain injury to show how to apply the scoring systems. Subsequently, a number of practice runs were performed to ensure the assessors (M.Ní.B) understanding of the MRI scoring systems. Following the intensive training, a subsample (n=10) of scans was rescored by the assessor for intra-rater reliability using intraclass correlation coefficient (ICC). To test the reliability between readers for each of the three scores described above, the interrater agreement was calculated on a subsample of scans (n=10) between the assessor (M.Ní.B) and an experienced paediatric neuroradiologist (A.T.B) using Cronbach alpha. Patient identifiers were removed from the imaging before evaluation and both MRI readers were blinded to the clinical data and clinical outcomes and reviewed the MRIs in random order.

3.2.5 Neurodevelopmental outcome

Neurodevelopmental outcome was assessed using the Bayley-III at 2 years of age administered by a clinical psychologist unaware of the MRI scores (Bayley, 2006). Rates of developmental delay were determined using Bayley-III test norms (mean=100, SD=15) with Bayley-III score 70-84 (-1 SD) indicating mild impairment, and <70 (-2 SD) indicating severe impairment.

3.2.6 Statistical Analyses

Infant characteristics were compared using student's t-tests, Mann-Whitney U tests, χ^2 or Fisher exact test where appropriate. Normality was assessed using the Shapiro-Wilk test. Agreement between the assessor (M.Ni.B) and an experienced paediatric neuroradiologist (A.T.B) was performed on a subsample (n=10) using Cronbach alpha. Multiple linear regression analyses were performed to assess the association between MRI scores and Bayley-III composite scores. All regression analyses were adjusted for postmenstrual age (PMA) at MRI scan and sex. Statistical analyses were performed using RStudio 1.1463 (The R Foundation for Statistical Computing, Vienna, Austria).

3.3 Results

3.3.1 Clinical characteristics

135 infants presented with NE between February 2011 and June 2015. Two died before MRI completion, and a further 43 infants either did not have MRI available (n=35) for further analysis or was performed at more than 14 days of life (n=8). We report findings from 90 neonatal MR scans and 86 follow-up assessments at 2 years. Combined data for both neonatal MR scans and follow-up assessments were available in 66 subjects.

The grades of encephalopathy according to Sarnat and Sarnat were as follows: 3 (3%) infants were exposed to perinatal asphyxia but with no neurological signs, 13 (15%) had Mild NE, 61 (70%) had Moderate NE, and 10 (11%) had Severe NE. Sarnat grading information was not available for 1 infant. 67 (74%) infants required TH in accordance with the TOBY criteria and clinical seizures developed in 56 (63%) infants.

Bayley-III, which was performed at 2 years, was obtained in 86/135 infants; and of these, 66 (73%) patients underwent Bayley-III and neonatal MRI. 24 patients who underwent neonatal MRI were lost to follow-up; four of which died in the early perinatal period.

Compared with infants lost to follow-up (n=24), patients with complete data (neonatal MRI + follow-up) (n=66) were significantly more likely to have the following features: higher gestational and postmenstrual age, more cases of moderate NE, less cases of severe NE and lower cord base excess values. Neonatal characteristics for the whole sample, baseline and follow up analysis subsamples are described in Table 3.1.

Table 3.1. Neonatal characteristics

Variable	Whole sample (n=135)	Baseline (MRI) (n=90)	Follow-up (Bayley-III) (n=86)	Complete (MRI and follow-up) (n=66)	No follow-up (n=24)	Complete ~ No follow-up p-value
Gestational age, weeks	40.57 (39.43-41.33)	40.70 (39.60-41.43)	40.84 (40-41.43)	40.93 (40-41.43)	40.22 (38.53-40.82)	0.02
Postmenstrual age, weeks	41.71 (40.67-42.47)	41.57 (40.42-42.43)	42 (41.03-42.57)	41.93 (40.92-42.43)	41.14 (39.40-41.85)	0.01
Age at scan, days	7 (6-9)	7 (5-8)	7 (6-8)	7 (6-8)	6 (4-8.25)	0.59
Birth Weight, kg	3.67 ± 0.67	3.67 ± 0.68	3.71 ± 0.65	3.70 ± 0.67	3.58 ± 0.74	0.45
Male	91 (69%)	62 (69%)	58 (68%)	44 (68%)	18 (75%)	0.79
<i>Mode of Delivery</i>						
LSCS	52 (44%)	36 (41%)	34 (41%)	26 (41%)	10 (42%)	0.81
SVD	34 (28%)	24 (27%)	20 (24%)	16 (25%)	8 (33%)	0.60
Inst.	34 (28%)	28 (32%)	29 (35%)	22 (34%)	6 (25%)	0.45
Outborn	28 (23%)	23 (28%)	19 (23%)	15 (24%)	8 (42%)	0.27
Twin pregnancy	5 (4%)	2 (2%)	1 (1%)	1 (2%)	1 (5%)	0.45
Apgar 1 min	3 (1-5)	2 (1-4)	3 (1-5)	2 (1-4.75)	2 (0.75-3)	0.30
Apgar 5 min	5 (3-7)	4.5 (2-6)	5 (3-7)	5 (2-6)	4 (2.75-6.25)	0.73
Apgar 10 min	6 (4-8)	5 (4-8)	6 (4-8)	5 (4-8)	5.5 (4-7.75)	1
<i>Grade of encephalopathy</i>						
Perinatal asphyxia	14 (11%)	3 (3%)	4 (5%)	1 (2%)	2 (9%)	0.18

Mild	33 (26%)	13 (15%)	17 (21%)	11 (17%)	3 (13%)	1
Moderate	67 (53%)	61 (70%)	56 (69%)	50 (77%)	11 (48%)	0.02
Severe	13 (10%)	10 (11%)	4 (5%)	3 (5%)	7 (30%)	0.004
Therapeutic hypothermia	77 (58%)	67 (74%)	57 (67%)	49 (74%)	18 (75%)	0.79
Seizures	62 (48%)	56 (63%)	48 (57%)	43 (66%)	13 (57%)	0.32
Mortality	6 (5%)	4 (5%)	0	0	4 (19%)	0.004
Cord pH 1	7.13 (6.97-7.25)	7.07 (6.94-7.23)	7.11 (6.97-7.24)	7.09 (6.97-7.23)	7.02 (6.90-7.21)	0.60
Cord pH 2	7.16 (7.06-7.25)	7.16 (7.06-7.24)	7.15 (7.04-7.23)	7.16 (7.06-7.22)	7.2 (7.07-7.28)	0.26
Cord BE 1 mmol/l	-10.53 ± 4.71	-10.89 ± 5.0	-10.88 ± 4.66	-10.94 ± 4.8	-10.75 ± 5.73	0.70
Cord BE 2 mmol/l	-9.1 (-12.6- -7.2)	-9.3 (-13- -7.35)	-9.7 (-13.73- -7.78)	-9.6 (-13.5- -7.75)	-7.75 (-9.75- -5.25)	0.02
Cord lactate 1, mmol/l	7.9 (5.7-11.6)	7.35 (6-10.43)	7.65 (6-11.9)	7.35 (6.4-10.43)	7.55 (4.5-11.83)	0.46
Adm. pH	7.1 ± 0.21	7.07 ± 0.22	7.1 ± 0.19	7.08 ± 0.19	6.99 ± 0.33	0.41
Adm. pCO ₂	6.34 (5.22-10)	6.54 (5.14-10.90)	6.72 (5.18-10.47)	6.91 (5.07-11.03)	5.67 (5.22-9.0)	0.77
Adm. bicarbonate, mmol/l	14.5 (11.55-17.25)	13.7 (11.40-15.9)	13.85 (11.4-16.18)	13.2 (11.4-14.9)	14.85 (11.3-20.4)	0.22
Adm. BE, mmol/l	-13.48 ± 6.76	-14.64 ± 6.17	-14.30 ± 5.65	-14.94 ± 5.38	-13.8 ± 8.12	0.52
Adm. lactate, mmol/l	10.57 ± 4.65	11.59 ± 4.03	11.47 ± 4.23	11.75 ± 3.91	10.95 ± 4.72	0.70

Data presented as N (percent), means ± SD, or median and (IQRs). Mann-Whitney U tests were used for continuous data and for categorical variables the χ^2 and Fisher exact tests were used for comparison. Abbreviations: LSCS = lower segment caesarean section; SVD = spontaneous vaginal delivery; Inst. = instrumental delivery; BE = base excess; Adm. = admission.

3.3.2 MRI scoring characteristics

Neonatal MRI was carried out at 7 (5-8) days in infants with baseline MRI data, and at 7 (6-8) days in infants with complete data (MRI and follow-up). 59 out of 90 (66%) infants with baseline MRI data and 43 out of 66 (65%) infants with complete data (MRI and follow-up) had scanning performed in the first week after birth. All infants had conventional MRI and DWI, and ¹H-MRS of the basal ganglia was obtained in 52 out of 90 (58%) infants with baseline data (MRI) and in 42 out of 66 (64%) infants with complete data (MRI and follow-up). For infants with baseline MRI data, ¹H-MRS in the basal ganglia revealed abnormal lactate peak in two infants (one of which died in the early perinatal period), abnormal NAA peak in one infant (died in the early perinatal period) and abnormal lactate and NAA peak in one infant. For infants with complete data (MRI and follow-up), abnormal lactate peak was observed in one infant, and abnormal lactate and NAA peak was observed in one infant. See table 2 for description of MRI scoring systems.

The most frequent pattern of injury with the Barkovich score was 2: abnormal signal in the cortex (Baseline: n=15 (14%), Complete: n=13 (20%)) and with the NICHD NRN score was 1B: more extensive cerebral lesions (Baseline: n=12 (13%); Complete: n=10 (15%)). The Weeke total score (Grey matter+¹H-MRS + White matter + Cerebellum + Additional subscores) was [median (IQR)] 4 (1-10) for infants with baseline MRI data, and 3.5 (1-9.75) for infants with complete data (MRI and follow-up).

MRI abnormalities were detected with the highest frequency using the Weeke score (Baseline (MRI): Barkovich 38% vs NICHD NRN 47% vs Weeke 77%; Complete (MRI and follow-up): Barkovich 40% vs NICHD NRN 50% vs Weeke 77%). Details of MRI findings are shown in Table 3. The inter-rater agreement was 0.625 for the Barkovich

score, 0.889 for the NICHD NRN score, and 0.969 for the Weeke total score. While the intra-rater agreement was 0.977 for the Barkovich score, 0.991 for the NICHD NRN score and 0.975 for the Weeke score.

Table 3.2. MRI scoring systems

Barkovich		NICHD NRN		Weeke			
BG/T	Description		Description	DGM+ ¹ H-MRS	WM	Cerebellum	Additional
0	Normal	0	Normal	Thalamus 1 – Focal (<50%) 2 – Extensive (≥50%)	Cortex 1 – Focal (1 lobe) 2 – Extensive (>1 lobe)	Cerebellum 1 – Focal (<0.5cm) 2 – Extensive (≥0.5cm or multiple lesions)	IVH 1 – Yes
1	Abnormal signal in basal ganglia or thalamus	1A	Minimal cerebral lesions	Basal ganglia 1 – Focal (<50%) 2 – Extensive (≥50%)	White matter 1 – Focal (1 lobe) 2 – Extensive (>1 lobe)	Cerebellar haemorrhage 1 – Single haemorrhage <0.5cm 2 – Multiple haemorrhages or ≥0.5cm	SDH 1 – Yes
2	Abnormal signal in cortex	1B	More extensive cerebral lesions	PLIC 1 – Partial myelination 2 – Absent myelination	PWML 1 – <6 2 – ≥6		CSVT 1 – Yes
3	Abnormal signal in cortex and basal nuclei (basal ganglia or thalami)	2A	Any BGT, ALIC, PLIC, or WS infarction noted without any other cerebral lesions	Brainstem 1 – Focal (<50%) 2 – Extensive (≥50%)	Parenchymal haemorrhage 1 – Single haemorrhage <1.5cm 2 – Multiple haemorrhages or ≥ 1.5cm		
4	Abnormal signal in entire cortex and basal nuclei.	2B	2A with cerebral lesions	Perirolandic cortex 1 – Mild 2 – Clear	Optic radiation 1 – Mild 2 – Clear		
		3	Cerebral hemispheric devastation	Hippocampus 1 – Yes	Corpus callosum 1 – Yes		
				Basal ganglia NAA			

				0 – Normal 1 – Reduced			
				Basal ganglia Lac 0 – Absent 1 – Increased			

Abbreviations: ALIC = anterior limb internal capsule; BG = Basal ganglia; BGT = Basal ganglia/thalamic; CSVT = cerebral sinovenous thrombosis; ¹H-MRS = proton magnetic resonance spectroscopy; IVH = intraventricular haemorrhage; Lac = lactate; NAA = N-acetylaspartate; PLIC = posterior limb internal capsule; PWML = punctate white matter lesions; SDH = subdural haemorrhage WS = Watershed. Weeke scoring system total score calculated by adding the 4 subscores (DGM+¹H-MRS + WM + cerebellum + additional).

Table 3.3 MRI scoring characteristics of the infants

MRI score	Baseline (MRI) (n=90)	Abnormal MRI	Complete (MRI and follow-up) (n=66)	Abnormal MRI
<i>Barkovich, BGT/WS</i>		34 (38%)		26 (40%)
0	56 (64%)		40 (61%)	
1	8 (10%)		8 (12%)	
2	15 (14%)		13 (20%)	
3	10 (11%)		5 (7%)	
4	1 (1%)		0	
<i>NICHD NRN</i>		42 (47%)		33 (50%)
0	48 (59%)		33 (50%)	
1A	10 (5%)		9 (14%)	
1B	12 (13%)		10 (15%)	
2A	9 (10%)		9 (14%)	
2B	8 (10%)		3 (4%)	
3	3 (3%)		2 (3%)	
<i>Weeke</i>		69 (77%)		51 (77%)
Total score	4 (1-10)		3.5 (1-9.75)	
Grey matter	0 (0-3)		0 (0-3)	
White matter	2 (0-6)		1.5 (0-4.75)	
Cerebellum	0 (0-2)		0 (0-0)	
Additional	0 (0-1)		0 (0-1)	

Data presented as N (percent), or median and (IQRs).

3.3 Neurodevelopmental characteristics

Bayley-III was obtained in 86/135 infants, and combined data for both neonatal scans and follow-up assessments were available in 66 infants. Bayley-III language composite scores were not available for one infant. Among the 86 infants with follow-up assessments, cognitive impairment was observed in 11 (13%) infants, 6 (7%) with mild impairment, and 5 (6%) with severe impairment. Language impairment was observed in 16 (19%) infants,

10 (12%) with mild impairment and 6 (7%) with severe impairment. Motor impairment was observed in 9 (10%) infants, 3 (3%) with mild and 6 (7%) with severe impairment.

For infants with complete data (MRI and follow-up data) cognitive impairment was observed in 9 (14%) infants, 5 (8%) with mild impairment and 4 (6%) with severe impairment. Language impairment was observed in 10 (16%) infants, 7 (11%) with mild impairment and 3 (5%) with severe impairment. Motor impairment was observed in 7 (11%) infants, 2 (3%) with mild and 5 (8%) with severe impairment. Neurodevelopmental characteristics of the infants are summarized in Table 4.

Table 3.4. Neurodevelopmental characteristics of the infants

Outcomes	Follow-up (Bayley-III) (n=86)	Complete (MRI and follow-up) (n=66)
Bayley-III cognitive composite score	105 (95-110)	105 (95-110)
Bayley-III language composite score	100 (89-115)	100 (89-115)
Bayley-III motor composite score	103 (97-112)	107 (97-112)
Impairment at 2 years		
Mild cognitive impairment (Bayley-III cognitive composite score 70-84)	6 (7%)	5 (8%)
Mild language impairment (Bayley-III language composite score 70-84)	10 (12%)	7 (11%)
Mild motor impairment (Bayley-III motor composite score 70-84)	3 (3%)	2 (3%)
Severe cognitive impairment (Bayley-III cognitive composite score <70)	5 (6%)	4 (6%)
Severe language impairment (Bayley-III language composite score <70)	6 (7%)	3 (5%)
Severe motor impairment (Bayley-III motor composite score <70)	6 (7%)	5 (8%)

Data presented as N (percent), or median and (IQRs)

3.4 Relationship between MRI scores and neurodevelopmental outcome

Analysis of infants with complete data (MRI scores and follow-up) revealed a significant correlation between Bayley-III cognitive composite score and Barkovich BGT/WS score

(adjusted $R^2 = 0.1269$, $p=0.0102$), NICHD NRN score (adjusted $R^2 = 0.2236$, $p=0.0026$), and Weeke total score (adjusted $R^2 = 0.2645$, $p<0.0001$). There was no association between Bayley-III language composite scores and Barkovich BGT/WS and NICHD NRN scores ($p>0.05$ in both cases). However, we did find a significant correlation between Bayley-III language composite scores and Weeke total score (adjusted $R^2 = 0.1747$, $p=0.0022$).

Lastly, we found a significant association between Bayley-III motor composite score and Barkovich BGT/WS score (adjusted $R^2 = 0.1053$, $p=0.0204$), NICHD NRN score (adjusted $R^2 = 0.2703$, $p=0.0006$), and Weeke total score (adjusted $R^2 = 0.3018$, $p<0.0001$). After adjusting for Sarnat grading, therapeutic hypothermia treatment and whether MRI was performed at ≤ 7 and >7 days of age, all p -values remained statistically significant.

After adjustment for whether MRI was performed at ≤ 7 and >7 days of age, we found a significant association between Bayley-III cognitive composite score and Barkovich BGT/WS score (adjusted $R^2 = 0.1283$, $p=0.0152$), NICHD NRN score (adjusted $R^2 = 0.2209$, $p=0.0040$), and Weeke total score (adjusted $R^2 = 0.2671$, $p=0.0001$); Bayley-III language composite scores and Weeke total score (adjusted $R^2 = 0.1656$, $p=0.0052$); and Bayley-III motor composite score and Barkovich BGT/WS score (adjusted $R^2 = 0.1401$, $p=0.0106$), NICHD NRN score (adjusted $R^2 = 0.2703$, $p=0.0006$), and Weeke total score (adjusted $R^2 = 0.3365$, $p<0.0001$). There was no association between Bayley-III language composite scores and Barkovich BGT/WS and NICHD NRN scores.

3.4 Discussion

We investigated the association of three MRI scoring systems (Barkovich, NICHD NRN and Weeke scores) with Bayley-III composite scores at 2 years in infants with NE. The inter-rater agreement was good for the Barkovich score, and excellent for NICHD NRN and Weeke scores. We found the Weeke scoring system identified MRI abnormalities with the highest frequency. We also show Barkovich, NICHD NRN and Weeke scoring systems were associated with Bayley-III cognitive and motor composite scores at 2 years. However, only the Weeke score was associated with Bayley-III language composite scores. These results lend support for the use of MRI scoring systems for prognosticating cognitive and motor outcome in infants with NE, and suggest that a detailed assessment of all MRI abnormalities has added predictive value for language outcome.

Several MRI studies have identified a range of brain abnormalities that are useful in evaluating brain injury severity. Mild to moderate hypoxic-ischemic injury produces brain lesions in WS areas, parasagittal cortex and subcortical white matter, while severe hypoxic-ischemic injury causes lesions in the thalamus, putamen, hippocampus, brainstem, corticospinal tracts and sensorimotor cortex (Bano et al., 2017). Many MRI scores have been developed and validated in this population, with a variable level of these brain abnormalities included (Barkovich et al., 1998; Shankaran et al., 2012; Weeke et al., 2018; Al Amrani et al., 2018; Rollins et al., 2014; Massaro et al., 2015a; Trivedi et al., 2017; Lally et al., 2019). While the overall objective of MRI scoring systems is to guide interpretation in order to reduce subjectivity, standardize communication and aid reproducibility, there is no clear consensus which system describes the most common and significant abnormalities that are relevant to predicting neurodevelopmental outcome. Two of the most commonly used scoring systems are Barkovich and NICHD NRN which group

patterns of injury in BG and WS areas and are quick and easy to use, whereas the MRI score recently developed by Weeke et al., (2018) assesses all brain abnormalities observed on MRI is more time intensive. These scoring systems also vary in the sequences used, with conventional sequences used in the Barkovich and NICHD NRN scores, and DWI and ¹H-MRS utilised in the Weeke score. Furthermore, these scores were developed and validated in infants with variable severities of NE and described for application beyond the first week of life for Barkovich and NICHD NRN scores, and within the first week of life for the Weeke score. While we acknowledge that we cannot make a direct fair comparison of the predictive ability of each MRI score, we are not intending to do so, nor are we attempting to promote one scoring system over the other. The aim of this paper was to illustrate the strengths of each scoring system for predicting outcome, and the added advantage of a more detailed approach. There is a clinical need to determine the strengths of these MRI scoring systems in predicting outcome, as these insights carry important implications for the development of behavioural interventions in the care of children with NE.

A previous study compared the ability of Barkovich, NICHD NRN, and Weeke MRI scores to detect brain abnormalities in infants with NE (24). They showed the Weeke score detected MRI abnormalities with the highest frequency compared with Barkovich and NICHD NRN scores. Similar to Machie et al., (2021) we also found the Weeke score detected brain abnormalities with a higher frequency than Barkovich and NICHD NRN scoring systems. Here, we extend this research to determine how this finding relates to predicting neurodevelopmental outcomes.

We found Barkovich and NICHD NRN scores were associated with Bayley-III cognitive and motor composite scores at 2 years. This is consistent with previous studies which have established these MRI scores as good predictors of cognitive and motor outcomes in infants with NE. The Barkovich BG/W score has been associated with poor neuromotor and cognitive outcomes (Barkovich et al., 1998), and BGT pattern has been associated with severely impaired motor (Miller et al., 2005; Martinez-Biarge et al., 2011; Harteman et al., 2013) and cognitive outcomes (Miller et al., 2005) and WS pattern with cognitive impairments (Miller et al., 2005, Steinman et al., 2009). Additionally, the NICHD NRN score has been shown to be a marker of moderate or severe disability at 18-22 months (Shankaran et al., 2012), and death or IQ<70 at 6-7 years of age (Shankaran et al., 2015). However, there are limitations to the use of Barkovich and NICHD NRN scores, as classification of injury by these systems provide only a distinct number of brain injury severity levels, and are subject to inter-rater reliability. While we report the inter-rater reliability of all three MRI scores to be good, we found that the Barkovich score had the lowest inter-reliability of the three scores assessed. The Weeke score, which showed excellent inter-rater reliability in our study, assesses all brain abnormalities observed on MRI using a comprehensive point by point basis with distinct descriptions of brain injury. Similar to Barkovich and NICHD-NRN scores, we also found that the Weeke score was associated with Bayley-III cognitive and motor composite scores at 2 years. This is consistent with the Weeke et al. study which showed the Weeke grey matter subscore had high predictive value for adverse outcome at 2 years (defined as death, GMFCS \geq II, or Bayley-III <85 for motor or cognitive composite score).

Despite the large number of children with impaired language development after NE (Marlow et al., 2005) there have been less studies attempting to identify biomarkers of

impaired language ability. Interestingly, the Weeke score was the only scoring system associated with Bayley-III language composite scores. The Weeke score includes an assessment of brain regions including the corpus callosum, brainstem, hippocampus, and cerebellum, not accounted for by Barkovich and NICHD NRN scores. The corpus callosum which supports the acquisition of spoken language in healthy infants (Swanson et al., 2017) has been identified in a recent systematic review by Dibble et al. as a particular region of interest with altered diffusion in infants with NE (Dibble et al., 2020). Additionally, microstructural abnormalities of the corpus callosum have been associated with language outcomes in infants born preterm (Counsell et al., 2008) and with NE (Massaro et al., 2015b). Lesions of the brainstem have also been reported in NE, and are associated with the most severe outcomes (Martinez-Biarge et al., 2011) with speech, language and communication problems commonly seen in infants with these types of lesions. In infants with NE, reduced volumes of the hippocampus has been identified (Gadian et al., 2000) and is associated with visuospatial memory at 9-10 years of age (Annink et al., 2019), and injury to the hippocampus has been associated with neurocognition and memory at school-age in NE (Annink et al., 2021). The cerebellum which is also important for language functioning (Murdoch, 2010) is increasingly being identified as a brain region vulnerable to hypoxia in infants with NE (Alderliesten et al., 2013), and in preterm infants, cerebellar abnormalities have been associated with neurodevelopmental outcomes (Hortensius et al., 2018). Reduced structural connectivity involving both the hippocampus and cerebellum has also been previously identified in populations at-risk of neurodevelopmental impairments (Ní Bhroin et al., 2020).

The Weeke score also assesses IVH, SDH and CSVT as part of the additional subscore.

While we were not able to assess the association of this subscore with outcome due to the

limited number of infants presenting with these abnormalities, a previous study found intracranial haemorrhages had no association with outcome in infants with NE treated with TH (Lakatos et al., 2019). It will therefore be important for future studies to assess whether the inclusion of this subscore adds additional prognostic information.

We were unable to compare the predictive ability of MRI scores for neurodevelopmental outcome between infants with MRIs performed early (≤ 7 days) or late (> 7 days), because only a limited number of MRIs were performed in the first week of life. It is thought that early MRI indicates the timing of injury and later MRI the extent of the injury (Executive summary: neonatal encephalopathy and neurologic outcome, second edition. Report of the American College of Obstetricians and Gynecologists' Task Force on Neonatal Encephalopathy), but there is no consensus which is more valuable in determining prognosis. Late MRI has been shown to be a good predictor of outcome (Rutherford et al., 2010; Shankaran et al., 2012) and a previous study found no difference between early and late MRI scans in predicting outcome (Rollins et al., 2014). However, a meta-analysis by Ouwehand et al. (2020) found MRI injury scoring methods were more predictive during the first week than the second week of life, and a recent study showed better predictive ability of Barkovich and NICHD NRN scores when MRI was performed early (≤ 7 days) compared with late (> 7 days) (O'Kane et al., 2021). Moreover, pseudonormalization of DWI can occur after the first week of life, restricting the value of the Weeke score to the first week (Bednarek et al., 2012; Barkovich et al., 2006). Further studies are needed to determine the optimal timing of imaging in this population to most accurately quantify brain injury severity using MRI scoring systems and predict outcome.

Finally, it is worth considering the inclusion of resting state functional MRI (rs-fMRI) as another modality which may offer additional predictive utility to assess the impact of brain injury. rs-fMRI noninvasively measures the temporal correlation of low frequency (<0.1Hz) fluctuations in blood oxygen level-dependent (BOLD) signals across the brain while the subject is at rest. A recent systematic review identified altered functional connectivity in brain regions important for motor and language functioning that were associated with motor and language outcomes in individuals after perinatal brain injury (Ní Bhroin et al., 2021). They also identified altered brain network functional connectivity involving a number of resting-state networks that were associated with motor outcomes. Disrupted functional connectivity has been previously shown to predict motor impairment better than structural MRI score (Linke et al., 2018), therefore, therapeutic approaches aimed at measuring rs-fMRI may also facilitate early identification of infants with NE at risk of neurodevelopmental impairments.

Our study has some limitations. Firstly, its retrospective design, small sample size and lack of follow-up in a number of infants (24 out of 90, 27%). In addition, 37 infants did not have MRI data available, two of whom died. The study cohort was heterogeneous that included varying severities of NE. Unfortunately, our sample size was not large enough to assess whether these findings would generalize to infants with varied NE severity and further studies with larger sample sizes are needed to investigate this. Our study did not include identification and classification of cerebral palsy, deafness or blindness and should only be interpreted accordingly. Furthermore, not all infants had MRI scanning performed in the first week of life, 31 out of 90 (34%) infants with baseline MRI data and 23 out of 66 (35%) infants with complete data, had MRI scanning performed in the second week of life. Neurodevelopmental follow-up was obtained at 2 years of age, however, additional

studies are needed to assess the predictive value of these MRI scores at later school ages. Finally, due to the heterogeneity of the study cohort showing various brain injury patterns, the number of infants with specific injury patterns was limited. Limitations aside, our findings add to the literature by suggesting that (1) Barkovich, NICHD NRN and Weeke scores are associated with Bayley-III cognitive and motor composite scores at 2 years, but that (2) only the more detailed MRI score by Weeke et al. is associated with Bayley-III language composite scores at 2 years. Accordingly, more detailed scoring systems may have added prognostic value for neurodevelopmental outcome in newborns with NE.

3.5 Conclusion

This study investigated the association of three different MRI scoring systems (Barkovich, NICHD NRN, Weeke) with neurodevelopmental outcome at 2 years in infants with NE. We confirm the predictive value of existing MRI scoring systems for cognitive and motor outcomes, and show that more detailed scoring systems have added prognostic value for language outcome. Future studies should examine how generalizable these findings are to infants with varied severity levels of NE.

Chapter 4: Reduced structural connectivity in cortico-striatal-thalamic network in neonates with congenital heart disease.

Abstract: Impaired brain development has been observed in newborns with congenital heart disease (CHD). We performed graph theoretical analyses and network-based statistics (NBS) to assess global brain network topology and identify subnetworks of altered connectivity in infants with CHD prior to cardiac surgery. Fifty-eight infants with critical/serious CHD prior to surgery and 116 matched healthy controls as part of the developing Human Connectome Project (dHCP) underwent MRI on a 3T system and high angular resolution diffusion MRI (HARDI) was obtained. Multi-tissue constrained spherical deconvolution, anatomically constrained probabilistic tractography (ACT) and spherical-deconvolution informed filtering of tractograms (SIFT2) was used to construct weighted structural networks. Network topology was assessed and NBS was used to identify structural connectivity differences between CHD and control groups. Structural networks were partitioned into core and peripheral nodes, and edges classed as core, peripheral, or feeder. NBS identified one subnetwork with reduced structural connectivity in CHD infants involving basal ganglia, amygdala, hippocampus, cerebellum, vermis, and temporal and parieto-occipital lobe, primarily affecting core nodes and edges. However, we did not find significantly different global network characteristics in CHD neonates. This locally affected sub-network with reduced connectivity could explain, at least in part, the neurodevelopmental impairments associated with CHD.

This chapter is based upon: Ní Bhroin M, Abo Seada S, Bonthron AF, Kelly CJ, Christiaens D, Schuh A, Pietsch M, Hutter J, Tournier JD, Cordero-Grande L, Rueckert D, Hajnal JV, Pushparajah K, Simpson J, Edwards AD, Rutherford MA, Counsell SJ, Batalle D. Reduced structural connectivity in cortico-striatal-thalamic network in neonates with congenital heart disease. *Neuroimage Clin.* 2020;28:102423. doi: 10.1016/j.nicl.2020.102423.

4.1. Introduction

Congenital heart disease is the most common congenital disorder, with an estimated incidence of 6-8 per 1000 live births (van der Bom et al., 2011). Recent advances in surgical procedures and perioperative care have led to a significant decrease in mortality rates and most children born with CHD now survive to adulthood (Wren & O'Sullivan, 2001). As mortality rates have declined, research efforts have shifted to understanding and improving neurodevelopmental outcomes and quality of life for survivors of CHD.

Neurodevelopmental impairments are common (Marino et al., 2012) and can involve several developmental domains, including cognition, executive function, motor and language skills, and behavioural impairments (Gaynor et al., 2015; Latal, 2016).

Magnetic resonance imaging (MRI) studies have identified a high incidence of acquired brain lesions and impaired brain development in infants with CHD (Glauser et al., 1990; Miller et al., 2004; Miller et al., 2007; Hinton et al., 2008; Ortinou et al., 2012; von Rhein et al., 2015; Kelly et al., 2017; Kelly et al., 2019a; Kelly et al., 2019b; McQuillen et al., 2006; Claessens et al., 2016). Brain dysmaturation in this population encompasses reduced total and regional brain volume (Ortinou et al., 2012; von Rhein et al., 2015); impaired cortical gyrification (Kelly et al., 2017; Claessens et al., 2016) and microstructural development (Kelly et al., 2019a); reduced *N*-acetylaspartate (NAA) to choline ratios and elevated mean diffusivity in deep grey and white matter; and reduced white matter fractional anisotropy (Miller et al., 2007).

Recent advances in MRI have made it possible to describe global organization properties of structural and functional brain networks through the application of graph theoretical approaches (Bullmore & Sporns, 2009). Graph theory analysis applied to connectivity matrices can extract important network features (Hagmann et al., 2012) and has been used to investigate alterations in brain development in preterm infants (van den Heuvel et al.,

2015; Bataille et al., 2017). The presence of a high capacity central core, or rich club, has been observed in adults (van den Heuvel & Sporns, 2011) and in infants (Ball et al., 2014). Previous reports in populations at-risk of neurodevelopmental impairment have found that core-connectivity is maintained and peripheral (i.e. local) connectivity is disrupted (Fischi-Gomez et al., 2016; Karolis et al., 2016; Bataille et al., 2017; Ball et al 2014). In neonates with CHD, recent studies have demonstrated reduced functional connectivity (De Asis-Cruz et al., 2018) and alterations in structural network topology pre-operatively (Schmithorst et al., 2018). However, it is not clear whether altered structural network topology in infants with CHD prior to surgery can be explained by disruptions to core-peripheral connections.

In this study we used high angular resolution multi-shell diffusion imaging to characterise brain organisation of the structural network in newborns with CHD and controls. Our aims were to (i) determine global and local network features in newborns with CHD and healthy controls, (ii) assess core and peripheral network organisation in both groups and (iii) identify subnetworks of altered connectivity in infants with CHD using network-based statistics (NBS) (Zalesky et al., 2010).

4.2. Materials and methods

The project was approved by the National Research Ethics Service West London committee (CHD 07/H0707/105; Controls 14/LO/1169). Informed written consent was obtained from the parents of all participants before scanning.

4.2.1 Participants

The study included fifty-eight infants with critical or serious CHD. Critical CHD was defined as hypoplastic left heart syndrome, pulmonary atresia with intact ventricular

septum, transposition of the great arteries, interruption of the aortic arch and all infants dying or requiring surgery within the first 28 days of life with the following conditions: coarctation of the aorta; aortic valve stenosis; pulmonary valve stenosis; tetralogy of Fallot; pulmonary atresia with ventricular septal defect; total anomalous pulmonary venous connection. Serious CHD was defined as any cardiac lesion not defined as critical, which requires cardiac catheterisation or surgery, or results in death before age one (Ewer et al., 2011; Kelly et al., 2019b). Exclusion criteria included suspected or confirmed chromosomal abnormality or congenital syndrome, neonatal surgery before recruitment (excluding cardiac catheterization procedures), suspected congenital infection, or arterial ischaemic infarction on MRI. Twelve infants with transposition of the great arteries underwent balloon atrial septostomy prior to MRI. Thirty-one infants with CHD were on a prostaglandin infusion to maintain ductal patency at the time of scan and none required mechanical ventilation at the time of scanning.

A control group of 116 healthy infants was matched to the CHD group by gestational age (GA) at birth, post-menstrual age (PMA) at scan and sex. Healthy infants were recruited contemporaneously from the postnatal ward at St Thomas' Hospital as part of the developing Human Connectome Project (dHCP) (<http://www.developingconnectome.org/>). Table 4.1 shows the demographic characteristics of the two groups.

Table 4.1. Demographic Characteristics of the CHD and Control Cohorts

Variable	Newborns with CHD (n=58)	Control newborns (n=116)	<i>p</i> -value
Gestational age at birth, weeks	38.43 (38–38.86)	38.71 (37.86–39.29)	0.1579
Postmenstrual age at scan, weeks	39.07 (38.57–39.71)	39.14 (38.43–39.71)	0.884
Male sex, n (%)	33 (57%)	66 (57%)	1
Birth weight (kg)	3.06 (2.77–3.45)	3.11 (2.71–3.46)	0.6162

Birth head circumference (cm)	33.65 (32.4–35)	34 (33–35)	0.5306
Primary Heart lesion - n (%)			
Transposition of the great arteries	27 (46%)	–	
Coarctation of the aorta	12 (21%)	–	
Tetralogy of Fallot	7 (12%)	–	
Pulmonary stenosis	4 (7%)	–	
Hypoplastic left heart syndrome	3 (5%)	–	
Pulmonary atresia	3 (5%)	–	
Truncus arteriosus	1 (2%)	–	
Tricuspid atresia	1 (2%)	–	

Values presented as median (interquartile range) unless otherwise stated. *p*-values calculated using Mann-Whitney *U* test.

4.2.2 Data Acquisition

MR imaging was performed on a Philips 3 Tesla system (Best, The Netherlands) located in the neonatal intensive care unit in the Evelina Newborn Imaging Centre at St. Thomas Hospital using a 32-channel neonatal head coil and neonatal positioning device (Hughes et al., 2017). Pulse oximetry, temperature, electrocardiography and respiratory rate were monitored during the MR examinations which were supervised by a paediatrician trained in MR procedures. Infants were scanned in natural sleep and provided with ear protection comprising earplugs moulded from silicone based putty placed in the external auditory meatus (President Putty, Coltene Whaledent, Mahwah, NJ), neonatal earmuffs (MiniMuffs, Natus Medical Inc, San Carlos, CA) and an acoustic hood placed over the infant. T1-weighted images were acquired using the following parameters; repetition time (TR)=11 milliseconds, echo time (TE)=4.6 milliseconds, flip angle=9°, voxel size=0.8×0.8×0.8 mm. T2-weighted images were acquired using a multislice turbo echo sequence: TR=12 seconds, TE=156 milliseconds, flip angle=90°, in-plane resolution=0.8 mm, slice thickness=1.6, overlap=0.8 mm. Susceptibility-weighted imaging (SWI) was

acquired using a spoiled gradient-recalled echo sequence: TR=3.2 seconds, TE=25 milliseconds, flip angle=12°, voxel size=0.45x0.45x1.8mm. Diffusion MRI was acquired with a high angular resolution diffusion (HARDI) multi-shell protocol designed specifically for the neonatal brain; TR= 3.8 seconds, TE=90 milliseconds, volumes=300, multiband factor=4, sensitivity encoding E: 1.2; resolution: 1.5×1.5×3 mm with 1.5 mm slice overlap, diffusion gradient encoding: b=0 s/mm² (n=20), b=400 s/mm² (n=64), b=1000 s/mm² (n=88), b=2600 s/mm² (n=128) with interleaved phase encoding (Hutter et al., 2018).

4.2.3 Qualitative MRI analysis

MR images were reported by two neonatal neuroradiologists. All images were subsequently rereviewed to ensure consistency, and lesions classified as focal arterial ischaemic stroke (AIS), white matter injury (WMI), cerebellar haemorrhage or intraventricular haemorrhage as described previously (Kelly et al., 2019b). The location and properties of lesions on T1 and T2-weighted imaging, SWI and apparent diffusion coefficient (ADC) map were recorded. WMI was classified into normal (no WMI), mild (≤ 3 foci and all ≤ 2 mm), moderate (> 3 and ≤ 10 foci or any > 2 mm) or severe (> 10 foci) (Beca et al., 2013). Overall each baby was categorised into one of four brain injury groups; normal, mild (intraventricular haemorrhage, and/or cerebellar haemorrhage ≤ 2 mm, and/or mild WMI), moderate (cerebellar haemorrhage > 2 mm and/or moderate WMI) and severe (severe WMI) (Kelly et al., 2019b).

4.2.4 Pre-processing and network construction

All T2-weighted images were motion corrected and reconstructed to a 0.8mm isotropic resolution (Cordero-Grande et al., 2018), bias field corrected (Tustison et al., 2010), brain extracted (Smith et al., 2002) and segmented into white matter (WM), grey matter (GM),

deep grey matter (DGM), cerebrospinal fluid (CSF) and cerebellum using an extension of the Draw-EM algorithm (Makropoulos et al., 2014, 2018). Parcellation was performed using the anatomical automatic labelling (AAL) atlas (Tzourio-Mazoyer et al., 2002) mapped to neonates (Shi et al., 2011) resulting in 93 cortical, subcortical and cerebellar regions, and manually corrected using a high-resolution dHCP atlas (Schuh et al., 2018). The parcellation was normalised from template space to native T2-weighted space using the diffeomorphic symmetric image normalization method (SyN) in the Advanced Normalization Tools (ANTs) software package (Avants et al., 2008). Tissue maps and parcellation were registered using rigid registration with the Image Registration Toolkit (IRTK) (Studholme et al., 1999) from each infant's T2-weighted native space to diffusion native space with average $b=0$ volumes used as the target.

Diffusion MRI was reconstructed to an isotropic resolution of 1.5mm, denoised (Cordero-Grande et al., 2019; Veraart et al., 2016), Gibbs ringing artefacts suppressed (Kellner et al., 2016), and corrected for motion and image distortion using spherical harmonics and radial decomposition (SHARD) (Christiaens et al., 2019). Using a group averaged response function sampled in WM and in CSF from control infants, tissue and free water orientation distribution functions (ODFs) were estimated using multi-shell multi-tissue constrained spherical deconvolution (Jeurissen et al., 2014) and subsequently normalized to obtain quantitative measures of density (Raffelt et al., 2017). The normalised tissue ODFs were used to generate 10M streamlines from probabilistic tracking using anatomically constrained probabilistic tractography (ACT) (Smith et al., 2012) with biologically accurate weights (SIFT2) (Smith et al., 2015; Tournier et al., 2019).

The fibre density SIFT2 proportionality coefficient (μ) for each subject was obtained to achieve inter-subject connection density normalisation, and structural connectivity (SC)

was considered as the weighted sum ($SIFT2 * \mu$) of streamlines connecting each pair of regions, resulting in the construction of a 93x93 structural connectivity matrix for each subject.

4.2.5 Network measures

Graph theoretical analyses were carried out in order to assess topological properties of individual weighted networks using functions from the Brain Connectivity Toolbox (BCT) (Rubinov & Sporns, 2010) for Matlab (version R2018b). Global functioning of brain networks was characterized by assessing infrastructure, integration and segregation.

Network infrastructure was assessed by network density which measures the proportion of observed edges relative to the number of possible edges (Kaiser, 2011) and average strength which describes the connectivity of a node to other nodes by summing all of the edge weights in the network. In order to assess brain network integration, we measured global efficiency which takes the inverse of the average shortest path length between nodes to provide a measure of relative parallel information exchange between distributed regions across the network (Achard & Bullmore, 2007; Latora & Marchiori, 2001, 2003).

Local efficiency, which represents network segregation and measures the efficiency of information exchange among neighbouring nodes was also calculated. Local efficiency reflects the fault tolerance of the network, by assessing how well each subnetwork exchanges information following the removal of random nodes from the network (Achard & Bullmore, 2007). Each of these network features were calculated in original reconstructed networks (“raw” networks). In addition, we summarised how the organisation of structural connectivity changes with increasing age at scan by assessing the relationship of infrastructure, integration and segregation with PMA at MRI scan.

Calculation of all network characteristic formulations were based on definitions by Rubinov and Sporns (2010).

4.2.6 Core and Periphery partitioning and local characteristics

We partitioned structural connectivity networks into two distinct groups of nodes, which consisted of a core and periphery structure. This was achieved using an adapted version of the Kernighan-Lin algorithm for graph partitioning (Borgatti & Everett, 1999; Newman, 2006) available in the BCT toolbox (Rubinov & Sporns, 2010). This produces an optimal core-periphery structure such that core nodes are well-connected to other core and periphery nodes, while periphery nodes are not well connected to each other, and results in a set of highly connected and strongly interconnected hubs and a sparsely connected brain periphery. We defined a common core/periphery structure as nodes belonging to the core/periphery partitioning in 90% of subjects. To quantify the goodness of fit of the core/periphery partition we calculated the coreness statistic which estimates the degree of separation between core and peripheral nodes (Borgatti & Everett, 1999). For regional nodal characteristics of the core and periphery structure, we considered nodal efficiency measuring how well a specific node is integrated within the network via its shortest paths (Latora & Marchiori, 2001; Achard & Bullmore, 2007), and nodal strength which represents the sum of edge weights connected to each node.

4.2.7 Network based statistics

The structural connectomes were then evaluated with the network-based statistics (NBS) toolbox for MATLAB, which detects differences in structural connectivity between groups using permutation testing (Zalesky et al., 2010). NBS considers multiple comparisons when identifying subnetworks that exhibit significant structural differences between

groups. We used a general linear model (GLM) with 10,000 permutations and multiple comparison correction ($p=0.05$) when comparing the extent (i.e. total number of connections) between groups. In NBS, correction for multiple comparisons is carried out by cluster-based thresholding whereby connected components of a network are treated as a cluster. We used the primary test-statistics threshold ($t=3.1$) to define a set of supra-threshold connections in which the connections with a test statistic value exceeding this threshold are considered significant. Since NBS results are highly dependent on the primary test-statistics threshold, we tested a range of values ($t=2.5-3.5$) and show the results for $t=3.1$. The NBS analysis was controlled for relevant covariates including sex, GA at birth, PMA at scan, and overall brain injury score.

4.2.8 Statistical Analysis

Group comparisons were examined with a general linear model (GLM) using the multivariate analysis of covariance (MANCOVAN) toolbox by William Gruner (<https://www.mathworks.com/matlabcentral/fileexchange/27014-mancovan>) in Matlab R2018b (Mathworks Inc., Mattick, USA) with sex, GA at birth, PMA at scan, and overall brain injury score as fixed effects. Partial Spearman's correlations were used to assess the association between graph theory features and PMA at scan, while also controlling for sex, GA at birth and overall brain injury score. All analyses were carried out using Matlab R2018b. BrainNet Viewer was used for visualizations of nodes and edges (Xia et al., 2013).

4.3. Results

4.3.1. Clinical Characteristics

The analysis included 174 newborn infants, which comprised of 58 neonates with CHD scanned prior to surgery and 116 age-matched healthy controls. There was a higher

proportion of infants with CHD with mild ($p=0.0161$) and severe WMI ($p=0.0443$). Four (7%) infants with CHD had cerebellar haemorrhage. There were no cases of cerebellar haemorrhage or severe WMI in control infants. Details of imaging findings in both groups are shown in Table 4.2.

Table 4.2. Characteristics and MRI findings of the infants

Variable	Newborns with CHD (n=58)	Control newborns (n=116)	<i>p</i> -value
Cerebellar haemorrhage, n (%)	4 (7%)	0	0.0042
White matter Injury (WMI), n (%)			
Normal	40 (69%)	101 (87%)	0.0042
Mild	11 (19%)	8 (7%)	0.0161
Moderate	5 (9%)	7 (6%)	0.4028
Severe	2 (3%)	0	0.0443
Overall brain injury score, n (%)			
0 – Normal	37 (64%)	101 (87%)	0.0004
1 – Mild	13 (22%)	8 (7%)	0.0031
2 – Moderate	6 (10%)	7 (6%)	0.3080
3 – Severe	2 (3%)	0	0.0443

p-values calculated using Chi-squared statistics

4.3.2 Global network features

Increasing postmenstrual age at MRI scan was positively associated with average network strength ($\rho=0.3429$, $p<0.001$), global efficiency ($\rho=0.3935$, $p<0.001$) (Fig. 4.1A), and local efficiency ($\rho=0.3533$, $p<0.001$) (Fig. 4.1B), but negatively associated with total network density ($\rho=-0.3955$, $p<0.001$). No difference between groups was found when assessing infrastructure for total network density ($p=0.242$) and average network strength ($p=0.177$). Furthermore, when investigating network integration, we found no difference in global

efficiency ($p=0.150$) (Fig. 4.1A) between the two cohorts. Analysis of network segregation revealed that local efficiency was significantly higher in controls compared to neonates with CHD [MANCOVA: $F_{(5, 168)}=4.60, p=0.033$] (Fig. 4.1B). However, after removing one outlier from the analysis of local efficiency (defined as 3 scaled median absolute deviations (MAD) away from the median), statistical significance was lost ($p=0.103$).

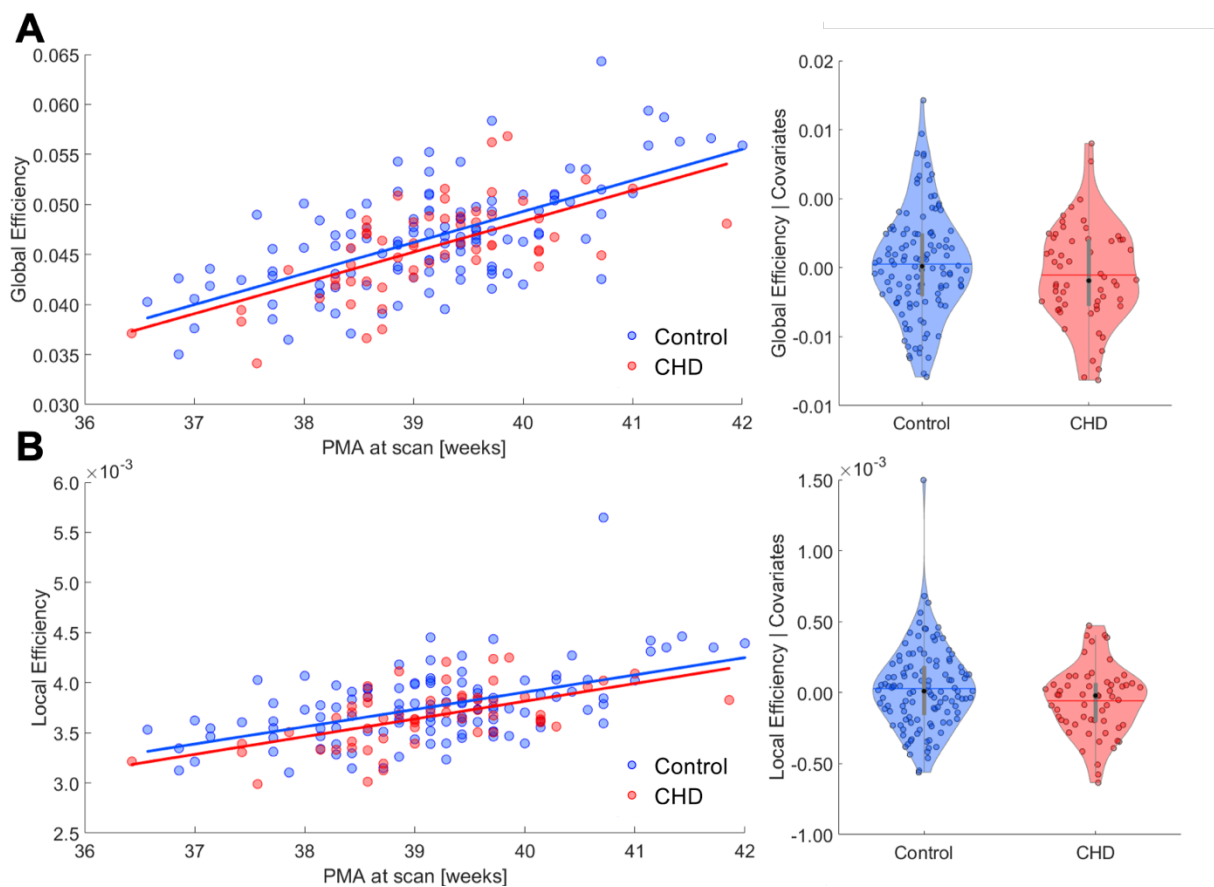


Figure 4.1. Global graph theory characteristics in CHD and control group. Relationship between global (A) and local efficiency (B) with post-menstrual age (PMA) at scan. Regression line indicates significant positive relationship. Violin plots representing distribution of residuals after correcting for PMA at scan, GA at birth, sex and overall brain injury score. Global efficiency did not differ between groups, whereas local efficiency in controls was significantly higher compared to CHD neonates ($p=0.033$). However, after removing the outlier, statistical significance was lost.

5.3.3 Core/Periphery partitioning and local characteristics

A common core/periphery structure was defined for the whole study population (see Table 4.3 for a full list of core and periphery nodes, represented in Fig. 4.2) as described in

Section 4.2.6. This analysis revealed a core comprised of 34 regions, which included the insula, precuneus, superior frontal cortex as well as subcortical thalamus and putamen. The coreness statistic was calculated for each subject and found to be significantly higher in CHD compared to control neonates [MANCOVA: $F_{(5, 168)} = 5.01, p = 0.026$].

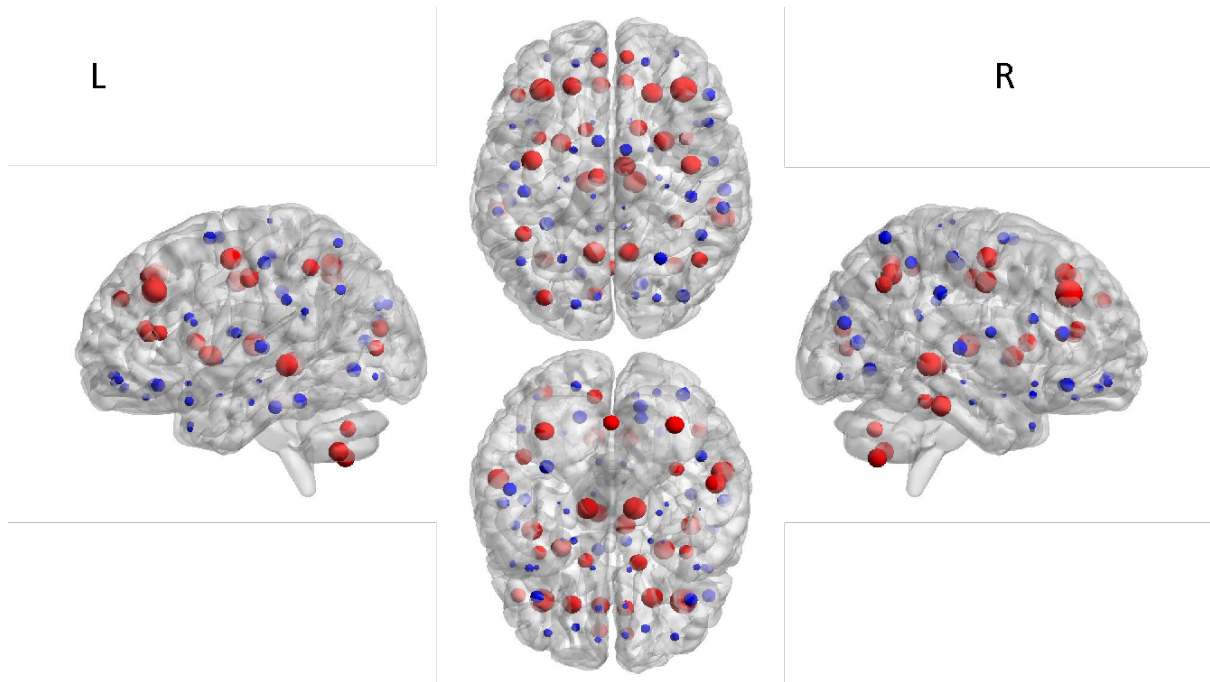


Figure 4.2. Distribution of core/periphery nodes common in CHD and control networks. In a network with a core-periphery organization core nodes (red) are well-connected to each other and nodes in the periphery (blue) are not well connected to one another. From left to right, lateral view of the left hemisphere, transverse view of both hemispheres (superior, inferior) and lateral view of the right hemisphere. Size of nodes represented by nodal strength. Images were generated using the BrainNet Viewer software (Xia et al. 2013).

Table 4.3. List of core (n=34) and peripheral nodes (n=59) common in CHD and control networks.

Core nodes		Peripheral nodes	
Precentral gyrus left & right	Middle temporal gyrus left & right	Orbitofrontal cortex (superior) left & right	Superior occipital gyrus left & right
Superior frontal gyrus (dorsal) left & right	Inferior temporal gyrus right	Orbitofrontal cortex (middle) left & right	Middle occipital gyrus right
Middle frontal gyrus left & right	Cerebellum left & right	Inferior frontal gyrus (opercular) left & right	Fusiform gyrus left
Inferior frontal gyrus (triangular) left	Vermis	Inferior frontal gyrus (triangular) right	Inferior occipital gyrus left & right
Superior frontal gyrus (medial) left & right		Orbitofrontal cortex (inferior) left & right	Postcentral gyrus left & right
Insula left & right		Rolandic operculum left & right	Superior parietal gyrus left & right
Anterior cingulate gyrus left & right		Supplementary motor area left & right	Inferior parietal lobule right
Median cingulate and paracingulate gyrus left & right		Olfactory left & right	Supramarginal gyrus left & right
Calcarine cortex left		Orbitofrontal cortex (medial) left & right	Angular gyrus left
Middle occipital gyrus left		Rectus gyrus left & right	Paracentral lobule left & right
Fusiform gyrus right		Posterior cingulate gyrus left & right	Pallidum left & right
Inferior parietal lobule left		Hippocampus left & right	Heschl gyrus left & right
Angular gyrus right		Parahippocampal gyrus left & right	Superior temporal gyrus left & right
Precuneus left & right		Amygdala left & right	Temporal pole (superior) left & right
Caudate left & right		Calcarine cortex right	Temporal pole (middle) left & right
Putamen left & right		Cuneus left & right	Inferior temporal gyrus left
Thalamus left & right		Lingual gyrus left & right	

We carried out a regional analysis in order to investigate whether core and/or peripheral (i.e. local) connections were affected in the CHD group. This was carried out by assessing group differences in nodal characteristics of core and peripheral structures and allowed us to determine whether nodes from either structures were affected as a consequence of CHD. Nodal efficiency of the core structure was significantly lower in CHD neonates compared to controls [MANCOVA: $F_{(5, 168)} = 4.03, p = 0.046$] (Fig. 3). Similarly, in the peripheral structure nodal efficiency was significantly lower in CHD neonates compared to controls [MANCOVA: $F_{(5, 168)} = 4.51, p = 0.035$] (Fig. 3). However, for both core and periphery average nodal efficiency, after removing the aforementioned outlier, statistical significance was lost. We found no difference in nodal strength in core and peripheral structures between groups.

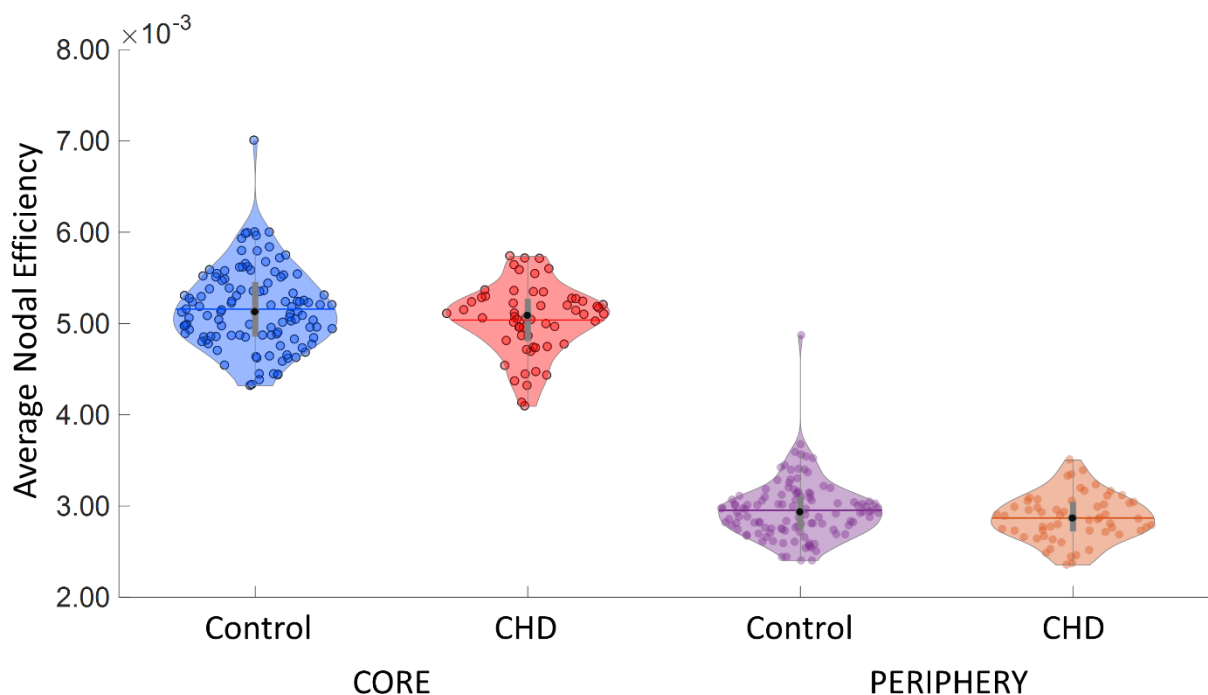


Figure 4.3. Average nodal efficiency of core and periphery nodes in CHD and control groups. Average nodal efficiency in CHD is significantly lower in core ($p = 0.046$) and periphery ($p = 0.035$). However, after removing outliers, no significant difference is found.

4.3.4 Subnetwork of brain regions with reduced connectivity in CHD

We further assessed whether specific sub-networks were affected in the CHD group using NBS. We found a single subnetwork comprising 23 nodes sharing 26 edges with reduced connectivity in CHD (Fig 4.4). This distributed network included connections between the vermis, bilateral hippocampus, thalamus, cerebellum, putamen, posterior cingulate gyrus, middle occipital gyrus, and left amygdala, inferior occipital gyrus, superior parietal gyrus, middle temporal gyrus, and right precentral gyrus, inferior parietal lobule and caudate.

This subnetwork comprised of 11 nodes situated in the right, and 11 nodes within the left hemisphere, as well as the vermis. Affected edges of the subnetwork included 9 right intra-hemispheric, 9 left intra-hemispheric, 6 inter-hemispheric connections, and 2 connecting to the vermis. We then assessed whether regions identified in the subnetwork belonged to either the core or periphery structure and assessed which connection type was most affected. Edges were defined as; core connections between core nodes, peripheral connections between peripheral nodes; and feeder connections between peripheral and core nodes. From the 23 nodes with reduced structural connectivity in infants with CHD, 13 were core nodes (out of a total of 34 core nodes, 38.23%), while 10 were peripheral nodes (out of a total of 59 peripheral nodes, 16.94%). Of the 26 edges with reduced connectivity in CHD, 10 (38.46%) were core, 10 (38.46%) were feeders and 6 (23.07%) were peripheral. We did not identify any subnetworks with increased connectivity in the CHD group compared with controls. Table 4.4 lists the nodes and edges comprising the disconnected sub-network in neonates with CHD and is represented in Figure 4.4.

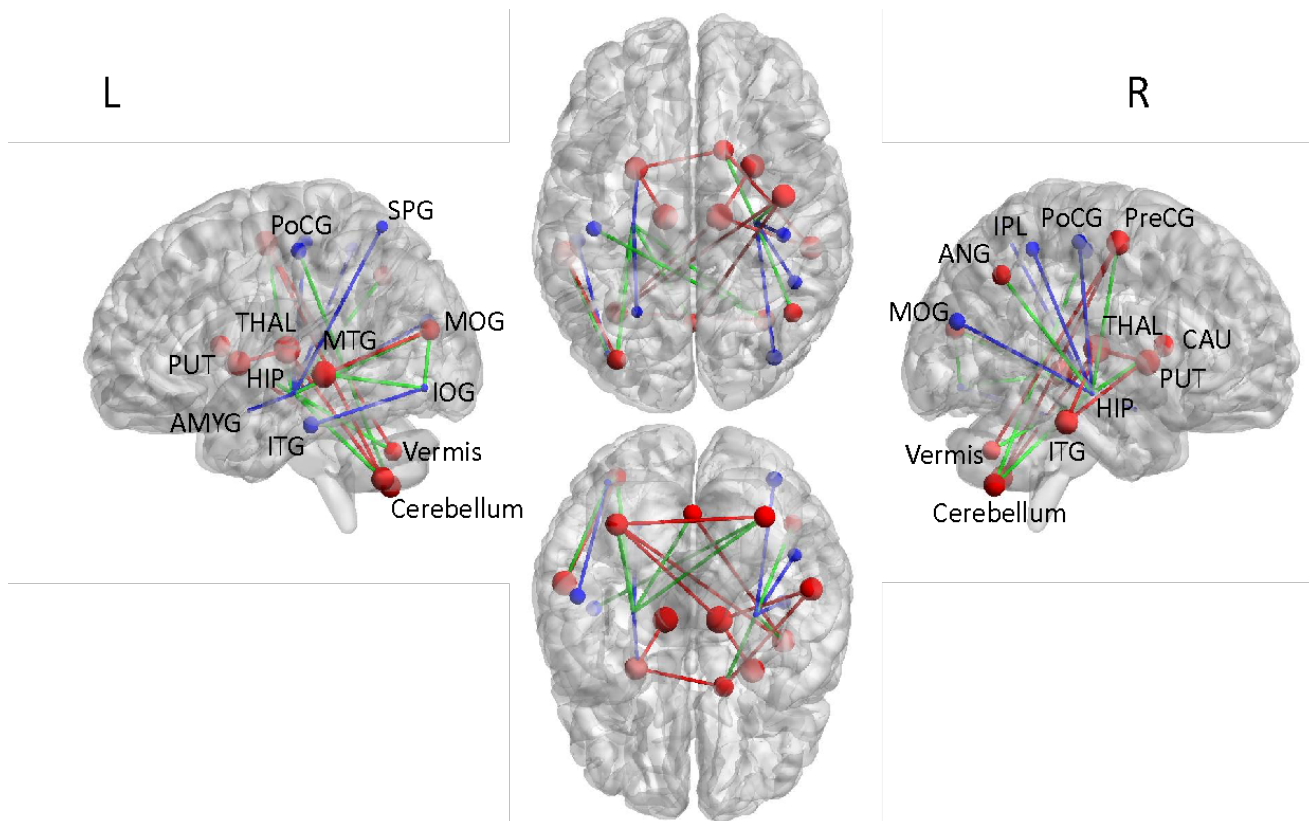


Figure 4.4. Illustration of NBS-derived subnetwork with reduced structural connectivity in CHD neonates compared to controls. From left to right, lateral view of the left hemisphere, transverse view of both hemispheres (superior, inferior) and lateral view of the right hemisphere. Each dot and line represents a node and edge in which structural connectivity is reduced in CHD neonates. Red and blue regions correspond to nodes from the core and peripheral structure, respectively. Size of nodes represented by nodal strength. Edge colours correspond to core-core edges in red (core), peripheral-peripheral edges in blue (peripheral) and core-peripheral edges in green (feeder). Abbreviations: PreCG, precentral gyrus; HIP, hippocampus; AMYG, amygdala; MOG, middle occipital gyrus; IOG, inferior occipital gyrus; PoCG, postcentral gyrus; SPG, superior parietal gyrus; IPL, inferior parietal lobule; ANG, angular gyrus; CAU, caudate; PUT, putamen; THAL, thalamus; MTG, middle temporal gyrus; ITG, inferior temporal gyrus. Images were generated using the BrainNet Viewer software (Xia et al. 2013).

Table 4.4. Subnetwork with reduced structural connectivity in CHD neonates.

#	Node	Node network	#	Edge	Edge type	t-value
1	Precentral gyrus right	Core	1	Hippocampus left–Middle occipital gyrus left	Feeder	3.11
2	Middle occipital gyrus left	Core	2	Precentral gyrus right–Hippocampus right	Feeder	3.12
3	Angular gyrus right	Core	3	Caudate right–Inferior temporal gyrus right	Core	3.13
4	Caudate right	Core	4	Precentral gyrus right–Cerebellum left	Core	3.13
5	Putamen left	Core	5	Middle occipital gyrus left–Middle temporal gyrus left	Core	3.15
6	Putamen right	Core	6	Middle occipital gyrus left–Inferior occipital gyrus left	Feeder	3.17
7	Thalamus left	Core	7	Hippocampus left–Superior parietal gyrus left	Peripheral	3.17
8	Thalamus right	Core	8	Inferior occipital gyrus left–Middle temporal gyrus left	Feeder	3.29
9	Middle temporal gyrus left	Core	9	Hippocampus right –Inferior parietal lobule right	Peripheral	3.31
10	Inferior temporal gyrus right	Core	10	Hippocampus left–Amygdala left	Peripheral	3.34
11	Cerebellum left	Core	11	Hippocampus left–Cerebellum left	Feeder	3.36
12	Cerebellum right	Core	12	Hippocampus right–Middle occipital gyrus right	Peripheral	3.4
13	Vermis	Core	13	Postcentral gyrus left–Cerebellum right	Feeder	3.43
14	Hippocampus left	Peripheral	14	Thalamus right–Cerebellum left	Core	3.51
15	Hippocampus right	Peripheral	15	Putamen right–Thalamus right	Core	3.52
16	Amygdala left	Peripheral	16	Thalamus right–Inferior temporal gyrus right	Core	3.52
17	Middle occipital gyrus right	Peripheral	17	Hippocampus right–Angular gyrus right	Feeder	3.58

18	Inferior occipital gyrus left	Peripheral	18	Precentral gyrus right–Vermis	Core	3.70
19	Postcentral gyrus left	Peripheral	19	Inferior occipital gyrus left–Inferior temporal gyrus left	Peripheral	3.72
20	Postcentral gyrus right	Peripheral	20	Hippocampus right–Postcentral gyrus right	Peripheral	3.77
21	Superior parietal gyrus left	Peripheral	21	Putamen left–Thalamus left	Core	3.77
22	Inferior parietal lobule right	Peripheral	22	Caudate right–Putamen left	Core	3.81
23	Inferior temporal gyrus left	Peripheral	23	Cerebellum left–Cerebellum right	Core	3.81
			24	Hippocampus left–Vermis	Feeder	3.93
			25	Hippocampus left–Cerebellum right	Feeder	3.97
			26	Hippocampus right–Caudate right	Feeder	4

4.4. Discussion

This study provides evidence for altered structural connectivity in a cortico-striatal-thalamic sub-network in newborns with CHD prior to surgery.

Human brain development is characterised by rapid changes in brain structure due to myelination, synaptogenesis and dendritic arborisation (Kostovic & Jovanov-Milosevic, 2006). Studies assessing structural brain organisation have revealed that the brain tends to be more segregated in the fetal (Song et al., 2017) and preterm brain (Batalle et al., 2017; Zhao et al., 2019; van den Heuvel et al., 2015; Ball et al., 2014; Tymofiyeva et al., 2012; Brown et al., 2014), improving in integration capacity during the first years of life (Hagmann et al. 2010, Dennis et al., 2013; Huang et al., 2015; Tymofiyeva et al., 2013; Khundrakpam et al., 2013; Fan et al., 2011; Yap et al., 2011) due to the development of long-range association fibres which support higher cognitive functions (Huang & Vasung, 2014, Bullmore & Sporns, 2012).

In infants with CHD pre-operatively, a recent diffusion tensor imaging (DTI)-based connectivity study identified reorganisation of global network topology of structural brain networks (Schmithorst et al., 2018), reporting disruptions to cost and global efficiency (integration). However, in our population we found that newborns with CHD had preserved network infrastructure and integration, while disruption in segregation had a small effect size, and was not statistically significant after the removal of outliers. To further understand the discrepancy with previously reported differences, we carried out a regional analysis to assess whether there were subtle alterations to core-peripheral connectivity. Core or rich club regions are brain hubs that form the backbone of the brain network (van den Heuvel et al., 2012; van den Heuvel & Sporns, 2013) allowing integration of specialized cortical regions (Senden et al., 2014). Our analysis revealed core regions that included the insula, precuneus, superior frontal cortex as well as subcortical thalamus and putamen, consistent with previous descriptions of rich club regions described in adults (van den Heuvel & Sporns, 2011) and neonates (Ball et al., 2014). However, similar to our global network results, we found only a small effect associated with CHD, which did not reach statistical significance after removing outliers.

Notwithstanding, we did find altered connectivity at the sub-network level using NBS, revealing one sub-network of structural connections in which connectivity strengths were significantly reduced in neonates with CHD compared to controls. This distributed network comprised connections predominantly in the cortico-striatal-thalamic network, involving regions in the basal ganglia, amygdala, hippocampus, cerebellum, vermis, and cortical regions in the temporal and parieto-occipital lobe. Our structural findings correspond with a recent resting state fMRI study of pre-operative CHD newborns which identified one subnetwork with reduced functional connectivity involving the putamen,

caudate and thalamus (De Asis-Cruz et al., 2018). The thalamus is an important site for the integration of networks supporting the ability to modulate behaviour (Haber & Calzavara, 2009), while the striatum, the main input station of the basal ganglia, is associated with the regulation of motor (Lehericy et al., 2005) and cognitive functioning (van Rooij et al., 2015). Disruptions to cortico-thalamic circuits have been previously reported in children with ADHD (Castellanos, 1997; Casey et al., 2007), and dysfunction of the cortico-striatal-thalamic network has been described in Parkinson's disease patients (Hacker et al., 2012) and cognitive disorders including, bipolar disorder (Chen et al., 2006) and Tourette syndrome (Makki et al., 2009) and in school age children born extremely prematurely with intrauterine growth restriction (IUGR) (Fischi-Gomez et al., 2015; Eixarch et al., 2016). Moreover, recent reports have documented subcortical morphological abnormalities in CHD patients across their lifespan (Wong et al., 2017; von Rhein et al., 2014; von Rhein et al., 2015; Owen et al., 2014; Ortinau et al., 2012). DTI and magnetic resonance spectroscopy (MRS) evaluation of term born newborns with CHD preoperatively revealed reduced fractional anisotropy (FA) in subcortical white matter tracts, and increased average diffusivity (AD), decreased ratio of NAA to choline and increased lactate to choline ratio in the basal ganglia and thalamus (Miller et al., 2007). Additionally, reduced volumes of subcortical structures have been reported in fetuses with hypoplastic left heart syndrome (HLHS) (Clouchoux et al. 2013) and in newborns (Owen et al., 2014), and are associated with impaired cognitive abilities in adolescents with CHD (von Rhein et al., 2014).

We also observed reduced structural connectivity in a number of regions that are important for memory, cognition, executive function and attention. Specifically, we observed reduced structural connectivity in the hippocampus and amygdala in infants with CHD,

structures that are important in memory (Scoville & Milner, 1957; Tulving, 2002), cognition (Squire, 2004), and emotion regulation (LeDoux, 1996), respectively. We also found reduced structural connectivity in the precentral gyrus. Reduced FA in the precentral white matter has previously been shown to correlate with deficits in executive function and inattention/hyperactivity symptoms in adolescents with CHD (Rollins et al., 2014). We identified reduced structural connectivity in the cerebellum and vermis, regions that are crucial for motor control, coordination (Morton et al., 2004) and evidence suggests that the cerebellum may also play an important role in cognitive processing and emotional control (Schmahmann & Caplan, 2006).

Of note, core regions were affected more than peripheral in the subnetwork with reduced structural connectivity in infants with CHD. Additionally, we showed decreased feeder connections with core regions of the right precentral gyrus, angular gyrus, and caudate, left middle occipital and temporal gyrus and bilateral cerebellum. Core components play a key role in the efficient integration of information processing among distant brain regions, therefore disruptions to core connectivity have a widespread effect on information transfer in the brain (van den Heuvel & Sporns, 2011; van den Heuvel et al., 2012). Although it is widely believed that damage to core connections severely impacts the global efficiency to the network (van den Heuvel & Sporns, 2011), we did not find such alterations in global efficiency between CHD and matched controls. While studies of preterm infants suggest core connections are relatively preserved (Fischi-Gomez et al., 2016; Karolis et al., 2016; Bataille et al., 2017), our findings are consistent with a previous functional connectivity study in infants with CHD which found that rich club regions were primarily affected in a subnetwork of nodes with reduced functional connectivity (De Asis-Cruz et al., 2018). Our findings suggest core connections in regions associated with important aspects of

behaviour including cognition, behaviour modulation, motor control, and emotion regulation, are more vulnerable in newborns with CHD.

Our study has some limitations. Our CHD cohort is heterogeneous. Infants had a wide range of complex CHD which may affect structural brain development and subsequent network topology differently. Our sample size was not large enough to assess differences in network topology related to CHD types. Further studies with larger sample sizes are needed to elucidate whether changes in structural network topology are associated with different CHD types. A common core/periphery structure was defined as nodes belonging to the core/periphery partitioning in 90% of subjects. However, it has been shown that newborns with CHD have fewer rich club nodes compared to controls (De-Asis Cruz et al., 2018). In this case assessing the core/periphery partitioning for the whole group may have influenced our findings. In addition, neurodevelopmental outcome data are not available for this cohort and so we were not able to assess the relationship between our findings and subsequent outcome. However, developmental follow-up of our cohort is currently underway and we will assess this relationship in future studies.

4.5. Conclusion

Using network-based statistics we reveal altered structural connectivity in infants with CHD prior to surgery compared to healthy control infants. We found one subnetwork with reduced structural connectivity in newborns with CHD predominantly affecting core nodes belonging to the cortico-striatal-thalamic network suggesting vulnerability of core connectivity in CHD. Alterations in the sub-network topology of structural connectivity could explain, at least in part, the neurodevelopmental sequelae associated with CHD.

Chapter 5: Relationship between resting-state fMRI functional connectivity with motor and language outcome after perinatal brain injury – A systematic review

Abstract: Perinatal brain injury (PBI) is a significant cause of adverse outcomes. The objective of this systematic review was to identify patterns of altered brain function, quantified using FC changes in rs-fMRI data, that were associated with motor and language outcomes in individuals with a history of PBI. A total of 10 studies were included in the systematic review, representing 260 individuals with a history of PBI. Motor and language outcomes were measured at time points ranging from 4 months to 29 years 1 month. Relations between FC and motor measures revealed increased intra-hemispheric FC, reduced inter-hemispheric FC and impaired lateralization of motor-related brain regions associated with motor outcomes. Altered FC within sensorimotor, visual, cerebellum and frontoparietal networks, and between sensorimotor, visual, auditory and higher-order networks, including cerebellum, frontoparietal, default-mode, salience, self-referential and attentional networks were also associated with motor outcomes. In studies assessing the relationship between rs-fMRI and language outcome, reduced intra-hemispheric FC, increased inter-hemispheric FC and right-hemisphere lateralization of language-related brain regions correlated with language outcomes. Evidence from this systematic review suggests a possible association between diaschisis and motor and language impairments in individuals after PBI. These findings support the need to explore the contributions of additional brain regions functionally connected but remote from the primary lesioned brain area for targeted treatments and appropriate intervention, though more studies with increased standardization across neuroimaging and neurodevelopmental assessments are needed.

This chapter is based upon: Ní Bhroin M, Molloy EJ, Bokde ALW. Relationship between resting-state fMRI functional connectivity with motor and language outcome after perinatal brain injury - A systematic review. *Eur J Paediatr Neurol.* 2021 Jul;33:36-49. doi: 10.1016/j.ejpn.2021.05.007.

5.1 Introduction

Perinatal brain injury (PBI) due to hypoxia-ischaemia, cerebral infarction, or haemorrhage are leading causes of severe motor deficits such as cerebral palsy, and language, visual and behavioural deficits (Ganesan et al., 2000; Edwards et al., 2010). Although these conditions are of different origin, they all disrupt the normal developmental trajectory of the brain, presenting considerable risk for motor and language development.

Prediction of outcome after perinatal brain injury is difficult and has been increasingly facilitated by magnetic resonance imaging (MRI) to provide information regarding the location and severity of brain lesions. In newborns with hypoxia-ischaemia, basal ganglia/thalamic (BGT) and watershed (WS) patterns of brain injury relate with motor and language impairments (Barkovich et al., 1998; Rutherford et al., 2010; de Vries et al., 2010), and in preterm infants, white matter injury (WMI) in the frontal lobe are associated with adverse language outcome (Guo et al., 2017), and punctate white matter lesions (PWML) with motor outcome (Tusor et al., 2017). While in infants with perinatal stroke, involvement of cerebral cortex, basal ganglia and posterior internal capsule is associated with the development of cerebral palsy (Boardman et al., 2005; Kirton et al., 2013; Dinomais et al., 2015).

Resting state functional magnetic resonance imaging (rs-fMRI) may offer additional predictive utility by assessing the impact of perinatal brain lesions on functional connectivity in brain regions adjacent to and remote from the primary site of injury. rs-fMRI measures the temporal correlation of low frequency (<0.1Hz) fluctuations in blood oxygen level-dependent (BOLD) signal across the brain while the subject is at rest (Biswal et al., 1995). Using rs-fMRI, a number of resting state networks (RSNs) involved in

primary functions (sensorimotor, auditory, visual) and higher-order functions (default-mode, salience, executive control and attentional) have been identified (Damoiseaux et al., 2006). Several studies have assessed the emergence of resting-state networks in term and preterm-born infants (Fransson et al., 2007; De Asis-Cruz et al., 2015; Gao et al., 2011; Doria et al., 2010) and developmental trajectories of RSNs during typical development (Doria et al., 2010). These studies have established primary functional networks are established by term-equivalent age (TEA) in both term and preterm-born infants, followed by higher order networks, in parallel with structural brain development and the maturational sequence of cognitive, language and motor abilities¹⁶.

Studies using rs-fMRI have identified impaired functional network topology in infants with perinatal brain lesions (Tusor et al., 2014, Li et al., 2019). Infants with severe neonatal encephalopathy (NE) exhibited decreased local efficiency, clustering coefficient, and reduced nodal efficiency in left supramarginal gyrus, bilateral superior temporal gyrus, and right middle temporal gyrus (Li et al., 2019). Additionally, infants with NE with an unfavourable outcome had significantly lower functional connectivity scores within auditory and motor networks compared to infants with NE with a favourable outcome (Tusor et al., 2014). In addition, brain injury sustained during the perinatal period may adversely affect subsequent functional network development by interfering with myelination and synaptogenesis. Disrupted functional connectivity has provided insight into many neurological and psychiatric conditions (Zhang et al., 2010) and populations at risk of neurodevelopmental impairments including infants with intrauterine growth restriction (IUGR) (Batalle et al., 2016), children with attention deficit hyperactivity disorder (ADHD) (Wang et al., 2009) and Tourette syndrome (Church et al., 2009), and adolescents with autism (Redcay et al., 2013). We therefore performed this systematic review to identify differences in functional connectivity between typically developing

individuals and individuals with a history of perinatally acquired brain lesions, and examine the relationship between altered functional connectivity with motor and language outcomes in affected individuals.

5.2 Materials and Methods

The systematic review was performed following guidelines from the Meta-analysis of Observational Studies in Epidemiology (MOOSE) (Stroup et al., 2000) and Preferred Reporting Items for Systematic Reviews and Meta-Analyses the (PRISMA) statements (Hutton et al., 2015). Relevant papers were selected using the PRISMA flowchart (Figure 5.1).

5.2.1 Search strategy

The search was conducted by the first author of this article (MNB) using the bibliographical databases PubMed, Medline, and Embase in November 2019 and updated on March 2021 using combinations of the key terms: “perinatal/neonatal brain injury” or “neonatal/ hypoxic ischaemic encephalopathy” or “perinatal/neonatal stroke” or “cerebral palsy” AND “resting-state fMRI” or “functional connectivity” or “functional network connectivity” AND “neurodevelopmental outcome” or “motor outcome” or “language outcome”. We also searched the reference list of related studies and reviews to include other studies that might be eligible for review.

5.2.2 Study selection

Studies were included based on the following inclusion criteria: (1) participants with a history of perinatal brain lesions confirmed with MRI, (2) a control group comprised of healthy controls was present (3) neurodevelopmental outcome was assessed, and (4) rs-fMRI was obtained and its relationship with neurodevelopmental outcome was analysed

(can include task-based fMRI studies if rs-fMRI is identifiable and can be extracted). Cross-sectional, cohort, and case-control study designs were included in the search. Studies were excluded if there was insufficient data on lesion characteristics of the participants, they did not assess the relationship between rs-fMRI and neurodevelopmental outcome, animal models were used, or studies were not published in English. Rehabilitation studies, reviews, case reports, and unpublished research were also excluded. The selection of studies was based on the screening of titles and abstracts, followed by the screening of full texts of remaining reports. Selected studies were assessed for quality and bias with the application of the Strengthening the Reporting of Observational Studies in Epidemiology (STROBE)(von Elm et al., 2008).

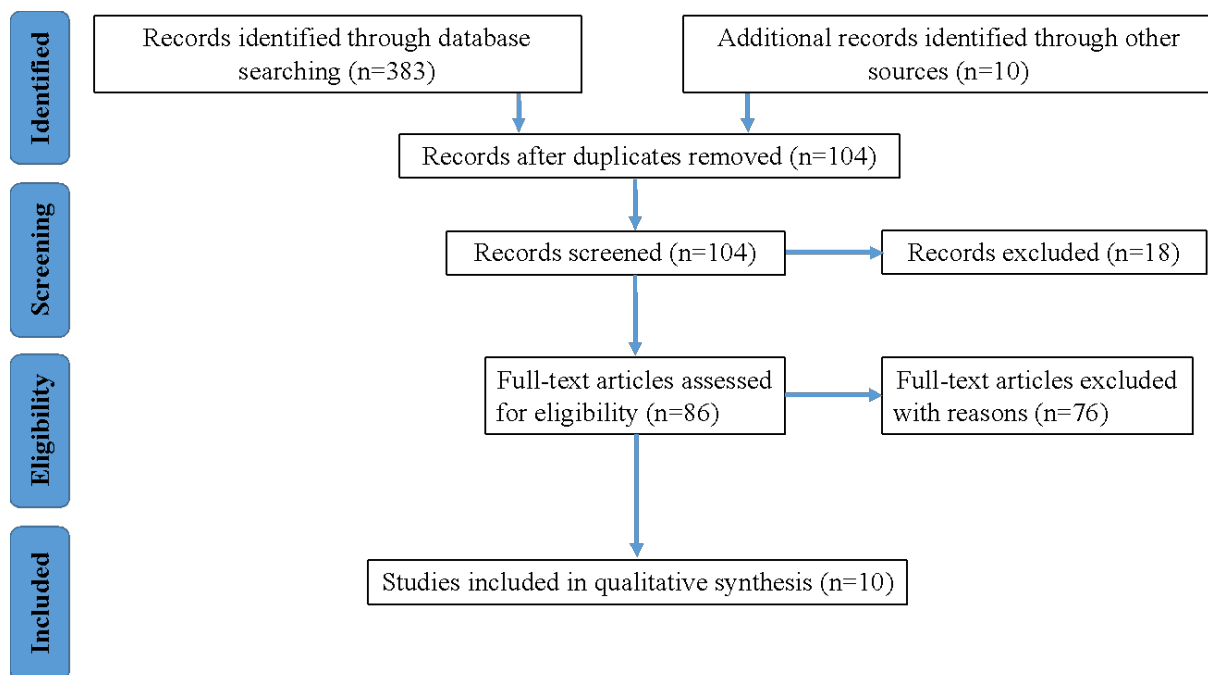


Figure 5.1 Search strategy and selected articles

* Two^{31,32} and three studies^{27-28,35} recruited from the same database.

5.2.3 Data extraction

One reviewer (MNB) extracted data from the included studies. Data extracted from the studies included: clinical definition, population characteristics, neuroimaging details including the neuroimaging method used to describe brain lesions, lesion characteristics,

age at rs-fMRI scan, age at time of outcome assessment, outcome assessment method used and outcome of the assessment, rs-fMRI findings and reported relationships between FC of brain regions and RSNs that showed a statistically significant relationship with outcome.

5.3 Results

5.3.1 Study selection

The search yielded 383 articles, which after the removal of duplicates, left 104 individual studies. The titles and abstracts of these records were screened for their eligibility, resulting in an initial selection of 86 papers. The full manuscript of these papers was further assessed, and 10 studies were included in our final list for review. These studies were further subdivided according to whether the relationship between rs-fMRI with motor (n=7) or language (n=3) outcome was assessed. These studies all met the guidelines outlined in the STROBE statement regarding quality and bias (Table 5.4).

The 10 studies included in this systematic review comprised 260 individuals with a history of perinatal brain injury (145 [55%] males) and 290 controls (159 [55%] males), with results summarised in Table 6.2. Of the studies assessing motor outcome, one study assessed whether rs-fMRI at term-equivalent age (TEA) would be predictive of motor impairments at follow-up at 4 and 8 months of age (Linke et al., 2018), and the remaining 6 studies investigated the relationship between rs-fMRI and motor functioning cross-sectionally in individuals between 3 and 19 years of age (Saunders et al., 2019; Woodward et al., 2019; Linke et al., 2018; Simon-Martinez et al., 2019; Qin et al., 2018; Qin et al., 2019; Wheelock et al., 2018). 3 studies also assessed the association between rs-fMRI and language performance at the same time-point in individuals between 3 years 6 months and 29 years 1 month (Dick et al., 2013; Carlson et al., 2019; Francois et al., 2019).

5.3.2 Lesion location

The location of lesions was reported as occurring in left or right-hemispheres, and/or in cortical or subcortical regions. Studies assessing the relationship between resting-state fMRI and motor outcome identified lesions in the basal ganglia (Saunders. et al., 2019; Qin et al., 2018; Qin et al., 2019), thalamus (Qin et al., 2018; Qin et al., 2019), internal capsule (Woodward et al., 2019), white matter (Linke et al., 2018; Simon-Martinez et al., 2019; Qin et al., 2018; Wheelock et al., 2018), grey matter (Linke et al., 2018; Qin et al., 2018; Qin ET AL., 2019), and IVH (Linke et al., 2018), while studies assessing the relationship between resting-state fMRI and language outcome reported lesions in the thalamus (Dick et al., 2013), white matter (Dick et al., 2013), temporo-parietal junction (Dick et al., 2013), PVL (Dick et al., 2013), language related brain regions (Francois et al., 2019), and predominantly affecting the left hemisphere (Carlson et al., 2019; Francois et al., 2018).

5.3.3 Neurodevelopmental assessments

A total of 19 distinctive neurodevelopmental outcome assessment instruments were applied. Motor outcome was assessed using Assessment of Daily Living (ADL) (Qin et al., 2018; Qin et al., 2019), Assisting Hand Assessment (AHA) (Saunders et al., 2019; Woodward et al., 2019), Alberta Infant Motor Scale (AIMs) (Linke et al., 2018), Gross Motor Functional Classification System (GMFCS) (Qin et al., 2018; Qin et al., 2019; Wheelock et al., 2018), Infant Neurological Battery (INFANIB) (Linke et al., 2018), Movement ABC for children (MABC) (Wheelock et al., 2018), Jebsen-Taylor Hand Function Test (JTHFT) (Simon-Martinez et al., 2019), Melbourne Assessment of Unilateral Upper limb Function (MA) (Saunders et al., 2019; Woodward et al., 2019), Manual Ability Classification System (MACS) (Simon-Martinez et al., 2019), Test of Infant Motor Performance (TIMP) (Linke et al., 2018). Language outcome was assessed

using Clinical evaluation of language fundamentals (CELF) (Dick et al., 2013), Children's memory scale (CMS) (Carlson et al., 2019), California Verbal learning test (CVLT) (Carlson et al., 2019), Continuous Visual Memory Test (CVMT) (Carlson et al., 2019), mean length of utterance (MLU) (Francois et al., 2019), A Developmental NEUROPSYchological Assessment (NEPSY) (Carlson et al., 2019; Francois et al., 2019), Peabody picture vocabulary test (PPVT) (Francois et al., 2019). Lastly, cognitive outcome was assessed using Wechsler Adult Intelligence Scale (WAIS) (Carlson et al., 2019), Wechsler Intelligence Scale for Children (WISC) (Carlson et al., 2019), Woodcock-Johnson Tests of Cognitive Abilities (WJ) (Carlson et al., 2019). Follow-up length varied between 4 months and 29 years 1 month.

5.3.4 ROI-based functional connectivity analysis and motor outcome

Overall, individuals after perinatal brain lesions showed widespread atypical functional connectivity compared with typically developing peers. These alterations in brain functional organization were related to motor and language abilities. In studies employing a cross sectional design and using an ROI-based correlation analysis approach to assess the relationship with motor outcome, increased intra-hemispheric functional connectivity (Woodward et al., 2019; Linke et al., 2018; Simon-Martinez et al., 2019), reduced inter-hemispheric functional connectivity³² and impaired lateralization (Qin et al., 2019) of motor-related brain regions were found to be associated with motor outcomes, while one study did not report any significant results (Saunders et al., 2019). Specifically, increased intra-hemispheric functional connectivity from the primary motor cortex to supplementary motor area negatively correlated with AHA (Woodward et al., 2019), and to parietal operculum and supramarginal gyrus negatively correlated with JTHFT scores (Simon-Martinez et al., 2019). While reduced inter-hemispheric functional connectivity of the calcarine cortex positively correlated with ADL scores and negatively correlated with

GMFCS scores (Qin et al., 2019). In addition, increased left-hemisphere lateralization of the supplementary motor area positively correlated with GMFCS scores (Qin et al., 2019) and reduced left-hemisphere lateralization of inferior parietal lobule negatively correlated with ADL scores (Qin et al., 2019).

5.3.5 Network based analysis and motor outcome

In studies employing a cross sectional design to investigate the association between functional network topology and motor outcome, disrupted within and between network functional connectivity was associated with motor outcomes. Reduced functional connectivity within the cerebellum and between primary-extrastriate visual, anterior default mode-self-referential, and posterior default mode-salience networks negatively correlated with GMFCS scores (Qin et al., 2019) and reduced functional connectivity between right frontoparietal-primary visual, right frontoparietal-cerebellum, and anterior default mode-self-referential networks positively correlated with ADL scores (Qin et al., 2019). Additionally, children with perinatal brain injury born preterm exhibited weaker associations between basal ganglia-motor network and balance scores, salience-motor network and aiming and catching scores, and between thalamus-motor network and MABC total scores, aiming and catching scores, and manual dexterity scores, when compared with term-born controls (Wheelock et al., 2018). Children with perinatal brain injury born preterm also demonstrated stronger associations within frontoparietal control and cerebellar networks and MABC total scores, default mode network and balance subscale scores, and between basal ganglia-auditory networks and aiming and catching subscale scores, and dorsal attention-default mode networks and balance subscale scores compared with term-born controls (Wheelock et al., 2018).

One study investigated whether the functional network topology measured at TEA would be predictive of later motor outcomes (Linke et al., 2018). They found disruption to functional connectivity was positively associated with AIMS at 4 months and AIMS and INFANIB at 8 months, with disruption to functional connectivity within sensorimotor and frontoparietal networks and between sensorimotor-default mode, sensorimotor-ventral attention, and between default mode-visual networks contributing most to the correlation with AIMS and INFANIB at 8 months (Linke et al., 2018).

5.3.6 ROI-based functional connectivity analysis and language outcome

In studies employing a cross sectional design and using an ROI-based correlation analysis approach to assess the relationship with language outcome, statistically significant associations between reduced intra-hemispheric, increased inter-hemispheric and right-hemisphere lateralization of language-related brain regions with language functioning was identified. Reduced intra-hemispheric functional connectivity between left inferior frontal gyrus and superior temporal gyrus was positively associated with WJ scores (Carlson et al., 2019). Additionally, increased inter-hemispheric functional connectivity of the superior temporal gyrus positively correlated with CELF (Dick et al., 2013) and CMS (Carlson et al., 2019) scores, and increased functional connectivity of the angular gyrus negatively correlated with CELF scores (Dick et al., 2013). Furthermore, increased right-hemisphere lateralization of superior temporal and inferior frontal gyrus was positively associated with MLU scores (Francois et al., 2019).

Studies reporting disrupted functional connectivity between brain regions associated with motor and language outcomes in individuals after perinatal brain lesions were visualised using BrainNet Viewer software (www.nitrc.org/projects/bnv) (Xia et al., 2013) (Fig. 6.2). Specifically, spatial coordinates for each brain region was obtained using the anatomical

automatic labelling (AAL) atlas (Tzourio-Mazoyer et al., 2002). Next, a figure demonstrating increased (red) or decreased (blue) intra- and inter-hemispheric FC, and right/left hemisphere lateralization (functional dominance of one hemisphere over the other) of brain regions associated with motor and language outcomes was generated (Fig. 6.2). Studies reporting altered functional connectivity within and between resting-state networks (RSNs) associated with motor outcomes is summarised in Table 5.3.

Table 5.1. rs-fMRI studies assessing motor and language outcomes following perinatal brain injury (PBI).

Article	Clinical definition	Sample characteristics	Neuroimaging details	Lesion location	Outcome	Analytic method	rs-fMRI findings	Brain behaviour relationship
Motor outcome								
Saunders et al., 2018	AIS, PVI – Hemiparetic cerebral palsy	20 PBI, 11/9 M/F, AIS – n=10 14.7 (4.1) [6-19] PVI – n=10 13.5 (5.1) [9-19] 18 controls, 7/11 M/F, 15.3 (5.1) [7.0–19.0] Mean (SD) [range] years	3T MRI 32-channel head coil T1-weighted images were used to assess injury rs-scan details Eyes open TR/TE = 2,000/30 ms, ~5–6 min)	AIS- Basal ganglia - 7 70% left-sided lesion PVI- Basal ganglia - 1 50% left-sided lesion	AHA MA AHA: AIS = 67.3 ± 20.4 PVI = 72.0 ± 14.5 MA: AIS = 80.9 ± 21.0 PVI = 88.4 ± 9.7 Mean ± SD	ROI analysis – primary motor cortex (M1) lesioned and non-lesioned hemisphere Lateralization of primary motor cortex = (mean Z-score ROI 1 – mean Z-score ROI 2)/(mean Z-score ROI 1 + mean Z-score ROI 2) * strength of brain activity within an ROI in one hemisphere is compared with the strength of activity in a homologous ROI in the opposite hemisphere.	AIS > PVI, Controls M1 lesioned hemisphere– anterior supramarginal gyrus lesioned hemisphere AIS < PVI, Controls M1 lesioned hemisphere– precentral and postcentral gyri in lesioned and non-lesioned hemisphere AIS < Controls M1 lesioned hemisphere– supplementary motor area	No association between lateralization of primary motor cortex with motor outcome.

							<p>AIS > PVI, Controls M1 non-lesioned hemisphere–supplementary motor area</p> <p>AIS < PVI, Controls M1 non-lesioned hemisphere–postcentral gyrus lesioned hemisphere</p> <p>PVI < Controls M1 non-lesioned hemisphere–supplementary motor area</p> <p>AIS < Control PVI < Control Lateralization from lesioned M1</p> <p>AIS < Control Lateralization from non-lesioned M1</p>	
--	--	--	--	--	--	--	--	--

Woodward et al., 2019	PVI – unilateral cerebral palsy	15 PVI, 9/6 M/F 11.3 (9.1-14.5) 21 Controls, 11/10 M/F, 12.6 (9.5-15.5) Median (IQR) years	3T MRI 32-channel head coil. T1-weighted images were used to assess injury rs-scan details Eyes open TR/TE = 2000/30 ms.	Left posterior frontal cortex - 1 Right frontal cortex - 4 Left frontal cortex - 4 Right interal capsule - 1 Left interal capsule - 1 Left frontoparietal - 3 Right frontoparietal - 1	AHA MA AHA: 73.14 ± 15.85 MA: 87.96 ± 10.58 Mean ± SD	ROI analysis – 5 regions left and right primary motor cortices (precentral gyri), left and right primary somatosensory cortices (postcentral gyri), left and right supplementary motor areas, and left and right thalamus, non-lesioned anterior temporal pole.	PVI < Controls Left thalamus–right thalamus	Contralesional primary motor cortex– contralesional supplementary motor area → negatively associated with AHA
Linke et al., 2018	Stroke, NE, IVH, Seizures	53 PVI, 40/13 M/F, 29 [25-41], Median [range] weeks *Outcome assessed at 4 and 8 months FC compared with normative connectivity pattern between the same ROIs	1.5T MRI T1- and T2-weighted images were used to assess injury rs-scan details Sedated natural sleep TR/TE = 1920/60ms, Four 7-minute runs	White matter injury - 37 Grey matter injury - 37 No injury - 20	AIMS INFANIB TIMP NA	Whole brain analysis using 28 ROIs compared with 14 adults. The similarity of each infants FC to the adults gave a measure of disruption to FC. Assessed which of the 7 RSN (language,	Auditory networks spatially less similar to the auditory network from healthy adults than other networks	Disruption to FC → positively associated with AIMS at 4 months Disruption to FC → positively associated with AIMS, INFANIB at 8 months Disruption to FC within sensorimotor & frontoparietal

		obtained from a group of healthy 14 adults.	Adult fMRI data similarly comprised two 7-minute functional EPI runs (Siemens 3T Prisma, TR/TE=686/30 ms)			sensorimotor, visual, default mode, dorsal attention, ventral attention, frontoparietal) drove correlation between disruption to FC and outcome assessed by within and between network connectivity		networks → positively associated with AIMS, INFANIB at 8 months Disruption to FC between sensorimotor–default-mode, sensorimotor–ventral attention, default-mode–visual → positively associated with AIMS, INFANIB at 8 months
Simon-Martinez et al., 2019	uCP	24 PBI, 9/15 M/F 9 Contralateral CST wiring, 2/7 M/F, 14.54 (4.18) 6 Bilateral CST, 3/3 M/F, 10.88 (3.41) 9 Ipsilateral CST,	3T MRI 32-channel T1-MPRAGE images were used to assess injury rs-scan details Awake TR/TE = 1700/33ms 7 min	PWML	MACS JTHFT MACS levels I = 8 II = 11 III = 5 JTHFT - NA	ROI analysis – primary motor cortex (M1) to bilateral primary sensory cortex, bilateral dorsal and ventral premotor cortex; and the supplementary motor cortex. (i) intra-hemispheric FC of M1 with the other ROIs within each	Contralateral CST > Ipsilateral CST, control Intra-hemispheric FC M1–dorsal premotor cortex Bilateral and ipsilateral CST > Control M1-ventral premotor cortex *not survive	Contralesional primary motor cortex – contralesional parietal operculum and supramarginal gyrus → higher FC predicted poorer hand dexterity - JTHFT

		<p>4/5 M/F, 13.36 (5.11)</p> <p>*CST – connects thalamus to motor cortex</p> <p>60 Controls, 46/14 M/F, 14.54 (4.80)</p> <p>Mean (SD) years</p>				<p>hemisphere (ii) inter- hemispheric FC from M1 to other ROIs (iii) inter- hemispheric FC between M1-M1.</p> <p>Calculated Laterality index = (mean Z-score ROI 1 – mean Z-score ROI 2)/(mean Z- score ROI 1 + mean Z-score ROI 2)</p> <p>Exploratory seed- to-voxel FC analysis to identify FC of M1 to other brain regions not included in ROI- ROI approach</p>	<p>multiple comparison correction</p> <p>uCP < Control non-dominant M1– both occipital lobes</p> <p>uCP > Control non-dominant M1– ipsilateral temporal pole and insular cortex</p> <p>All CST wiring groups < Control non-dominant M1– non-dominant occipital lobe, contralateral occipital lobe</p> <p>Contralateral and bilateral CST < Control dominant M1– dominant occipital lobe, contralateral occipital lobe</p> <p>Bilateral CST > Control</p>	
--	--	---	--	--	--	---	--	--

							dominant M1– ipsilateral supramarginal gyrus and parietal operculum	
Qin et al., 2018	DCP, SCP	34 PBI, 20/14 M/F 16 DCP, 10/6 M/F, 9.6 ± 5.0 18 SCP, 10/8 M/F, 8.9 ± 3.1 18 Controls, 11/7 M/F, 9.5 ± 2.2 Mean ± SD years	3T MRI 8-channel T1-weighted images were used to assess injury rs-scan details Eyes closed, asleep (sedated) TR/TE = 2000/30 ms	WMI - 21, consisting of PVL, ventricular enlargement CGM - 1, occipital lesion BGT - 4 Normal - 8	GMFCS ADL DCP: GMFCS II = 3 III = 7 IV = 5 V = 1 ADL = 38.44 ± 18 SCP: GMFCS I = 9 II = 5 III = 4 ADL = 82.55 ± 3.4 Mean ± SD	Independent component analysis (ICA) – 14 RSN Cerebellum, sensorimotor network 1 &2, dorsal attention, anterior default- mode, posterior default mode, self- referential, primary visual, extrastriate visual, auditory, left and right frontoparietal, salience Within and between RSN analysis Correlations between RSN and	DCP, SCP < Control Within Cerebellum, sensorimotor network 2, left frontoparietal, salience networks (superior frontal gyrus) DCP, SCP > Control Within salience network (anterior cingulum) DCP, SCP > Control primary visual– extrastriate visual network primary visual– right frontoparietal network	FC within Cerebellum→ negatively associated with GMFCS FC between primary visual– extrastriate visual network → negatively associated with GMFCS FC between primary visual– right frontoparietal network→ positively associated with ADL

						clinical measurements	<p>posterior DMN–left frontoparietal network</p> <p>DCP > Control right frontoparietal–cerebellum antDMN–self-referential network</p> <p>DCP, SCP < Control posterior DMN–salience network</p>	<p>FC between right frontoparietal–Cerebellum→ positively associated with ADL</p> <p>FC between anterior default mode–self-referential network → negatively associated with GMFCS, positively associated with ADL</p> <p>FC between posterior default mode–salience network → negatively associated with GMFCS</p>
Qin et al., 2019	DCP *Right-handed	24 DCP, 12/12 M/F, 8.5 ± 4.6 20 controls, 12/8 M//F, 9 ± 2.2	3T MRI T1- and T2-weighted images were used to assess injury	White matter lesions (predominantly PVL) - 9 CGM - 6 BGT - 3 Normal - 8	GMFCS ADL GMFCS II = 5 III = 9 IV = 9	Voxel-mirror homotopic connectivity (VMHC) ICA = 12 RSN	DCP < Control Inter-hemispheric FC – Cerebellum, precentral, SMA, anterior cingulate, middle cingulate,	Calcarine cortex Inter-hemispheric FC→ negatively associated with GMFCS, positively

		Mean ± SD years	rs-scan details Eyes closed TR/TE = 8400/150 ms		V = 3 ADL = 38.44 ± 18 Mean ± SD	<p>Cerebellum, dorsal attention, auditory, primary visual, extrastriate visual, central executive, salience, anterior default mode, posterior default mode, left and right frontoparietal, sensorimotor</p> <p>Correlations of inter-hemispheric FC of VMHC</p> <p>Regions showing significant difference for VMHC and lateralization between DCP and controls chosen as ROIs</p> <p>VMHC - Cerebellum (Crus 1, 6 L), calcarine, cingulum anterior, cingulum middle, superior frontal gyrus, precentral gyrus,</p>	<p>and frontal and calcarine areas</p> <p>DCP < Control Lateralization in right anterior cingulate cortex and right insula in central executive network, right temporal middle gyrus in left frontoparietal network, and left parietal inferior in right frontoparietal network</p> <p>DCP > Control Lateralization in left supplementary motor area and left precentral areas in salience network, right frontal middle gyrus in left frontoparietal network, left angular gyrus in right frontoparietal network</p>	<p>associated with ADL</p> <p>Left hemisphere lateralization of Inferior parietal lobule in right frontoparietal network → negatively associated with ADL</p> <p>Left hemisphere lateralization of supplementary motor area in right frontoparietal network → positively associated with GMFCS</p>
--	--	--------------------	--	--	--	--	---	--

						<p>supplementary motor area in left and right hemispheres</p> <p>Lateralization – central executive – (right anterior, right insula) left frontoparietal – (right middle temporal gyrus, right frontal middle gyrus) right frontoparietal – (left angular gyrus, left inferior parietal lobule) salience – (left supplementary area left precentral gyrus)</p>	
Wheelock et al., 2018	Very preterm birth (<32 weeks gestation)	<p>58 PBI, 26/32 M/F, 12.3 ± 0.1</p> <p>65 Controls, 24/31 M/F, 12.2 ± 0.1</p> <p>Mean ± SD years</p>	<p>3T MRI 8-channel coil T1-weighted images were used to assess injury</p> <p>rs-scan details Eyes open</p>	<p>WMI Severe - 0 mild - 39 moderate - 7 none - 12 IVH - 2 PVL - 1</p>	<p>GMFCS MABC</p> <p>GMFCS I = 9 II = 2</p> <p>MABC Manual Dexterity</p>	<p>288 ROIs, comprising 15 RSNs used to investigate associations between FC of ROI pairs and MABC using enrichment analysis</p>	<p>Control > PBI Thalamus–Motor → MABC total scores Aiming and catching, manual dexterity</p> <p>Basal ganglia–Motor → balance</p>

			TR/TE = 2500/35 ms Range 10-20 minutes (average 14 minutes)		PBI: 8.2 ± 2.2 Control: 9.6 ± 2.3 Aiming Catching PBI: 9.8 ± 2.9 Control: 11.2 ± 2.7 Mean ± SD Balance PBI: 10 Control: 14 Total standard PBI: 10 Control: 11 Median	Motor, cingulo- opercular, auditory, default mode, memory, visual, frontoparietal, salience, ventral attention, dorsal attention, medial temporal, reward, basal ganglia, thalamus, cerebellum Tested for differences in brain- behaviour relationships between very preterm and term groups		Saliency-Motor→ Aiming and catching PBI > Control Within frontoparietal and cerebellum networks→ MABC Total scores Basal ganglia- Auditory→ Aiming and catching Dorsal attention- DMN→ balance Within DMN→ balance Shared brain- behav correlation Thalamus-Basal ganglia→ Balance
Language outcome								
Dick et al., 2013	Left-sided perinatal	14 PBI, 5/9 M/F,	3T MRI	Frontal cortex - 1	CELF III, Johnson-Newport	ROI analysis – 16 ROIs	NA	Controls

	<p>stroke – unilateral cerebral palsy in 12 patients</p> <p>Predominantly left-handed</p>	<p>14.6 [7.17-29.08]</p> <p>25 Controls, 9/16 M/F, 16.91 [8.6 - 38.11]</p> <p>Mean [range] years</p>	<p>T1-weighted images were used to assess injury</p> <p>rs-scan details TR/TE 2000/25 ms</p>	<p>Inferior frontal gyrus - 2 Middle frontal gyrus - 1 Superior temporal gyrus - 4 Middle temporal gyrus - 1 Supramarginal gyrus - 4 Precentral gyrus - 2 Postcentral gyrus - 1 Lateral occipital gyrus - 2 Superior parietal gyrus - 1 Angular gyrus - 2 PWML - 5 WMI - 1 Precuneus - 1 Frontal vascular injury - 1 Vascular lesion - 1 PVL - 1 Insula - 3 Thalamus - 3 Caudate - 3 Putamen - 2</p>	<p>grammaticality judgment task, WAIS-III (>16 years) WISC-III (<16 years)</p> <p>Receptive language Listening to paragraphs PBI: 7.4 ± 2.6 Control: 9.8 ± 2.6 Verbal comprehension PBI: 94.9 ± 20.6 Control: 100.9 ± 17.7 Newport Grammaticality index PBI: 120.6 ± 17.9 Control: 131.0 ± 7 CELF Receptive PBI: 88.8 ± 22 Control: 100.3 ± 20.7</p> <p>Performance IQ measure Perceptual organization index</p>	<p>inferior frontal gyrus; pars triangularis, pars opercularis, supramarginal and angular gyri of the inferior parietal lobule, posterior superior temporal gyrus and sulcus, the posterior middle temporal gyrus, and one cerebellar ROI, per hemisphere</p>		<p>Increased Inter-hemispheric FC angular and superior temporal gyrus → negatively associated Verbal comprehension</p> <p>PBI Inter-hemispheric FC superior temporal gyrus posterior → positively associated with all receptive language measures (listening to paragraphs, verbal comprehension, Newport grammaticality index, CELF receptive)</p> <p>Interhemispheric FC angular gyrus → negatively associated with Listening on paragraphs</p>
--	---	--	--	---	---	---	--	---

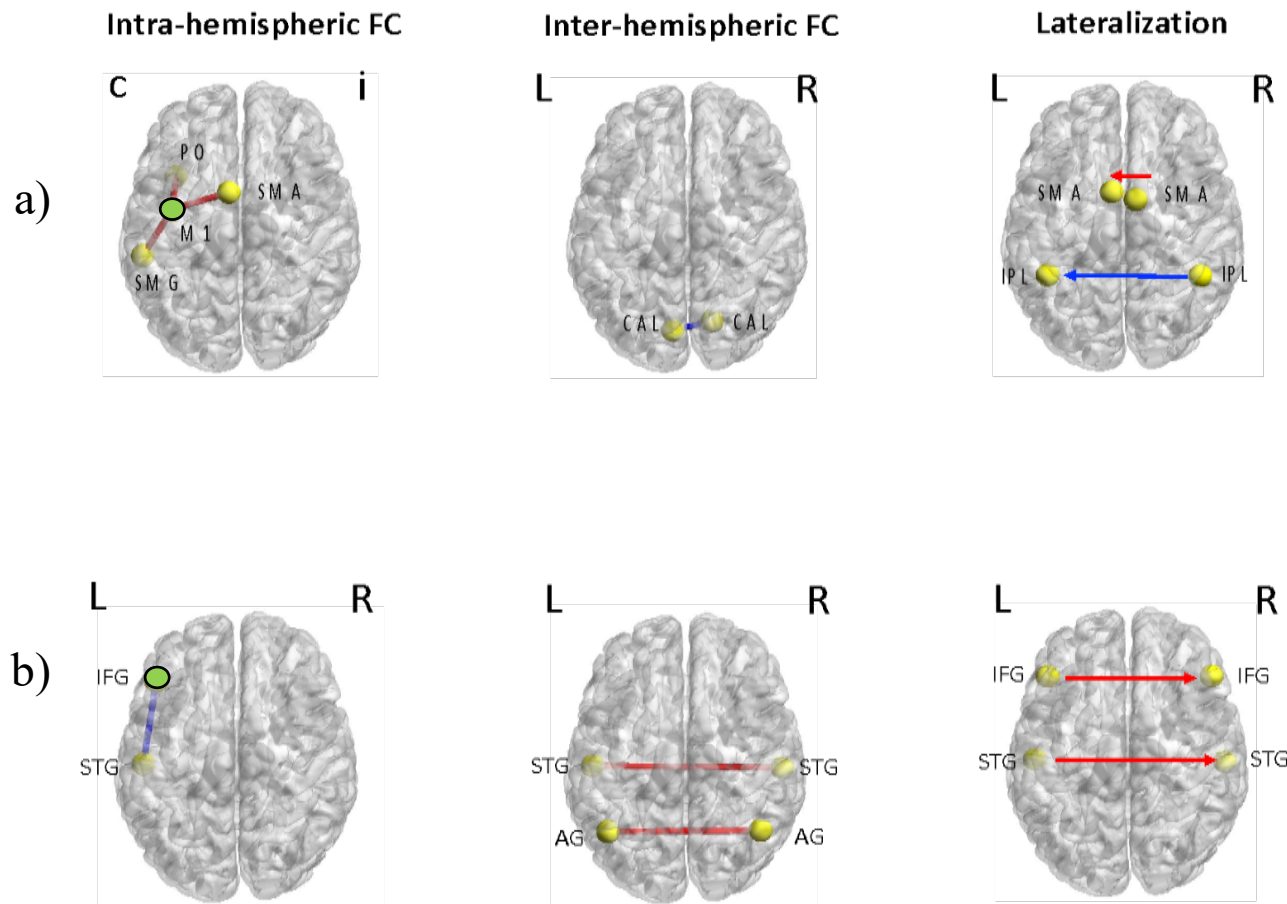
					PBI: 94.6 ± 20.7 Control: 108.7 ± 11.8			
Carlson et al., 2019	AIS, PVI	32 PBI, 20/12 M/F 17 AIS, 10/7 M/F, 14.0 14.2 (4.1) [6.6-19.0] years 15 PVI, 10/5 M/F, 12.8 11.4 (4.0) [6.7-19.7] 34 Controls, 19/15 M/F, 13.2 13.1 (3.6) [6.5-19.0] Mean median (SD) [range] years	3T MRI T1-weighted images were used to assess injury rs-scan details Eyes open TR/TE 2000/30 ms 5 minutes	AIS – Left-sided lesion – 12 Right-sided lesion – 5 PVI – Left-sided lesion – 9 Right-sided lesion – 6	WISC-IV NEPSY-II WJ-III CVLT-C CMS CVMT Intellectual functioning WISC-IV Full scale IQ: 21.3 (24.9) [0.4-79] Processing speed index: 13.1 (14.2) [0.1-50] Expressive language WISC-IV Vocabulary: 22.5 (20.1) [0.4-75] Comprehension: 16.3 (11.7) [2-37] NEPSY-II Word generation (Semantic): 50.1 (28.6) [0.1-99]	ROI analysis – 6 ROIs left and right inferior frontal gyri left and right posterior superior temporal gyri left and right frontal poles as non-language reference points Lateralitization	Control > Left stroke left inferior frontal gyrus–left inferior frontal gyrus, left middle temporal gyrus, left caudate nucleus, left anterior thalamus Right stroke < Control left inferior frontal gyrus–right inferior frontal gyrus AIS < Control, PVI left inferior frontal gyrus–right	Intra-hemispheric FC left inferior frontal gyrus–left superior temporal gyrus → positively correlated with WJ-III understanding directions Inter-hemispheric FC left superior temporal gyrus–right superior temporal gyrus → positively correlated with CMS stories in right-sided stroke patients

					<p>Word generation (initial letter): 8.5 (9.3) [0.4-25]</p> <p>Receptive language WJ-III Understanding directions 48.0 (31.2) [7-95]</p> <p>Verbal memory CVLT-C Total trials 1-5: 58.8 (27.2) [8-95] CMS Stories (delayed): 60.6 (27.4) [5-95]</p> <p>Visual memory CVMT Total: 40.6 (32.8) [10-90] CMS Faces (delayed): 29.6 (30.5) [0.4-75]</p> <p>Mean %ile (SD) [range]</p>		<p>inferior frontal gyrus left superior temporal gyrus–right superior temporal gyrus left inferior frontal gyrus–right superior temporal gyrus</p>	
--	--	--	--	--	---	--	--	--

Francois et al., 2019	Left-sided AIS	<p>6 PBI, 4/2 M/F, 3.8 ± 0.26 [3.5-4]</p> <p>9 controls, 6/3 M/F, 4.3±1.09</p> <p>Mean ± SD [range] years</p>	<p>a. T MRI MRI-based diagnostics were performed on anatomic data acquired on a 1.5 T whole-body MRI within 7 days and MRI performed again at 3.8 ± 0.26</p> <p>rs-scan details TR/TE 3000/60 ms 5 minutes</p>	<p>Middle frontal gyrus Inferior frontal gyrus Middle temporal gyrus Superior temporal gyrus Precentral gyrus Postcentral gyrus Supramarginal gyrus Middle occipital gyrus Angular gyrus</p>	<p>GMFCS, NEPSY-II, PPVT-III MLU</p> <p>NEPSY Normative range (8-12)</p> <p>Comprehension of instruction: 9 (7-11) Body part naming and identification: 8 (5-11) Word generation: 8 (5-12) Phonological processing: 7 (5-9) Speeded naming: 9 (8-10) Memory for designs: 9 (7-11) Narrative memory: 8 (7-9) Sentence repetition: 8 (6-10) Block construction: 8 (5-10)</p>		NA	Right-hemisphere lateralization of superior temporal gyrus–inferior frontal gyrus → positively associated with MLU
-----------------------	----------------	---	--	--	--	--	----	--

					Design copying: 7 (5-9) Imitating hand positions: 10 (8-12) Visuomotor precision: 8 (6-10) Median (IQR)			
--	--	--	--	--	---	--	--	--

Abbreviations: IQR, interquartile range; M/F, male/female; ms, milliseconds SD, standard deviation; TR/TE, Repetition time/echo time; AIS, arterial ischemic stroke; CST, corticospinal tract wiring; DCP, dyskinetic cerebral palsy; IVH, intraventricular haemorrhage; NE, neonatal encephalopathy; PBI, perinatal brain injury; PVI, periventricular venous infarction; SCP, spastic cerebral palsy; uCP; unilateral cerebral palsy; BGT, basal ganglia thalamic; CGM, cortical grey matter; PVL, periventricular leukomalacia; PWML, punctate white matter lesion; WMI, white matter injury; ADL, Assessment of Daily Living; AHA, Assisting Hand Assessment; AIMS, Alberta Infant Motor Scale; CELF, Clinical evaluation of language fundamentals; CMS, Children’s memory scale; CVLT, California Verbal learning test; CVMT, Continuous Visual Memory Test; GMFCS, Gross Motor Functional Classification System; INFANIB, Infant Neurological Battery; JTHFT, Jebsen-Taylor Hand Function Test; MA, Melbourne Assessment of Unilateral Upper limb Function; MACS, Manual Ability Classification System; MABC, Movement ABC for children; MLU, mean length of utterance; NEPSY, A Developmental NEUROPSYchological Assessment; PPVT; Peabody picture vocabulary test; TIMP, Test of Infant Motor Performance; WAIS, Wechsler Adult Intelligence Scale; WISC, Wechsler Intelligence Scale for Children; WJ, Woodcock-Johnson Tests of Cognitive Abilities; FC, functional connectivity; ICA, independent component analysis; ROI, region-of-interest; RSN, resting-state network; VMHC, Voxel-mirror homotopic connectivity.



Article	ROI		Outcome
Intra-hemispheric FC			
Simon-Martinez et al., 2019	cM1	cPO	JTHFT (-)
Woodward et al., 2019	cM1	cSMA	AHA (-)
Simon-Martinez et al., 2019	cM1	cSMG	JTHFT (-)
Inter-hemispheric FC			
Qin et al., 2019	L CaI	R CaI	ADL (-) GMFCS (-)
Lateralization			
Qin et al., 2019		L SMA	GMFCS (+)
Qin et al., 2019		L IPL	ADL (-)

Article	ROI		Outcome
Intra-hemispheric FC			
Carlson et al., 2019	L IFG	L STG	WJ (+)
Inter-hemispheric FC			
Dick et al., 2013	L STG	R STG	CELF (+)
Carlson et al., 2019			CMS (+)
Carlson et al., 2019	L AG	R AG	CELF (-)
Lateralization			
Francois et al., 2019		R IFG	MLU (+)
		R STG	MLU (+)

Figure 5.2 Abnormal resting-state functional connectivity (FC) of brain regions associated with motor (*a*) and language (*b*) outcomes in individuals with a history of perinatal brain injury. Brain regions with altered intra-hemispheric FC (first column), inter-hemispheric FC (second column) and lateralization (third column) compared with typically developing controls. Red connections indicate connections between brain regions with increased FC and blue connections correspond to connections between brain regions with reduced FC. Seeds indicated by green circle. +/- represent positive and negative correlation of FC with clinical outcome, respectively

Table 5.2 Summary of relations between functional network topology and motor outcome

Articles	Resting-state network		FC strength	Outcome	Age at outcome
Linke et al., 2018	Within-network	SMN	↓	AIMS, INFANIB (+)	8 months
Linke et al., 2018 Wheelock et al., 2018		FPN	↓ ↑	AIMS, INFANIB (+) MABC (+)	8 months 12 years
Qin et al., 2018 Wheelock et al., 2018		Cerebellum	↓ ↑	GMFCS (-), MABC (+)	3-18 years 12 years
Wheelock et al., 2018		DMN	↑	Balance (+)	12 years
	Between-network				
Linke et al., 2018	SMN	DMN	↓	AIMS, INFANIB (+)	8 months
Linke et al., 2018	SMN	VAN	↓	AIMS, INFANIB (+)	8 months
Linke et al., 2018	DMN	VIS	↓	AIMS, INFANIB (+)	8 months
Wheelock et al., 2018	BG	AUD	↑	MABC (+)	12 years
Wheelock et al., 2018	DAN	DMN	↑	MABC (+)	12 years
Wheelock et al., 2018	THAL	BG	↑	MABC (+)	12 years
Wheelock et al., 2018	BG	Motor	↓	Balance (-)	12 years
Wheelock et al., 2018	SN	Motor	↓	Aiming and catching scores (-)	12 years
Wheelock et al., 2018	Thalamus	Motor	↓	MABC, Aiming and catching, manual dexterity (-)	12 years
Qin et al., 2018	primVN	extraVN	↓	GMFCS (-)	3-18 years

Qin et al., 2018	primVN	RFPN	↓	ADL (+)	3-18 years
Qin et al., 2018	RFPN	Cerebellum	↓	ADL (+)	3-18 years
Qin et al., 2018	antDMN	SRN	↓	ADL (+), GMFCS (-)	3-18 years
Qin et al., 2018	postDMN	SN	↓	GMFCS (-)	3-18 years

↑/↓ represents increased and decreased functional connectivity (FC), respectively; +/- represent positive and negative correlation of FC with clinical outcome, respectively.

Abbreviations: DMN, default-mode network; SMN, sensorimotor network; VAN, ventral attention network; VIS, visual network; antDMN, anterior default mode network; extraVN, extrastriate visual network; FPC, frontoparietal control network; LFPN, left frontoparietal network; postDMN, posterior default mode network; primVN, primary visual network; RFPN, right frontoparietal network; SN, salience network; SRN, self-referential network; VIS, visual network; ADL, Assessment of Daily Living; AHA, Assisting Hand Assessment; AIMS, Alberta Infant Motor Scale; GMFCS, Gross Motor Functional Classification System; INFANIB, Infant Neurological Battery; MABC, Movement ABC for children.

Table 5.3 STROBE reporting for each study												
Characteristics	Item no.		Saunders et al., 2018	Woodward et al., 2019	Linke et al., 2018	Simon-Martinez et al., 2019	Qin et al., 2018	Qin et al., 2019	Wheelock et al., 2018	Dick et al., 2013	Carlson et al., 2019	Francois et al., 2019
Title and abstract	1	a b	Y Y	Y Y	Y Y	Y Y	Y Y	Y Y	Y Y	Y Y	Y Y	Y Y
Introduction												
Background/rationale	2		Y	Y	Y	Y	Y	Y	Y	Y	Y	Y
Objectives	3		Y	Y	Y	Y	Y	Y	Y	Y	Y	Y
Methods												
Study design	4		Y	Y	Y	Y	Y	Y	Y	Y	Y	Y
Setting	5		Y	Y	Y	Y	Y	Y	Y	Y	Y	Y
Participants	6	a b	Y NA	Y NA	Y NA	Y NA	Y NA	Y NA	Y NA	Y NA	Y NA	Y NA
Variables	7		Y	Y	Y	Y	Y	Y	Y	Y	Y	Y
Data sources/measurement	8		Y	Y	Y	Y	Y	Y	Y	Y	Y	Y
Bias	9		Y	Y	Y	Y	Y	Y	Y	Y	Y	Y

Study size	10		Y	Y	Y	Y	Y	Y	Y	Y	Y	Y
Quantitative variables	11		Y	Y	Y	Y	Y	Y	Y	Y	Y	Y
Statistical methods	12	a b c d e	Y Y NA NA NA	Y Y NA Y NA	Y Y NA Y NA	Y Y NA NA NA	Y Y NA NA NA	Y Y NA NA NA	Y Y NA NA NA	Y Y NA NA NA	Y Y NA Y NA	Y Y NA NA NA
Results												
Participants	13	a b c	Y NA NA	Y Y NA	Y Y NA	Y Y NA	Y Y NA	Y Y NA	Y Y NA	Y Y NA	Y Y NA	Y Y NA
Descriptive data	14	a b c	Y Y Y	Y Y Y	Y Y Y	Y Y Y	Y Y Y	Y Y Y	Y Y Y	Y Y Y	Y Y Y	Y Y Y
Outcome data	15		Y	Y	Y	Y	Y	Y	Y	Y	Y	Y
Main results	16	a b c	Y NA NA	Y NA NA	Y NA NA	Y NA NA	Y NA NA	Y NA NA	Y NA NA	Y NA NA	Y NA NA	Y NA NA
Other analyses	17		Y	Y	Y	Y	Y	Y	Y	Y	Y	Y
Discussion												
Key results	18	Y	Y	Y	Y	Y	Y	Y	Y	Y	Y	Y
Limitations	19	Y	Y	Y	Y	Y	Y	Y	Y	NA	Y	Y

Interpretation	20	Y	Y	Y	Y	Y	Y	Y	Y	Y	Y	Y
Generalisability	21	Y	Y	Y	Y	Y	Y	Y	Y	Y	Y	Y
Other information												
Funding	22	Y	Y	Y	Y	Y	Y	Y	Y	Y	Y	Y

N/A – not applicable, Y – yes.

5.4 Discussion

Evidence from this systematic review suggests a possible association between diaschisis and motor and language impairments in individuals after perinatal brain lesions. This result is demonstrated by altered intra- and inter-hemispheric connectivity and impaired lateralization of brain regions important for motor and language functioning, as well as altered connectivity within and between RSNs of primary (sensorimotor, visual, auditory) and higher-order (cerebellum, frontoparietal, default-mode, salience, self-referential and attentional) functions. These alterations in brain functional organization are of particular interest as they satisfy the criteria of diaschisis. Thus there is a need to explore brain regions functionally connected but remote from the primary lesioned brain area for targeted treatments and appropriate intervention in individuals after perinatal brain injury.

When evaluating the effects of perinatal brain injury on outcome based on conventional MRI, the usual approach is to investigate the association of neurodevelopmental outcome with injury to brain regions of well-defined function. For example, in infants with neonatal encephalopathy, existing MRI scoring systems rely on the location of brain lesions to produce a score of brain injury severity (Barkovich et al., 1998; Shankaran et al., 2012). Depending on the scoring system, lesions may be divided into those occurring within BGT and WS areas, thus dividing the brain into broad patterns of injury. However, a limitation of this lesion mapping approach is that lesions widely distributed may lead to similar functional impairments, and thus there is no single region that may lead to language or motor impairments but there is a number of regions that may be associated with impairments.

Another approach is to understand not only the location of the lesion but how the functional interaction of the lesion to the rest of the brain is altered. The central concept is

that the functional impairments (outcomes) reflect the dysfunction in large scale brain networks which mediate either language or motor function. Thus a lesion in the brain may lead to impairments in distal brain regions and cause similar symptoms even if lesion locations do not overlap.

The findings from this systematic review seem to be consistent with the concept of ‘diaschisis’ introduced by von Manakow in 1914 (von Monakow, 1914). The term refers to changes in brain areas functionally connected but remote from the primary lesioned brain area, and includes four key aspects (i) presence of a focal lesion, (ii) decrease in activity at a remote (distal) region due to direct inhibitory or excitatory effects, (iii) interruption of connections between lesion and remote areas, and (iv) the symptoms change over time.

Most importantly, this systematic review revealed altered functional connectivity in regions important for language and motor functioning remote from the primary lesioned area. In studies assessing motor outcome, this result is demonstrated by statistically significant associations between motor functioning and an increase in intra-hemispheric functional connectivity from the primary motor cortex to supplementary motor area (a component of sensorimotor network) (Woodward et al., 2019), supramarginal gyrus (a component of ventral attention network) (Simon-Martinez et al., 2019) and parietal operculum (a component of dorsal attention network) (Simon-Martinez et al., 2019) in the contralesional hemisphere, a decrease in inter-hemispheric connectivity of the calcarine cortex (a component of visual network) (Qin et al., 2019), as well as increased left-hemisphere lateralization of the supplementary motor area (a component of sensorimotor network) (Qin et al., 2019) and decreased left-hemisphere lateralization of the inferior parietal lobule (a component of frontoparietal network) (Qin et al., 2019). These brain

regions are crucial for motor processing (Weilke et al., 2001; Ben-Shabat et al., 2015; Andersen et al., 2009) suggesting altered connectivity between motor-related cortical regions have been compromised by early injury and are associated with adverse motor functioning in later life.

Our findings also show alterations in functional connectivity were not restricted to motor processing areas but that perinatal brain injury had a global impact on functional network processing. Widespread alterations of within and between network connectivity affecting a number of RSNs involved in primary and higher-order functions was revealed, involving the sensorimotor, visual, auditory, cerebellum, frontoparietal, default-mode, salience, self-referential and attentional networks. In particular, two studies revealed reduced within and between network connectivity of primary and higher order networks associated with motor impairments (Woodward et al., 2019; Qin et al., 2018). Specifically, disruption to functional connectivity within sensorimotor and frontoparietal networks and between sensorimotor-default mode, sensorimotor-ventral attention, default mode-visual networks scanned at TEA was predictive of motor impairments at 8 months (Linke et al., 2018), and Qin et al. revealed reduced functional connectivity within the cerebellum and between primary-extrastriate visual, anterior default mode-self-referential, posterior default mode-salience, right frontoparietal-primary visual, right frontoparietal-cerebellum, and anterior default mode-self-referential networks were associated with motor impairments in children and adolescents with cerebral palsy (Qin et al., 2018). A recent rs-fMRI study in preterm-born infants with mild brain injury scanned at TEA (Eyre et al., 2021) also showed decreased functional connectivity in both primary and higher-order RSNs, and the findings from this review suggest these alterations remain compromised into adolescence, and are associated with later motor impairments.

In contrast to the observed relationship between maladaptive motor performance and reduced connectivity within frontoparietal (Linke et al., 2018) and cerebellum³¹ networks, one study in very preterm children with perinatal brain injury (Qin et al., 2019) showed that enrichment of within network connectivity in cerebellum and frontoparietal networks positively correlated with improved motor performance. These findings suggest individuals who develop adaptive alternative developmental trajectories in the face of widespread alterations in typical functional network processing that would otherwise pose risk for the development of adverse motor outcomes have improved motor functioning. Children with perinatal brain injury born very preterm also exhibited altered functional connectivity within default mode network, and between basal ganglia, auditory, dorsal attention, default mode, motor, salience and thalamus networks (Qin et al., 2019), showing the importance of considering networks which may not have traditionally been associated with motor outcomes in future investigations.

In studies assessing language outcome, functional connectivity of only regions involved in language-processing were investigated. These studies revealed individuals after perinatal brain lesions demonstrated a decrease in intra-hemispheric connectivity (Carlson et al., 2019), an increase in inter-hemispheric connectivity (Dick et al., 2013, Carlson et al., 2019; Francois et al., 2019), and an increase in right hemisphere lateralization of language-related areas, and were associated with language functioning. Specifically, reduced intra-hemispheric connectivity from left inferior frontal gyrus to superior temporal gyrus (Carlson et al., 2019), increased inter-hemispheric connectivity of the superior temporal gyrus (Carlson et al., 2019), and increased inter-hemispheric connectivity of the angular gyrus were associated with poorer language performance (Dick et al., 2013). Whereas, increased inter-hemispheric connectivity of the superior temporal gyrus³⁴ and increased right hemisphere lateralization of the inferior frontal gyrus and superior temporal gyrus

correlated with better language functioning (Francois et al., 2019). Studies have demonstrated the presence of inter-hemispheric connectivity of language-related regions in typically developing fetuses (Anderson et al., 2013, Thomason et al., 2013), maturing to a pattern of primarily intra-hemispheric connectivity of language-related regions in the left hemisphere in adults (Vigneau et al., 2011; Perani et al., 2011; Friederici et al., 2011). The findings from this review provide evidence for long-lasting effects of perinatal brain injury on the normal maturation of the language network and suggests a failure to progress beyond an early basic language network, possibly due to disrupted synaptic pruning. It also provides evidence for preserved language performance supported by compensatory activity in the right perisylvian cortex in individuals after perinatal brain lesions, suggesting healthy brain regions are able to take up functions previously the responsibility of damaged areas, though more studies are needed to confirm this.

We also searched for studies that assessed the relationship between rs-fMRI and cognitive outcomes after perinatal brain injury. While no studies met the inclusion criteria, we did find one study performed in children and adolescents after AIS, with lesions in BGT, and frontal temporal and parietal cortices in the left-hemisphere, and with lower cognitive functions, which demonstrated increased functional connectivity in the posterior precuneus (a component of default mode network) compared with children with PVI (Ilves et al., 2016). However, they did not assess the relationship between rs-fMRI and cognitive outcome, and it will be important for future studies to examine this relationship.

We found a number of discrepancies in this review, which may be attributed to the heterogeneity of the study population (e.g. hypoxia-ischaemia, IVH, perinatal stroke, PVL, haemorrhage), wide range in age (i.e between 4 months, up to 29 years of age), varied levels of impairment, analysis of rs-fMRI, injury-related factors (e.g. severity and

location), varied outcome assessment tools used and the age at which these tools were administered. Specifically, Wheelock et al. (2018) observed a positive association between increased functional connectivity within cerebellum and frontoparietal networks and improved motor performance, whereas Qin et al. (2018) and Linke et al. (2018) showed reduced functional connectivity within the cerebellum and frontoparietal networks were associated with adverse motor abilities. Children in Wheelock et al. (2018) had mild white matter brain injuries with no evidence of subcortical injury, had less severe motor impairments and motor outcome was assessed using MABC (Age at outcome: mean \pm SD, 12.3 \pm 0.1 years). In contrast, both Qin et al. (2018) and Linke et al. (2018) found evidence of grey matter injury, and children assessed in Qin et al. (Qin et al., 2018) had cerebral palsy, and motor outcome was assessed using TIMP, AIMS, and INFANIB at 4 and 8 months in Linke et al. (2018), and GMFCS in Qin et al. (2018) (Age at outcome: mean \pm SD, DCP - 9.6 \pm 5.0, SCP - 8.9 \pm 3.1). In addition, Dick et al. (2013) revealed improved language functioning was associated with increased inter-hemispheric functional connectivity of the superior temporal gyrus, whereas Carlson et al. (2019) demonstrated poorer language functioning was associated with increased inter-hemispheric functional connectivity of the superior temporal gyrus. In Dick et al. (2013) children had left-sided perinatal stroke, whereas, in Carlson et al. (2019) children had right-sided perinatal stroke, and language outcome was assessed using CELF in Dick et al. (2013) (Age at outcome: range, 7.17-29.08), and CMS in Carlson et al. (2019) (Age at outcome: range, 6.6-19.7).

This structured review brings into focus that even though the locations of the lesions may vary, the regions that have been found to have altered functional connectivity are within brain regions and brain networks typically found to be associated with either motor or language function. Our findings also highlight the need to consider networks which may not have traditionally been associated with motor and language outcome. Notably, one

study included in this review demonstrated disrupted functional connectivity predicted motor impairment better than structural MRI score (Linke et al., 2018). Accordingly, therapeutic practices directed at measuring diaschisis may have the potential to mitigate the motor and language impairments associated with perinatal brain injury.

5.5 Limitations

This systematic review has some limitations that need to be considered. Given the limited amount of literature available the number of studies included in this review was relatively small. Additionally, the heterogeneity of the study population may have affected the combination and interpretation of the results. Other factors include the variability of clinical tools used to capture motor and language outcomes and the age of the child when these were administered. Furthermore, the study population covered a wide age-range comprising infants at 4 months, up to individuals of 29 years of age. While the findings from this review suggest a long-lasting effect of perinatal brain injury, longitudinal studies with outcome assessed at multiple time-points are required to understand how altered functional connectivity due to perinatal brain injury develops over time.

5.6 Conclusion

The study of the relationship between resting-state fMRI and motor and language outcomes in individuals after perinatal brain lesions is still in its infancy and warrants further investigation. Together these findings show that resting-state functional connectivity of individuals with a history of perinatal brain injury remains compromised up to adulthood, with intra- and inter-hemispheric connectivity, lateralization and within- and between network connectivity affected. From the studies reviewed here, a possible association between diaschisis and motor and language impairments emerged, and may represent a potential biomarker of impaired language and motor ability in individuals after

perinatal brain injury. However, we remain cautious in the conclusions that can be made due to the heterogeneity and wide age-range of the study population under review, and discrepancies in some findings. We propose areas warranting further investigation throughout this systematic review. In particular, (1) further examination of additional networks which may not have traditionally been associated with motor and language outcomes; (2) an assessment of how altered functional connectivity patterns due to perinatal brain injury develop over time by performing longitudinal studies with multiple assessment time-points; (3) address how diaschisis mediates the rs-fMRI–neurodevelopmental outcome relationship; (4) explore whether the effects of perinatal brain lesions on rs-fMRI translate to cognition; (5) that distinguish between biological mechanisms which may lay behind such effects (e.g. hypoxia-ischaemia, cerebral infarction, or haemorrhage); and (6) that assess whether particular brain regions are innately specialized for motor or language functioning, or, if there is limited functional localization in early brain development. Although several questions remain unanswered, this systematic review suggests a possible association between diaschisis and motor and language impairments in individuals after perinatal brain lesions. There is therefore a need to explore the contribution of brain regions functionally connected but remote from the primary lesioned brain area for targeted treatments and appropriate intervention in individuals after perinatal brain injury.

Chapter 6: Metastable resting state neural dynamics of brain networks in the infant brain

6.1 Introduction

rs-fMRI measures the temporal synchronization of low frequency spontaneous fluctuations in the BOLD signal (Biswal et al., 1995) (Biswal et al., 1995; Fox et al., 2007). Using rs-fMRI a number of RSNs have been identified that are associated with primary functions (i.e. sensorimotor, auditory and visual processing) and rapidly respond to external inputs, and those involved in higher-order functions (i.e. self-awareness, memory, attention and executive functioning) that sustain diverse and complex mental operations (Damoiseaux et al., 2006; Smith et al., 2009, Power et al., 2011). Many studies in fetuses and newborn infants (Alcauter et al., 2015a; Arichi et al., 2010; Fransson et al., 2009, 2007, Gao et al., 2014a, 2014b, 2013, 2009; Lin et al., 2008; Schöpf et al., 2012; Smyser et al., 2010; Thomason et al., 2015) have revealed primary networks display a mature configuration, whilst higher-order networks are largely fragmented (Doria et al., 2010; Fransson et al., 2009; Gao et al., 2014a, 2014b; Smyser et al., 2010) with the developmental trajectories of RSNs showing remarkable similarities with neurodevelopmental milestones.

Most rs-fMRI studies to date have largely emphasized the investigation of phase-coherent states and focused on static FC properties to predict behaviours (Ní Bhroin et al., 2020; Markett et al., 2020; Zhang et al., 2020). FC analyses are based on the assumption that connectivity is static across the entire fMRI examination, failing to establish a link between the dynamics of coordinated brain activity. Recent studies have shown that the brain is a complex dynamic system (Kringelbach & Deco, 2020; Vasa et al., 2015) and consider the dynamics of functional brain networks in terms of the synchrony and asynchrony (metastability) of oscillatory activity of brain network regions over time (Deco et al. 2015; Kelso 2012). Synchrony has been linked with information exchange (Fries,

2005), while metastability is considered to be important for adaptive information processing (Kelso, 2012; Tognoli and Kelso, 2014). The ability to flexibly engage in a variety of cognitive functions is crucial for adaptation to the ever-changing environment, and studies have shown that the brain navigates different functional network configurations to allow efficient information flow and adaptive changes in response to internal and external stimuli (Kelso, 2012; Hellyer et al., 2015; Hellyer et al., 2014; Deco & Kringelbach, 2016; Senden et al., 2017; Cabral et al., 2011; Shanahan, 2010; Tognoli & Kelso, 2014).

Previous studies in adults have established that synchrony and metastability differ between RSNs (Hellyer et al., 2015; Hellyer et al., 2014; Deco & Kringelbach, 2016) in a manner related to the brain network state required (Lee & Frangou, 2017). Moreover, dynamic FC of association areas is higher than primary areas in adults (Zhang et al., 2016). At birth, dynamic FC of primary order RSNs decreases, and increases in higher order RSN over the first 2 years of age (Wen et al., 2020). It is currently unclear whether spontaneous brain activity of RSNs in the infant brain operate in a metastable manner. Therefore in the present study, we aimed to address the knowledge gaps outlined above using rs-fMRI data obtained from a cohort of healthy neonates from the developing Human Connectome Project (dHCP), to better understand the dynamic properties of RSNs in early life and further our understanding of the establishment of metastability and brain functional organisation.

6.2 Materials and Methods

6.2.1 Participants

We used the 2019 (second) neonatal dataset release from the Developing Human Connectome project (dHCP) (<http://www.developingconnectome.org>). The study was

approved by the UK National Research Ethics Authority. Informed written parental consent was obtained prior to imaging and data release. Recruited neonates underwent MRI scanning on a Philips 3 Tesla system (Best, The Netherlands) located in the Evelina Newborn Imaging Centre at St. Thomas Hospital using a 32-channel neonatal head coil and neonatal positioning device (Hughes et al., 2017) supervised by a neonatal nurse/paediatrician trained in MR procedures. Neonates were scanned during natural undisturbed sleep following feeding, and immobilization of the infants was done using a vacuum evacuated bag (Med-Vac, CFI Medical Solutions, Fenton, MI, USA). Infants were provided with hearing protection using earplugs moulded from silicone based putty placed in the external auditory meatus (President Putty, Coltene Whaledent, Mahwah, NJ), earmuffs (MiniMuffs, Natus Medical Inc., San Carlos, CA, USA) and an acoustic hood was placed over the infant.

We selected 464 functional neonatal datasets acquired at term equivalent age from the 2019 (second) dHCP data release. Only infants scanned at 37–44.5 weeks PMA in term-born infants were considered for inclusion. Eighteen were excluded because of a radiology score of 5 (e.g. incidental finding with possible / likely significance for both clinical and imaging analysis e.g. major lesions within white matter cortex, cerebellum, and or basal ganglia; small head/brain <1st centile) (n=15), or radiology score of Q (poor quality anatomical data) (n=3). Five were excluded because they were imaged with sedation (one infant also had a radiology score of 5). A further 137 were excluded because of motion (see 6.2.3 MRI preprocessing section). This left an initial sample of 181 neonates (81 female, 37-44.5 weeks).

6.2.2 Data acquisition

High-temporal resolution BOLD fMRI optimized for neonates was acquired over 15 minutes 3 seconds (2300 volumes) using a multi slice gradient-echo echo planar imaging (EPI) sequence with multiband excitation (multiband factor 9). The repetition time (TR) was 392 ms, echo time (TE) 38 ms, flip angle 34° , and acquired spatial resolution 2.15 mm isotropic (Price et al., 2015). For clinical diagnosis and registration purposes, high-resolution T₁- and T₂-weighted anatomical imaging were also acquired in the same scanning session, which were acquired with a spatial resolution of 0.8 mm isotropic (T₁-weighted: field of view (FOV) $145 \times 122 \times 100$ mm, repetition time 4795 ms; T₂-weighted: FOV = $145 \times 145 \times 108$ mm, TR = 12000 ms, TE = 156 ms) (Cordero-Grande et al., 2018).

6.2.3 MRI pre-processing

All infant fMRI data had been pre-processed using a functional MRI pre-processing pipeline optimized for neonatal imaging and specifically developed for the dHCP, detailed in Fitzgibbon et al. 2020. This included distortion-correction, motion correction, 2-stage registration of the functional image to the T2-weighted structural image and a combined transform from the functional image to a weekly T2-weighted template (Schuh et al., 2018), and ICA denoising using ICA-FIX (Griffanti et al., 2014; Salimi-Khorshidi et al., 2014). Structural data was pre-processed using the dHCP neonatal structural processing pipeline (Makropoulos et al., 2018) which included bias correction, brain extraction using BET from FSL, and segmentation of T2-weighted images using the Developing Brain Region Annotation With Expectation-Maximization (DRAW-EM) for automatic brain MRI segmentation of the developing neonatal brain (Makropoulos et al., 2018).

Since head motion during fMRI data acquisition has been shown to significantly alter rs-fMRI analysis (Satterthwaite et al., 2012; Power et al., 2012; Whitehead et al., 2018;

Denisova et al., 2019) rs-fMRI data were cropped to 10.45 minutes (i.e. 1600 volumes) with the least amount of motion (estimated by calculating the framewise displacement of each volume) selected for further analysis. Participants with high framewise displacement (>0.5 mm) in more than 5% of the cropped dataset were excluded entirely from analysis (i.e. 80 volumes of the 1600 total volumes). The number of motion-outlier volumes remaining in the cropped dataset was recorded for each subject and included as a covariate in all subsequent analyses.

6.2.4 Functional data analysis

Pre-processed functional data from 17 healthy term-born infants scanned at 43.5–44.5 weeks PMA were used to define the RSNs using group ICA. These subjects were excluded from all subsequent analyses.

Probabilistic group ICA by temporal concatenation across subjects was carried out using FSL MELODIC (Beckmann et al., 2004). The ICA dimensionality was set at 25, which resulted in an output consisting of 25 group-average spatial maps representing 25 independent components. The maps were visually inspected and each component was manually labelled as signal (RSN) or noise, following guidelines in Fitzgibbon et al., 2020 and Griffanti et al., 2017 by using the IC spatial map, time series and power spectral density (i.e. magnitude of the Fourier transform of the time series).

All ICA analyses were spatially smoothed with a Gaussian kernel of 3mm (full-width at half-maximum (FWHM)). The spatial components extracted by the ICA were thresholded using an alternative hypothesis test based on fitting a Gaussian mixture model to the distribution of voxel intensities within spatial maps (Beckmann et al., 2005) and controlling the local false-discovery rate at 0.5 ($p < 0.5$) to get an equal balance between false positives and false negatives.

For the remaining dataset that was used for the metastability analysis, the fMRI BOLD signal was bandpass filtered in order to obtain meaningful signal phases (Glerean et al., 2012). Zuo et al. (2012) previously explored the BOLD signal at specific sub-bands and found that the slow-4 (0.027–0.073 Hz) band was mainly identified in the grey matter, with a noise component around 0.03 Hz attributed to respiratory-related fluctuations (Beckmann et al., 2005; Birn et al., 2006). Based on these studies, we chose frequency band specific fMRI signals in the 0.033–0.07 Hz frequency range, minus the 0.03 Hz critical frequency.

6.2.5 Defining brain functional parcels

The individual spatial ICA maps were subsequently projected to the UNC Cedars infant atlas (Shi et al., 2018) which parcellates the infant brain into 223 functionally homogeneous regions using the infant-specific structural (i.e., AAL) atlas as spatial constraint. The atlas was downloaded from the NeuroImaging Tools & Resources Collaboratory (NITRC) database (<https://www.nitrc.org/projects/functionalatlas>).

We then decomposed the RSNs identified in the group ICA analysis (see 6.2.4 Functional data analysis section) into individual regions of interest (ROIs) defined by the UNC Cedars infant atlas (Shi et al., 2018). In determining whether a region from the UNC Cedars infant atlas belonged to a particular RSN as defined by the ICA analysis this was achieved by:

- 1) dividing the volume of the region in the ICA map by the total volume of the region in the age-respective atlas template. For a brain region to be considered as part of the ICA, the volume of the region had to exceed 30% of the total volume, 2) and exhibit the highest mean z-value when compared to other ICA map's.

This resulted in 17 ICA networks as well as the thalamus (see Table 6.1, represented in Figure 6.1). There were 19 regions in the neonate template that did not reach our criteria (Parahippocampal gyrus left, #102; Fusiform gyrus left, #134; Fusiform gyrus left, #138; Fusiform gyrus right, #140; Fusiform gyrus right, #141; Fusiform gyrus right, #142; Fusiform gyrus right, #143; Caudate left, #171; Caudate left, #172; Caudate right, #173; Caudate right, #174; Caudate right, #175; Putamen left, #176; Putamen right, #177; Pallidum left, #178; Pallidum right, #179; Inferior temporal gyrus left, #212; Inferior temporal gyrus left, #213; Inferior temporal gyrus left, #215).

After identifying ROIs for each of the networks, we extracted ROI-specific time series from the pre-processed data for use in the metastability analysis.

Table 6.1 List of ROIs belonging to each ICA network in neonates						
RSN	Regions	#	RSN	Regions	#	
Medial motor	Median cingulate and paracingulate gyrus L	92	Auditory left	Supramarginal gyrus L	158	
	Precuneus L	166		Supramarginal gyrus L	159	
	Precuneus R	168		Angular gyrus L	161	
	Paracentral lobule L	169		Heschl gyrus L	184	
	Paracentral lobule R	170		Superior temporal gyrus L	186	
Lateral motor	Precentral gyrus L	2		Temporal pole: superior temporal gyrus L	194	
	Precentral gyrus R	4		Middle temporal gyrus L	204	
	Rolandic operculum L	53		Dorsal frontal	Superior frontal gyrus, dorsolateral L	6
	Supramarginal gyrus L	157			Superior frontal gyrus, dorsolateral L	7
	Supramarginal gyrus R	160	Superior frontal gyrus, dorsolateral L		8	
Somatosensory right	Postcentral gyrus R	146	Superior frontal gyrus, dorsolateral L		9	

	Superior parietal gyrus R	149		Superior frontal gyrus, dorsolateral L	10
	Superior parietal gyrus R	150		Superior frontal gyrus, dorsolateral R	16
	Inferior parietal lobule R	155		Superior frontal gyrus, dorsolateral R	17
Premotor	Precentral gyrus L	1		Superior frontal gyrus, dorsolateral R	18
	Precentral gyrus R	3		Superior frontal gyrus, orbital part L	27
	Superior frontal gyrus dorsal L	15		Superior frontal gyrus, orbital part R	30
	Superior frontal gyrus dorsal R	21		Middle frontal gyrus, orbital part L	41
	Superior motor area L	55		Middle frontal gyrus, orbital part R	44
	Superior motor area L	56		Superior frontal gyrus, medial L	62
	Superior motor area R	57		Superior frontal gyrus, medial R	63
	Median cingulate and paracingulate gyrus L	91		Superior frontal gyrus, medial R	64
	Median cingulate and paracingulate gyrus R	93		Superior frontal gyrus, medial R	65
	Median cingulate and paracingulate gyrus R	94		Superior frontal gyrus, medial R	66
	Median cingulate and paracingulate gyrus R	95		Superior frontal gyrus, medial R	67
Posterior parietal	Median cingulate and paracingulate gyrus R	96		Superior frontal gyrus, medial orbital L	68
	Posterior cingulate gyrus L	97		Superior frontal gyrus, medial orbital R	69
	Posterior cingulate gyrus R	98		Superior frontal gyrus, medial orbital R	70
	Cuneus R	117		Superior frontal gyrus, medial orbital R	71
	Precuneus L	165		Gyrus rectus L	72
	Precuneus R	167		Gyrus rectus L	75
Somatosensory left	Postcentral gyrus L	145		Gyrus rectus R	78

	Superior parietal gyrus L	148		Gyrus rectus R	79
Visual 1	Calcarine cortex L	110		Gyrus rectus R	81
	Calcarine cortex R	111		Anterior cingulate and paracingulate gyrus L	89
	Calcarine cortex R	112		Anterior cingulate and paracingulate gyrus R	90
	Calcarine cortex R	113	Auditory right	Rolandic operculum R	54
	Cuneus L	114		Insula R	86
	Cuneus R	116		Angular gyrus R	164
	Lingual gyrus L	118		Heschl gyrus L	183
	Lingual gyrus R	121		Heschl gyrus R	185
	Superior parietal gyrus L	147		Superior temporal gyrus R	187
Inferior parietal lobule L	151	Superior temporal gyrus R		189	
Inferior parietal lobule L	152	Superior temporal gyrus R		191	
Inferior parietal lobule L	153	Superior temporal gyrus R		192	
Inferior parietal lobule L	154	Superior temporal gyrus R	193		
Inferior parietal lobule R	156	Visual association left	Parahippocampal gyrus L	103	
Superior frontal gyrus dorsolateral L	11		Parahippocampal gyrus R	106	
Superior frontal gyrus dorsolateral L	12		Lingual gyrus L	119	
Superior frontal gyrus dorsolateral L	13		Middle occipital gyrus L	126	
Superior frontal gyrus dorsolateral L	14		Middle occipital gyrus L	127	
Superior frontal gyrus dorsolateral R	19		Inferior occipital gyrus L	130	
Superior frontal gyrus dorsolateral R	20		Middle temporal gyrus L	203	
Superior frontal gyrus dorsolateral R	22	Inferior temporal gyrus L	211		

	Superior frontal gyrus dorsolateral R	23	Ventral frontal	Precentral gyrus R	5
	Superior frontal gyrus, orbital part L	24		Middle frontal gyrus, orbital part L	39
	Superior frontal gyrus, orbital part L	25		Middle frontal gyrus, orbital part L	40
	Superior frontal gyrus, orbital part L	26		Middle frontal gyrus, orbital part R	42
	Superior frontal gyrus, orbital part R	28		Middle frontal gyrus, orbital part R	43
	Superior frontal gyrus, orbital part R	29		Inferior frontal gyrus, opercular part L	45
	Superior frontal gyrus, orbital part R	31		Inferior frontal gyrus, opercular part R	46
	Superior frontal gyrus, orbital part R	32		Inferior frontal gyrus, triangular part L	47
	Middle frontal gyrus L	33		Inferior frontal gyrus, triangular part R	48
	Middle frontal gyrus L	34		Inferior frontal gyrus, triangular part R	49
	Middle frontal gyrus R	35		Inferior frontal gyrus, orbital part L	50
	Middle frontal gyrus R	36		Inferior frontal gyrus, orbital part R	51
	Middle frontal gyrus R	37		Inferior frontal gyrus, orbital part R	52
	Middle frontal gyrus R	38		Olfactory cortex L	59
	Supplementary motor area R	58		Olfactory cortex R	60
Visual association right	Lingual gyrus R	120		Olfactory cortex R	61
	Superior occipital gyrus R	124		Rectal gyrus L	73
	Superior occipital gyrus R	125	Rectal gyrus L	74	
	Middle occipital gyrus R	128	Rectal gyrus L	76	
	Middle occipital gyrus R	129	Rectal gyrus L	77	

	Inferior occipital gyrus R	131
	Inferior temporal R	216
Temporoparietal	Hippocampus R	100
	Fusiform gyrus R	144
	Angular gyrus R	162
	Angular gyrus R	163
	Superior temporal gyrus R	188
	Superior temporal gyrus R	190
	Temporal pole: superior temporal gyrus L	195
	Temporal pole: superior temporal gyrus L	196
	Temporal pole: superior temporal gyrus L	197
	Temporal pole: superior temporal gyrus R	198
	Temporal pole: superior temporal gyrus R	199
	Temporal pole: superior temporal gyrus R	200
	Temporal pole: superior temporal gyrus R	201
	Temporal pole: superior temporal gyrus R	202
	Middle temporal gyrus R	205
	Middle temporal gyrus R	206

	Rectal gyrus R	80
	Rectal gyrus R	82
	Rectal gyrus R	83
	Insula L	84
	Insula L	85
	Insula R	87
	Anterior cingulate and paracingulate gyrus L	88
	Hippocampus L	99
	Hippocampus R	101
	Parahippocampal gyrus L	104
	Parahippocampal gyrus L	105
	Parahippocampal gyrus R	107
	Amygdala L	108
	Amygdala R	109
	Fusiform gyrus L	132
	Fusiform gyrus L	133
	Fusiform gyrus L	135
	Fusiform gyrus L	136

	Temporal pole: middle temporal gyrus L	207		Fusiform gyrus L	137
	Temporal pole: middle temporal gyrus L	208		Fusiform gyrus R	139
	Temporal pole: middle temporal gyrus L	209	Visual 2	Cuneus L	115
	Temporal pole: middle temporal gyrus R	210		Superior occipital gyrus L	122
	Inferior temporal gyrus L	214		Superior occipital gyrus L	123
	Inferior temporal gyrus R	217	Thalamus	Thalamus L	180
	Inferior temporal gyrus R	218		Thalamus R	181
	Inferior temporal gyrus R	219		Thalamus R	182
	Inferior temporal gyrus R	220			
	Inferior temporal gyrus R	221			
	Inferior temporal gyrus R	222			

6.2.6 Calculating metastability

All FC metastability analyses were performed in native functional space. Mean BOLD signals were transformed into complex phase representation using the Hilbert transform to obtain associated analytic signals. The analytic signal represents a narrowband signal, $s(t)$, in the time domain as a rotating vector with an instantaneous phase, $\phi(t)$, and instantaneous amplitude, $A(t)$, i.e., $s(t)=A(t)\cos(\phi(t))$. The phase and amplitude are given by the argument and the modulus, respectively, of the complex signal $z(t)$, given by $z(t)=s(t)+i.H[s(t)]$, where i is the imaginary unit and $H[s(t)]$ is the Hilbert transform of $s(t)$ (Glerean et al., 2012; Bedrosian et al., 1963). In order to avoid border effects

associated with the Hilbert transform the first and last ten time points were removed (Ponce-Alvarez et al., 2015). We computed the instantaneous phase values for each ICA and the Kuramoto order parameter, $R(t)$ (a proxy for the instantaneous whole-brain synchronization) was estimated for the set of regions comprising a RSN, and the set of regions comprising two RSNs when evaluating their interactions, as:

$$R_{RSN}(t) = \frac{1}{N} \sum_{k=1}^N e^{i\theta_k(t)}$$

where $K = \{1, \dots, N\}$ is region number and $\theta_k(t)$ is the instantaneous phase of oscillator k at time t . For each RSN, metastability (variation in synchronization over time) was defined as the standard deviation (SD) of R_{RSN} across time, and synchrony (mean synchrony) as the mean of R_{RSN} across time, where 0 indicates perfect asynchronization and 1 indicates perfect synchronization (Cabral et al., 2011; Deco & Kringelbach, 2016; Shanahan, 2010; Lee et al. 2017; Lee and Frangou 2017). We estimated global metastability by considering the interactions of all RSNs concomitantly. A large standard deviation of Kuramoto order parameter values would therefore characterize brains that traverse a broad set of dynamic states over time, measured as high metastability.

6.2.7 Statistical analysis

Group differences in demographic characteristics and motion parameters were examined using Mann-Whitney U-test and χ^2 tests where appropriate. We performed Analysis of Covariance (ANCOVA) to examine differences in network dynamics (synchrony and metastability) between RSNs. Sex, overall brain injury score, and number of motion outliers were entered as covariates in all analyses. For each ANCOVA, when the overall model was significant at $p < 0.05$, we conducted post-hoc pairwise comparisons for which

the threshold of statistical significance was adjusted using Bonferroni based on the number of variables in each model. Partial Spearman’s correlations were used to assess the association between metastability measures and PMA at scan, controlling for sex, overall brain injury score, and number of motion outliers. All statistical comparisons were performed using RStudio 1.1463 (The R Foundation for Statistical Computing, Vienna, Austria).

6.3 Results

6.3.1 Demographic and clinical characteristics

The study included 181 newborn infants, comprising 17 infants that defined the RSN, and 164 infants that were used in the metastability analysis. The median number of motion-outlier volumes in the term-born group used for ICA analysis was 5 (2-8) and for the metastability analysis was 26 (10.75-46) ($p=0.0011$, Mann-Whitney U-test). Details of demographic characteristics are shown in Table 6.2.

Table 6.2 Demographic characteristics of the study population

	Infants that defined RSN	Infants used for analysis
Group	Term-born infants scanned at 43.5-44.5 weeks PMA (n=17)	Term-born infants scanned at 37-43.5 weeks PMA (n=164)
Female, n (%)	12 (71%)	69 (42%)
GA at birth, median (IQR), weeks	40.71 (40.43-41.29)	40 (39-40.86)
Weight at birth, median (IQR), kg	3.75 (3.4-3.85)	3.35 (2.94-3.69)
PMA at scan, median (IQR), weeks	44 (43.71-44.14)	41 (39.96-42)
Head circumference, median (IQR), cm	36 (35.5-37.4)	33.5 (35-36)
Type of pregnancy		
Singleton, n (%)	17 (100%)	154 (94%)
Radiology score, n (%)		

Score 1	13 (76%)	79 (48%)
Score 2	4 (24%)	66 (40%)
Score 3	—	14 (9%)
Score 4	—	5 (3%)
Motion outliers median (IQR)	5 (2-8)	26 (10.75-46)

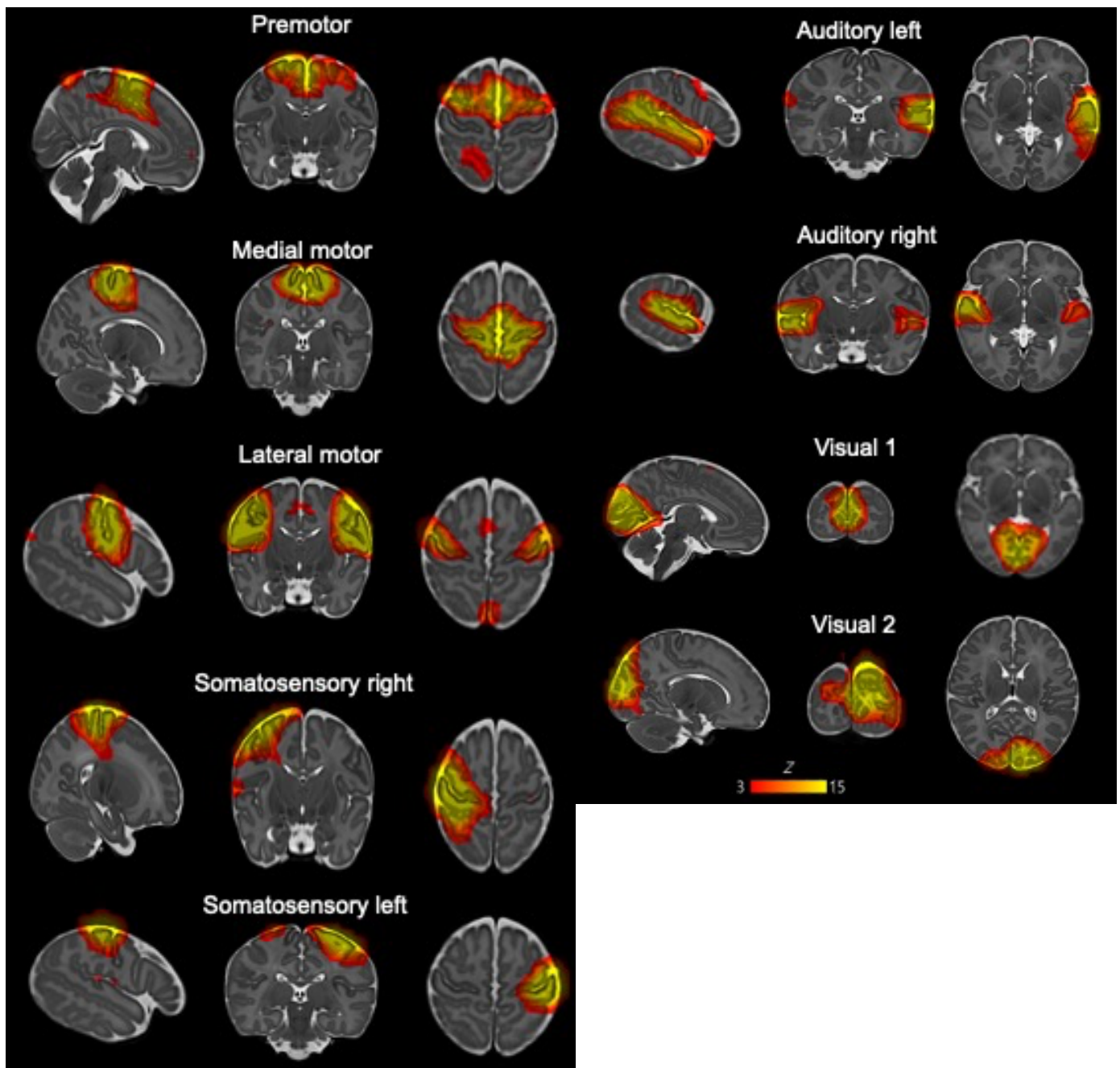
Abbreviations: RSN: resting state network, PMA: postmenstrual age at scan, IQR: interquartile range. Data presented as n (percent) or median and (IQRs)

Radiology score: Score 1: Normal appearance for age; Score 2: Incidental findings with unlikely significance for clinical outcome or analysis (e.g. subdural haemorrhage, isolated subependymal cysts, mild inferior vermis rotation); Score 3: Incidental findings with unlikely clinical significance but possible analysis significance (e.g. several punctate lesions or other focal white matter/ cortical lesions not thought to be of clinical significance); Score 4: Incidental findings with possible clinical significance. Unlikely analysis significance (e.g. isolated non brain anomaly for example on pituitary/ on tongue)

6.3.2 Resting state networks

17 RSNs were identified by group ICA in a subsample of term-born infants scanned between 43.5-44.5 weeks PMA (n=17). Nine RSNs including primary motor or sensory cortical areas categorized as primary networks: medial motor, lateral motor, premotor, somatosensory (left and right), visual (1, 2), auditory (left and right) were identified (Figure 6.1A). The remaining 8 RSNs were considered higher order/association networks: parietal (including inferior parietal lobule and superior parietal gyrus), posterior parietal (including the precuneus and posterior cingulate cortices), temporoparietal (including Broca's area and Wernicke's area), prefrontal (including cingulate gyrus, frontal gyrus and rectus gyrus), dorsal frontal (including frontal and SMA), ventral frontal (including medial prefrontal cortex, association cortices, anterior cingulate and insula) and visual association left and right networks (including occipital and temporal cortices and parahippocampus) (Figure 6.1B). Figure 6.1 shows RSN spatial maps captured by group-ICA.

A) Primary order RSN



B) Higher order RSN

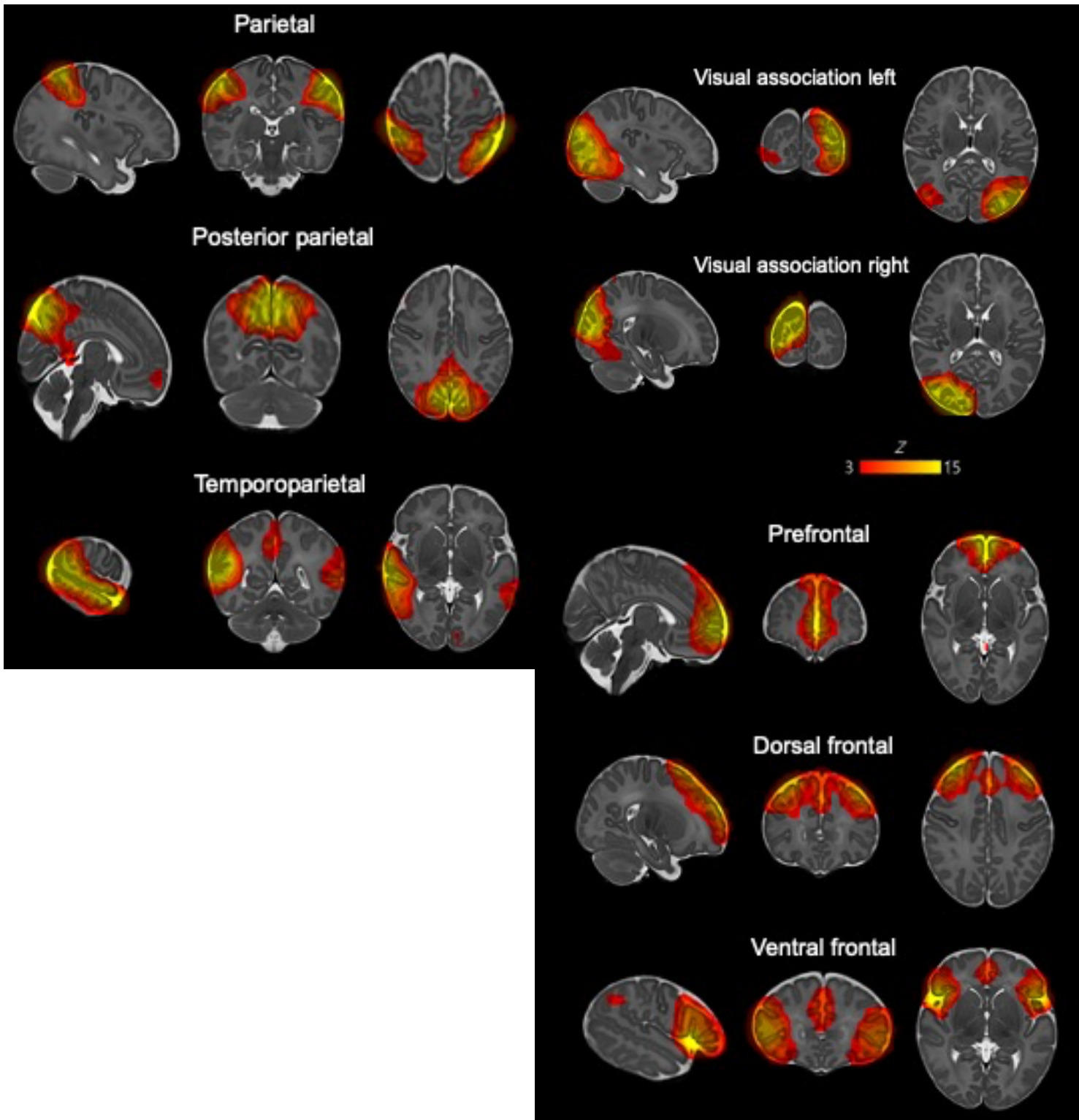


Figure 6.1 Spatial maps of resting state networks (RSNs) identified by group independent component analysis (ICA) in 17 term-born infants scanned at 43.5-44.5 weeks PMA. Example sagittal, coronal and sagittal slices for spatial patterns in primary (A) and higher-order (B) RSNs, thresholded at $Z > 3$ and overlaid on a T2 structural template (Schuh et al., 2018) displayed in radiological convention.

6.3.3 Metastability and synchrony within resting state networks

For each RSN, synchrony and metastability using phase-transformed rs-fMRI time series from 164 healthy neonates was computed. The distribution of global synchrony and metastability across participants and for each RSN is shown in Figure 6.2. The thalamus had the highest metastability (0.25 ± 0.01), while the lowest metastability was observed in temporoparietal network (0.18 ± 0.02). The highest synchrony values were observed in somatosensory left network (0.85 ± 0.05), and the lowest values were observed in temporoparietal network (0.41 ± 0.09). Analyses of covariance (covarying for sex, PMA at scan, brain injury score and number of motion outliers) showed that RSNs differed in metastability ($F_{17} = 68.04$; $p < 0.0001$) and synchrony ($F_{17} = 325.27$; $p < 0.0001$). Subsequent Bonferroni corrected post-hoc pairwise comparisons ($n=324$) showing significant differences in metastability and synchrony between RSNs is found in Supplementary table 6.1.

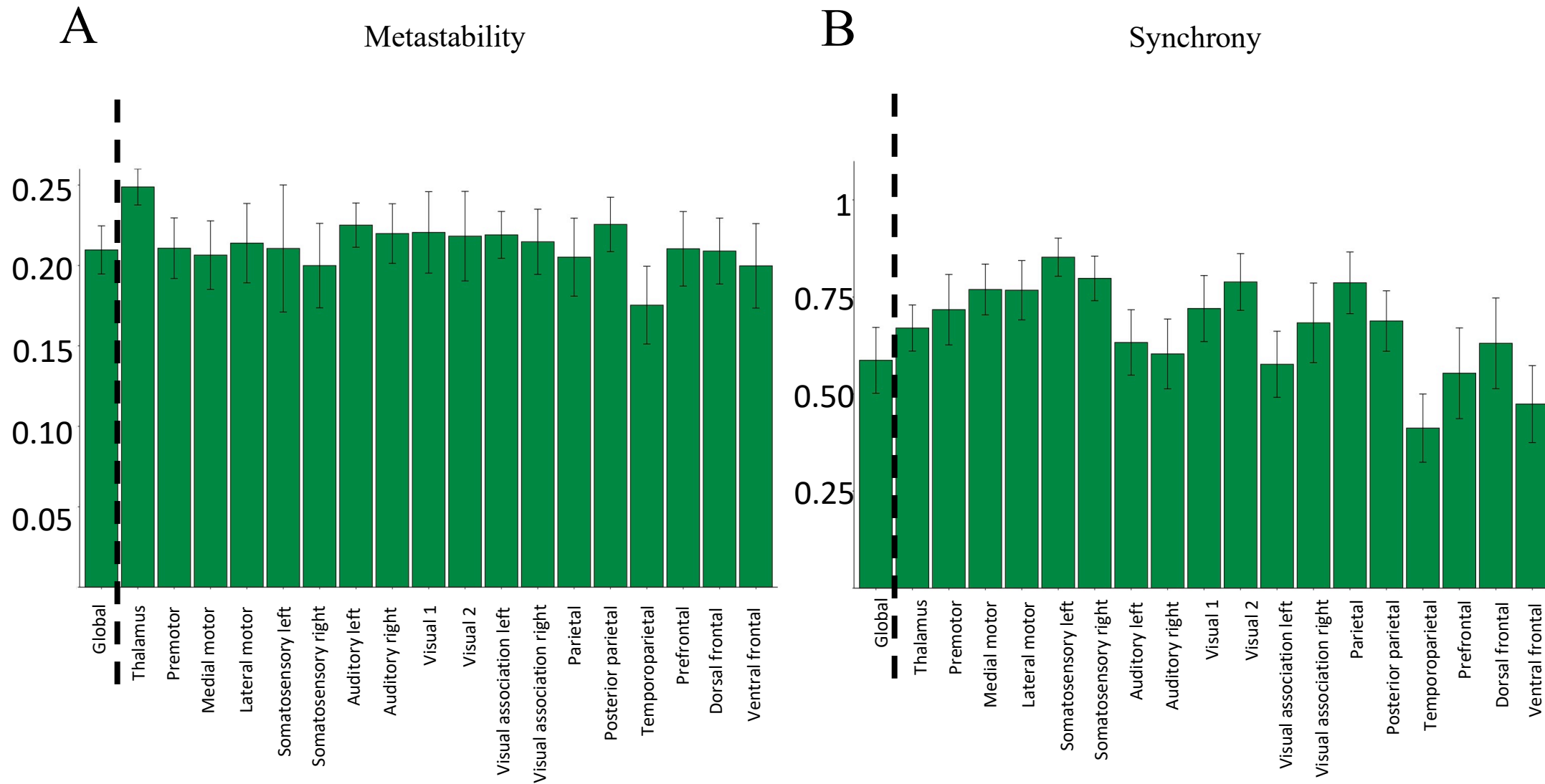
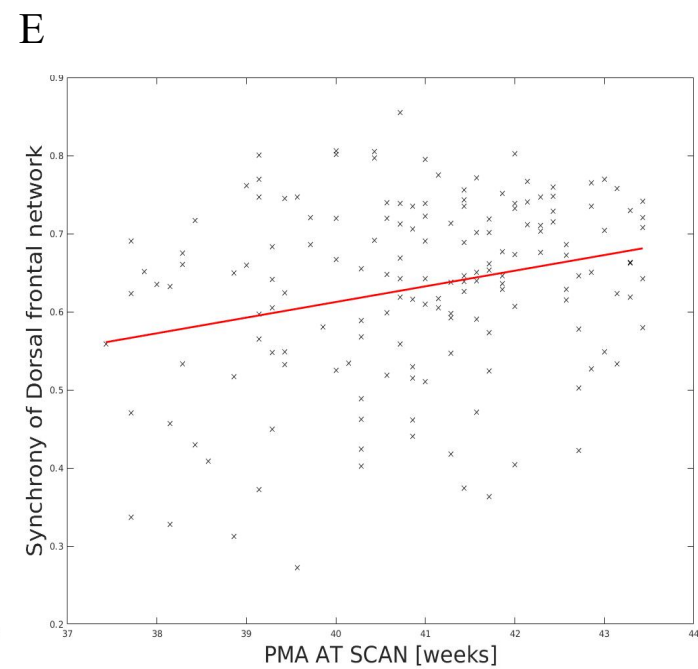
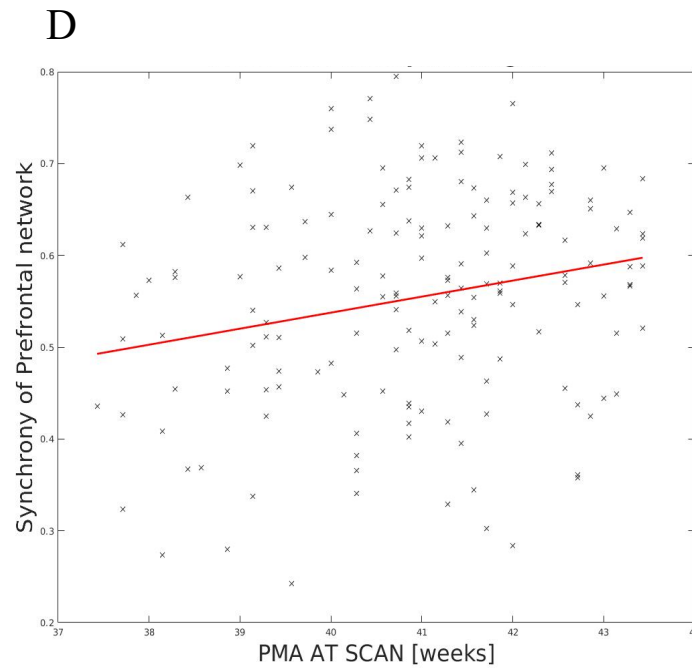
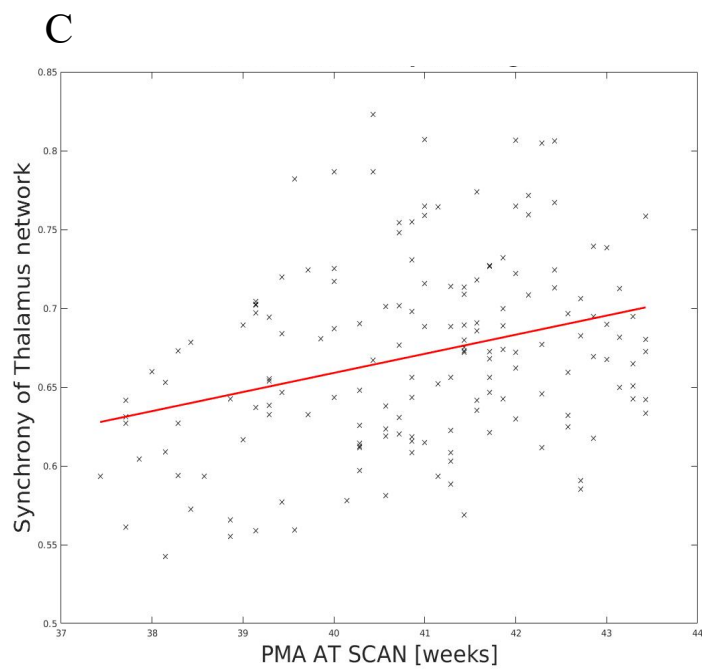
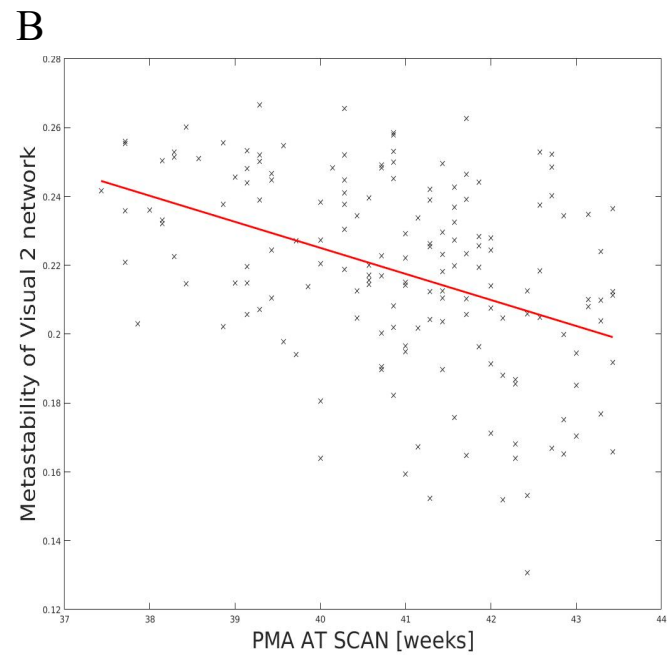
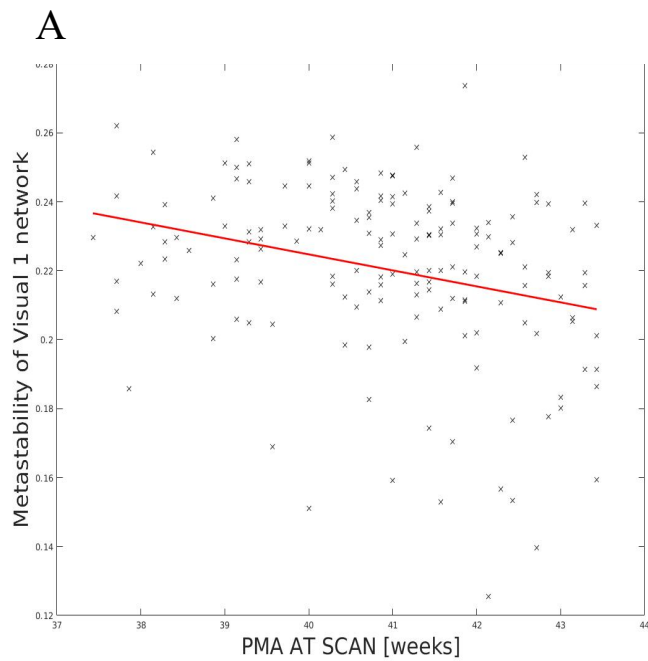


Figure 6.2 Resting state network metastability (A) and synchrony (B). Figures A and B show the mean and standard error of mean (SEM) of metastability and synchrony for each resting-state network (RSN) across term-born infants scanned at 37-43.5 weeks PMA.

6.3.4 Effect of postmenstrual age at scan

To characterize normal development in dynamic network properties in term born infants scanned from 37–43.5 weeks, we analysed the association between metastability and synchrony of RSNs and PMA at scan. Increasing postmenstrual age at scan was negatively associated with metastability of visual 1 (figure 6.3A) and visual 2 networks (figure 6.3B) (Visual 1: $\rho=-0.288$, $p=0.0002$; Visual 2: $\rho=-0.399$, $p<0.0001$, FDR-corrected). Increasing postmenstrual age at scan was also positively correlated with synchrony of the thalamus (figure 6.3C), prefrontal (figure 6.3D), dorsal frontal (figure 6.3E), visual 1 (figure 6.3F), visual association networks (figure 6.3G) and global synchrony (figure 6.3H) (thalamus: $\rho=0.302$, $p<0.0001$; prefrontal: $\rho=0.191$, $p=0.0409$; dorsal frontal: $\rho=0.206$, $p=0.0310$; visual 1: $\rho=0.395$, $p<0.0001$; visual association right: $\rho=0.272$, $p=0.0023$; global synchrony: $\rho=0.157$, $p<0.001$, FDR-corrected).



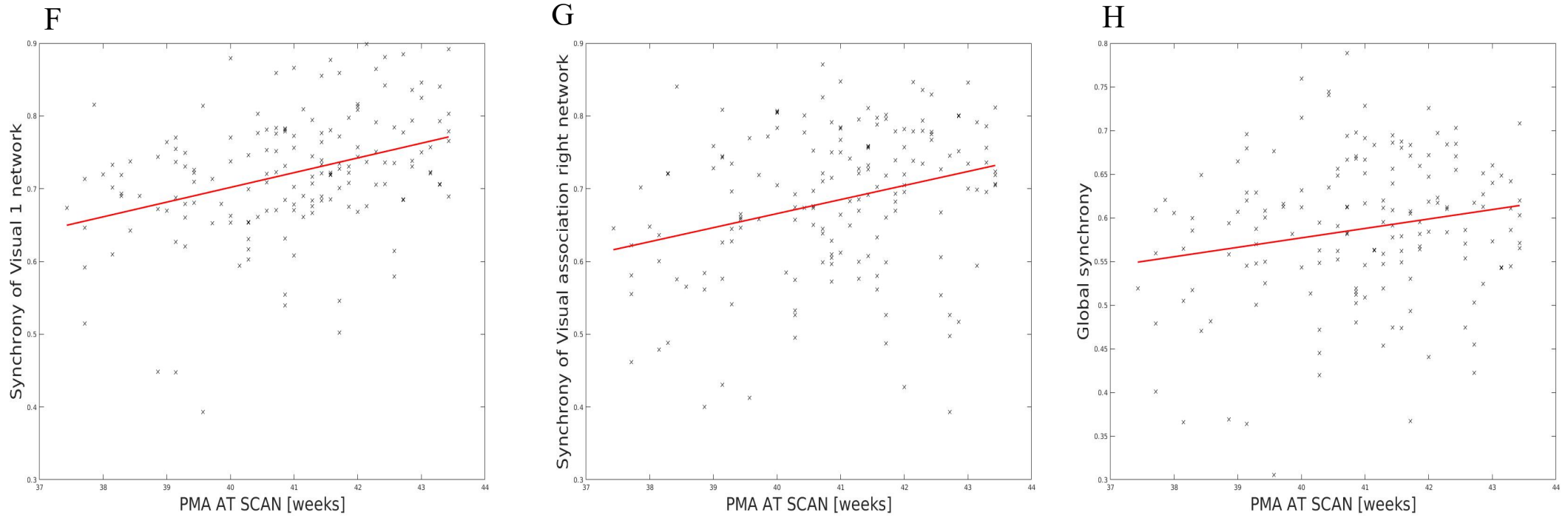


Figure 6.3 Relationship between postmenstrual age at scan (PMA) and resting state network metastability and synchrony in term-born infants scanned at 37-43.5 weeks PMA.

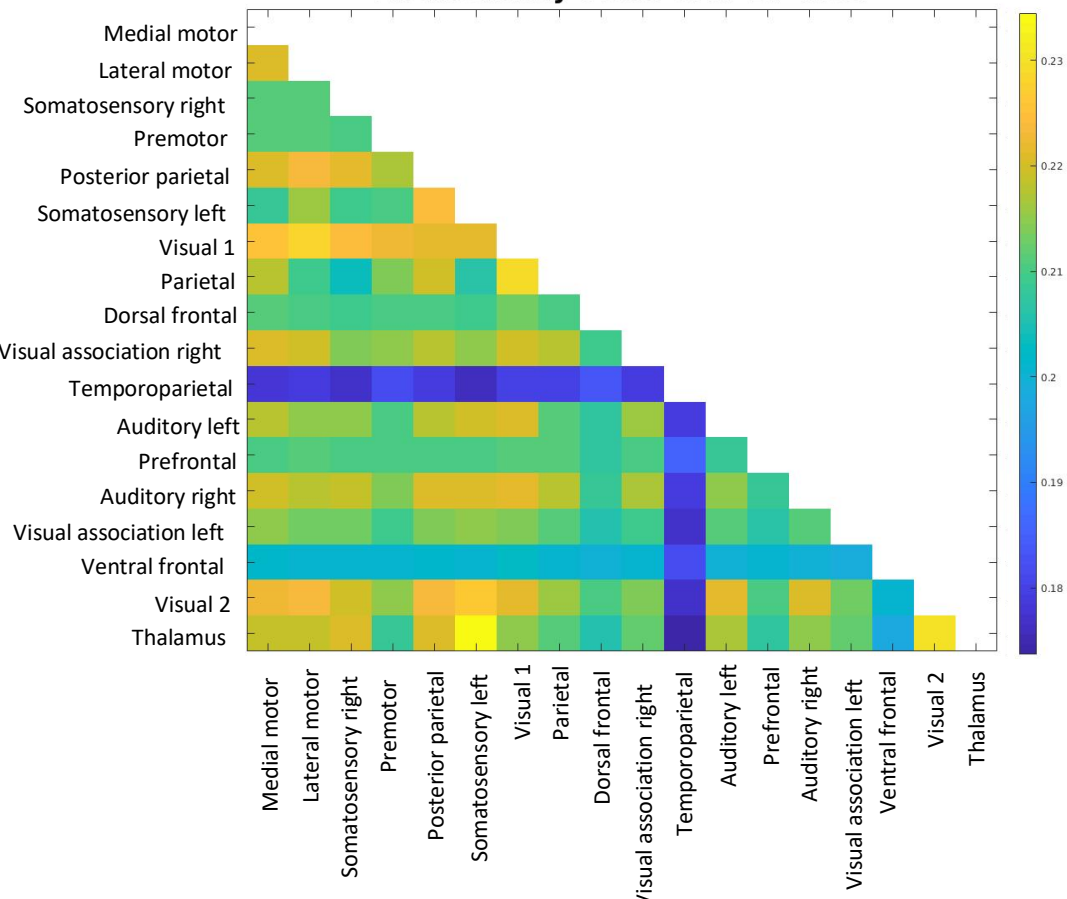
6.3.5 Metastability and synchrony between resting state networks

We then estimated an 'interaction matrix' reflecting the metastable and synchronous interactions of the 17 RSNs and thalamus for each infant. The average interaction matrix for metastability and synchrony are shown in figure 6.4.

Primary-order RSNs including visual 1 and 2, medial and lateral motor, somatosensory left and right, auditory left and right, and thalamus had high metastable interactions with other primary-order RSN, but lower metastable interactions with higher-order RSNs. Higher-order RSNs including prefrontal, dorsal and ventral frontal, visual association left and right, parietal and temporoparietal had low metastable interactions with all other RSNs.

Primary order RSNs including lateral motor, somatosensory left and right, visual 1 and 2 had high synchronous interactions with other primary order RSNs and lower synchronous interactions with higher-order RSNs, while higher-order RSNs had low synchronous interactions with all RSNs.

Metastability 0.033-0.07 BP filter



Synchrony 0.033-0.07 BP filter

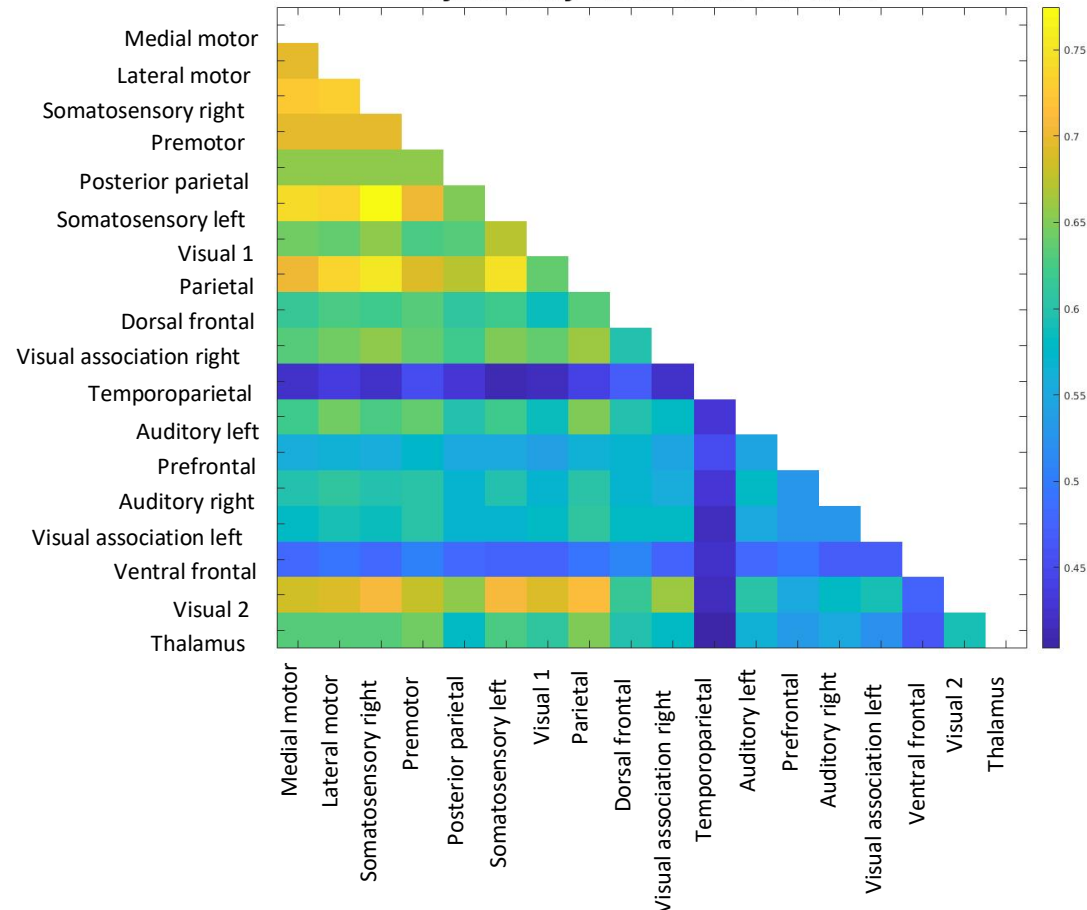


Figure 6.4 Average interaction matrix reflecting the metastable and synchronous interactions. Metastable interactions of the 17 resting state networks defined by group ICA and thalamus on the left. On the right, average interaction matrix reflecting the synchronous interactions of the 17 resting state networks and thalamus.

6.4 Discussion

The present study evaluated dynamic FC estimated through use of the Kuramoto order within- and between RSNs and determined the association of dynamic FC of RSNs with increasing age at scan. The findings presented here complement previous static FC studies in early development and provide novel insights into the brain's functional organization during this period.

We identified nine primary order RSNs involved in somatomotor, auditory and visual processing, and eight higher-order/association RSNs in line with previous studies at this age (Doria et al., 2010; Fransson et al., 2007; 2009; Fransson et al., 2007; Smyser et al., 2010; Gao et al., 2014; Gao et al., 2015; Fransson et al., 2011; Eyre et al., 2020).

Additionally, we found that the thalamus had the highest metastability indicating greater variation in mean phase coherence over time. This suggests the thalamus has flexible interactions between network regions enabling exploratory cognitive states and efficient responses to changing external inputs (Werner, 2007; Deco et al., 2009; Fritz et al., 2010; Power et al. 2011; Smith et al. 2009). The thalamus plays a critical role as the relay centre of sensory, motor and cognitive signals in the brain, which are essential for early survival (Smyser et al., 2016; Jones, 2000, 2007; Parnaudeau et al., 2018). Moreover, the vulnerability of this structure to early disruptions in populations at risk of impairments has been demonstrated in preterm infants (Boardman et al., 2006; Nosarti et al., 2008; Ball et al., 2012), infants with NE (Miller et al., 2005; de Vries et al., 2010; Martinez-Biarge et al., 2010; Ní Bhroin et al., 2020) and infants with CHD (Ní Bhroin et al., 2021). There is also evidence of an association between thalamus injury and impaired motor outcomes in infants with NE (Miller et al., 2005; de Vries et al., 2010; Ní Bhroin et al., 2020) and cognition in prematurity (Ball et al., 2015). Therefore, early disruptions (e.g. prematurity,

neonatal insults) may affect the brain such that dynamics of the thalamus become more stable.

The lowest metastability and synchrony was observed in the temporoparietal network, suggesting that brain regions of this brain network are not flexibly connected with each other. The temporoparietal network comprises regions associated with language function (Ferstl et al., 2008; Friederici et al., 2011; Vigneau et al., 2006; Dehaene-Lambertz et al., 2006; Redcay et al., 2008), and therefore, these findings may reflect largely immature language functioning at birth.

Primary order RSNs were found to have high metastable and synchronous interactions with other primary order RSNs, and higher-order RSNs had low metastable and synchronous interactions with all other RSNs. These differences may be due to primary order RSNs maturing earlier than higher-order RSNs and correspond to changes in brain structure, whereby an extended period of structural development takes place in association regions compared with primary regions (Gao et al. 2015a, 2015b; Cao et al. 2017). The maturational sequence of brain function and structure means the resources of the infant brain are concentrated on primary RSNs which are essential for early survival, followed by prolonged development of higher-order RSNs (Cole et al., 2013).

We also found visual networks demonstrated decreased dynamic flexibility with increasing age at scan. This finding is consistent with a previous study showing decreased temporal dynamics within the visual network in the first two years of age (Wen et al., 2020) and provides additional evidence for different developmental patterns between primary and higher-order RSNs. Additionally, association networks had increased dynamic flexibility

with increasing age at scan. A previous study showed that dynamic flexibility of higher-order networks develop in the first two years of life reflecting the continuing maturation of cognitive flexibility for performing high-level functions (Wen et al., 2020). Indeed, in adults association brain areas display higher temporal variability than primary brain areas (Zhang et al., 2016). As the brain matures, the number of possible functional network states is increased to respond to various new emerging external stimuli. Therefore, the brain becomes optimized as a more variable system to ensure the information processing capacity among the increasing number of brain states (Deco et al., 2009). Taken together, our findings highlight the relevance of investigating neural dynamics in neonates, and offers a potential theoretical framework for linking resting state activity to cognition and behaviour and a basis to better understand how early disruptions may affect brain metastable neural dynamics.

Our study has some limitations. First, rs-fMRI is sensitive to subject motion (Power et al. 2012; Van Dijk et al. 2012), therefore to decrease the effects of motion-related noise in our data, we scrubbed volumes with a frame-wise displacement exceeding 0.5 mm.

Furthermore, the lack of monitoring of cardiac and respiratory effects represents another limitation of the present study. Lastly, there are numerous statistical concerns regarding whether resting-state FC reflects genuine neural network dynamics or artefacts such as head motion (Laumann et al., 2016) or signal processing steps (Leonardi & Van de Ville, 2015). Hence we suggest that evaluation of these possible explanatory factors of variability in network dynamics account for these effects in future studies.

6.5 Conclusion

The present study used computational modelling (using the Kuramoto oscillator model) to test whether spontaneous brain activity in the functional organisation of the infant brain operates in a metastable state. Our findings suggest that the thalamus plays a strong role in cognitive flexibility in the neonate brain. We also provide evidence of metastability in primary resting state networks maturing earlier than the higher-order resting state networks, consistent with many conventional static FC studies. Overall, these findings highlight the relevance of resting-state metastable neural dynamics in neonates, and offers a potential theoretical framework for linking altered resting state activity due to early disruptions (e.g. prematurity, neonatal insults) and associated neurodevelopmental impairments.

Chapter 7: Discussion

7.1 Summary of findings

Despite reductions in mortality after neonatal brain injury in recent decades, improvements in motor, language and cognitive outcomes has been comparatively modest. Advanced imaging modalities have dramatically advanced our understanding of the human brain, however, our understanding of how brain development may be disrupted in individuals predisposed to neurodevelopmental disorders is limited. The studies included in this thesis examined the structure and function of the brain in early development in an attempt to provide further insight into how brain injury may disrupt typical neurodevelopment, and provide MR biomarkers of injury that have the potential to predict outcome. The key findings from Chapters 3-6 are summarised below.

In Chapter 3, we compared the ability of three MRI scoring systems (Barkovich, NICHD NRN and Weeke) to predict neurodevelopmental outcome at 2 years in infants with NE. MRI scoring systems have been developed to standardize the classification of findings on MRI and are established as good prognostic markers of outcome. Numerous scoring systems exist, however, there is no consensus which system should be used in clinical practice. Therefore, the scope of this chapter was to determine the prognostic ability of two conventional-based MRI scoring systems which evaluate well recognised patterns of injury, and a more detailed system which assesses all brain abnormalities observed using conventional MRI, DWI and H-MRS on a point-by-point basis. The findings from this chapter revealed that all three MRI scoring systems were associated with Bayley-III cognitive and motor composite scores, while only the more detailed Weeke score was associated with Bayley-III language composite scores at 2 years. This results suggests that

the inclusion of brain abnormalities such as intracranial haemorrhage and cerebellum as well as DWI and H-MRS which have not been incorporated into previous MRI systems may have added prognostic value. Therefore, this result lends support for the use of more detailed scoring systems due their added predictive value for language outcome and presents limitations of conventional based MRI scores.

In Chapter 4, evidence is provided for altered structural connectivity mainly affecting core regions belonging to the cortico-striatal-thalamic network. Previous MRI studies have identified a high incidence of acquired brain lesions and impaired brain development in newborns with CHD. Therefore this chapter investigated alterations in brain development by describing global organization properties of structural brain networks through the application of graph theory. The findings from this chapter suggest that regions associated with important aspects of behaviour including cognition, behaviour modulation, motor control, and emotion regulation are more vulnerable in newborns with CHD, and make progress towards understanding the reported neurodevelopmental sequelae associated with CHD. Interestingly, this analysis also revealed newborns with CHD had preserved infrastructure and integration, while disruption in segregation had a small effect size and was not statistically significant after the removal of outliers.

Since the results of Chapter 3 and Chapter 4 demonstrated alterations in brain structure in populations at-risk of neurodevelopmental impairment, we then wanted to identify altered brain function, quantified using resting state fMRI data, and examine its association with motor and language outcomes in individuals with a history of perinatal brain injury by performing a systematic review. The findings from this chapter revealed increased intra-

hemispheric FC, reduced inter-hemispheric FC and impaired lateralization of motor-related brain regions, as well as altered FC within and between primary order and higher-order networks associated with motor outcomes. Additionally, reduced intra-hemispheric FC, increased inter-hemispheric FC and right-hemisphere lateralization of language-related brain regions was associated with language outcomes.. Overall these findings suggest widespread alterations in rs-FC in individuals with a history of perinatal brain injury which remain compromised up to adulthood, and suggest that resting state fMRI may offer additional predictive utility in determining neurodevelopmental outcomes after perinatal brain injury.

Following the findings from Chapter 5 in which widespread alterations in rs-FC were associated with neurodevelopmental outcomes, we then wanted to better understand the dynamics of functional brain networks in the healthy neonate brain. This was performed in order to establish whether the healthy neonate brain operates in a metastable regime, and appreciate the differential patterns of brain network dynamics in early development. These findings have the potential to be used to advance our understanding of brain functional network activity in early development, and may prove useful as an early marker of atypical neurodevelopmental trajectories following injury. Therefore in Chapter 6, functional brain network dynamics was assessed by examining synchrony and metastability using resting-state fMRI data from a cohort of healthy neonates from the developing human connectome project. This analysis revealed the thalamus had the highest metastability compared with other RSNs, which suggests that the thalamus is the most temporally dynamic in the neonate brain, and is in a state of maximum network switching. This may be explained by the fact that the thalamus is involved in externally-driven functions, and therefore requires a greater capacity to alter its functional configuration in response to diverse and rapidly

changing external inputs. Interestingly, the lowest metastability was observed in the temporoparietal network, which suggests that brain regions in this network are not flexibly connected with each other. This network comprises regions associated with language functioning and therefore these findings may reflect largely immature language functioning at birth. We also found the thalamus and visual network had high metastable interactions with other primary order networks, and may reflect maturity of these networks at this age. Metastability of the visual network was found to decrease with increasing age at scan, providing additional evidence for different developmental patterns between primary and higher-order RSNs. Overall, the findings presented in this chapter may provide new references and valuable insights of brain functional activity in neonates and may have the potential to assist in the early identification of infants at risk of neurodevelopmental impairments.

Together the work of this thesis advance our previous knowledge of how altered brain structure and function after early injury may relate with later impairments and offers support for the use of neuroimaging biomarkers with the goal of improving neurodevelopmental outcomes. First, we found existing MRI scoring systems are predictive of neurodevelopmental outcomes in infants with NE, with more detailed scoring systems having added prognostic value. Next, we found altered structural connectivity in brain regions associated with important aspects of behaviour in newborns with CHD. We also found associations between altered functional connectivity and motor and language outcome after perinatal brain injury. And finally the findings from this thesis also highlight the relevance of understanding resting state neural dynamics to provide further insight into neurodevelopment

7.2 Future perspectives

Possible directions for future study to extend upon the work presented in this thesis are presented below

7.2.1 Does the inclusion of rs-fMRI in MRI scoring systems have added prognostic benefit

The findings from Chapter 3 demonstrated that structural MRI scoring systems were associated with motor and cognitive outcome but had limited predictive ability for language outcome. This suggests that even though structural MRI has high sensitivity for detecting brain injury related to neurodevelopmental outcome, its predictive ability remains limited. Future work might focus on understanding whether the inclusion of rs-fMRI as an additional modality for assessment in MRI scoring systems may have additional prognostic benefit. rs-fMRI is a non-invasive tool used to study brain function and organisation, with the potential to complement information available through imaging modalities that are currently used in MRI scores. rs-fMRI functional connectivity indirectly measures neural activity by assessing the temporal correlation of spontaneous, low-frequency (<0.1Hz) fluctuations in BOLD signal across the brain while the subject is at rest (Biswal et al., 1995). The findings from the systematic review in Chapter 5 highlight the feasibility of rs-fMRI to explore alterations in RSNs after perinatal brain injury and its association with outcome and also suggest that the inclusion of rs-fMRI in future MRI scoring systems may have additional predictive utility. Specifically, altered functional connectivity in regions important for language functioning remote from the primary lesioned area was revealed to be associated with language outcome (Dick et al., 2013, Carlson et al., 2019; Francois et al., 2019). Additionally, in studies assessing motor outcome, statistically significant associations between altered functional connectivity and

motor functioning was revealed (Woodward et al., 2019; Simon-Martinez et al., 2019; Qin et al., 2019; Linke et al., 2018; Qin et al., 2018). These findings therefore suggest that early alterations of RSN present a correlation with clinical manifestation, and support the use of rs-fMRI for early diagnostics and treatment.

7.2.1 Is altered structural connectivity associated with neurodevelopmental outcome in CHD?

Many survivors of CHD are at increased risk of neurodevelopmental impairments affecting multiple domains such as executive functioning, cognition, motor and language skills and behavioural impairments (Gaynor et al., 2015; Latal et al., 2016). Therefore, an understanding of the mechanisms underpinning impaired neurodevelopment is of crucial importance. In Chapter 4 we reported intact global network topology but reduced structural brain connectivity in a sub-network affecting the basal ganglia, amygdala, hippocampus, cerebellum, vermis, and temporal and parieto-occipital lobe. However, we were not able to assess the relationship between neonatal brain network organization and subsequent outcome as the infants with CHD in this thesis did not have neurodevelopmental outcome data available. This relationship has not been previously characterized; therefore, it will be important for future studies to assess this.

Neurodevelopmental follow-up of this cohort is underway, and we will be able to understand the association between altered structural brain network topology identified in Chapter 4 with subsequent outcome once this phase is complete.

7.2.2 What are the consequences of neonatal brain injury on metastability and synchrony of RSNs in the brain?

Another approach is to link dynamic neural activity, the structural connectivity and neurodevelopment. Studies have found that healthy neural dynamics operate in a

metastable regime, however, little is known of how disruptions to network topology affect these neural dynamics following neonatal brain injury. A previous study in traumatic brain injury patients (Hellyer et al., 2015) investigated the relationship between metastable neural dynamics and cognition, and found decreased neural metastability was associated with structural connectivity damage, reduced information processing and cognitive flexibility. The findings from this study suggest that altered resting-state dynamics may be a clinical correlate of neurocognitive impairments, and highlight the relevance of utilising this investigational approach in infants with brain injury. This was one of the topics of my PhD however due to timing constraints, the analysis of resting-state metastable neural dynamics was instead performed in a cohort of healthy neonates. The findings from Chapter 6 could be used to serve as a reference to provide valuable insights of brain functional activity in neonates and may assist in the early identification of infants at risk of neurodevelopmental impairments. rs-fMRI data is currently being collected in a cohort of infants with NE by our research group and the impact of neonatal brain injury on metastability and synchrony of RSNs in the brain will be assessed in future studies.

7.3 Limitations

Although limitations encountered within each study have been discussed, there are some notable limitations of this thesis that should be noted.

Most of the studies had small sample sizes and we should be cautious not to over interpret the findings presented in this thesis. Therefore replication and further comparison using larger populations is needed. Additionally, another limitation encountered in Chapter 2 is the attrition rate. However, we found minimal statistical differences in demographic and clinical factors between the cohort that was examined and those who did not return for

follow-up. Also, previous studies have found that individuals lost to follow-up may be at greatest risk of psychosocial disadvantage (Wolke et al., 2009) and it will be important for future studies to assess this.

There was also a variety of exclusion criteria implemented by the different studies in this thesis which could have influenced the generalisability of findings. Furthermore, we included distinct NE and CHD subtypes in our studies in order to give a true reflection of the clinical profile. Future studies should explore the underlying aetiological pathways leading to distinct NE, stroke, and CHD subtypes and how this might impact the findings identified in this thesis and their clinical implications.

The long-term adverse neurodevelopmental consequences of perinatal brain injury highlight the need for identifying early biomarkers of neurodevelopmental impairment. While this thesis highlights the benefits of utilising advanced MRI techniques, the lack of outcome data in some of the studies included here restricts the interpretation of our results. It will be important for future studies to understand the predictive value of some of the findings presented in this thesis.

7.4 Conclusions

The overall aim of this thesis was to better understand atypical brain development after perinatal brain injury with the goal of improving outcomes for these infants by identification of neuroimaging biomarkers. The studies presented in this thesis reveal the adverse effects of perinatal risk factors on the developing brain by demonstrating altered brain structure and function in infants at risk of neurodevelopmental impairments. Specifically we identified associations between MRI scoring systems with cognitive,

motor and language outcome in infants with NE, and altered rs-fMRI functional connectivity and motor and language outcome after perinatal brain injury. We also identified altered structural network topology in infants with CHD. Lastly, resting-state dynamics in a cohort of healthy neonates was characterised. The findings in this thesis are potentially valuable for understanding atypical brain development as well as for the development of future biomarkers of abnormal brain development for infants after PBI.

References

- Achard, S., & Bullmore, E. (2007). Efficiency and cost of economical brain functional networks. *PLoS computational biology*, *3*(2), e17. doi: 10.1371/journal.pcbi.0030017
- Al Amrani, F., Kwan, S., Gilbert, G., Saint-Martin, C., Shevell, M., & Wintermark, P. (2017). Early Imaging and Adverse Neurodevelopmental Outcome in Asphyxiated Newborns Treated With Hypothermia. *Pediatric neurology*, *73*, 20–27. doi: 10.1016/j.pediatrneurol.2017.04.025
- Al Amrani, F., Marcovitz, J., Sanon, P. N., Khairy, M., Saint-Martin, C., Shevell, M., & Wintermark, P. (2018). Prediction of outcome in asphyxiated newborns treated with hypothermia: Is a MRI scoring system described before the cooling era still useful?. *European journal of paediatric neurology : EJPN : official journal of the European Paediatric Neurology Society*, *22*(3), 387–395. doi: 10.1016/j.ejpn.2018.01.017
- Alcauter, S., Lin, W., Smith, J. K., Short, S. J., Goldman, B. D., Reznick, J. S., Gilmore, J. H., & Gao, W. (2014). Development of thalamocortical connectivity during infancy and its cognitive correlations. *The Journal of neuroscience : the official journal of the Society for Neuroscience*, *34*(27), 9067–9075. doi: 10.1523/JNEUROSCI.0796-14.2014
- Alcauter, S., Lin, W., Smith, J. K., Goldman, B. D., Reznick, J. S., Gilmore, J. H., & Gao, W. (2015). Frequency of spontaneous BOLD signal shifts during infancy and correlates with cognitive performance. *Developmental cognitive neuroscience*, *12*, 40–50. doi: 10.1016/j.dcn.2014.10.004
- Alderliesten, T., Nikkels, P. G., Benders, M. J., de Vries, L. S., & Groenendaal, F. (2013). Antemortem cranial MRI compared with postmortem histopathologic examination of the brain in term infants with neonatal encephalopathy following perinatal asphyxia. *Archives of disease in childhood. Fetal and neonatal edition*, *98*(4), F304–F309. doi: 10.1136/archdischild-2012-301768
- Ancora, G., Testa, C., Grandi, S., Tonon, C., Sbravati, F., Savini, S., Manners, D. N., Gramegna, L. L., Tani, G., Malucelli, E., Corvaglia, L. T., Faldella, G., & Lodi, R. (2013). Prognostic value of brain proton MR spectroscopy and diffusion tensor imaging in newborns with hypoxic-ischemic encephalopathy treated by brain cooling. *Neuroradiology*, *55*(8), 1017–1025. doi: 10.1007/s00234-013-1202-5
- Andersen, R. A., & Cui, H. (2009). Intention, action planning, and decision making in parietal-frontal circuits. *Neuron*, *63*(5), 568–583. doi: 10.1016/j.neuron.2009.08.028
- Anderson, A. L., & Thomason, M. E. (2013). Functional plasticity before the cradle: a review of neural functional imaging in the human fetus. *Neuroscience and biobehavioral reviews*, *37*(9 Pt B), 2220–2232. doi: 10.1016/j.neubiorev.2013.03.013
- Andropoulos, D. B., Ahmad, H. B., Haq, T., Brady, K., Stayer, S. A., Meador, M. R., Hunter, J. V., Rivera, C., Voigt, R. G., Turcich, M., He, C. Q., Shekerdemian, L. S., Dickerson, H. A., Fraser, C. D., Dean McKenzie, E., Heinle, J. S., & Blaine Easley, R. (2014). The association between brain injury, perioperative anesthetic exposure, and 12-month neurodevelopmental outcomes after neonatal cardiac surgery: a retrospective cohort study. *Paediatric anaesthesia*, *24*(3), 266–274. doi: 10.1111/pan.12350
- Annink, K. V., de Vries, L. S., Groenendaal, F., Eijssermans, R., Mocking, M., van Schooneveld, M., Dudink, J., van Straaten, H., Benders, M., Lequin, M., & van der Aa, N. E. (2021). Mammillary body atrophy and other MRI correlates of school-age outcome following neonatal hypoxic-ischemic encephalopathy. *Scientific reports*, *11*(1), 5017. doi: 10.1038/s41598-021-83982-8
- Annink, K. V., de Vries, L. S., Groenendaal, F., van den Heuvel, M. P., van Haren, N., Swaab, H., van Handel, M., Jongmans, M. J., Benders, M. J., & van der Aa, N. E. (2019). The

- long-term effect of perinatal asphyxia on hippocampal volumes. *Pediatric research*, 85(1), 43–49. doi: 10.1038/s41390-018-0115-8
- Arichi, T., Moraux, A., Melendez, A., Doria, V., Groppo, M., Merchant, N., Combs, S., Burdet, E., Larkman, D. J., Counsell, S. J., Beckmann, C. F., & Edwards, A. D. (2010). Somatosensory cortical activation identified by functional MRI in preterm and term infants. *NeuroImage*, 49(3), 2063–2071. doi: 10.1016/j.neuroimage.2009.10.038
- Aslam, S., Strickland, T., & Molloy, E. J. (2019). Neonatal Encephalopathy: Need for Recognition of Multiple Etiologies for Optimal Management. *Frontiers in pediatrics*, 7, 142. doi: 10.3389/fped.2019.00142
- Avants, B. B., Epstein, C. L., Grossman, M., & Gee, J. C. (2008). Symmetric diffeomorphic image registration with cross-correlation: evaluating automated labeling of elderly and neurodegenerative brain. *Medical image analysis*, 12(1), 26–41. doi: 10.1016/j.media.2007.06.004
- Azzopardi, D., Strohm, B., Marlow, N., Brocklehurst, P., Deierl, A., Eddama, O., Goodwin, J., Halliday, H. L., Juszczak, E., Kapellou, O., Levene, M., Linsell, L., Omar, O., Thoresen, M., Tusor, N., Whitelaw, A., Edwards, A. D., & TOBY Study Group (2014). Effects of hypothermia for perinatal asphyxia on childhood outcomes. *The New England journal of medicine*, 371(2), 140–149. doi: 10.1056/NEJMoa1315788
- Azzopardi, D., & Edwards, A. D. (2010). Magnetic resonance biomarkers of neuroprotective effects in infants with hypoxic ischemic encephalopathy. *Seminars in fetal & neonatal medicine*, 15(5), 261–269. doi: 10.1016/j.siny.2010.03.001
- Badawi, N., Kurinczuk, J. J., Keogh, J. M., Alessandri, L. M., O'Sullivan, F., Burton, P. R., Pemberton, P. J., & Stanley, F. J. (1998). Intrapartum risk factors for newborn encephalopathy: the Western Australian case-control study. *BMJ (Clinical research ed.)*, 317(7172), 1554–1558. doi: 10.1136/bmj.317.7172.1554
- Barnett, A., Mercuri, E., Rutherford, M., Haataja, L., Frisone, M. F., Henderson, S., Cowan, F., & Dubowitz, L. (2002). Neurological and perceptual-motor outcome at 5 - 6 years of age in children with neonatal encephalopathy: relationship with neonatal brain MRI. *Neuropediatrics*, 33(5), 242–248. doi: 10.1055/s-2002-36737
- Boichot, C., Walker, P. M., Durand, C., Grimaldi, M., Chapuis, S., Gouyon, J. B., & Brunotte, F. (2006). Term neonate prognoses after perinatal asphyxia: contributions of MR imaging, MR spectroscopy, relaxation times, and apparent diffusion coefficients. *Radiology*, 239(3), 839–848. doi: 10.1148/radiol.2393050027
- Bourgeois, J. P., & Rakic, P. (1993). Changes of synaptic density in the primary visual cortex of the macaque monkey from fetal to adult stage. *The Journal of neuroscience : the official journal of the Society for Neuroscience*, 13(7), 2801–2820. doi: 10.1523/JNEUROSCI.13-07-02801.1993
- Bourgeois, J. P. (1997). Synaptogenesis, heterochrony and epigenesis in the mammalian neocortex. *Acta paediatrica (Oslo, Norway : 1992). Supplement*, 422, 27–33. doi: 10.1111/j.1651-2227.1997.tb18340.x
- Ball, G., Srinivasan, L., Aljabar, P., Counsell, S. J., Durighel, G., Hajnal, J. V., Rutherford, M. A., & Edwards, A. D. (2013). Development of cortical microstructure in the preterm human brain. *Proceedings of the National Academy of Sciences of the United States of America*, 110(23), 9541–9546. doi: 10.1073/pnas.1301652110
- Ball, G., Aljabar, P., Zebari, S., Tusor, N., Arichi, T., Merchant, N., Robinson, E. C., Ogundipe, E., Rueckert, D., Edwards, A. D., & Counsell, S. J. (2014). Rich-club organization of the newborn human brain. *Proceedings of the National Academy of Sciences of the United States of America*, 111(20), 7456–7461. doi: 10.1073/pnas.1324118111

- Bano, S., Chaudhary, V., & Garga, U. C. (2017). Neonatal Hypoxic-ischemic Encephalopathy: A Radiological Review. *Journal of pediatric neurosciences*, *12*(1), 1–6. doi: 10.4103/1817-1745.205646
- Barkovich, A. J., Kjos, B. O., Jackson, D. E., Jr, & Norman, D. (1988). Normal maturation of the neonatal and infant brain: MR imaging at 1.5 T. *Radiology*, *166*(1 Pt 1), 173–180. doi: 10.1148/radiology.166.1.3336675
- Barkovich, A. J., Hajnal, B. L., Vigneron, D., Sola, A., Partridge, J. C., Allen, F., & Ferriero, D. M. (1998). Prediction of neuromotor outcome in perinatal asphyxia: evaluation of MR scoring systems. *AJNR. American journal of neuroradiology*, *19*(1), 143–149.
- Barkovich, A. J., Baranski, K., Vigneron, D., Partridge, J. C., Hallam, D. K., Hajnal, B. L., & Ferriero, D. M. (1999). Proton MR spectroscopy for the evaluation of brain injury in asphyxiated, term neonates. *AJNR. American journal of neuroradiology*, *20*(8), 1399–1405.
- Barkovich, A. J., Miller, S. P., Bartha, A., Newton, N., Hamrick, S. E., Mukherjee, P., Glenn, O. A., Xu, D., Partridge, J. C., Ferriero, D. M., & Vigneron, D. B. (2006). MR imaging, MR spectroscopy, and diffusion tensor imaging of sequential studies in neonates with encephalopathy. *AJNR. American journal of neuroradiology*, *27*(3), 533–547.
- Barr, R., Hayne, H. (2003). It's not what you know, its who you know: older siblings facilitate imitation during infancy. *International Journal of Early years Education* *11*, 7-21.
- Baslow M. H. (2000). Functions of N-acetyl-L-aspartate and N-acetyl-L-aspartylglutamate in the vertebrate brain: role in glial cell-specific signaling. *Journal of neurochemistry*, *75*(2), 453–459. doi: 10.1046/j.1471-4159.2000.0750453.x
- Batalle, D., Muñoz-Moreno, E., Tornador, C., Bargallo, N., Deco, G., Eixarch, E., & Gratacos, E. (2016). Altered resting-state whole-brain functional networks of neonates with intrauterine growth restriction. *Cortex; a journal devoted to the study of the nervous system and behavior*, *77*, 119–131. doi: 10.1016/j.cortex.2016.01.012
- Batalle, D., Hughes, E. J., Zhang, H., Tournier, J. D., Tusor, N., Aljabar, P., Wali, L., Alexander, D. C., Hajnal, J. V., Nosarti, C., Edwards, A. D., & Counsell, S. J. (2017). Early development of structural networks and the impact of prematurity on brain connectivity. *NeuroImage*, *149*, 379–392. doi: 10.1016/j.neuroimage.2017.01.065
- Bates, E., & Dick, F. (2002). Language, gesture, and the developing brain. *Developmental psychobiology*, *40*(3), 293–310. doi: 10.1002/dev.10034
- Batki, A., Baron-Cohen, S., Wheelwright, S., Connellan, J., Ahluwalia, J. (2000). Is there an innate gaze module? *Infant Behavior and Development*, *23*, 223-229. doi: 10.1016/S0163-6383(01)00037-6.
- Bayley, N. Bayley Scales of Infants and Toddler Development. 3rd ed. San Antonio (TX): Harcourt Assessment; 2006.
- Beca, J., Gunn, J. K., Coleman, L., Hope, A., Reed, P. W., Hunt, R. W., Finucane, K., Brizard, C., Dance, B., & Shekerdemian, L. S. (2013). New white matter brain injury after infant heart surgery is associated with diagnostic group and the use of circulatory arrest. *Circulation*, *127*(9), 971–979. doi: 10.1161/CIRCULATIONAHA.112.001089
- Beckmann, C. F., DeLuca, M., Devlin, J. T., & Smith, S. M. (2005). Investigations into resting-state connectivity using independent component analysis. *Philosophical transactions of the Royal Society of London. Series B, Biological sciences*, *360*(1457), 1001–1013. doi: 10.1098/rstb.2005.1634
- Bednarek, N., Mathur, A., Inder, T., Wilkinson, J., Neil, J., & Shimony, J. (2012). Impact of therapeutic hypothermia on MRI diffusion changes in neonatal encephalopathy. *Neurology*, *78*(18), 1420–1427. doi: 10.1212/WNL.0b013e318253d589

- Bedrosian, E. (1963). A product theorem for Hilbert transforms. *Proceedings of the IEEE*, *51*, 868-869.
- Ben-Shabat, E., Matyas, T. A., Pell, G. S., Brodtmann, A., & Carey, L. M. (2015). The Right Supramarginal Gyrus Is Important for Proprioception in Healthy and Stroke-Affected Participants: A Functional MRI Study. *Frontiers in neurology*, *6*, 248. doi: 10.3389/fneur.2015.00248
- Bellinger, D. C., Wypij, D., duPlessis, A. J., Rappaport, L. A., Jonas, R. A., Wernovsky, G., & Newburger, J. W. (2003). Neurodevelopmental status at eight years in children with dextro-transposition of the great arteries: the Boston Circulatory Arrest Trial. *The Journal of thoracic and cardiovascular surgery*, *126*(5), 1385–1396. doi: 10.1016/s0022-5223(03)00711-6
- Bellinger, D. C., Wypij, D., Rivkin, M. J., DeMaso, D. R., Robertson, R. L., Jr, Dunbar-Masterson, C., Rappaport, L. A., Wernovsky, G., Jonas, R. A., & Newburger, J. W. (2011). Adolescents with d-transposition of the great arteries corrected with the arterial switch procedure: neuropsychological assessment and structural brain imaging. *Circulation*, *124*(12), 1361–1369. doi: 10.1161/CIRCULATIONAHA.111.026963
- Belliveau, J. W., Kennedy, D. N., Jr, McKinstry, R. C., Buchbinder, B. R., Weisskoff, R. M., Cohen, M. S., Vevea, J. M., Brady, T. J., & Rosen, B. R. (1991). Functional mapping of the human visual cortex by magnetic resonance imaging. *Science*, *254*(5032), 716–719. doi: 10.1126/science.1948051
- Bergelson, E., & Swingle, D. (2012). At 6-9 months, human infants know the meanings of many common nouns. *Proceedings of the National Academy of Sciences of the United States of America*, *109*(9), 3253–3258. doi: 10.1073/pnas.1113380109
- Birn, R. M., Diamond, J. B., Smith, M. A., & Bandettini, P. A. (2006). Separating respiratory-variation-related fluctuations from neuronal-activity-related fluctuations in fMRI. *NeuroImage*, *31*(4), 1536–1548. doi: 10.1016/j.neuroimage.2006.02.048
- Biswal, B., Yetkin, F. Z., Haughton, V. M., & Hyde, J. S. (1995). Functional connectivity in the motor cortex of resting human brain using echo-planar MRI. *Magnetic resonance in medicine*, *34*(4), 537–541. doi: 10.1002/mrm.1910340409
- Bloch F, Hansen WW, Packard ME. (1946). Nuclear induction. *Physical Review*, *69*, 127.
- Bly, L. (1994). Motor skills acquisition in the first year. Therapy Skill Builders; San Antonio, TX.
- Boardman, J. P., Counsell, S. J., Rueckert, D., Kapellou, O., Bhatia, K. K., Aljabar, P., Hajnal, J., Allsop, J. M., Rutherford, M. A., & Edwards, A. D. (2006). Abnormal deep grey matter development following preterm birth detected using deformation-based morphometry. *NeuroImage*, *32*(1), 70–78. doi: 10.1016/j.neuroimage.2006.03.029
- Boardman, J. P., Ganesan, V., Rutherford, M. A., Saunders, D. E., Mercuri, E., & Cowan, F. (2005). Magnetic resonance image correlates of hemiparesis after neonatal and childhood middle cerebral artery stroke. *Pediatrics*, *115*(2), 321–326. doi: 10.1542/peds.2004-0427
- Boichot, C., Walker, P. M., Durand, C., Grimaldi, M., Chapuis, S., Gouyon, J. B., & Brunotte, F. (2006). Term neonate prognoses after perinatal asphyxia: contributions of MR imaging, MR spectroscopy, relaxation times, and apparent diffusion coefficients. *Radiology*, *239*(3), 839–848. doi: 10.1148/radiol.2393050027
- Bonifacio, S. L., deVries, L. S., & Groenendaal, F. (2015). Impact of hypothermia on predictors of poor outcome: how do we decide to redirect care?. *Seminars in fetal & neonatal medicine*, *20*(2), 122–127. doi: 10.1016/j.siny.2014.12.011
- Borgatti, S. P., Everett, M. G. (1999). Models of core/periphery structures. *Social Networks*, *21*, 375–395. doi: 10.1016/S0378-8733(99)00019-2.

- Brody, B. A., Kinney, H. C., Kloman, A. S., & Gilles, F. H. (1987). Sequence of central nervous system myelination in human infancy. I. An autopsy study of myelination. *Journal of neuropathology and experimental neurology*, *46*(3), 283–301. doi: 10.1097/00005072-198705000-00005
- Brown, C. J., Miller, S. P., Booth, B. G., Andrews, S., Chau, V., Poskitt, K. J., & Hamarneh, G. (2014). Structural network analysis of brain development in young preterm neonates. *NeuroImage*, *101*, 667–680. doi: 10.1016/j.neuroimage.2014.07.030
- Brown, R. (1828). A brief account of microscopical observations made in the months of June, July and August, 1827, on the particles contained in the pollen of plants; and on the general existence of active molecules in organic and inorganic bodies. *Philosophical Magazine*, *4*, 161–173.
- Bullmore, E., & Sporns, O. (2012). The economy of brain network organization. *Nature reviews. Neuroscience*, *13*(5), 336–349. doi: 10.1038/nrn3214
- Bullmore, E., & Sporns, O. (2009). Complex brain networks: graph theoretical analysis of structural and functional systems. *Nature reviews. Neuroscience*, *10*(3), 186–198. doi: 10.1038/nrn2575
- Burkhardt, B. E., Rücker, G., & Stiller, B. (2015). Prophylactic milrinone for the prevention of low cardiac output syndrome and mortality in children undergoing surgery for congenital heart disease. *The Cochrane database of systematic reviews*, (3), CD009515. doi: 10.1002/14651858.CD009515.pub2
- Bushnell, I. W. R., Sai, F., Mullin, J.T. (1989). Neonatal recognition of the mother's face. *British Journal of Developmental Psychology*, *7*, 3-15.
- Bushnell, I.W.R. (2001). Mother's face recognition in newborn infants: learning and memory. *Infants and Child Development*, *10*, 67-74. doi:10.1002/icd.248
- Cabral, J., Hugues, E., Sporns, O., & Deco, G. (2011). Role of local network oscillations in resting-state functional connectivity. *NeuroImage*, *57*(1), 130–139. doi: 10.1016/j.neuroimage.2011.04.010
- Calhoun, V. D., Miller, R., Pearlson, G., & Adalı, T. (2014). The chronnectome: time-varying connectivity networks as the next frontier in fMRI data discovery. *Neuron*, *84*(2), 262–274. doi: 10.1016/j.neuron.2014.10.015
- Cao, M., He, Y., Dai, Z., Liao, X., Jeon, T., Ouyang, M., Chalak, L., Bi, Y., Rollins, N., Dong, Q., & Huang, H. (2017). Early Development of Functional Network Segregation Revealed by Connectomic Analysis of the Preterm Human Brain. *Cerebral cortex*, *27*(3), 1949–1963. doi: 10.1093/cercor/bhw038
- Carlson, H. L., Sugden, C., Brooks, B. L., & Kirton, A. (2019). Functional connectivity of language networks after perinatal stroke. *NeuroImage. Clinical*, *23*, 101861. doi: 10.1016/j.nicl.2019.101861
- Carlson SM, Beck DM. (2009). Symbols as tools in the development of executive function. In: Winsler A, Fernyhough C, Montero I, editors. Private Speech, Executive Functioning, and the Development of Verbal Self-regulation. New York: Cambridge University Press; pp. 163–175.
- Casey, B. J., Epstein, J. N., Buhle, J., Liston, C., Davidson, M. C., Tonev, S. T., Spicer, J., Niogi, S., Millner, A. J., Reiss, A., Garrett, A., Hinshaw, S. P., Greenhill, L. L., Shafritz, K. M., Vitolo, A., Kotler, L. A., Jarrett, M. A., & Glover, G. (2007). Frontostriatal connectivity and its role in cognitive control in parent-child dyads with ADHD. *The American journal of psychiatry*, *164*(11), 1729–1736. doi: 10.1176/appi.ajp.2007.06101754
- Cassidy, A. R., White, M. T., DeMaso, D. R., Newburger, J. W., & Bellinger, D. C. (2015). Executive Function in Children and Adolescents with Critical Cyanotic Congenital

- Heart Disease. *Journal of the International Neuropsychological Society*, 21(1), 34–49. doi: 10.1017/S1355617714001027
- Castellanos, F. X. (1997). Toward a pathophysiology of attention-deficit/hyperactivity disorder. *Clinical pediatrics*, 36(7), 381–393. doi: 10.1177/000992289703600702
- Chalak, L. F., Nguyen, K. A., Prempunpong, C., Heyne, R., Thayyil, S., Shankaran, S., Laptook, A. R., Rollins, N., Pappas, A., Koclas, L., Shah, B., Montaldo, P., Techasaensiri, B., Sánchez, P. J., & Sant'Anna, G. (2018). Prospective research in infants with mild encephalopathy identified in the first six hours of life: neurodevelopmental outcomes at 18-22 months. *Pediatric research*, 84(6), 861–868. doi: 10.1038/s41390-018-0174-x
- Chalak, L., Ferriero, D. M., Gressens, P., Molloy, E., & Bearer, C. (2019). A 20 years conundrum of neonatal encephalopathy and hypoxic ischemic encephalopathy: are we closer to a consensus guideline?. *Pediatric research*, 86(5), 548–549. doi: 10.1038/s41390-019-0547-9
- Chen, C. H., Lennox, B., Jacob, R., Calder, A., Lupson, V., Bisbrown-Chippendale, R., Suckling, J., & Bullmore, E. (2006). Explicit and implicit facial affect recognition in manic and depressed States of bipolar disorder: a functional magnetic resonance imaging study. *Biological psychiatry*, 59(1), 31–39. doi: 10.1016/j.biopsych.2005.06.008
- Cheong, J. L., Coleman, L., Hunt, R. W., Lee, K. J., Doyle, L. W., Inder, T. E., Jacobs, S. E., & Infant Cooling Evaluation Collaboration (2012). Prognostic utility of magnetic resonance imaging in neonatal hypoxic-ischemic encephalopathy: substudy of a randomized trial. *Archives of pediatrics & adolescent medicine*, 166(7), 634–640. doi: 10.1001/archpediatrics.2012.284
- Christiaens, D., Cordero-Grande, L., Pietsch, M., Hutter, J., Price, A. N., Hughes, E. J., Vecchiato, K., Deprez, M., Edwards, A. D., Hajnal, J. V., & Tournier, J. D. (2021). Scattered slice SHARD reconstruction for motion correction in multi-shell diffusion MRI. *NeuroImage*, 225, 117437. doi: 10.1016/j.neuroimage.2020.117437
- Church, J. A., Fair, D. A., Dosenbach, N. U., Cohen, A. L., Miezin, F. M., Petersen, S. E., & Schlaggar, B. L. (2009). Control networks in paediatric Tourette syndrome show immature and anomalous patterns of functional connectivity. *Brain : a journal of neurology*, 132(Pt 1), 225–238. doi: 10.1093/brain/awn223
- Claessens, N. H., Moeskops, P., Buchmann, A., Latal, B., Knirsch, W., Scheer, I., Išgum, I., de Vries, L. S., Benders, M. J., & von Rhein, M. (2016). Delayed cortical gray matter development in neonates with severe congenital heart disease. *Pediatric research*, 80(5), 668–674. doi: 10.1038/pr.2016.145
- Claessens, N., Algra, S. O., Ouweland, T. L., Jansen, N., Schappin, R., Haas, F., Eijssermans, M., de Vries, L. S., Benders, M., & CHD Lifespan Study Group Utrecht (2018). Perioperative neonatal brain injury is associated with worse school-age neurodevelopment in children with critical congenital heart disease. *Developmental medicine and child neurology*, 60(10), 1052–1058. doi: 10.1111/dmcn.13747
- Clouchoux, C., du Plessis, A. J., Bouyssi-Kobar, M., Tworetzky, W., McElhinney, D. B., Brown, D. W., Gholipour, A., Kudelski, D., Warfield, S. K., McCarter, R. J., Robertson, R. L., Jr, Evans, A. C., Newburger, J. W., & Limperopoulos, C. (2013). Delayed cortical development in fetuses with complex congenital heart disease. *Cerebral cortex*, 23(12), 2932–2943. doi: 10.1093/cercor/bhs281
- Conway, J. M., Walsh, B. H., Boylan, G. B., & Murray, D. M. (2018). Mild hypoxic ischaemic encephalopathy and long term neurodevelopmental outcome - A systematic review. *Early human development*, 120, 80–87. doi: 10.1016/j.earlhumdev.2018.02.007

- Cole, M. W., Reynolds, J. R., Power, J. D., Repovs, G., Anticevic, A., & Braver, T. S. (2013). Multi-task connectivity reveals flexible hubs for adaptive task control. *Nature neuroscience*, *16*(9), 1348–1355. doi: 10.1038/nn.3470
- Corbetta, M., & Shulman, G. L. (2002). Control of goal-directed and stimulus-driven attention in the brain. *Nature reviews. Neuroscience*, *3*(3), 201–215. doi: 10.1038/nrn755
- Cordero-Grande, L., Christiaens, D., Hutter, J., Price, A. N., & Hajnal, J. V. (2019). Complex diffusion-weighted image estimation via matrix recovery under general noise models. *NeuroImage*, *200*, 391–404. doi: 10.1016/j.neuroimage.2019.06.039
- Cordero-Grande, L., Hughes, E. J., Hutter, J., Price, A. N., & Hajnal, J. V. (2018). Three-dimensional motion corrected sensitivity encoding reconstruction for multi-shot multi-slice MRI: Application to neonatal brain imaging. *Magnetic resonance in medicine*, *79*(3), 1365–1376. doi: 10.1002/mrm.26796
- Cordes, D., Haughton, V. M., Arfanakis, K., Carew, J. D., Turski, P. A., Moritz, C. H., Quigley, M. A., & Meyerand, M. E. (2001). Frequencies contributing to functional connectivity in the cerebral cortex in "resting-state" data. *AJNR. American journal of neuroradiology*, *22*(7), 1326–1333.
- Córdova-Palomera, A., Kaufmann, T., Persson, K., Alnæs, D., Doan, N. T., Moberget, T., Lund, M. J., Barca, M. L., Engvig, A., Brækhus, A., Engedal, K., Andreassen, O. A., Selbæk, G., & Westlye, L. T. (2017). Disrupted global metastability and static and dynamic brain connectivity across individuals in the Alzheimer's disease continuum. *Scientific reports*, *7*, 40268. doi: 10.1038/srep40268
- Corkum, V., & Moore, C. (1998). The origins of joint visual attention in infants. *Developmental psychology*, *34*(1), 28–38. doi: 10.1037/0012-1649.34.1.28
- Counsell, S. J., Maalouf, E. F., Fletcher, A. M., Duggan, P., Battin, M., Lewis, H. J., Herlihy, A. H., Edwards, A. D., Bydder, G. M., & Rutherford, M. A. (2002). MR imaging assessment of myelination in the very preterm brain. *AJNR. American journal of neuroradiology*, *23*(5), 872–881.
- Counsell, S. J., Edwards, A. D., Chew, A. T., Anjari, M., Dyet, L. E., Srinivasan, L., Boardman, J. P., Allsop, J. M., Hajnal, J. V., Rutherford, M. A., & Cowan, F. M. (2008). Specific relations between neurodevelopmental abilities and white matter microstructure in children born preterm. *Brain : a journal of neurology*, *131*(Pt 12), 3201–3208. doi: 10.1093/brain/awn268
- Cowan, W. M., Fawcett, J. W., O'Leary, D. D., & Stanfield, B. B. (1984). Regressive events in neurogenesis. *Science*, *225*(4668), 1258–1265. doi: 10.1126/science.6474175
- Cowan, F., Rutherford, M., Groenendaal, F., Eken, P., Mercuri, E., Bydder, G. M., Meiners, L. C., Dubowitz, L. M., & de Vries, L. S. (2003). Origin and timing of brain lesions in term infants with neonatal encephalopathy. *Lancet*, *361*(9359), 736–742. doi: 10.1016/S0140-6736(03)12658-X
- Dammann, O., Ferriero, D., & Gressens, P. (2011). Neonatal encephalopathy or hypoxic-ischemic encephalopathy? Appropriate terminology matters. *Pediatric research*, *70*(1), 1–2. doi: 10.1203/PDR.0b013e318223f38d
- Damoiseaux, J. S., Rombouts, S. A., Barkhof, F., Scheltens, P., Stam, C. J., Smith, S. M., & Beckmann, C. F. (2006). Consistent resting-state networks across healthy subjects. *Proceedings of the National Academy of Sciences of the United States of America*, *103*(37), 13848–13853. doi: 10.1073/pnas.0601417103
- De Asis-Cruz, J., Bouyssi-Kobar, M., Evangelou, I., Vezina, G., & Limperopoulos, C. (2015). Functional properties of resting state networks in healthy full-term newborns. *Scientific reports*, *5*, 17755. doi: 10.1038/srep17755

- De Asis-Cruz, J., Donofrio, M. T., Vezina, G., & Limperopoulos, C. (2017). Aberrant brain functional connectivity in newborns with congenital heart disease before cardiac surgery. *NeuroImage. Clinical*, *17*, 31–42. doi: 10.1016/j.nicl.2017.09.020
- de Graaf-Peters, V. B., & Hadders-Algra, M. (2006). Ontogeny of the human central nervous system: what is happening when?. *Early human development*, *82*(4), 257–266. doi: 10.1016/j.earlhumdev.2005.10.013
- de Vries, L. S., & Groenendaal, F. (2010). Patterns of neonatal hypoxic-ischaemic brain injury. *Neuroradiology*, *52*(6), 555–566. doi: 10.1007/s00234-010-0674-
- de Vries, L. S., & Jongmans, M. J. (2010). Long-term outcome after neonatal hypoxic-ischaemic encephalopathy. *Archives of disease in childhood. Fetal and neonatal edition*, *95*(3), F220–F224. doi: 10.1136/adc.2008.148205
- DeCasper, A. J., & Fifer, W. P. (1980). Of human bonding: newborns prefer their mothers' voices. *Science (New York, N.Y.)*, *208*(4448), 1174–1176. doi: 10.1126/science.7375928
- Deco, G., Jirsa, V., McIntosh, A. R., Sporns, O., & Kötter, R. (2009). Key role of coupling, delay, and noise in resting brain fluctuations. *Proceedings of the National Academy of Sciences of the United States of America*, *106*(25), 10302–10307. doi: 10.1073/pnas.0901831106
- Deco, G., Tononi, G., Boly, M., & Kringelbach, M. L. (2015). Rethinking segregation and integration: contributions of whole-brain modelling. *Nature reviews. Neuroscience*, *16*(7), 430–439. doi: 10.1038/nrn3963
- Deco, G., & Kringelbach, M. L. (2016). Metastability and Coherence: Extending the Communication through Coherence Hypothesis Using A Whole-Brain Computational Perspective. *Trends in neurosciences*, *39*(3), 125–135. doi: 10.1016/j.tins.2016.01.001
- Dehaene-Lambertz, G., Hertz-Pannier, L., Dubois, J., Mériaux, S., Roche, A., Sigman, M., & Dehaene, S. (2006). Functional organization of perisylvian activation during presentation of sentences in preverbal infants. *Proceedings of the National Academy of Sciences of the United States of America*, *103*(38), 14240–14245. doi: 10.1073/pnas.0606302103
- Denisova, K. (2019). Age attenuates noise and increases symmetry of head movements during sleep resting-state fMRI in healthy neonates, infants, and toddlers. *Infant behavior & development*, *57*, 101317. doi: 10.1016/j.infbeh.2019.03.008
- Dennis, E. L., & Thompson, P. M. (2013). Mapping connectivity in the developing brain. *International journal of developmental neuroscience : the official journal of the International Society for Developmental Neuroscience*, *31*(7), 525–542. doi: 10.1016/j.ijdevneu.2013.05.007
- Dibble, M., O'Dea, M. I., Hurley, T., Byrne, A., Colleran, G., Molloy, E. J., & Bokde, A. (2020). Diffusion tensor imaging in neonatal encephalopathy: a systematic review. *Archives of disease in childhood. Fetal and neonatal edition*, *105*(5), 480–488. doi: 10.1136/archdischild-2019-318025
- Dick, A. S., Raja Beharelle, A., Solodkin, A., & Small, S. L. (2013). Interhemispheric functional connectivity following prenatal or perinatal brain injury predicts receptive language outcome. *The Journal of neuroscience : the official journal of the Society for Neuroscience*, *33*(13), 5612–5625. doi: 10.1523/JNEUROSCI.2851-12.2013
- Dimitropoulos, A., McQuillen, P. S., Sethi, V., Moosa, A., Chau, V., Xu, D., Brant, R., Azakie, A., Campbell, A., Barkovich, A. J., Poskitt, K. J., & Miller, S. P. (2013). Brain injury and development in newborns with critical congenital heart disease. *Neurology*, *81*(3), 241–248. doi: 10.1212/WNL.0b013e31829b9bdc
- Dinomais, M., Hertz-Pannier, L., Groeschel, S., Chabrier, S., Delion, M., Husson, B., Kossorotoff, M., Renaud, C., Nguyen The Tich, S., & AVCnn Study Group (2015).

- Long term motor function after neonatal stroke: Lesion localization above all. *Human brain mapping*, 36(12), 4793–4807. doi: 10.1002/hbm.22950
- Dixon, G., Badawi, N., Kurinczuk, J. J., Keogh, J. M., Silburn, S. R., Zubrick, S. R., & Stanley, F. J. (2002). Early developmental outcomes after newborn encephalopathy. *Pediatrics*, 109(1), 26–33. doi: 10.1542/peds.109.1.26
- Dobbing, J., & Sands, J. (1973). Quantitative growth and development of human brain. *Archives of disease in childhood*, 48(10), 757–767. doi: 10.1136/adc.48.10.757
- Doria, V., Beckmann, C. F., Arichi, T., Merchant, N., Groppo, M., Turkheimer, F. E., Counsell, S. J., Murgasova, M., Aljabar, P., Nunes, R. G., Larkman, D. J., Rees, G., & Edwards, A. D. (2010). Emergence of resting state networks in the preterm human brain. *Proceedings of the National Academy of Sciences of the United States of America*, 107(46), 20015–20020. doi: 10.1073/pnas.1007921107
- Du, Y., Pearlson, G. D., Yu, Q., He, H., Lin, D., Sui, J., Wu, L., & Calhoun, V. D. (2016). Interaction among subsystems within default mode network diminished in schizophrenia patients: A dynamic connectivity approach. *Schizophrenia research*, 170(1), 55–65. doi: 10.1016/j.schres.2015.11.021
- Dubois, J., Hertz-Pannier, L., Dehaene-Lambertz, G., Cointepas, Y., & Le Bihan, D. (2006). Assessment of the early organization and maturation of infants' cerebral white matter fiber bundles: a feasibility study using quantitative diffusion tensor imaging and tractography. *NeuroImage*, 30(4), 1121–1132. doi: 10.1016/j.neuroimage.2005.11.022
- Dubois, J., Dehaene-Lambertz, G., Kulikova, S., Poupon, C., Hüppi, P. S., & Hertz-Pannier, L. (2014). The early development of brain white matter: a review of imaging studies in fetuses, newborns and infants. *Neuroscience*, 276, 48–71. doi: 10.1016/j.neuroscience.2013.12.044
- DuPont, T. L., Chalak, L. F., Morriss, M. C., Burchfield, P. J., Christie, L., & Sánchez, P. J. (2013). Short-term outcomes of newborns with perinatal acidemia who are not eligible for systemic hypothermia therapy. *The Journal of pediatrics*, 162(1), 35–41. doi: 10.1016/j.jpeds.2012.06.042
- Edmonds, C. J., Cianfaglione, R., Cornforth, C., & Vollmer, B. (2021). Children with neonatal Hypoxic Ischaemic Encephalopathy (HIE) treated with therapeutic hypothermia are not as school ready as their peers. *Acta paediatrica*, 110(10), 2756–2765. doi: 10.1111/apa.16002
- Edwards, A. D., Brocklehurst, P., Gunn, A. J., Halliday, H., Juszczak, E., Levene, M., Strohm, B., Thoresen, M., Whitelaw, A., & Azzopardi, D. (2010). Neurological outcomes at 18 months of age after moderate hypothermia for perinatal hypoxic ischaemic encephalopathy: synthesis and meta-analysis of trial data. *BMJ (Clinical research ed.)*, 340, c363. doi: 10.1136/bmj.c363
- Eixarch, E., Muñoz-Moreno, E., Bargallo, N., Bataille, D., & Gratacos, E. (2016). Motor and cortico-striatal-thalamic connectivity alterations in intrauterine growth restriction. *American journal of obstetrics and gynecology*, 214(6), 725.e1–725.e7259. doi: 10.1016/j.ajog.2015.12.028
- Elmahdy, H., El-Mashad, A. R., El-Bahrawy, H., El-Gohary, T., El-Barbary, A., & Aly, H. (2010). Human recombinant erythropoietin in asphyxia neonatorum: pilot trial. *Pediatrics*, 125(5), e1135–e1142. doi: 10.1542/peds.2009-2268
- Emde, R. N., & Harmon, R. J. (1972). Endogenous and exogenous smiling systems in early infancy. *Journal of the American Academy of Child Psychiatry*, 11(2), 177–200. doi: 10.1016/s0002-7138(10)60071-4
- Ewer, A. K., Middleton, L. J., Furnston, A. T., Bhojar, A., Daniels, J. P., Thangaratinam, S., Deeks, J. J., Khan, K. S., & PulseOx Study Group (2011). Pulse oximetry screening for

- congenital heart defects in newborn infants (PulseOx): a test accuracy study. *Lancet (London, England)*, 378(9793), 785–794. doi: 10.1016/S0140-6736(11)60753-8
- Executive summary: Neonatal encephalopathy and neurologic outcome, second edition. Report of the American College of Obstetricians and Gynecologists' Task Force on Neonatal Encephalopathy. (2014). *Obstetrics and gynecology*, 123(4), 896–901. doi: 10.1097/01.AOG.0000445580.65983.d2
- Eyre, M., Fitzgibbon, S. P., Ciarrusta, J., Cordero-Grande, L., Price, A. N., Poppe, T., Schuh, A., Hughes, E., O'Keeffe, C., Brandon, J., Cromb, D., Vecchiato, K., Andersson, J., Duff, E. P., Counsell, S. J., Smith, S. M., Rueckert, D., Hajnal, J. V., Arichi, T., O'Muirheartaigh, J., ... Edwards, A. D. (2021). The Developing Human Connectome Project: typical and disrupted perinatal functional connectivity. *Brain : a journal of neurology*, 144(7), 2199–2213. doi: 10.1093/brain/awab118
- Einstein A. (1905) Über die von der molekularkinetischen Theorie der Wärme geforderte Bewegung von in ruhenden Flüssigkeiten suspendierten Teilchen. *Annalen der Physik* 322, 549–560. doi:10.1002/andp.19053220806
- Fan, Y., Shi, F., Smith, J. K., Lin, W., Gilmore, J. H., & Shen, D. (2011). Brain anatomical networks in early human brain development. *NeuroImage*, 54(3), 1862–1871. doi: 10.1016/j.neuroimage.2010.07.025
- Farroni, T., Csibra, G., Simion, F., & Johnson, M. H. (2002). Eye contact detection in humans from birth. *Proceedings of the National Academy of Sciences of the United States of America*, 99(14), 9602–9605. doi: 10.1073/pnas.152159999
- Farroni, T., Johnson, M. H., & Csibra, G. (2004). Mechanisms of eye gaze perception during infancy. *Journal of cognitive neuroscience*, 16(8), 1320–1326. doi: 10.1162/0898929042304787
- Fenson, L., Dale, P. S., Reznick, J. S., Thal, D. J., Bates, E., Hartung, J.p., Pethick, S. J. & Reilly, J.S. (1993). *The MacArthur communicative development inventories: User's guide and technical manual*. San Diego: Singular.
- Fenson, L., Dale, P. S., Reznick, J. S., Bates, E., Thal, D. J., & Pethick, S. J. (1994). Variability in early communicative development. *Monographs of the Society for Research in Child Development*, 59(5), 1–185.
- Ferriero D. M. (2004). Neonatal brain injury. *The New England journal of medicine*, 351(19), 1985–1995. doi: 10.1056/NEJMra041996
- Ferstl, E. C., Neumann, J., Bogler, C., & von Cramon, D. Y. (2008). The extended language network: a meta-analysis of neuroimaging studies on text comprehension. *Human brain mapping*, 29(5), 581–593. doi: 10.1002/hbm.20422
- Finder, M., Boylan, G. B., Twomey, D., Ahearne, C., Murray, D. M., & Hallberg, B. (2020). Two-Year Neurodevelopmental Outcomes After Mild Hypoxic Ischemic Encephalopathy in the Era of Therapeutic Hypothermia. *JAMA pediatrics*, 174(1), 48–55. doi: 10.1001/jamapediatrics.2019.4011
- Finer, N. N., Robertson, C. M., Peters, K. L., & Coward, J. H. (1983). Factors affecting outcome in hypoxic-ischemic encephalopathy in term infants. *American journal of diseases of children (1960)*, 137(1), 21–25. doi: 10.1001/archpedi.1983.02140270017006
- Fitzgibbon, S. P., Harrison, S. J., Jenkinson, M., Baxter, L., Robinson, E. C., Bastiani, M., Bozek, J., Karolis, V., Cordero Grande, L., Price, A. N., Hughes, E., Makropoulos, A., Passerat-Palmbach, J., Schuh, A., Gao, J., Farahibozorg, S. R., O'Muirheartaigh, J., Ciarrusta, J., O'Keeffe, C., Brandon, J., ... Andersson, J. (2020). The developing Human Connectome Project (dHCP) automated resting-state functional processing framework for newborn infants. *NeuroImage*, 223, 117303. doi: 10.1016/j.neuroimage.2020.117303

- Fischi-Gomez, E., Muñoz-Moreno, E., Vasung, L., Griffa, A., Borradori-Tolsa, C., Monnier, M., Lazeyras, F., Thiran, J. P., & Hüppi, P. S. (2016). Brain network characterization of high-risk preterm-born school-age children. *NeuroImage. Clinical*, *11*, 195–209. doi: 10.1016/j.nicl.2016.02.001
- Fischi-Gómez, E., Vasung, L., Meskaldji, D. E., Lazeyras, F., Borradori-Tolsa, C., Hagmann, P., Barisnikov, K., Thiran, J. P., & Hüppi, P. S. (2015). Structural Brain Connectivity in School-Age Preterm Infants Provides Evidence for Impaired Networks Relevant for Higher Order Cognitive Skills and Social Cognition. *Cerebral cortex*, *25*(9), 2793–2805. doi: 10.1093/cercor/bhu073
- Fox, M. D., Snyder, A. Z., Vincent, J. L., Corbetta, M., Van Essen, D. C., & Raichle, M. E. (2005). The human brain is intrinsically organized into dynamic, anticorrelated functional networks. *Proceedings of the National Academy of Sciences of the United States of America*, *102*(27), 9673–9678. doi: 10.1073/pnas.0504136102
- Fox, M. D., & Raichle, M. E. (2007). Spontaneous fluctuations in brain activity observed with functional magnetic resonance imaging. *Nature reviews. Neuroscience*, *8*(9), 700–711. doi: 10.1038/nrn2201
- François, C., Ripollés, P., Ferreri, L., Muchart, J., Sierpowska, J., Fons, C., Solé, J., Rebollo, M., Zatorre, R. J., Garcia-Alix, A., Bosch, L., & Rodriguez-Fornells, A. (2019). Right Structural and Functional Reorganization in Four-Year-Old Children with Perinatal Arterial Ischemic Stroke Predict Language Production. *eNeuro*, *6*(4), ENEURO.0447-18.2019. doi: 10.1523/ENEURO.0447-18.2019
- Fransson, P., Skiöld, B., Horsch, S., Nordell, A., Blennow, M., Lagercrantz, H., & Aden, U. (2007). Resting-state networks in the infant brain. *Proceedings of the National Academy of Sciences of the United States of America*, *104*(39), 15531–15536. doi: 10.1073/pnas.0704380104
- Fransson, P., Skiöld, B., Engström, M., Hallberg, B., Mosskin, M., Aden, U., Lagercrantz, H., & Blennow, M. (2009). Spontaneous brain activity in the newborn brain during natural sleep—an fMRI study in infants born at full term. *Pediatric research*, *66*(3), 301–305. doi: 10.1203/PDR.0b013e3181b1bd84
- Fransson, P., Aden, U., Blennow, M., & Lagercrantz, H. (2011). The functional architecture of the infant brain as revealed by resting-state fMRI. *Cerebral cortex*, *21*(1), 145–154. doi: 10.1093/cercor/bhq071
- Friederici, A. D., Brauer, J., & Lohmann, G. (2011). Maturation of the language network: from inter- to intrahemispheric connectivities. *PloS one*, *6*(6), e20726. doi: 10.1371/journal.pone.0020726
- Fries, P. (2005). A mechanism for cognitive dynamics: neuronal communication through neuronal coherence. *Trends in cognitive sciences*, *9*(10), 474–480. doi: 10.1016/j.tics.2005.08.011
- Gadian, D. G., Aicardi, J., Watkins, K. E., Porter, D. A., Mishkin, M., & Vargha-Khadem, F. (2000). Developmental amnesia associated with early hypoxic-ischaemic injury. *Brain : a journal of neurology*, *123 Pt 3*, 499–507. doi: 10.1093/brain/123.3.499
- Ganesan, V., Hogan, A., Shack, N., Gordon, A., Isaacs, E., & Kirkham, F. J. (2000). Outcome after ischaemic stroke in childhood. *Developmental medicine and child neurology*, *42*(7), 455–461. doi: 10.1017/s0012162200000852
- Gao, W., Zhu, H., Giovanello, K. S., Smith, J. K., Shen, D., Gilmore, J. H., & Lin, W. (2009). Evidence on the emergence of the brain's default network from 2-week-old to 2-year-old healthy pediatric subjects. *Proceedings of the National Academy of Sciences of the United States of America*, *106*(16), 6790–6795. doi: 10.1073/pnas.0811221106
- Gao, W., Gilmore, J. H., Shen, D., Smith, J. K., Zhu, H., & Lin, W. (2013). The synchronization within and interaction between the default and dorsal attention

- networks in early infancy. *Cerebral cortex*, 23(3), 594–603. doi: 10.1093/cercor/bhs043
- Gao, W., Alcauter, S., Smith, J. K., Gilmore, J. H., & Lin, W. (2015). Development of human brain cortical network architecture during infancy. *Brain structure & function*, 220(2), 1173–1186. doi: 10.1007/s00429-014-0710-3
- Gao, W., Alcauter, S., Elton, A., Hernandez-Castillo, C. R., Smith, J. K., Ramirez, J., & Lin, W. (2015). Functional Network Development During the First Year: Relative Sequence and Socioeconomic Correlations. *Cerebral cortex (New York, N.Y. : 1991)*, 25(9), 2919–2928. doi: 10.1093/cercor/bhu088
- Gao, W., Gilmore, J. H., Giovanello, K. S., Smith, J. K., Shen, D., Zhu, H., & Lin, W. (2011). Temporal and spatial evolution of brain network topology during the first two years of life. *PloS one*, 6(9), e25278. doi: 10.1371/journal.pone.0025278
- Garel, C., Chantrel, E., Brisse, H., Elmaleh, M., Luton, D., Oury, J. F., Sebag, G., & Hassan, M. (2001). Fetal cerebral cortex: normal gestational landmarks identified using prenatal MR imaging. *AJNR. American journal of neuroradiology*, 22(1), 184–189.
- Gaynor, J. W., Stopp, C., Wypij, D., Andropoulos, D. B., Atallah, J., Atz, A. M., Beca, J., Donofrio, M. T., Duncan, K., Ghanayem, N. S., Goldberg, C. S., Hövels-Gürich, H., Ichida, F., Jacobs, J. P., Justo, R., Latal, B., Li, J. S., Mahle, W. T., McQuillen, P. S., Menon, S. C., ... International Cardiac Collaborative on Neurodevelopment (ICCON) Investigators (2015). Neurodevelopmental outcomes after cardiac surgery in infancy. *Pediatrics*, 135(5), 816–825. doi: 10.1542/peds.2014-3825
- Geangu, E., Benga, O., Stahl, D., & Striano, T. (2010). Contagious crying beyond the first days of life. *Infant behavior & development*, 33(3), 279–288. doi: 10.1016/j.infbeh.2010.03.004
- Gelb, B. D., & Chung, W. K. (2014). Complex genetics and the etiology of human congenital heart disease. *Cold Spring Harbor perspectives in medicine*, 4(7), a013953. doi: 10.1101/cshperspect.a013953
- Gilmore, J. H., Knickmeyer, R. C., & Gao, W. (2018). Imaging structural and functional brain development in early childhood. *Nature reviews. Neuroscience*, 19(3), 123–137. doi: 10.1038/nrn.2018.1
- Glauser, T. A., Rorke, L. B., Weinberg, P. M., & Clancy, R. R. (1990). Congenital brain anomalies associated with the hypoplastic left heart syndrome. *Pediatrics*, 85(6), 984–990.
- Glerean, E., Salmi, J., Lahnakoski, J. M., Jääskeläinen, I. P., & Sams, M. (2012). Functional magnetic resonance imaging phase synchronization as a measure of dynamic functional connectivity. *Brain connectivity*, 2(2), 91–101. doi: 10.1089/brain.2011.0068
- Gluckman, P. D., Wyatt, J. S., Azzopardi, D., Ballard, R., Edwards, A. D., Ferriero, D. M., Polin, R. A., Robertson, C. M., Thoresen, M., Whitelaw, A., & Gunn, A. J. (2005). Selective head cooling with mild systemic hypothermia after neonatal encephalopathy: multicentre randomised trial. *Lancet*, 365(9460), 663–670. doi: 10.1016/S0140-6736(05)17946-X
- Gonzalez, F. F., & Miller, S. P. (2006). Does perinatal asphyxia impair cognitive function without cerebral palsy?. *Archives of disease in childhood. Fetal and neonatal edition*, 91(6), F454–F459. doi: 10.1136/adc.2005.092445
- Gredebäck, G., & Daum, M. M. (2015). The Microstructure of Action Perception in Infancy: Decomposing the Temporal Structure of Social Information Processing. *Child development perspectives*, 9(2), 79–83. doi: 10.1111/cdep.12109
- Greicius, M. D., Krasnow, B., Reiss, A. L., & Menon, V. (2003). Functional connectivity in the resting brain: a network analysis of the default mode hypothesis. *Proceedings of*

- the National Academy of Sciences of the United States of America*, 100(1), 253–258. doi: 10.1073/pnas.0135058100
- Griffanti, L., Salimi-Khorshidi, G., Beckmann, C. F., Auerbach, E. J., Douaud, G., Sexton, C. E., Zsoldos, E., Ebmeier, K. P., Filippini, N., Mackay, C. E., Moeller, S., Xu, J., Yacoub, E., Baselli, G., Ugurbil, K., Miller, K. L., & Smith, S. M. (2014). ICA-based artefact removal and accelerated fMRI acquisition for improved resting state network imaging. *NeuroImage*, 95, 232–247. doi: 10.1016/j.neuroimage.2014.03.034
- Griffanti, L., Douaud, G., Bijsterbosch, J., Evangelisti, S., Alfaro-Almagro, F., Glasser, M. F., Duff, E. P., Fitzgibbon, S., Westphal, R., Carone, D., Beckmann, C. F., & Smith, S. M. (2017). Hand classification of fMRI ICA noise components. *NeuroImage*, 154, 188–205. doi: 10.1016/j.neuroimage.2016.12.036
- Gunn, A. J., & Gluckman, P. D. (2007). Head cooling for neonatal encephalopathy: the state of the art. *Clinical obstetrics and gynecology*, 50(3), 636–651. doi: 10.1097/GRF.0b013e31811e3181
- Gunn, A. J., & Bennet, L. (2008). Timing of injury in the fetus and neonate. *Current opinion in obstetrics & gynecology*, 20(2), 175–181. doi: 10.1097/GCO.0b013e3282f4ef9e
- Gunn, J. K., Beca, J., Hunt, R. W., Goldsworthy, M., Brizard, C. P., Finucane, K., Donath, S., & Shekerdemian, L. S. (2016). Perioperative risk factors for impaired neurodevelopment after cardiac surgery in early infancy. *Archives of disease in childhood*, 101(11), 1010–1016. doi: 10.1136/archdischild-2015-309449
- Guo, T., Duerden, E. G., Adams, E., Chau, V., Branson, H. M., Chakravarty, M. M., Poskitt, K. J., Synnes, A., Grunau, R. E., & Miller, S. P. (2017). Quantitative assessment of white matter injury in preterm neonates: Association with outcomes. *Neurology*, 88(7), 614–622. doi: 10.1212/WNL.0000000000003606
- Gupta, R. K., Hasan, K. M., Trivedi, R., Pradhan, M., Das, V., Parikh, N. A., & Narayana, P. A. (2005). Diffusion tensor imaging of the developing human cerebrum. *Journal of neuroscience research*, 81(2), 172–178. doi: 10.1002/jnr.20547
- Haber, S. N., & Calzavara, R. (2009). The cortico-basal ganglia integrative network: the role of the thalamus. *Brain research bulletin*, 78(2-3), 69–74. doi: 10.1016/j.brainresbull.2008.09.013
- Hacker, C. D., Perlmuter, J. S., Criswell, S. R., Ances, B. M., & Snyder, A. Z. (2012). Resting state functional connectivity of the striatum in Parkinson's disease. *Brain : a journal of neurology*, 135(Pt 12), 3699–3711. doi: 10.1093/brain/aww281
- Hagmann, P., Grant, P. E., & Fair, D. A. (2012). MR connectomics: a conceptual framework for studying the developing brain. *Frontiers in systems neuroscience*, 6, 43. doi: 10.3389/fnsys.2012.00043
- Hagmann, P., Sporns, O., Madan, N., Cammoun, L., Pienaar, R., Wedeen, V. J., Meuli, R., Thiran, J. P., & Grant, P. E. (2010). White matter maturation reshapes structural connectivity in the late developing human brain. *Proceedings of the National Academy of Sciences of the United States of America*, 107(44), 19067–19072. doi: 10.1073/pnas.1009073107
- Hansen, E., Poole, T. A., Nguyen, V., Lerner, M., Wigal, T., Shannon, K., Wigal, S. B., & Batra, A. S. (2012). Prevalence of ADHD symptoms in patients with congenital heart disease. *Pediatrics international : official journal of the Japan Pediatric Society*, 54(6), 838–843. doi: 10.1111/j.1442-200X.2012.03711.x
- Harteman, J. C., Groenendaal, F., Toet, M. C., Benders, M. J., Van Haastert, I. C., Nievelstein, R. A., Koopman-Elseboom, C., & de Vries, L. S. (2013). Diffusion-weighted imaging changes in cerebral watershed distribution following neonatal encephalopathy are not invariably associated with an adverse outcome. *Developmental medicine and child neurology*, 55(7), 642–653. doi: 10.1111/dmcn.12122

- Hellyer, P. J., Shanahan, M., Scott, G., Wise, R. J., Sharp, D. J., & Leech, R. (2014). The control of global brain dynamics: opposing actions of frontoparietal control and default mode networks on attention. *The Journal of neuroscience : the official journal of the Society for Neuroscience*, *34*(2), 451–461. doi: 10.1523/JNEUROSCI.1853-13.2014
- Hellyer, P. J., Scott, G., Shanahan, M., Sharp, D. J., & Leech, R. (2015). Cognitive Flexibility through Metastable Neural Dynamics Is Disrupted by Damage to the Structural Connectome. *The Journal of neuroscience : the official journal of the Society for Neuroscience*, *35*(24), 9050–9063. doi: 10.1523/JNEUROSCI.4648-14.2015
- Hinton, R. B., Andelfinger, G., Sekar, P., Hinton, A. C., Gendron, R. L., Michelfelder, E. C., Robitaille, Y., & Benson, D. W. (2008). Prenatal head growth and white matter injury in hypoplastic left heart syndrome. *Pediatric research*, *64*(4), 364–369. doi: 10.1203/PDR.0b013e3181827bf4
- Hodapp, R. M., Goldfield, E. C., & Boyatzis, C. J. (1984). The use and effectiveness of maternal scaffolding in mother-infant games. *Child development*, *55*(3), 772–781.
- Hongwanishkul, D., Happaney, K. R., Lee, W. S., & Zelazo, P. D. (2005). Assessment of hot and cool executive function in young children: age-related changes and individual differences. *Developmental neuropsychology*, *28*(2), 617–644. doi: 10.1207/s15326942dn2802_4
- Hortensius, L. M., Dijkshoorn, A., Ecury-Goossen, G. M., Steggerda, S. J., Hoebeek, F. E., Benders, M., & Dudink, J. (2018). Neurodevelopmental Consequences of Preterm Isolated Cerebellar Hemorrhage: A Systematic Review. *Pediatrics*, *142*(5), e20180609. doi: 10.1542/peds.2018-0609
- Hövels-Gürich, H. H., Konrad, K., Wiesner, M., Minkenberg, R., Herpertz-Dahlmann, B., Messmer, B. J., & Von Bernuth, G. (2002). Long term behavioural outcome after neonatal arterial switch operation for transposition of the great arteries. *Archives of disease in childhood*, *87*(6), 506–510. doi: 10.1136/adc.87.6.506
- Hövels-Gürich, H. H., Konrad, K., Skorzenski, D., Nacken, C., Minkenberg, R., Messmer, B. J., & Seghaye, M. C. (2006). Long-term neurodevelopmental outcome and exercise capacity after corrective surgery for tetralogy of Fallot or ventricular septal defect in infancy. *The Annals of thoracic surgery*, *81*(3), 958–966. doi: 10.1016/j.athoracsur.2005.09.010
- Hövels-Gürich, H. H., Konrad, K., Skorzenski, D., Herpertz-Dahlmann, B., Messmer, B. J., & Seghaye, M. C. (2007). Attentional dysfunction in children after corrective cardiac surgery in infancy. *The Annals of thoracic surgery*, *83*(4), 1425–1430. doi: 10.1016/j.athoracsur.2006.10.069
- Hövels-Gürich, H. H. (2016). Factors Influencing Neurodevelopment after Cardiac Surgery during Infancy. *Frontiers in pediatrics*, *4*, 137. doi: 10.3389/fped.2016.00137
- Huang, C. C., Wang, S. T., Chang, Y. C., Lin, K. P., & Wu, P. L. (1999). Measurement of the urinary lactate:creatinine ratio for the early identification of newborn infants at risk for hypoxic-ischemic encephalopathy. *The New England journal of medicine*, *341*(5), 328–335. doi: 10.1056/NEJM199907293410504
- Huang, H., Shu, N., Mishra, V., Jeon, T., Chalak, L., Wang, Z. J., Rollins, N., Gong, G., Cheng, H., Peng, Y., Dong, Q., & He, Y. (2015). Development of human brain structural networks through infancy and childhood. *Cerebral cortex*, *25*(5), 1389–1404. doi: 10.1093/cercor/bht335
- Huang, H., & Vasung, L. (2014). Gaining insight of fetal brain development with diffusion MRI and histology. *International journal of developmental neuroscience : the official journal of the International Society for Developmental Neuroscience*, *32*, 11–22. doi: 10.1016/j.ijdevneu.2013.06.005

- Huang, Z., Wang, Q., Zhou, S., Tang, C., Yi, F., & Nie, J. (2020). Exploring functional brain activity in neonates: A resting-state fMRI study. *Developmental cognitive neuroscience*, *45*, 100850. doi: 10.1016/j.dcn.2020.100850
- Hughes, E. J., Winchman, T., Padormo, F., Teixeira, R., Wurie, J., Sharma, M., Fox, M., Hutter, J., Cordero-Grande, L., Price, A. N., Allsop, J., Bueno-Conde, J., Tumor, N., Arichi, T., Edwards, A. D., Rutherford, M. A., Counsell, S. J., & Hajnal, J. V. (2017). A dedicated neonatal brain imaging system. *Magnetic resonance in medicine*, *78*(2), 794–804. doi: 10.1002/mrm.26462
- Huisman, T. A., Martin, E., Kubik-Huch, R., & Marincek, B. (2002). Fetal magnetic resonance imaging of the brain: technical considerations and normal brain development. *European radiology*, *12*(8), 1941–1951. doi: 10.1007/s00330-001-1209-x
- Hunt, R. W., Neil, J. J., Coleman, L. T., Kean, M. J., & Inder, T. E. (2004). Apparent diffusion coefficient in the posterior limb of the internal capsule predicts outcome after perinatal asphyxia. *Pediatrics*, *114*(4), 999–1003. doi: 10.1542/peds.2003-0935-L
- Hüppi, P. S., Maier, S. E., Peled, S., Zientara, G. P., Barnes, P. D., Jolesz, F. A., & Volpe, J. J. (1998). Microstructural development of human newborn cerebral white matter assessed in vivo by diffusion tensor magnetic resonance imaging. *Pediatric research*, *44*(4), 584–590. doi: 10.1203/00006450-199810000-00019
- Hutchison, R. M., Womelsdorf, T., Allen, E. A., Bandettini, P. A., Calhoun, V. D., Corbetta, M., Della Penna, S., Duyn, J. H., Glover, G. H., Gonzalez-Castillo, J., Handwerker, D. A., Keilholz, S., Kiviniemi, V., Leopold, D. A., de Pasquale, F., Sporns, O., Walter, M., & Chang, C. (2013). Dynamic functional connectivity: promise, issues, and interpretations. *NeuroImage*, *80*, 360–378. doi: 10.1016/j.neuroimage.2013.05.079
- Huttenlocher, P. R., De Courten, C., Garey, L. J., & Van der Loos, H. (1982). Synaptic development in human cerebral cortex. *International journal of neurology*, *16-17*, 144–154.
- Huttenlocher, P. R., de Courten, C., Garey, L. J., & Van der Loos, H. (1982). Synaptogenesis in human visual cortex--evidence for synapse elimination during normal development. *Neuroscience letters*, *33*(3), 247–252. doi: 10.1016/0304-3940(82)90379-2.
- Huttenlocher, P. R., de Courten, C., Garey, L. J., & Van der Loos, H. (1982). Synaptogenesis in human visual cortex--evidence for synapse elimination during normal development. *Neuroscience letters*, *33*(3), 247–252. doi: 10.1016/0304-3940(82)90379-2
- Huttenlocher P. R. (1990). Morphometric study of human cerebral cortex development. *Neuropsychologia*, *28*(6), 517–527. doi: 10.1016/0028-3932(90)90031-i
- Huttenlocher, P. R., & Dabholkar, A. S. (1997). Regional differences in synaptogenesis in human cerebral cortex. *The Journal of comparative neurology*, *387*(2), 167–178. doi: 10.1002/(sici)1096-9861(19971020)387:2<167::aid-cne1>3.0.co;2-z
- Hutter, J., Tournier, J. D., Price, A. N., Cordero-Grande, L., Hughes, E. J., Malik, S., Steinweg, J., Bastiani, M., Sotiropoulos, S. N., Jbabdi, S., Andersson, J., Edwards, A. D., & Hajnal, J. V. (2018). Time-efficient and flexible design of optimized multishell HARDI diffusion. *Magnetic resonance in medicine*, *79*(3), 1276–1292. doi: 10.1002/mrm.26765
- Hutton, B., Salanti, G., Caldwell, D. M., Chaimani, A., Schmid, C. H., Cameron, C., Ioannidis, J. P., Straus, S., Thorlund, K., Jansen, J. P., Mulrow, C., Catalá-López, F., Gøtzsche, P. C., Dickersin, K., Boutron, I., Altman, D. G., & Moher, D. (2015). The PRISMA extension statement for reporting of systematic reviews incorporating

- network meta-analyses of health care interventions: checklist and explanations. *Annals of internal medicine*, 162(11), 777–784. doi: 10.7326/M14-2385
- Ilardi, D., Ono, K. E., McCartney, R., Book, W., & Stringer, A. Y. (2017). Neurocognitive functioning in adults with congenital heart disease. *Congenital heart disease*, 12(2), 166–173. doi: 10.1111/chd.12434
- Ilves, N., Ilves, P., Laugesaar, R., Juurmaa, J., Männamaa, M., Lõo, S., Loorits, D., Tomberg, T., Kolk, A., Talvik, I., & Talvik, T. (2016). Resting-State Functional Connectivity and Cognitive Impairment in Children with Perinatal Stroke. *Neural plasticity*, 2016, 2306406. doi: 10.1155/2016/2306406
- Innocenti, G. M., & Price, D. J. (2005). Exuberance in the development of cortical networks. *Nature reviews. Neuroscience*, 6(12), 955–965. doi: 10.1038/nrn1790
- Izbudak, I., & Grant, P. E. (2011). MR imaging of the term and preterm neonate with diffuse brain injury. *Magnetic resonance imaging clinics of North America*, 19(4), 709–vii. doi: 10.1016/j.mric.2011.08.014
- Jacobs, S. E., Berg, M., Hunt, R., Tarnow-Mordi, W. O., Inder, T. E., & Davis, P. G. (2013). Cooling for newborns with hypoxic ischaemic encephalopathy. *The Cochrane database of systematic reviews*, 2013(1), CD003311. doi: 10.1002/14651858.CD003311.pub3
- Jacobs, S. E., Morley, C. J., Inder, T. E., Stewart, M. J., Smith, K. R., McNamara, P. J., Wright, I. M., Kirpalani, H. M., Darlow, B. A., Doyle, L. W., & Infant Cooling Evaluation Collaboration (2011). Whole-body hypothermia for term and near-term newborns with hypoxic-ischemic encephalopathy: a randomized controlled trial. *Archives of pediatrics & adolescent medicine*, 165(8), 692–700. doi: 10.1001/archpediatrics.2011.43
- Jakovcevski, I., & Zecevic, N. (2005). Sequence of oligodendrocyte development in the human fetal telencephalon. *Glia*, 49(4), 480–491. doi: 10.1002/glia.20134
- Jary, S., Smit, E., Liu, X., Cowan, F. M., & Thoresen, M. (2015). Less severe cerebral palsy outcomes in infants treated with therapeutic hypothermia. *Acta paediatrica*, 104(12), 1241–1247. doi: 10.1111/apa.13146
- Jeurissen, B., Tournier, J. D., Dhollander, T., Connelly, A., & Sijbers, J. (2014). Multi-tissue constrained spherical deconvolution for improved analysis of multi-shell diffusion MRI data. *NeuroImage*, 103, 411–426. doi: 10.1016/j.neuroimage.2014.07.061
- Johnson, M. H., Dziurawiec, S., Ellis, H., & Morton, J. (1991). Newborns' preferential tracking of face-like stimuli and its subsequent decline. *Cognition*, 40(1-2), 1–19. doi: 10.1016/0010-0277(91)90045-6
- Jones, E.G. (2000). *The thalamus*. Cambridge, England: Cambridge University Press.
- Jones S. S. (2007). Imitation in infancy: the development of mimicry. *Psychological science*, 18(7), 593–599. doi: 10.1111/j.1467-9280.2007.01945.x
- Judas, M., Rados, M., Jovanov-Milosevic, N., Hrabac, P., Stern-Padovan, R., & Kostovic, I. (2005). Structural, immunocytochemical, and mr imaging properties of periventricular crossroads of growing cortical pathways in preterm infants. *AJNR. American journal of neuroradiology*, 26(10), 2671–2684.
- Kaiser, M. (2011). A tutorial in connectome analysis: topological and spatial features of brain networks. *NeuroImage*, 57(3), 892–907. doi: 10.1016/j.neuroimage.2011.05.025
- Karsdorp, P. A., Everaerd, W., Kindt, M., & Mulder, B. J. (2007). Psychological and cognitive functioning in children and adolescents with congenital heart disease: a meta-analysis. *Journal of pediatric psychology*, 32(5), 527–541. doi: 10.1093/jpepsy/jsl047
- Karolis, V. R., Froudust-Walsh, S., Brittain, P. J., Kroll, J., Ball, G., Edwards, A. D., Dell'Acqua, F., Williams, S. C., Murray, R. M., & Nosarti, C. (2016). Reinforcement of the Brain's Rich-Club Architecture Following Early Neurodevelopmental Disruption

- Caused by Very Preterm Birth. *Cerebral cortex (New York, N.Y. : 1991)*, 26(3), 1322–1335. doi: 10.1093/cercor/bhv305
- Kasmi, L., Bonnet, D., Montreuil, M., Kalfa, D., Geronikola, N., Bellinger, D. C., & Calderon, J. (2017). Neuropsychological and Psychiatric Outcomes in Dextro-Transposition of the Great Arteries across the Lifespan: A State-of-the-Art Review. *Frontiers in pediatrics*, 5, 59. doi: 10.3389/fped.2017.00059
- Kellner, E., Dhital, B., Kiselev, V. G., & Reisert, M. (2016). Gibbs-ringing artifact removal based on local subvoxel-shifts. *Magnetic resonance in medicine*, 76(5), 1574–1581. doi: 10.1002/mrm.26054
- Kelly, C. J., Christiaens, D., Batalle, D., Makropoulos, A., Cordero-Grande, L., Steinweg, J. K., O'Muirheartaigh, J., Khan, H., Lee, G., Victor, S., Alexander, D. C., Zhang, H., Simpson, J., Hajnal, J. V., Edwards, A. D., Rutherford, M. A., & Counsell, S. J. (2019). Abnormal Microstructural Development of the Cerebral Cortex in Neonates With Congenital Heart Disease Is Associated With Impaired Cerebral Oxygen Delivery. *Journal of the American Heart Association*, 8(5), e009893. doi: 10.1161/JAHA.118.009893
- Kelly, C. J., Arulkumaran, S., Tristão Pereira, C., Cordero-Grande, L., Hughes, E. J., Teixeira, R., Steinweg, J. K., Victor, S., Pushparajah, K., Hajnal, J. V., Simpson, J., Edwards, A. D., Rutherford, M. A., & Counsell, S. J. (2019). Neuroimaging findings in newborns with congenital heart disease prior to surgery: an observational study. *Archives of disease in childhood*, 104(11), 1042–1048. doi: 10.1136/archdischild-2018-314822
- Kelly, C. J., Makropoulos, A., Cordero-Grande, L., Hutter, J., Price, A., Hughes, E., Murgasova, M., Teixeira, R., Steinweg, J. K., Kulkarni, S., Rahman, L., Zhang, H., Alexander, D. C., Pushparajah, K., Rueckert, D., Hajnal, J. V., Simpson, J., Edwards, A. D., Rutherford, M. A., & Counsell, S. J. (2017). Impaired development of the cerebral cortex in infants with congenital heart disease is correlated to reduced cerebral oxygen delivery. *Scientific reports*, 7(1), 15088. doi: 10.1038/s41598-017-14939-z
- Kelso, J. A. (2012). Multistability and metastability: understanding dynamic coordination in the brain. *Philosophical transactions of the Royal Society of London. Series B, Biological sciences*, 367(1591), 906–918. doi: 10.1098/rstb.2011.0351
- Kendall, G. S., Melbourne, A., Johnson, S., Price, D., Bainbridge, A., Gunny, R., Huertas-Ceballos, A., Cady, E. B., Ourselin, S., Marlow, N., & Robertson, N. J. (2014). White matter NAA/Cho and Cho/Cr ratios at MR spectroscopy are predictive of motor outcome in preterm infants. *Radiology*, 271(1), 230–238. doi: 10.1148/radiol.13122679
- Kersbergen, K. J., Leemans, A., Groenendaal, F., van der Aa, N. E., Viergever, M. A., de Vries, L. S., & Benders, M. (2014). Microstructural brain development between 30 and 40 weeks corrected age in a longitudinal cohort of extremely preterm infants. *NeuroImage*, 103, 214–224. doi: 10.1016/j.neuroimage.2014.09.039
- Khundrakpam, B. S., Reid, A., Brauer, J., Carbonell, F., Lewis, J., Ameis, S., Karama, S., Lee, J., Chen, Z., Das, S., Evans, A. C., & Brain Development Cooperative Group (2013). Developmental changes in organization of structural brain networks. *Cerebral cortex*, 23(9), 2072–2085. doi: 10.1093/cercor/bhs187
- Kinney, H. C., Brody, B. A., Kloman, A. S., & Gilles, F. H. (1988). Sequence of central nervous system myelination in human infancy. II. Patterns of myelination in autopsied infants. *Journal of neuropathology and experimental neurology*, 47(3), 217–234. doi: 10.1097/00005072-198805000-00003
- Kinney, H. C., Karthigasan, J., Borenshteyn, N. I., Flax, J. D., & Kirschner, D. A. (1994). Myelination in the developing human brain: biochemical correlates. *Neurochemical research*, 19(8), 983–996. doi: 10.1007/BF00968708

- Kirton, A., & Deveber, G. (2013). Life after perinatal stroke. *Stroke*, *44*(11), 3265–3271. doi: 10.1161/STROKEAHA.113.000739
- Kiviniemi, V., Jauhiainen, J., Tervonen, O., Pääkkö, E., Oikarinen, J., Vainionpää, V., Rantala, H., & Biswal, B. (2000). Slow vasomotor fluctuation in fMRI of anesthetized child brain. *Magnetic resonance in medicine*, *44*(3), 373–378. doi: 10.1002/1522-2594(200009)44:3<373::aid-mrm5>3.0.co;2-p
- Kostović, I., Judas, M., Petanjek, Z., & Simić, G. (1995). Ontogenesis of goal-directed behavior: anatomo-functional considerations. *International journal of psychophysiology : official journal of the International Organization of Psychophysiology*, *19*(2), 85–102. doi: 10.1016/0167-8760(94)00081-o
- Kostović, I., & Jovanov-Milosević, N. (2006). The development of cerebral connections during the first 20-45 weeks' gestation. *Seminars in fetal & neonatal medicine*, *11*(6), 415–422. doi: 10.1016/j.siny.2006.07.001
- Kostović, I., & Judas, M. (2010). The development of the subplate and thalamocortical connections in the human foetal brain. *Acta paediatrica (Oslo, Norway : 1992)*, *99*(8), 1119–1127. doi: 10.1111/j.1651-2227.2010.01811.x
- Kostović, I., Jovanov-Milošević, N., Radoš, M., Sedmak, G., Benjak, V., Kostović-Srzić, M., Vasung, L., Čuljat, M., Radoš, M., Hüppi, P., & Judaš, M. (2014). Perinatal and early postnatal reorganization of the subplate and related cellular compartments in the human cerebral wall as revealed by histological and MRI approaches. *Brain structure & function*, *219*(1), 231–253. doi: 10.1007/s00429-012-0496-0
- Kostović, I., Sedmak, G., & Judaš, M. (2019). Neural histology and neurogenesis of the human fetal and infant brain. *NeuroImage*, *188*, 743–773. doi: 10.1016/j.neuroimage.2018.12.043
- Kringelbach, M. L., & Deco, G. (2020). Brain States and Transitions: Insights from Computational Neuroscience. *Cell reports*, *32*(10), 108128. doi: 10.1016/j.celrep.2020.108128
- Lakatos, A., Kolossváry, M., Szabó, M., Jermendy, Á., Barta, H., Gyebnár, G., Rudas, G., & Kozák, L. R. (2019). Neurodevelopmental effect of intracranial hemorrhage observed in hypoxic ischemic brain injury in hypothermia-treated asphyxiated neonates - an MRI study. *BMC pediatrics*, *19*(1), 430. doi: 10.1186/s12887-019-1777-z
- Lally, P. J., Montaldo, P., Oliveira, V., Soe, A., Swamy, R., Bassett, P., Mendoza, J., Atreja, G., Kariholu, U., Pattanayak, S., Sashikumar, P., Harizaj, H., Mitchell, M., Ganesh, V., Harigopal, S., Dixon, J., English, P., Clarke, P., Muthukumar, P., Satodia, P., ... MARBLE consortium (2019). Magnetic resonance spectroscopy assessment of brain injury after moderate hypothermia in neonatal encephalopathy: a prospective multicentre cohort study. *The Lancet. Neurology*, *18*(1), 35–45. doi: 10.1016/S1474-4422(18)30325-9
- Lambert, L. M., Minich, L. L., Newburger, J. W., Lu, M., Pemberton, V. L., McGrath, E. A., Atz, A. M., Xu, M., Radojewski, E., Servedio, D., McCrindle, B. W., & Pediatric Heart Network Investigators (2009). Parent- versus child-reported functional health status after the Fontan procedure. *Pediatrics*, *124*(5), e942–e949. doi: 10.1542/peds.2008-1697
- Larson-Prior, L. J., Zempel, J. M., Nolan, T. S., Prior, F. W., Snyder, A. Z., & Raichle, M. E. (2009). Cortical network functional connectivity in the descent to sleep. *Proceedings of the National Academy of Sciences of the United States of America*, *106*(11), 4489–4494. doi: 10.1073/pnas.0900924106
- Larson-Prior, L. J., Zempel, J. M., Nolan, T. S., Prior, F. W., Snyder, A. Z., & Raichle, M. E. (2009). Cortical network functional connectivity in the descent to sleep. *Proceedings*

- of the National Academy of Sciences of the United States of America, 106(11), 4489–4494. doi: 10.1073/pnas.0900924106
- Latal, B. (2016). Neurodevelopmental Outcomes of the Child with Congenital Heart Disease. *Clinics in perinatology*, 43(1), 173–185. doi: 10.1016/j.clp.2015.11.012
- Latal, B., Wohlrab, G., Brotschi, B., Beck, I., Knirsch, W., & Bernet, V. (2016). Postoperative Amplitude-Integrated Electroencephalography Predicts Four-Year Neurodevelopmental Outcome in Children with Complex Congenital Heart Disease. *The Journal of pediatrics*, 178, 55–60.e1. doi: 10.1016/j.jpeds.2016.06.050
- Latora, V., & Marchiori, M. (2003). Economic small-world behavior in weighted networks. *European Physical Journal B*, 32, 249–263. doi: 10.1140/epjb/e2003-00095-5.
- Latora, V., & Marchiori, M. (2001). Efficient behavior of small-world networks. *Physical review letters*, 87(19), 198701. doi: 10.1103/PhysRevLett.87.198701
- Laumann, T. O., Snyder, A. Z., Mitra, A., Gordon, E. M., Gratton, C., Adeyemo, B., Gilmore, A. W., Nelson, S. M., Berg, J. J., Greene, D. J., McCarthy, J. E., Tagliazucchi, E., Laufs, H., Schlaggar, B. L., Dosenbach, N., & Petersen, S. E. (2017). On the Stability of BOLD fMRI Correlations. *Cerebral cortex (New York, N.Y. : 1991)*, 27(10), 4719–4732. doi: 10.1093/cercor/bhw265
- LeDoux, J.E. (1996). *The emotional brain: The mysterious underpinnings of emotional life*. New York: Simon & Schuster.
- Lee, A. C., Kozuki, N., Blencowe, H., Vos, T., Bahalim, A., Darmstadt, G. L., Niermeyer, S., Ellis, M., Robertson, N. J., Cousens, S., & Lawn, J. E. (2013). Intrapartum-related neonatal encephalopathy incidence and impairment at regional and global levels for 2010 with trends from 1990. *Pediatric research*, 74 Suppl 1(Suppl 1), 50–72. doi: 10.1038/pr.2013.206
- Lee, B. L., & Glass, H. C. (2021). Cognitive outcomes in late childhood and adolescence of neonatal hypoxic-ischemic encephalopathy. *Clinical and experimental pediatrics*, 10.3345/cep.2021.00164. doi: 10.3345/cep.2021.00164
- Lee, W. H., Moser, D. A., Ing, A., Doucet, G. E., & Frangou, S. (2019). Behavioral and Health Correlates of Resting-State Metastability in the Human Connectome Project. *Brain topography*, 32(1), 80–86. doi: 10.1007/s10548-018-0672-5
- Lee, W. H., & Frangou, S. (2017). Linking functional connectivity and dynamic properties of resting-state networks. *Scientific reports*, 7(1), 16610. doi: 10.1038/s41598-017-16789-1
- Lehéricy, S., Benali, H., Van de Moortele, P. F., Péligrini-Issac, M., Waechter, T., Ugurbil, K., & Doyon, J. (2005). Distinct basal ganglia territories are engaged in early and advanced motor sequence learning. *Proceedings of the National Academy of Sciences of the United States of America*, 102(35), 12566–12571. doi: 10.1073/pnas.0502762102
- Leonardi, N., & Van De Ville, D. (2015). On spurious and real fluctuations of dynamic functional connectivity during rest. *NeuroImage*, 104, 430–436. doi: 10.1016/j.neuroimage.2014.09.007
- Levitt P. (2003). Structural and functional maturation of the developing primate brain. *The Journal of pediatrics*, 143(4 Suppl), S35–S45. doi: 10.1067/s0022-3476(03)00400-1
- Li, H. X., Yu, M., Zheng, A. B., Zhang, Q. F., Hua, G. W., Tu, W. J., & Zhang, L. C. (2019). Resting-state network complexity and magnitude changes in neonates with severe hypoxic ischemic encephalopathy. *Neural regeneration research*, 14(4), 642–648. doi: 10.4103/1673-5374.247468

- Liégeois, R., Laumann, T. O., Snyder, A. Z., Zhou, J., & Yeo, B. (2017). Interpreting temporal fluctuations in resting-state functional connectivity MRI. *NeuroImage*, *163*, 437–455. doi: 10.1016/j.neuroimage.2017.09.012
- Limperopoulos, C., Majnemer, A., Shevell, M. I., Rosenblatt, B., Rohlicek, C., & Tchervenkov, C. (1999). Neurologic status of newborns with congenital heart defects before open heart surgery. *Pediatrics*, *103*(2), 402–408. doi: 10.1542/peds.103.2.402
- Limperopoulos, C., Majnemer, A., Shevell, M. I., Rohlicek, C., Rosenblatt, B., Tchervenkov, C., & Darwish, H. Z. (2002). Predictors of developmental disabilities after open heart surgery in young children with congenital heart defects. *The Journal of pediatrics*, *141*(1), 51–58. doi: 10.1067/mpd.2002.125227
- Limperopoulos, C., Tworetzky, W., McElhinney, D. B., Newburger, J. W., Brown, D. W., Robertson, R. L., Jr, Guizard, N., McGrath, E., Geva, J., Annese, D., Dunbar-Masterson, C., Trainor, B., Laussen, P. C., & du Plessis, A. J. (2010). Brain volume and metabolism in fetuses with congenital heart disease: evaluation with quantitative magnetic resonance imaging and spectroscopy. *Circulation*, *121*(1), 26–33. doi: 10.1161/CIRCULATIONAHA.109.865568
- Lin, W., Zhu, Q., Gao, W., Chen, Y., Toh, C. H., Styner, M., Gerig, G., Smith, J. K., Biswal, B., & Gilmore, J. H. (2008). Functional connectivity MR imaging reveals cortical functional connectivity in the developing brain. *AJNR. American journal of neuroradiology*, *29*(10), 1883–1889. doi: 10.3174/ajnr.A1256
- Linke, A. C., Wild, C., Zubiaurre-Elorza, L., Herzmann, C., Duffy, H., Han, V. K., Lee, D., & Cusack, R. (2018). Disruption to functional networks in neonates with perinatal brain injury predicts motor skills at 8 months. *NeuroImage. Clinical*, *18*, 399–406. doi: 10.1016/j.nicl.2018.02.002
- Lodygensky, G. A., Battin, M. R., & Gunn, A. J. (2018). Mild Neonatal Encephalopathy-How, When, and How Much to Treat?. *JAMA pediatrics*, *172*(1), 3–4. doi: 10.1001/jamapediatrics.2017.3044
- Lowe, M. J., Mock, B. J., & Sorenson, J. A. (1998). Functional connectivity in single and multislice echoplanar imaging using resting-state fluctuations. *NeuroImage*, *7*(2), 119–132. doi: 10.1006/nimg.1997.0315
- Machie, M., Weeke, L., de Vries, L. S., Rollins, N., Brown, L., & Chalak, L. (2021). MRI Score Ability to Detect Abnormalities in Mild Hypoxic-Ischemic Encephalopathy. *Pediatric neurology*, *116*, 32–38. doi: 10.1016/j.pediatrneurol.2020.11.015
- Mahle, W. T., Clancy, R. R., McGaurn, S. P., Goin, J. E., & Clark, B. J. (2001). Impact of prenatal diagnosis on survival and early neurologic morbidity in neonates with the hypoplastic left heart syndrome. *Pediatrics*, *107*(6), 1277–1282. doi: 10.1542/peds.107.6.1277
- Mahle, W. T., Tavani, F., Zimmerman, R. A., Nicolson, S. C., Galli, K. K., Gaynor, J. W., Clancy, R. R., Montenegro, L. M., Spray, T. L., Chiavacci, R. M., Wernovsky, G., & Kurth, C. D. (2002). An MRI study of neurological injury before and after congenital heart surgery. *Circulation*, *106*(12 Suppl 1), I109–I114.
- Majnemer, A., Limperopoulos, C., Shevell, M. I., Rohlicek, C., Rosenblatt, B., & Tchervenkov, C. (2009). A new look at outcomes of infants with congenital heart disease. *Pediatric neurology*, *40*(3), 197–204. doi: 10.1016/j.pediatrneurol.2008.09.014
- Makki, M. I., Govindan, R. M., Wilson, B. J., Behen, M. E., & Chugani, H. T. (2009). Altered fronto-striato-thalamic connectivity in children with Tourette syndrome assessed with diffusion tensor MRI and probabilistic fiber tracking. *Journal of child neurology*, *24*(6), 669–678. doi: 10.1177/0883073808327838

- Makropoulos, A., Gousias, I. S., Ledig, C., Aljabar, P., Serag, A., Hajnal, J. V., Edwards, A. D., Counsell, S. J., & Rueckert, D. (2014). Automatic whole brain MRI segmentation of the developing neonatal brain. *IEEE transactions on medical imaging*, *33*(9), 1818–1831. doi: 10.1109/TMI.2014.2322280
- Makropoulos, A., Aljabar, P., Wright, R., Hüning, B., Merchant, N., Arichi, T., Tusor, N., Hajnal, J. V., Edwards, A. D., Counsell, S. J., & Rueckert, D. (2016). Regional growth and atlas of the developing human brain. *NeuroImage*, *125*, 456–478. doi: 10.1016/j.neuroimage.2015.10.047
- Makropoulos, A., Robinson, E. C., Schuh, A., Wright, R., Fitzgibbon, S., Bozek, J., Counsell, S. J., Steinweg, J., Vecchiato, K., Passerat-Palmbach, J., Lenz, G., Mortari, F., Tenev, T., Duff, E. P., Bastiani, M., Cordero-Grande, L., Hughes, E., Tusor, N., Tournier, J. D., Hutter, J., ... Rueckert, D. (2018). The developing human connectome project: A minimal processing pipeline for neonatal cortical surface reconstruction. *NeuroImage*, *173*, 88–112. doi: 10.1016/j.neuroimage.2018.01.054
- Mañeru, C., Junqué, C., Botet, F., Tallada, M., & Guardia, J. (2001). Neuropsychological long-term sequelae of perinatal asphyxia. *Brain injury*, *15*(12), 1029–1039. doi: 10.1080/02699050110074178
- Marelli, A., Miller, S. P., Marino, B. S., Jefferson, A. L., & Newburger, J. W. (2016). Brain in Congenital Heart Disease Across the Lifespan: The Cumulative Burden of Injury. *Circulation*, *133*(20), 1951–1962. doi: 10.1161/CIRCULATIONAHA.115.019881
- Marino, B. S., Lipkin, P. H., Newburger, J. W., Peacock, G., Gerdes, M., Gaynor, J. W., Mussatto, K. A., Uzark, K., Goldberg, C. S., Johnson, W. H., Jr, Li, J., Smith, S. E., Bellinger, D. C., Mahle, W. T., & American Heart Association Congenital Heart Defects Committee, Council on Cardiovascular Disease in the Young, Council on Cardiovascular Nursing, and Stroke Council (2012). Neurodevelopmental outcomes in children with congenital heart disease: evaluation and management: a scientific statement from the American Heart Association. *Circulation*, *126*(9), 1143–1172. doi: 10.1161/CIR.0b013e318265ee8a
- Marlow, N., Rose, A. S., Rands, C. E., & Draper, E. S. (2005). Neuropsychological and educational problems at school age associated with neonatal encephalopathy. *Archives of disease in childhood. Fetal and neonatal edition*, *90*(5), F380–F387. doi: 10.1136/adc.2004.067520
- Martinez-Biarge, M., Diez-Sebastian, J., Rutherford, M. A., & Cowan, F. M. (2010). Outcomes after central grey matter injury in term perinatal hypoxic-ischaemic encephalopathy. *Early human development*, *86*(11), 675–682. doi: 10.1016/j.earlhumdev.2010.08.013
- Martinez-Biarge, M., Diez-Sebastian, J., Kapellou, O., Gindner, D., Allsop, J. M., Rutherford, M. A., & Cowan, F. M. (2011). Predicting motor outcome and death in term hypoxic-ischemic encephalopathy. *Neurology*, *76*(24), 2055–2061. doi: 10.1212/WNL.0b013e31821f442d
- Massaro, A. N., Evangelou, I., Brown, J., Fatemi, A., Vezina, G., McCarter, R., Glass, P., & Limperopoulos, C. (2015). Neonatal neurobehavior after therapeutic hypothermia for hypoxic ischemic encephalopathy. *Early human development*, *91*(10), 593–599. doi: 10.1016/j.earlhumdev.2015.07.008
- Massaro, A. N., Evangelou, I., Brown, J., Fatemi, A., Vezina, G., McCarter, R., Glass, P., & Limperopoulos, C. (2015). Neonatal neurobehavior after therapeutic hypothermia for hypoxic ischemic encephalopathy. *Early human development*, *91*(10), 593–599. doi: 10.1016/j.earlhumdev.2015.07.008

- Massaro, A. N., Evangelou, I., Fatemi, A., Vezina, G., Mccarter, R., Glass, P., & Limperopoulos, C. (2015). White matter tract integrity and developmental outcome in newborn infants with hypoxic-ischemic encephalopathy treated with hypothermia. *Developmental medicine and child neurology*, *57*(5), 441–448. doi: 10.1111/dmcn.12646
- Masur, E. F. (1995). Infants' early verbal imitation and their later lexical development. *Merrill-Palmer Quarterly*, *41*(3), 286–306.
- Matthiesen, N. B., Henriksen, T. B., Agergaard, P., Gaynor, J. W., Bach, C. C., Hjortdal, V. E., & Østergaard, J. R. (2016). Congenital Heart Defects and Indices of Placental and Fetal Growth in a Nationwide Study of 924 422 Liveborn Infants. *Circulation*, *134*(20), 1546–1556. doi: 10.1161/CIRCULATIONAHA.116.021793
- Mebius, M. J., Kooi, E., Bilardo, C. M., & Bos, A. F. (2017). Brain Injury and Neurodevelopmental Outcome in Congenital Heart Disease: A Systematic Review. *Pediatrics*, *140*(1), e20164055. doi: 10.1542/peds.2016-4055
- Mendis S, Puska P, Norrving B. (2011). Organization WH, Federation WH, Organization WS. Global atlas on cardiovascular disease prevention and control. Geneva: World Health Organization.
- Mercuri, E., Ricci, D., Cowan, F. M., Lessing, D., Frisone, M. F., Haataja, L., Counsell, S. J., Dubowitz, L. M., & Rutherford, M. A. (2000). Head growth in infants with hypoxic-ischemic encephalopathy: correlation with neonatal magnetic resonance imaging. *Pediatrics*, *106*(2 Pt 1), 235–243. doi: 10.1542/peds.106.2.235
- McKinstry, R. C., Miller, J. H., Snyder, A. Z., Mathur, A., Schefft, G. L., Almlı, C. R., Shimony, J. S., Shiran, S. I., & Neil, J. J. (2002). A prospective, longitudinal diffusion tensor imaging study of brain injury in newborns. *Neurology*, *59*(6), 824–833. doi: 10.1212/wnl.59.6.824
- McQuillen, P. S., Barkovich, A. J., Hamrick, S. E., Perez, M., Ward, P., Glidden, D. V., Azakie, A., Karl, T., & Miller, S. P. (2007). Temporal and anatomic risk profile of brain injury with neonatal repair of congenital heart defects. *Stroke*, *38*(2 Suppl), 736–741. doi: 10.1161/01.STR.0000247941.41234.90
- McQuillen, P. S., Hamrick, S. E., Perez, M. J., Barkovich, A. J., Glidden, D. V., Karl, T. R., Teitel, D., & Miller, S. P. (2006). Balloon atrial septostomy is associated with preoperative stroke in neonates with transposition of the great arteries. *Circulation*, *113*(2), 280–285. doi: 10.1161/CIRCULATIONAHA.105.566752
- Miller, S. P., McQuillen, P. S., Hamrick, S., Xu, D., Glidden, D. V., Charlton, N., Karl, T., Azakie, A., Ferriero, D. M., Barkovich, A. J., & Vigneron, D. B. (2007). Abnormal brain development in newborns with congenital heart disease. *The New England journal of medicine*, *357*(19), 1928–1938. doi: 10.1056/NEJMoa067393
- Miller, S. P., McQuillen, P. S., Vigneron, D. B., Glidden, D. V., Barkovich, A. J., Ferriero, D. M., Hamrick, S. E., Azakie, A., & Karl, T. R. (2004). Preoperative brain injury in newborns with transposition of the great arteries. *The Annals of thoracic surgery*, *77*(5), 1698–1706. doi: .1016/j.athoracsur.2003.10.084
- Miller, S. P., Ramaswamy, V., Michelson, D., Barkovich, A. J., Holshouser, B., Wycliffe, N., Glidden, D. V., Deming, D., Partridge, J. C., Wu, Y. W., Ashwal, S., & Ferriero, D. M. (2005). Patterns of brain injury in term neonatal encephalopathy. *The Journal of pediatrics*, *146*(4), 453–460. doi: 10.1016/j.jpeds.2004.12.026
- Molloy, E. J., & Bearer, C. (2018). Neonatal encephalopathy versus Hypoxic-Ischemic Encephalopathy. *Pediatric research*, *84*(5), 574. doi: 10.1038/s41390-018-0169-7

- Morton, S. M., & Bastian, A. J. (2004). Prism adaptation during walking generalizes to reaching and requires the cerebellum. *Journal of neurophysiology*, *92*(4), 2497–2509. doi: 10.1152/jn.00129.2004
- Moseley, M. E., Cohen, Y., Kucharczyk, J., Mintorovitch, J., Asgari, H. S., Wendland, M. F., Tsuruda, J., & Norman, D. (1990). Diffusion-weighted MR imaging of anisotropic water diffusion in cat central nervous system. *Radiology*, *176*(2), 439–445. doi: 10.1148/radiology.176.2.236765
- Murdoch B. E. (2010). The cerebellum and language: historical perspective and review. *Cortex; a journal devoted to the study of the nervous system and behavior*, *46*(7), 858–868. doi: 10.1016/j.cortex.2009.07.018
- Mulkey, S. B., Ou, X., Ramakrishnaiah, R. H., Glasier, C. M., Swearingen, C. J., Melguizo, M. S., Yap, V. L., Schmitz, M. L., & Bhutta, A. T. (2014). White matter injury in newborns with congenital heart disease: a diffusion tensor imaging study. *Pediatric neurology*, *51*(3), 377–383. doi: 10.1016/j.pediatrneurol.2014.04.00
- Murray, D. M., Boylan, G. B., Ryan, C. A., & Connolly, S. (2009). Early EEG findings in hypoxic-ischemic encephalopathy predict outcomes at 2 years. *Pediatrics*, *124*(3), e459–e467. doi: 10.1542/peds.2008-2190
- Natarajan, G., Pappas, A., & Shankaran, S. (2016). Outcomes in childhood following therapeutic hypothermia for neonatal hypoxic-ischemic encephalopathy (HIE). *Seminars in perinatology*, *40*(8), 549–555. doi: 10.1053/j.semperi.2016.09.007
- Nelson, K. B., Bingham, P., Edwards, E. M., Horbar, J. D., Kenny, M. J., Inder, T., Pfister, R. H., Raju, T., & Soll, R. F. (2012). Antecedents of neonatal encephalopathy in the Vermont Oxford Network Encephalopathy Registry. *Pediatrics*, *130*(5), 878–886. doi: 10.1542/peds.2012-0714
- Newman M. E. (2006). Modularity and community structure in networks. *Proceedings of the National Academy of Sciences of the United States of America*, *103*(23), 8577–8582. doi: 10.1073/pnas.0601602103
- Ní Bhroin, M., Abo Seada, S., Bonthron, A. F., Kelly, C. J., Christiaens, D., Schuh, A., Pietsch, M., Hutter, J., Tournier, J. D., Cordero-Grande, L., Rueckert, D., Hajnal, J. V., Pushparajah, K., Simpson, J., Edwards, A. D., Rutherford, M. A., Counsell, S. J., & Bataille, D. (2020). Reduced structural connectivity in cortico-striatal-thalamic network in neonates with congenital heart disease. *NeuroImage. Clinical*, *28*, 102423. doi: 10.1016/j.nicl.2020.102423
- Ní Bhroin, M., Molloy, E. J., & Bokde, A. (2021). Relationship between resting-state fMRI functional connectivity with motor and language outcome after perinatal brain injury - A systematic review. *European journal of paediatric neurology : EJPN : official journal of the European Paediatric Neurology Society*, *33*, 36–49. doi: 10.1016/j.ejpn.2021.05.007
- Nosarti, C., Giouroukou, E., Healy, E., Rifkin, L., Walshe, M., Reichenberg, A., Chitnis, X., Williams, S. C., & Murray, R. M. (2008). Grey and white matter distribution in very preterm adolescents mediates neurodevelopmental outcome. *Brain : a journal of neurology*, *131*(Pt 1), 205–217. doi: 10.1093/brain/awm282
- O'Hare, F. M., Watson, R. W., O'Neill, A., Segurado, R., Sweetman, D., Downey, P., Mooney, E., Murphy, J., Donoghue, V., & Molloy, E. J. (2017). Serial cytokine alterations and abnormal neuroimaging in newborn infants with encephalopathy. *Acta paediatrica*, *106*(4), 561–567. doi: 10.1111/apa.13745
- O'Kane, A., Vezina, G., Chang, T., Bendush, N., Ridore, M., Gai, J., Bost, J., Glass, P., & Massaro, A. N. (2021). Early Versus Late Brain Magnetic Resonance Imaging after Neonatal Hypoxic Ischemic Encephalopathy Treated with Therapeutic

- Hypothermia. *The Journal of pediatrics*, 232, 73–79.e2. doi: 10.1016/j.jpeds.2021.01.050
- Ogawa, S., Lee, T. M., Kay, A. R., & Tank, D. W. (1990). Brain magnetic resonance imaging with contrast dependent on blood oxygenation. *Proceedings of the National Academy of Sciences of the United States of America*, 87(24), 9868–9872. doi: 10.1073/pnas.87.24.9868
- Oishi, K., Mori, S., Donohue, P. K., Ernst, T., Anderson, L., Buchthal, S., Faria, A., Jiang, H., Li, X., Miller, M. I., van Zijl, P. C., & Chang, L. (2011). Multi-contrast human neonatal brain atlas: application to normal neonate development analysis. *NeuroImage*, 56(1), 8–20. doi: 10.1016/j.neuroimage.2011.01.051
- Oliveira, V., Singhvi, D. P., Montaldo, P., Lally, P. J., Mendoza, J., Manerkar, S., Shankaran, S., & Thayyil, S. (2018). Therapeutic hypothermia in mild neonatal encephalopathy: a national survey of practice in the UK. *Archives of disease in childhood. Fetal and neonatal edition*, 103(4), F388–F390. doi: 10.1136/archdischild-2017-313320
- Oller D, K. (1978). Infant vocalization and the development of speech. *Allied Health and Behavioral Science*, 1, 523-549.
- Ortinou, C., Beca, J., Lambeth, J., Ferdman, B., Alexopoulos, D., Shimony, J. S., Wallendorf, M., Neil, J., & Inder, T. (2012). Regional alterations in cerebral growth exist preoperatively in infants with congenital heart disease. *The Journal of thoracic and cardiovascular surgery*, 143(6), 1264–1270. doi: 10.1016/j.jtcvs.2011.10.039
- Oudgenoeg-Paz, O., Volman, M. C., & Leseman, P. P. (2012). Attainment of sitting and walking predicts development of productive vocabulary between ages 16 and 28 months. *Infant behavior & development*, 35(4), 733–736. doi: 10.1016/j.infbeh.2012.07.010
- Ouwehand, S., Smidt, L., Dudink, J., Benders, M., de Vries, L. S., Groenendaal, F., & van der Aa, N. E. (2020). Predictors of Outcomes in Hypoxic-Ischemic Encephalopathy following Hypothermia: A Meta-Analysis. *Neonatology*, 117(4), 411–427. doi: 10.1159/000505519
- Owen, M., Shevell, M., Donofrio, M., Majnemer, A., McCarter, R., Vezina, G., Bouyssi-Kobar, M., Evangelou, I., Freeman, D., Weisenfeld, N., & Limperopoulos, C. (2014). Brain volume and neurobehavior in newborns with complex congenital heart defects. *The Journal of pediatrics*, 164(5), 1121–1127.e1. doi: 10.1016/j.jpeds.2013.11.033
- Papez, J. W. (1995) A proposed mechanism of emotion. *J Neuropsychiatry Clinical Neuroscience*, 7(1), 103-12. doi: 10.1176/jnp.7.1.103. PMID: 7711480.
- Pandi-Perumal, S. R., BaHammam, A. S., Brown, G. M., Spence, D. W., Bharti, V. K., Kaur, C., Hardeland, R., & Cardinali, D. P. (2013). Melatonin antioxidative defense: therapeutical implications for aging and neurodegenerative processes. *Neurotoxicity research*, 23(3), 267–300. doi: 10.1007/s12640-012-9337-4
- Pappas, A., Shankaran, S., McDonald, S. A., Vohr, B. R., Hintz, S. R., Ehrenkranz, R. A., Tyson, J. E., Yolton, K., Das, A., Bara, R., Hammond, J., Higgins, R. D., & Hypothermia Extended Follow-up Subcommittee of the Eunice Kennedy Shriver NICHD Neonatal Research Network (2015). Cognitive outcomes after neonatal encephalopathy. *Pediatrics*, 135(3), e624–e634. doi: 10.1542/peds.2014-1566
- Parnaudeau, S., Bolkan, S. S., & Kellendonk, C. (2018). The Mediodorsal Thalamus: An Essential Partner of the Prefrontal Cortex for Cognition. *Biological psychiatry*, 83(8), 648–656. doi: 10.1016/j.biopsych.2017.11.008
- Paus, T., Collins, D. L., Evans, A. C., Leonard, G., Pike, B., & Zijdenbos, A. (2001). Maturation of white matter in the human brain: a review of magnetic resonance studies. *Brain research bulletin*, 54(3), 255–266. doi: 10.1016/s0361-9230(00)00434-2

- Perani, D., Saccuman, M. C., Scifo, P., Anwender, A., Spada, D., Baldoli, C., Poloniato, A., Lohmann, G., & Friederici, A. D. (2011). Neural language networks at birth. *Proceedings of the National Academy of Sciences of the United States of America*, *108*(38), 16056–16061. doi: 10.1073/pnas.1102991108
- Petanjek, Z., Judaš, M., Šimic, G., Rasin, M. R., Uylings, H. B., Rakic, P., & Kostovic, I. (2011). Extraordinary neoteny of synaptic spines in the human prefrontal cortex. *Proceedings of the National Academy of Sciences of the United States of America*, *108*(32), 13281–13286. doi: 10.1073/pnas.1105108108
- Peyvandi, S., Latal, B., Miller, S. P., & McQuillen, P. S. (2019). The neonatal brain in critical congenital heart disease: Insights and future directions. *NeuroImage*, *185*, 776–782. doi: 10.1016/j.neuroimage.2018.05.045
- Pin, T. W., Eldridge, B., & Galea, M. P. (2009). A review of developmental outcomes of term infants with post-asphyxia neonatal encephalopathy. *European journal of paediatric neurology : EJPN : official journal of the European Paediatric Neurology Society*, *13*(3), 224–234. doi: 10.1016/j.ejpn.2008.05.001
- Piper, M. S., Darrah, J. (1994). *Motor assessment of the Developing Infant*. Philadelphia, PA: W.B. Saunders Company.
- Ponce-Alvarez, A., Deco, G., Hagmann, P., Romani, G. L., Mantini, D., & Corbetta, M. (2015). Resting-state temporal synchronization networks emerge from connectivity topology and heterogeneity. *PLoS computational biology*, *11*(2), e1004100. doi: 10.1371/journal.pcbi.1004100
- Porter, E. J., Counsell, S. J., Edwards, A. D., Allsop, J., & Azzopardi, D. (2010). Tract-based spatial statistics of magnetic resonance images to assess disease and treatment effects in perinatal asphyxial encephalopathy. *Pediatric research*, *68*(3), 205–209. doi: 10.1203/PDR.0b013e3181e9f1ba
- Power, J. D., Cohen, A. L., Nelson, S. M., Wig, G. S., Barnes, K. A., Church, J. A., Vogel, A. C., Laumann, T. O., Miezin, F. M., Schlaggar, B. L., & Petersen, S. E. (2011). Functional network organization of the human brain. *Neuron*, *72*(4), 665–678. doi: 10.1016/j.neuron.2011.09.006
- Power, J. D., Barnes, K. A., Snyder, A. Z., Schlaggar, B. L., & Petersen, S. E. (2012). Spurious but systematic correlations in functional connectivity MRI networks arise from subject motion. *NeuroImage*, *59*(3), 2142–2154. doi: 10.1016/j.neuroimage.2011.10.018
- Price, T., Wee, C. Y., Gao, W., & Shen, D. (2014). Multiple-network classification of childhood autism using functional connectivity dynamics. *Medical image computing and computer-assisted intervention : MICCAI ... International Conference on Medical Image Computing and Computer-Assisted Intervention*, *17*(Pt 3), 177–184. doi: 10.1007/978-3-319-10443-0_23
- Purcell, E. M., Torrey, H. C., Pound, R. V. (1946). Resonance absorption by nuclear magnetic moments in a solid. *Physical review*, *69*, 37–38.
- Qin, Y., Li, Y., Sun, B., He, H., Peng, R., Zhang, T., Li, J., Luo, C., Sun, C., & Yao, D. (2018). Functional Connectivity Alterations in Children with Spastic and Dyskinetic Cerebral Palsy. *Neural plasticity*, *2018*, 7058953. doi: 10.1155/2018/7058953
- Qin, Y., Sun, B., Zhang, H., Li, Y., Zhang, T., Luo, C., Sun, C., & Yao, D. (2019). Aberrant Interhemispheric Functional Organization in Children with Dyskinetic Cerebral Palsy. *BioMed research international*, *2019*, 4362539. doi: 10.1155/2019/4362539
- Raichle M. E. (2015). The brain's default mode network. *Annual review of neuroscience*, *38*, 433–447. <https://doi.org/10.1146/annurev-neuro-071013-014030>
- Raffelt, D., Dhollander, T., Tournier, J. -D., Tabbara, R., Smith, R. E. Pierre, E., Connelly A. (2017). Bias field correction and intensity normalisation for quantitative analysis of

- apparent fibre density. *Proceedings of the International Society for Magnetic Resonance in Medicine*, 25:3541. doi: archive.ismrm.org/2017/3541
- Rashid, B., Damaraju, E., Pearlson, G. D., & Calhoun, V. D. (2014). Dynamic connectivity states estimated from resting fMRI Identify differences among Schizophrenia, bipolar disorder, and healthy control subjects. *Frontiers in human neuroscience*, 8, 897. doi: 10.3389/fnhum.2014.00897
- Redcay, E., Moran, J. M., Mavros, P. L., Tager-Flusberg, H., Gabrieli, J. D., & Whitfield-Gabrieli, S. (2013). Intrinsic functional network organization in high-functioning adolescents with autism spectrum disorder. *Frontiers in human neuroscience*, 7, 573. doi: 10.3389/fnhum.2013.00573
- Rivkin, M. J., Watson, C. G., Scoppettuolo, L. A., Wypij, D., Vajapeyam, S., Bellinger, D. C., DeMaso, D. R., Robertson, R. L., Jr, & Newburger, J. W. (2013). Adolescents with D-transposition of the great arteries repaired in early infancy demonstrate reduced white matter microstructure associated with clinical risk factors. *The Journal of thoracic and cardiovascular surgery*, 146(3), 543–9.e1. doi: 10.1016/j.jtcvs.2012.12.006
- Robertson, C., & Finer, N. (1985). Term infants with hypoxic-ischemic encephalopathy: outcome at 3.5 years. *Developmental medicine and child neurology*, 27(4), 473–484. doi: 10.1111/j.1469-8749.1985.tb04571.x
- Robertson, C. M., Finer, N. N., & Grace, M. G. (1989). School performance of survivors of neonatal encephalopathy associated with birth asphyxia at term. *The Journal of pediatrics*, 114(5), 753–760. doi: 10.1016/s0022-3476(89)80132-5
- Robertson, C. M., & Finer, N. N. (1993). Long-term follow-up of term neonates with perinatal asphyxia. *Clinics in perinatology*, 20(2), 483–500.
- Rollins, C. K., Watson, C. G., Asaro, L. A., Wypij, D., Vajapeyam, S., Bellinger, D. C., DeMaso, D. R., Robertson, R. L., Jr, Newburger, J. W., & Rivkin, M. J. (2014). White matter microstructure and cognition in adolescents with congenital heart disease. *The Journal of pediatrics*, 165(5), 936–44.e442. doi: 10.1016/j.jpeds.2014.07.028
- Rollins, N., Booth, T., Morriss, M. C., Sanchez, P., Heyne, R., & Chalak, L. (2014). Predictive value of neonatal MRI showing no or minor degrees of brain injury after hypothermia. *Pediatric neurology*, 50(5), 447–451. doi: 10.1016/j.pediatrneurol.2014.01.013
- Rubinov, M., & Sporns, O. (2010). Complex network measures of brain connectivity: uses and interpretations. *NeuroImage*, 52(3), 1059–1069. doi: 10.1016/j.neuroimage.2009.10.003
- Rutherford, M., Counsell, S., Allsop, J., Boardman, J., Kapellou, O., Larkman, D., Hajnal, J., Edwards, D., & Cowan, F. (2004). Diffusion-weighted magnetic resonance imaging in term perinatal brain injury: a comparison with site of lesion and time from birth. *Pediatrics*, 114(4), 1004–1014. doi: .1542/peds.2004-0222
- Rutherford, M., Ramenghi, L. A., Edwards, A. D., Brocklehurst, P., Halliday, H., Levene, M., Strohm, B., Thoresen, M., Whitelaw, A., & Azzopardi, D. (2010). Assessment of brain tissue injury after moderate hypothermia in neonates with hypoxic-ischaemic encephalopathy: a nested substudy of a randomised controlled trial. *The Lancet. Neurology*, 9(1), 39–45. doi: 10.1016/S1474-4422(09)70295-9
- Rutherford, M., Ward, P., Allsop, J., Malamateniou, C., & Counsell, S. (2005). Magnetic resonance imaging in neonatal encephalopathy. *Early human development*, 81(1), 13–25. doi: 10.1016/j.earlhumdev.2004.10.011
- Rutherford, M. A., Pennock, J. M., Counsell, S. J., Mercuri, E., Cowan, F. M., Dubowitz, L. M., & Edwards, A. D. (1998). Abnormal magnetic resonance signal in the internal capsule predicts poor neurodevelopmental outcome in infants with hypoxic-ischemic encephalopathy. *Pediatrics*, 102(2 Pt 1), 323–328. doi: 10.1542/peds.102.2.323

- Salimi-Khorshidi, G., Douaud, G., Beckmann, C. F., Glasser, M. F., Griffanti, L., & Smith, S. M. (2014). Automatic denoising of functional MRI data: combining independent component analysis and hierarchical fusion of classifiers. *NeuroImage*, *90*, 449–468. doi: 10.1016/j.neuroimage.2013.11.046
- Samuelsen, G. B., Larsen, K. B., Bogdanovic, N., Laursen, H., Graem, N., Larsen, J. F., & Pakkenberg, B. (2003). The changing number of cells in the human fetal forebrain and its subdivisions: a stereological analysis. *Cerebral cortex (New York, N.Y. : 1991)*, *13*(2), 115–122. doi: 10.1093/cercor/13.2.115
- Sánchez Fernández, I., Morales-Quezada, J. L., Law, S., & Kim, P. (2017). Prognostic Value of Brain Magnetic Resonance Imaging in Neonatal Hypoxic-Ischemic Encephalopathy: A Meta-analysis. *Journal of child neurology*, *32*(13), 1065–1073. doi: 10.1177/0883073817726681
- Sarnat, H. B., & Sarnat, M. S. (1976). Neonatal encephalopathy following fetal distress. A clinical and electroencephalographic study. *Archives of neurology*, *33*(10), 696–705. doi: 10.1001/archneur.1976.00500100030012
- Saunders, J., Carlson, H. L., Cortese, F., Goodyear, B. G., & Kirton, A. (2019). Imaging functional motor connectivity in hemiparetic children with perinatal stroke. *Human brain mapping*, *40*(5), 1632–1642. doi: 10.1002/hbm.24474
- Schaefer, C., von Rhein, M., Knirsch, W., Huber, R., Natalucci, G., Cafilisch, J., Landolt, M. A., & Latal, B. (2013). Neurodevelopmental outcome, psychological adjustment, and quality of life in adolescents with congenital heart disease. *Developmental medicine and child neurology*, *55*(12), 1143–1149. doi: 10.1111/dmcn.12242
- Schmahmann, J. D., Caplan, D. (2006). Cognition, emotion and the cerebellum. *Brain*, *129*, 290–293. doi: 10.1093/brain/awh729.
- Schmithorst, V. J., Votava-Smith, J. K., Tran, N., Kim, R., Lee, V., Ceschin, R., Lai, H., Johnson, J. A., De Toledo, J. S., Blüml, S., Paquette, L., & Panigrahy, A. (2018). Structural network topology correlates of microstructural brain dysmaturation in term infants with congenital heart disease. *Human brain mapping*, *39*(11), 4593–4610. doi: 10.1002/hbm.24308
- Schöpf, V., Kasprian, G., Brugger, P. C., & Prayer, D. (2012). Watching the fetal brain at 'rest'. *International journal of developmental neuroscience : the official journal of the International Society for Developmental Neuroscience*, *30*(1), 11–17. doi: 10.1016/j.ijdevneu.2011.10.006
- Schuh, A., Makropoulos, A., Robinson, E. C., Cordero-Grande, L., Hughes, E., Hutter, J., ... & Rueckert, D. (2018). Unbiased construction of a temporally consistent morphological atlas of neonatal brain development. *bioRxiv*, 251512.
- Scoville, W. B., Milner, B. (1957). Loss of recent memory after bilateral hippocampal lesions. *Journal of neurology, neurosurgery, and psychiatry*, *20*(1), 11–21. doi: 10.1136/jnnp.20.1.11
- Seeley, W. W., Menon, V., Schatzberg, A. F., Keller, J., Glover, G. H., Kenna, H., Reiss, A. L., & Greicius, M. D. (2007). Dissociable intrinsic connectivity networks for salience processing and executive control. *The Journal of neuroscience : the official journal of the Society for Neuroscience*, *27*(9), 2349–2356. doi: 10.1523/JNEUROSCI.5587-06.2007
- Senden, M., Deco, G., de Reus, M. A., Goebel, R., & van den Heuvel, M. P. (2014). Rich club organization supports a diverse set of functional network configurations. *NeuroImage*, *96*, 174–182. doi: 10.1016/j.neuroimage.2014.03.066
- Senden, M., Reuter, N., van den Heuvel, M. P., Goebel, R., & Deco, G. (2017). Cortical rich club regions can organize state-dependent functional network formation by engaging in oscillatory behavior. *NeuroImage*, *146*, 561–574. doi: 10.1016/j.neuroimage

- Sethi, V., Tabbutt, S., Dimitropoulos, A., Harris, K. C., Chau, V., Poskitt, K., Campbell, A., Azakie, A., Xu, D., Barkovich, A. J., Miller, S. P., & McQuillen, P. S. (2013). Single-ventricle anatomy predicts delayed microstructural brain development. *Pediatric research*, 73(5), 661–667. doi: 10.1038/pr.2013.29
- Shanahan, M. (2010). Metastable chimera states in community-structured oscillator networks. *Chaos*, 20, 013108. doi: 10.1063/1.3305451.
- Shankaran, S., Barnes, P. D., Hintz, S. R., Lupton, A. R., Zaterka-Baxter, K. M., McDonald, S. A., Ehrenkranz, R. A., Walsh, M. C., Tyson, J. E., Donovan, E. F., Goldberg, R. N., Bara, R., Das, A., Finer, N. N., Sanchez, P. J., Poindexter, B. B., Van Meurs, K. P., Carlo, W. A., Stoll, B. J., Duara, S., ... Eunice Kennedy Shriver National Institute of Child Health and Human Development Neonatal Research Network (2012). Brain injury following trial of hypothermia for neonatal hypoxic-ischaemic encephalopathy. *Archives of disease in childhood. Fetal and neonatal edition*, 97(6), F398–F404. doi: 10.1136/archdischild-2011-301524
- Shankaran, S., Lupton, A. R., Ehrenkranz, R. A., Tyson, J. E., McDonald, S. A., Donovan, E. F., Fanaroff, A. A., Poole, W. K., Wright, L. L., Higgins, R. D., Finer, N. N., Carlo, W. A., Duara, S., Oh, W., Cotten, C. M., Stevenson, D. K., Stoll, B. J., Lemons, J. A., Guillet, R., Jobe, A. H., ... National Institute of Child Health and Human Development Neonatal Research Network (2005). Whole-body hypothermia for neonates with hypoxic-ischemic encephalopathy. *The New England journal of medicine*, 353(15), 1574–1584. doi: 10.1056/NEJMcp050929
- Shankaran S, McDonald SA, Lupton AR, et al. Neonatal Magnetic Resonance Imaging Pattern of Brain Injury as a Biomarker of Childhood Outcomes following a Trial of Hypothermia for Neonatal Hypoxic-Ischemic Encephalopathy. *J Pediatr* 2015;167(5):987-93.e3. doi: 10.1016/j.jpeds.2015.08.013.
- Sheridan, M. (2008). *From Birth to Five Years: Children's Developmental Progress* (Routledge).
- Shi, F., Yap, P. T., Wu, G., Jia, H., Gilmore, J. H., Lin, W., & Shen, D. (2011). Infant brain atlases from neonates to 1- and 2-year-olds. *PloS one*, 6(4), e18746. doi: 10.1371/journal.pone.0018746
- Shi, F., Salzwedel, A. P., Lin, W., Gilmore, J. H., & Gao, W. (2018). Functional Brain Parcellations of the Infant Brain and the Associated Developmental Trends. *Cerebral cortex*, 28(4), 1358–1368. doi: 10.1093/cercor/bhx062
- Simon-Martinez, C., Jaspers, E., Alaerts, K., Ortibus, E., Balsters, J., Mailleux, L., Blommaert, J., Sleurs, C., Klingels, K., Amant, F., Uyttebroeck, A., Wenderoth, N., & Feys, H. (2019). Influence of the corticospinal tract wiring pattern on sensorimotor functional connectivity and clinical correlates of upper limb function in unilateral cerebral palsy. *Scientific reports*, 9(1), 8230. doi: 10.1038/s41598-019-44728-9
- Smith, R. E., Tournier, J. D., Calamante, F., & Connelly, A. (2012). Anatomically-constrained tractography: improved diffusion MRI streamlines tractography through effective use of anatomical information. *NeuroImage*, 62(3), 1924–1938. doi: 10.1016/j.neuroimage.2012.06.005
- Smith, R. E., Tournier, J. D., Calamante, F., & Connelly, A. (2015). SIFT2: Enabling dense quantitative assessment of brain white matter connectivity using streamlines tractography. *NeuroImage*, 119, 338–351. doi: 10.1016/j.neuroimage.2015.06.092
- Smith S. M. (2002). Fast robust automated brain extraction. *Human brain mapping*, 17(3), 143–155. doi: 10.1002/hbm.10062
- Smith, S. M., Fox, P. T., Miller, K. L., Glahn, D. C., Fox, P. M., Mackay, C. E., Filippini, N., Watkins, K. E., Toro, R., Laird, A. R., & Beckmann, C. F. (2009). Correspondence of the brain's functional architecture during activation and rest. *Proceedings of the*

- National Academy of Sciences of the United States of America*, 106(31), 13040–13045. doi: 10.1073/pnas.0905267106
- Smyser, C. D., Inder, T. E., Shimony, J. S., Hill, J. E., Degnan, A. J., Snyder, A. Z., & Neil, J. J. (2010). Longitudinal analysis of neural network development in preterm infants. *Cerebral cortex*, 20(12), 2852–2862. doi: 10.1093/cercor/bhq035
- Smyser, C. D., Snyder, A. Z., Shimony, J. S., Mitra, A., Inder, T. E., & Neil, J. J. (2016). Resting-State Network Complexity and Magnitude Are Reduced in Prematurely Born Infants. *Cerebral cortex*, 26(1), 322–333. doi: 10.1093/cercor/bhu251
- Song, L., Mishra, V., Ouyang, M., Peng, Q., Slinger, M., Liu, S., & Huang, H. (2017). Human Fetal Brain Connectome: Structural Network Development from Middle Fetal Stage to Birth. *Frontiers in neuroscience*, 11, 561. doi: 10.3389/fnins.2017.00561
- Song, S. K., Sun, S. W., Ramsbottom, M. J., Chang, C., Russell, J., & Cross, A. H. (2002). Dysmyelination revealed through MRI as increased radial (but unchanged axial) diffusion of water. *NeuroImage*, 17(3), 1429–1436. doi: 10.1006/nimg.2002.1267
- Sporns, O., Tononi, G., & Kötter, R. (2005). The human connectome: A structural description of the human brain. *PLoS computational biology*, 1(4), e42. doi: 10.1371/journal.pcbi.0010042
- Squire L. R. (2004). Memory systems of the brain: a brief history and current perspective. *Neurobiology of learning and memory*, 82(3), 171–177. doi: 10.1016/j.nlm.2004.06.005
- Steinman, K. J., Gorno-Tempini, M. L., Glidden, D. V., Kramer, J. H., Miller, S. P., Barkovich, A. J., & Ferriero, D. M. (2009). Neonatal watershed brain injury on magnetic resonance imaging correlates with verbal IQ at 4 years. *Pediatrics*, 123(3), 1025–1030. doi: 10.1542/peds.2008-1203
- Stejskal, E. O., Tanner, J. E. (1965). Spin Diffusion Measurements: Spin Echoes in the Presence of a Time-Dependent Field Gradient. *The Journal of Chemical Physics*, 42, 288–292. doi:10.1063/1.1695690
- Strohm, B., Hobson, A., Brocklehurst, P., Edwards, A. D., Azzopardi, D., & UK TOBY Cooling Register (2011). Subcutaneous fat necrosis after moderate therapeutic hypothermia in neonates. *Pediatrics*, 128(2), e450–e452. doi: 10.1542/peds.2010-3508
- Stroup, D. F., Berlin, J. A., Morton, S. C., Olkin, I., Williamson, G. D., Rennie, D., Moher, D., Becker, B. J., Sipe, T. A., & Thacker, S. B. (2000). Meta-analysis of observational studies in epidemiology: a proposal for reporting. Meta-analysis Of Observational Studies in Epidemiology (MOOSE) group. *JAMA*, 283(15), 2008–2012. doi: 10.1001/jama.283.15.2008
- Studholme, C., Hill, D. L. G., Hawkes, D.J. (1999) An overlap invariant entropy measure of 3D medical image alignment. *Pattern Recognition*, 32, 71–86. doi: 10.1016/S0031-3203(98)00091-0.
- Su, J., Shen, H., Zeng, L. L., Qin, J., Liu, Z., & Hu, D. (2016). Heredity characteristics of schizophrenia shown by dynamic functional connectivity analysis of resting-state functional MRI scans of unaffected siblings. *Neuroreport*, 27(11), 843–848. doi: 10.1097/WNR.0000000000000622
- Swanson, M. R., Wolff, J. J., Elison, J. T., Gu, H., Hazlett, H. C., Botteron, K., Styner, M., Paterson, S., Gerig, G., Constantino, J., Dager, S., Estes, A., Vachet, C., Piven, J., & IBIS Network (2017). Splenium development and early spoken language in human infants. *Developmental science*, 20(2), 10.1111/desc.12360. doi: 10.1111/desc.12360
- Thayyil, S., Chandrasekaran, M., Taylor, A., Bainbridge, A., Cady, E. B., Chong, W. K., Murad, S., Omar, R. Z., & Robertson, N. J. (2010). Cerebral magnetic resonance biomarkers in neonatal encephalopathy: a meta-analysis. *Pediatrics*, 125(2), e382–e395. doi: 10.1542/peds.2009-1046

- Thomason, M. E., Dassanayake, M. T., Shen, S., Katkuri, Y., Alexis, M., Anderson, A. L., Yeo, L., Mody, S., Hernandez-Andrade, E., Hassan, S. S., Studholme, C., Jeong, J. W., & Romero, R. (2013). Cross-hemispheric functional connectivity in the human fetal brain. *Science translational medicine*, 5(173), 173ra24. doi: 10.1126/scitranslmed.3004978
- Thomason, M. E., Grove, L. E., Lozon, T. A., Jr, Vila, A. M., Ye, Y., Nye, M. J., Manning, J. H., Pappas, A., Hernandez-Andrade, E., Yeo, L., Mody, S., Berman, S., Hassan, S. S., & Romero, R. (2015). Age-related increases in long-range connectivity in fetal functional neural connectivity networks in utero. *Developmental cognitive neuroscience*, 11, 96–104. doi: 10.1016/j.dcn.2014.09.001
- Tognoli, E., & Kelso, J. A. (2014). The metastable brain. *Neuron*, 81(1), 35–48. doi: 10.1016/j.neuron.2013.12.022
- Tooley, J. R., Eagle, R. C., Satas, S., & Thoresen, M. (2005). Significant head cooling can be achieved while maintaining normothermia in the newborn piglet. *Archives of disease in childhood. Fetal and neonatal edition*, 90(3), F262–F266. doi: 10.1136/adc.2003.044305
- Tournier, J. D., Calamante, F., & Connelly, A. (2007). Robust determination of the fibre orientation distribution in diffusion MRI: non-negativity constrained super-resolved spherical deconvolution. *NeuroImage*, 35(4), 1459–1472. doi: 10.1016/j.neuroimage.2007.02.016
- Tournier, J. D., Smith, R., Raffelt, D., Tabbara, R., Dhollander, T., Pietsch, M., Christiaens, D., Jeurissen, B., Yeh, C. H., & Connelly, A. (2019). MRtrix3: A fast, flexible and open software framework for medical image processing and visualisation. *NeuroImage*, 202, 116137. doi: 10.1016/j.neuroimage.2019.116137
- Triantafyllou, C., Polimeni, J. R., & Wald, L. L. (2011). Physiological noise and signal-to-noise ratio in fMRI with multi-channel array coils. *NeuroImage*, 55(2), 597–606. doi: 10.1016/j.neuroimage.2010.11.084
- Trivedi, S. B., Vesoulis, Z. A., Rao, R., Liao, S. M., Shimony, J. S., McKinstry, R. C., & Mathur, A. M. (2017). A validated clinical MRI injury scoring system in neonatal hypoxic-ischemic encephalopathy. *Pediatric radiology*, 47(11), 1491–1499. doi: 10.1007/s00247-017-3893-y
- Tuch, D. S., Reese, T. G., Wiegell, M. R., Makris, N., Belliveau, J. W., & Wedeen, V. J. (2002). High angular resolution diffusion imaging reveals intravoxel white matter fiber heterogeneity. *Magnetic resonance in medicine*, 48(4), 577–582. doi: 10.1002/mrm.10268
- Tulving E. (2002). Episodic memory: from mind to brain. *Annual review of psychology*, 53, 1–25. doi: 10.1146/annurev.psych.53.100901.135114
- Tusor, N., Wusthoff, C., Smeets, N., Merchant, N., Arichi, T., Allsop, J. M., Cowan, F. M., Azzopardi, D., Edwards, A. D., & Counsell, S. J. (2012). Prediction of neurodevelopmental outcome after hypoxic-ischemic encephalopathy treated with hypothermia by diffusion tensor imaging analyzed using tract-based spatial statistics. *Pediatric research*, 72(1), 63–69. doi: 10.1038/pr.2012.40
- Tusor, N., Benders, M. J., Counsell, S. J., Nongena, P., Ederies, M. A., Falconer, S., Chew, A., Gonzalez-Cinca, N., Hajnal, J. V., Gangadharan, S., Chatzi, V., Kersbergen, K. J., Kennea, N., Azzopardi, D. V., & Edwards, A. D. (2017). Punctate White Matter Lesions Associated With Altered Brain Development And Adverse Motor Outcome In Preterm Infants. *Scientific reports*, 7(1), 13250. doi: 10.1038/s41598-017-13753-x
- Tusor, N. (2014). Diffusion tensor imaging and resting state functional connectivity as advanced imaging biomarkers of outcome in infants with hypoxic ischaemic encephalopathy treated with hypothermia. PhD;Imperial College London.

- Tustison, N. J., Avants, B. B., Cook, P. A., Zheng, Y., Egan, A., Yushkevich, P. A., & Gee, J. C. (2010). N4ITK: improved N3 bias correction. *IEEE transactions on medical imaging*, *29*(6), 1310–1320. doi: 10.1109/TMI.2010.2046908
- Twomey, E., Twomey, A., Ryan, S., Murphy, J., & Donoghue, V. B. (2010). MR imaging of term infants with hypoxic-ischaemic encephalopathy as a predictor of neurodevelopmental outcome and late MRI appearances. *Pediatric radiology*, *40*(9), 1526–1535. doi: 10.1007/s00247-010-1692-9
- Tyagi, M., Fteropoulli, T., Hurt, C. S., Hirani, S. P., Rixon, L., Davies, A., Picaut, N., Kennedy, F., Deanfield, J., Cullen, S., & Newman, S. P. (2017). Cognitive dysfunction in adult CHD with different structural complexity. *Cardiology in the young*, *27*(5), 851–859. doi: 10.1017/S1047951116001396
- Tymofiyeva, O., Hess, C. P., Ziv, E., Lee, P. N., Glass, H. C., Ferriero, D. M., Barkovich, A. J., & Xu, D. (2013). A DTI-based template-free cortical connectome study of brain maturation. *PloS one*, *8*(5), e63310. doi: 10.1371/journal.pone.0063310
- Tymofiyeva, O., Hess, C. P., Ziv, E., Tian, N., Bonifacio, S. L., McQuillen, P. S., Ferriero, D. M., Barkovich, A. J., & Xu, D. (2012). Towards the "baby connectome": mapping the structural connectivity of the newborn brain. *PloS one*, *7*(2), e31029. doi: 10.1371/journal.pone.0031029
- Tzourio-Mazoyer, N., Landeau, B., Papathanassiou, D., Crivello, F., Etard, O., Delcroix, N., Mazoyer, B., & Joliot, M. (2002). Automated anatomical labeling of activations in SPM using a macroscopic anatomical parcellation of the MNI MRI single-subject brain. *NeuroImage*, *15*(1), 273–289. doi: 10.1006/nimg.2001.0978
- van den Heuvel, M. P., Kahn, R. S., Goñi, J., & Sporns, O. (2012). High-cost, high-capacity backbone for global brain communication. *Proceedings of the National Academy of Sciences of the United States of America*, *109*(28), 11372–11377. doi: 10.1073/pnas.1203593109
- van den Heuvel, M. P., Kersbergen, K. J., de Reus, M. A., Keunen, K., Kahn, R. S., Groenendaal, F., de Vries, L. S., & Benders, M. J. (2015). The Neonatal Connectome During Preterm Brain Development. *Cerebral cortex*, *25*(9), 3000–3013. doi: 10.1093/cercor/bhu095
- van den Heuvel, M. P., & Sporns, O. (2013). Network hubs in the human brain. *Trends in cognitive sciences*, *17*(12), 683–696. doi: 10.1016/j.tics.2013.09.012
- van den Heuvel, M. P., & Sporns, O. (2011). Rich-club organization of the human connectome. *The Journal of neuroscience : the official journal of the Society for Neuroscience*, *31*(44), 15775–15786. doi: 10.1523/JNEUROSCI.3539-11.2011
- van der Bom, T., Zomer, A. C., Zwinderman, A. H., Meijboom, F. J., Bouma, B. J., & Mulder, B. J. (2011). The changing epidemiology of congenital heart disease. *Nature reviews. Cardiology*, *8*(1), 50–60. doi: 10.1038/nrcardio.2010.166
- Van Dijk, K. R., Hedden, T., Venkataraman, A., Evans, K. C., Lazar, S. W., & Buckner, R. L. (2010). Intrinsic functional connectivity as a tool for human connectomics: theory, properties, and optimization. *Journal of neurophysiology*, *103*(1), 297–321. doi: 10.1152/jn.00783.2009
- Van Dijk, K. R., Sabuncu, M. R., & Buckner, R. L. (2012). The influence of head motion on intrinsic functional connectivity MRI. *NeuroImage*, *59*(1), 431–438. doi: 10.1016/j.neuroimage.2011.07.044
- van Handel, M., Swaab, H., de Vries, L. S., & Jongmans, M. J. (2007). Long-term cognitive and behavioral consequences of neonatal encephalopathy following perinatal asphyxia: a review. *European journal of pediatrics*, *166*(7), 645–654. doi: 10.1007/s00431-007-0437-8

- van Handel, M., Swaab, H., de Vries, L. S., & Jongmans, M. J. (2010). Behavioral outcome in children with a history of neonatal encephalopathy following perinatal asphyxia. *Journal of pediatric psychology, 35*(3), 286–295. doi: 10.1093/jpepsy/jsp049
- van Handel, M., de Sonnevile, L., de Vries, L. S., Jongmans, M. J., & Swaab, H. (2012). Specific memory impairment following neonatal encephalopathy in term-born children. *Developmental neuropsychology, 37*(1), 30–50. doi: 10.1080/87565641.2011.581320
- van Kooij, B. J., van Handel, M., Nievelstein, R. A., Groenendaal, F., Jongmans, M. J., & de Vries, L. S. (2010). Serial MRI and neurodevelopmental outcome in 9- to 10-year-old children with neonatal encephalopathy. *The Journal of pediatrics, 157*(2), 221–227.e2. doi: 10.1016/j.jpeds.2010.02.016
- van Rooij, D., Hartman, C. A., Mennes, M., Oosterlaan, J., Franke, B., Rommelse, N., Heslenfeld, D., Faraone, S. V., Buitelaar, J. K., & Hoekstra, P. J. (2015). Altered neural connectivity during response inhibition in adolescents with attention-deficit/hyperactivity disorder and their unaffected siblings. *NeuroImage. Clinical, 7*, 325–335. doi: 10.1016/j.nicl.2015.01.004
- van Schie, P. E., Becher, J. G., Dallmeijer, A. J., Barkhof, F., Weissenbruch, M. M., & Vermeulen, R. J. (2007). Motor outcome at the age of one after perinatal hypoxic-ischemic encephalopathy. *Neuropediatrics, 38*(2), 71–77. doi: 10.1055/s-2007-984449
- Váša, F., Shanahan, M., Hellyer, P. J., Scott, G., Cabral, J., & Leech, R. (2015). Effects of lesions on synchrony and metastability in cortical networks. *NeuroImage, 118*, 456–467. doi: 10.1016/j.neuroimage.2015.05.042
- Vasung, L., Lepage, C., Radoš, M., Pletikos, M., Goldman, J. S., Richiardi, J., Raguž, M., Fischi-Gómez, E., Karama, S., Huppi, P. S., Evans, A. C., & Kostovic, I. (2016). Quantitative and Qualitative Analysis of Transient Fetal Compartments during Prenatal Human Brain Development. *Frontiers in neuroanatomy, 10*, 11. doi: 10.3389/fnana.2016.00011
- Veraart, J., Novikov, D. S., Christiaens, D., Ades-Aron, B., Sijbers, J., & Fieremans, E. (2016). Denoising of diffusion MRI using random matrix theory. *NeuroImage, 142*, 394–406. doi: 10.1016/j.neuroimage.2016.08.016
- Verrall, C. E., Blue, G. M., Loughran-Fowlds, A., Kasparian, N., Gecz, J., Walker, K., Dunwoodie, S. L., Cordina, R., Sholler, G., Badawi, N., & Winlaw, D. (2019). 'Big issues' in neurodevelopment for children and adults with congenital heart disease. *Open heart, 6*(2), e000998. doi: 10.1136/openhrt-2018-000998
- Vermeulen, R. J., van Schie, P. E., Hendrikx, L., Barkhof, F., van Weissenbruch, M., Knol, D. L., & Pouwels, P. J. (2008). Diffusion-weighted and conventional MR imaging in neonatal hypoxic ischemia: two-year follow-up study. *Radiology, 249*(2), 631–639. doi: 10.1148/radiol.2492071581
- Vigneau, M., Beaucousin, V., Hervé, P. Y., Duffau, H., Crivello, F., Houdé, O., Mazoyer, B., & Tzourio-Mazoyer, N. (2006). Meta-analyzing left hemisphere language areas: phonology, semantics, and sentence processing. *NeuroImage, 30*(4), 1414–1432. doi: 10.1016/j.neuroimage.2005.11.002
- Vigneau, M., Beaucousin, V., Hervé, P. Y., Jobard, G., Petit, L., Crivello, F., Mellet, E., Zago, L., Mazoyer, B., & Tzourio-Mazoyer, N. (2011). What is right-hemisphere contribution to phonological, lexico-semantic, and sentence processing? Insights from a meta-analysis. *NeuroImage, 54*(1), 577–593. doi: 10.1016/j.neuroimage.2010.07.036
- Volpe, J. J. (2008). *Neurology of the Newborn*, 5th Edition. Philadelphia, PA: Saunders Elsevier
- Volpe J. J. (2012). Neonatal encephalopathy: an inadequate term for hypoxic-ischemic encephalopathy. *Annals of neurology, 72*(2), 156–166. doi: 10.1002/ana.23647

- von Elm, E., Altman, D. G., Egger, M., Pocock, S. J., Gøtzsche, P. C., Vandenbroucke, J. P., & STROBE Initiative (2008). The Strengthening the Reporting of Observational Studies in Epidemiology (STROBE) statement: guidelines for reporting observational studies. *Journal of clinical epidemiology*, *61*(4), 344–349. doi: 10.1016/j.jclinepi.2007.11.008
- von Monakow, C. (1914). Die Lokalisation im Grosshirn und der Abbau der Funktionen durch kortikale Herde, Wiesbaden, J. F. Bergmann.
- von Rhein, M., Buchmann, A., Hagmann, C., Dave, H., Bernet, V., Scheer, I., Knirsch, W., Latal, B., & Heart and Brain Research Group (2015). Severe Congenital Heart Defects Are Associated with Global Reduction of Neonatal Brain Volumes. *The Journal of pediatrics*, *167*(6), 1259–63.e1. doi: 10.1016/j.jpeds.2015.07.006
- von Rhein, M., Buchmann, A., Hagmann, C., Huber, R., Klaver, P., Knirsch, W., & Latal, B. (2014). Brain volumes predict neurodevelopment in adolescents after surgery for congenital heart disease. *Brain : a journal of neurology*, *137*(Pt 1), 268–276. doi: 10.1093/brain/awt322
- von Smoluchowski, M., (1906). Zur kinetischen Theorie der Brownschen Molekularbewegung und der Suspensionen. *Annals of Physics*, *326*, 756–780. doi:10.1002/andp.19063261405
- Walsh, B. H., Neil, J., Morey, J., Yang, E., Silvera, M. V., Inder, T. E., & Ortinau, C. (2017). The Frequency and Severity of Magnetic Resonance Imaging Abnormalities in Infants with Mild Neonatal Encephalopathy. *The Journal of pediatrics*, *187*, 26–33.e1. doi: 10.1016/j.jpeds.2017.03.065
- Wang, L., Zhu, C., He, Y., Zang, Y., Cao, Q., Zhang, H., Zhong, Q., & Wang, Y. (2009). Altered small-world brain functional networks in children with attention-deficit/hyperactivity disorder. *Human brain mapping*, *30*(2), 638–649. doi: 10.1002/hbm.20530
- Weeke, L. C., Groenendaal, F., Mudigonda, K., Blennow, M., Lequin, M. H., Meiners, L. C., van Haastert, I. C., Benders, M. J., Hallberg, B., & de Vries, L. S. (2018). A Novel Magnetic Resonance Imaging Score Predicts Neurodevelopmental Outcome After Perinatal Asphyxia and Therapeutic Hypothermia. *The Journal of pediatrics*, *192*, 33–40.e2. doi: 10.1016/j.jpeds.2017.09.043
- Weilke, F., Spiegel, S., Boecker, H., von Einsiedel, H. G., Conrad, B., Schwaiger, M., & Erhard, P. (2001). Time-resolved fMRI of activation patterns in M1 and SMA during complex voluntary movement. *Journal of neurophysiology*, *85*(5), 1858–1863. doi: 10.1152/jn.2001.85.5.1858
- Welin, A. K., Svedin, P., Lapatto, R., Sultan, B., Hagberg, H., Gressens, P., Kjellmer, I., & Mallard, C. (2007). Melatonin reduces inflammation and cell death in white matter in the mid-gestation fetal sheep following umbilical cord occlusion. *Pediatric research*, *61*(2), 153–158. doi: 10.1203/01.pdr.0000252546.20451.1a
- Wen, X., Wang, R., Yin, W., Lin, W., Zhang, H., & Shen, D. (2020). Development of Dynamic Functional Architecture during Early Infancy. *Cerebral cortex*, *30*(11), 5626–5638. doi: 10.1093/cercor/bhaa128
- Werner G. (2007). Metastability, criticality and phase transitions in brain and its models. *Bio Systems*, *90*(2), 496–508. doi: 10.1016/j.biosystems.2006.12.001
- Wernovsky, G., Rome, J. J., Tabbutt, S., Rychik, J., Cohen, M. S., Paridon, S. M., Webb, G., Dodds, K. M., Gallagher, M. A., Fleck, D. A., Spray, T. L., Vetter, V. L., & Gleason, M. M. (2006). Guidelines for the outpatient management of complex congenital heart disease. *Congenital heart disease*, *1*(1-2), 10–26. doi: 10.1111/j.1747-0803.2006.00002.x

- Wheellock, M. D., Austin, N. C., Bora, S., Eggebrecht, A. T., Melzer, T. R., Woodward, L. J., & Smyser, C. D. (2018). Altered functional network connectivity relates to motor development in children born very preterm. *NeuroImage*, *183*, 574–583. doi: 10.1016/j.neuroimage.2018.08.051
- Winter, J. D., Lee, D. S., Hung, R. M., Levin, S. D., Rogers, J. M., Thompson, R. T., & Gelman, N. (2007). Apparent diffusion coefficient pseudonormalization time in neonatal hypoxic-ischemic encephalopathy. *Pediatric neurology*, *37*(4), 255–262. doi: 10.1016/j.pediatrneurol.2007.06.005
- Wolf, R. L., Zimmerman, R. A., Clancy, R., & Haselgrove, J. H. (2001). Quantitative apparent diffusion coefficient measurements in term neonates for early detection of hypoxic-ischemic brain injury: initial experience. *Radiology*, *218*(3), 825–833. doi: 10.1148/radiology.218.3.r01fe47825
- Wong, A., Chavez, T., O'Neil, S., Votava-Smith, J., Miller, D., delCastillo, S., Panigrahy, A., & Paquette, L. (2017). Synchronous Aberrant Cerebellar and Opercular Development in Fetuses and Neonates with Congenital Heart Disease: Correlation with Early Communicative Neurodevelopmental Outcomes, Initial Experience. *AJP reports*, *7*(1), e17–e27. doi: 10.1055/s-0036-159793
- Woodward, K. E., Carlson, H. L., Kuczynski, A., Saunders, J., Hodge, J., & Kirton, A. (2019). Sensory-motor network functional connectivity in children with unilateral cerebral palsy secondary to perinatal stroke. *NeuroImage. Clinical*, *21*, 101670. doi: 10.1016/j.nicl.2019.101670
- Wren, C., & O'Sullivan, J. J. (2001). Survival with congenital heart disease and need for follow up in adult life. *Heart*, *85*(4), 438–443. doi: 10.1136/heart.85.4.438
- Xia, M., Wang, J., & He, Y. (2013). BrainNet Viewer: a network visualization tool for human brain connectomics. *PloS one*, *8*(7), e68910. doi: 10.1371/journal.pone.0068910
- Yakovlev, P. L., Lecours, A. R. (1967). The myelogenetic cycles of regional maturation of the brain. Regional development of the brain in early life, Blackwell, Oxford:3-69.
- Yap, P. T., Fan, Y., Chen, Y., Gilmore, J. H., Lin, W., & Shen, D. (2011). Development trends of white matter connectivity in the first years of life. *PloS one*, *6*(9), e24678. doi: 10.1371/journal.pone.0024678
- Zaidi, S., & Brueckner, M. (2017). Genetics and Genomics of Congenital Heart Disease. *Circulation research*, *120*(6), 923–940. doi: 10.1161/CIRCRESAHA.116.309140
- Zalesky, A., Fornito, A., & Bullmore, E. T. (2010). Network-based statistic: identifying differences in brain networks. *NeuroImage*, *53*(4), 1197–1207. doi: 10.1016/j.neuroimage.2010.06.041
- Zalesky, A., Fornito, A., Cocchi, L., Gollo, L. L., & Breakspear, M. (2014). Time-resolved resting-state brain networks. *Proceedings of the National Academy of Sciences of the United States of America*, *111*(28), 10341–10346. doi: 10.1073/pnas.1400181111
- Zhang, D., & Raichle, M. E. (2010). Disease and the brain's dark energy. *Nature reviews. Neurology*, *6*(1), 15–28. doi: 10.1038/nrneurol.2009.198
- Zhang, J., Cheng, W., Liu, Z., Zhang, K., Lei, X., Yao, Y., Becker, B., Liu, Y., Kendrick, K. M., Lu, G., & Feng, J. (2016). Neural, electrophysiological and anatomical basis of brain-network variability and its characteristic changes in mental disorders. *Brain : a journal of neurology*, *139*(Pt 8), 2307–2321. doi: 10.1093/brain/aww143
- Zhao, T., Mishra, V., Jeon, T., Ouyang, M., Peng, Q., Chalak, L., Wisnowski, J. L., Heyne, R., Rollins, N., Shu, N., & Huang, H. (2019). Structural network maturation of the preterm human brain. *NeuroImage*, *185*, 699–710. doi: 10.1016/j.neuroimage.2018.06.047
- Zhou, W. H., Cheng, G. Q., Shao, X. M., Liu, X. Z., Shan, R. B., Zhuang, D. Y., Zhou, C. L., Du, L. Z., Cao, Y., Yang, Q., Wang, L. S., & China Study Group (2010). Selective

- head cooling with mild systemic hypothermia after neonatal hypoxic-ischemic encephalopathy: a multicenter randomized controlled trial in China. *The Journal of pediatrics*, 157(3), 367–372.e3723. doi: 10.1016/j.jpeds.2010.03.030
- Zhu, C., Kang, W., Xu, F., Cheng, X., Zhang, Z., Jia, L., Ji, L., Guo, X., Xiong, H., Simbruner, G., Blomgren, K., & Wang, X. (2009). Erythropoietin improved neurologic outcomes in newborns with hypoxic-ischemic encephalopathy. *Pediatrics*, 124(2), e218–e226. doi: 10.1542/peds.2008-3553
- Zuo, X. N., Di Martino, A., Kelly, C., Shehzad, Z. E., Gee, D. G., Klein, D. F., Castellanos, F. X., Biswal, B. B., & Milham, M. P. (2010). The oscillating brain: complex and reliable. *NeuroImage*, 49(2), 1432–1445. doi: 10.1016/j.neuroimage.2009.09.037

Appendix A

Supplementary material of : Reduced structural connectivity in cortico-striatal-thalamic network in neonates with congenital heart disease

Supplementary results 1

Supplementary Table 1. Affected nodes and edges at different t thresholds (2.5 to 3.5 in steps of 0.1).

$t = 2.5$

61 nodes, 112 edges, $p=0.002$

#	Node	Node network	#	Edge	Edge type	t -value
1	Precentral gyrus left	Core	1	Inferior frontal gyrus (opercular) left to Supplementary motor area right	Peripheral	2.5
2	Precentral gyrus right	Core	2	Postcentral gyrus right to Cerebellum right	Feeder	2.5
3	Superior frontal gyrus (dorsal) left	Core	3	Thalamus left to Vermis	Core	2.5
4	Orbitofrontal cortex (superior) left	Peripheral	4	Olfactory right to Rectus gyms right	Peripheral	2.51
5	Middle frontal gyrus left	Core	5	Thalamus right to Cerebellum right	Core	2.51
6	Middle frontal gyrus right	Core	6	Angular gyrus right to Vermis	Core	2.51
7	Orbitofrontal cortex (medial) left	Peripheral	7	Superior frontal gyrus (dorsal) left to Hippocampus left	Feeder	2.52
8	Orbitofrontal cortex (medial) right	Peripheral	8	Hippocampus left to Thalamus left	Feeder	2.53
9	Inferior frontal gyrus (opercular) left	Peripheral	9	Precentral gyrus left to Postcentral gyrus right	Feeder	2.54
10	Inferior frontal gyrus (opercular) right	Peripheral	10	Rectus gyms left to Inferior occipital gyrus left	Peripheral	2.55

11	Inferior frontal gyrus (triangular) left	Core	11	Orbitofrontal cortex (medial) left to Orbitofrontal cortex (inferior) left	Peripheral	2.56
12	Inferior frontal gyrus (triangular) right	Peripheral	12	Orbitofrontal cortex (medial) left to Posterior cingulate gyrus right	Peripheral	2.56
13	Orbitofrontal cortex (inferior) left	Peripheral	13	Median cingulate and paracingulate gyrus left to Hippocampus left	Feeder	2.57
14	Rolandic operculum left	Peripheral	14	Inferior frontal gyrus (triangular) left to Hippocampus left	Feeder	2.58
15	Supplementary motor area left	Peripheral	15	Rectus gyrus left to Superior temporal gyrus left	Peripheral	2.58
16	Supplementary motor area right	Peripheral	16	Angular gyrus right to Cerebellum left	Core	2.59
17	Olfactory right	Peripheral	17	Thalamus left to Cerebellum right	Core	2.6
18	Superior frontal gyrus (medial) left	Core	18	Inferior frontal gyrus (triangular) left to Postcentral gyrus right	Feeder	2.61
19	Rectus gyrus left	Peripheral	19	Postcentral gyrus right to Temporal pole (superior) left	Peripheral	2.61
20	Rectus gyrus right	Peripheral	20	Angular gyrus left to Cerebellum right	Feeder	2.61
21	Insula left	Core	21	Olfactory right to Caudate right	Feeder	2.63
22	Anterior cingulate gyrus left	Core	22	Rectus gyrus left to Insula left	Feeder	2.64
23	Median cingulate and paracingulate gyrus left	Core	23	Rectus gyrus left to Angular gyrus left	Peripheral	2.65
24	Posterior cingulate	Peripheral	24	Precentral gyrus left to Supramarginal gyrus left	Feeder	2.66

	gyrus right					
25	Hippocampus left	Peripheral	25	Hippocampus left to Caudate left	Feeder	2.66
26	Hippocampus right	Peripheral	26	Middle frontal gyrus right to Anterior cingulate gyrus left	Core	2.68
27	Amygdala left	Peripheral	27	Hippocampus right to Cerebellum left	Feeder	2.68
28	Amygdala right	Peripheral	28	Middle frontal gyrus right to Vermis	Core	2.71
29	Cuneus right	Peripheral	29	Superior frontal gyrus (dorsal) left to Postcentral gyrus right	Feeder	2.72
30	Superior occipital gyrus left	Peripheral	30	Supplementary motor area left to Supramarginal gyrus left	Peripheral	2.72
31	Superior occipital gyrus right	Peripheral	31	Middle frontal gyrus right to Orbitofrontal cortex (medial) right	Feeder	2.73
32	Middle occipital gyrus left	Core	32	Rolandic operculum left to Rectus gyrus left	Peripheral	2.73
33	Middle occipital gyrus right	Peripheral	33	Middle frontal gyrus right to Postcentral gyrus right	Feeder	2.73
34	Inferior occipital gyrus left	Peripheral	34	Inferior frontal gyrus (opercular) right to Hippocampus right	Peripheral	2.74
35	Postcentral gyrus left	Peripheral	35	Superior frontal gyrus (dorsal) left to Supramarginal gyrus left	Feeder	2.74
36	Postcentral gyrus right	Peripheral	36	Posterior cingulate gyrus right to Precuneus right	Feeder	2.74
37	Superior parietal gyrus left	Peripheral	37	Postcentral gyrus right to Supramarginal gyrus left	Peripheral	2.75
38	Inferior parietal lobule left	Core	38	Superior occipital gyrus left to Paracentral lobule right	Peripheral	2.76

39	Inferior parietal lobule right	Peripheral	39	Inferior frontal gyrus (triangular) right to Hippocampus right	Peripheral	2.77
40	Supramarginal gyrus left	Peripheral	40	Hippocampus right to Thalamus right	Feeder	2.77
41	Supramarginal gyrus right	Peripheral	41	Middle occipital gyrus left to Cerebellum right	Core	2.77
42	Angular gyrus left	Peripheral	42	Postcentral gyrus right to Putamen left	Feeder	2.79
43	Angular gyrus right	Core	43	Precentral gyrus left to Cerebellum right	Core	2.79
44	Precuneus left	Core	44	Inferior frontal gyrus (opercular) right to Postcentral gyrus right	Peripheral	2.8
45	Precuneus right	Core	45	Hippocampus right to Cerebellum right	Feeder	2.82
46	Paracentral lobule right	Peripheral	46	Rolandic operculum left to Supplementary motor area right	Peripheral	2.83
47	Caudate left	Core	47	Middle frontal gyrus right to Hippocampus right	Feeder	2.83
48	Caudate right	Core	48	Caudate left to Caudate right	Core	2.83
49	Putamen left	Core	49	Supplementary motor area left to Cerebellum right	Feeder	2.83
50	Putamen right	Core	50	Orbitofrontal cortex (medial) right to Caudate right	Feeder	2.84
51	Thalamus left	Core	51	Inferior parietal lobule right to Vermis	Feeder	2.84
52	Thalamus right	Core	52	Middle frontal gyrus right to Inferior frontal gyrus (triangular) left	Core	2.85
53	Heschl gyrus left	Peripheral	53	Hippocampus left to Postcentral gyrus left	Peripheral	2.85
54	Superior temporal gyrus left	Peripheral	54	Hippocampus left to Inferior parietal lobule left	Feeder	2.85
55	Temporal pole	Peripheral	55	Precentral gyrus left to	Core	2.85

	(superior) left			Precuneus left		
56	Middle temporal gyrus left	Core	56	Supplementary motor area left to Hippocampus left	Peripheral	2.86
57	Inferior temporal gyrus left	Peripheral	57	Precentral gyrus right to Cerebellum right	Core	2.86
58	Inferior temporal gyrus right	Core	58	Middle frontal gyrus right to Orbitofrontal cortex (medial) left	Feeder	2.87
59	Cerebellum left	Core	59	Hippocampus left to Superior occipital gyrus left	Peripheral	2.87
60	Cerebellum right	Core	60	Amygdala right to Inferior parietal lobule right	Peripheral	2.89
61	Vermis	Core	61	Putamen left to Vermis	Core	2.9
			62	Rolandic operculum left to Supplementary motor area left	Peripheral	2.91
			63	Superior frontal gyrus (dorsal) left to Middle frontal gyrus right	Core	2.92
			64	Amygdala right to Angular gyrus right	Feeder	2.92
			65	Orbitofrontal cortex (superior) left to Middle frontal gyrus right	Feeder	2.97
			66	Inferior frontal gyrus (triangular) right to Postcentral gyrus right	Peripheral	2.98
			67	Postcentral gyrus right to Cerebellum left	Feeder	2.98
			68	Cuneus right to Middle occipital gyrus right	Peripheral	2.99
			69	Hippocampus right to Superior occipital gyrus right	Peripheral	3
			70	Superior occipital gyrus left to Postcentral gyrus right	Peripheral	3

			71	Thalamus right to Vermis	Core	3
			72	Inferior frontal gyrus (opercular) left to Postcentral gyrus right	Peripheral	3.02
			73	Hippocampus left to Angular gyrus left	Peripheral	3.05
			74	Rectus gyrus left to Heschl gyrus left	Peripheral	3.05
			75	Supplementary motor area left to Postcentral gyrus right	Peripheral	3.06
			76	Hippocampus right to Putamen right	Feeder	3.06
			77	Hippocampus right to Supramarginal gyrus right	Peripheral	3.07
			78	Middle frontal gyrus right to Caudate right	Core	3.07
			79	Median cingulate and paracingulate gyrus left to Postcentral gyrus right	Feeder	3.08
			80	Hippocampus left to Middle occipital gyrus left	Feeder	3.11
			81	Precentral gyrus right to Hippocampus right	Feeder	3.12
			82	Caudate right to Inferior temporal gyrus right	Core	3.13
			83	Precentral gyrus right to Cerebellum left	Core	3.13
			84	Middle frontal gyrus left to Middle frontal gyrus right	Core	3.14
			85	Orbitofrontal cortex (superior) left to Orbitofrontal cortex (medial) left	Peripheral	3.14
			86	Middle occipital gyrus left to Middle temporal gyrus left	Core	3.15
			87	Middle occipital gyrus left to Inferior occipital gyrus left	Feeder	3.17

			88	Hippocampus left to Superior parietal gyrus left	Peripheral	3.17
			89	Inferior occipital gyrus left to Middle temporal gyrus left	Feeder	3.29
			90	Hippocampus right to Inferior parietal lobule right	Peripheral	3.31
			91	Hippocampus left to Amygdala left	Peripheral	3.34
			92	Hippocampus left to Cerebellum left	Feeder	3.36
			93	Hippocampus right to Middle occipital gyrus right	Peripheral	3.4
			94	Postcentral gyrus left to Cerebellum right	Feeder	3.43
			95	Inferior frontal gyrus (triangular) left to Rolandic operculum left	Feeder	3.44
			96	Inferior frontal gyrus (opercular) left to Inferior frontal gyrus (triangular) left	Feeder	3.46
			97	Rectus gyrus left to Supramarginal gyrus left	Peripheral	3.47
			98	Rolandic operculum left to Superior frontal gyrus (medial) left	Feeder	3.49
			99	Thalamus right to Cerebellum left	Core	3.51
			100	Putamen right to Thalamus right	Core	3.52
			101	Thalamus right to Inferior temporal gyrus right	Core	3.52
			102	Hippocampus right to Angular gyrus right	Feeder	3.58
			103	Precentral gyrus right to Vermis	Core	3.7
			104	Superior frontal gyrus (dorsal) left to Rolandic	Feeder	3.71

				operculum left		
			105	Inferior occipital gyrus left to Inferior temporal gyrus left	Peripheral	3.72
			106	Hippocampus right to Postcentral gyrus right	Peripheral	3.77
			107	Putamen left to Thalamus left	Core	3.77
			108	Caudate right to Putamen left	Core	3.81
			109	Cerebellum left to Cerebellum right	Core	3.81
			110	Hippocampus left to Vermis	Feeder	3.93
			111	Hippocampus left to Cerebellum right	Feeder	3.97
			112	Hippocampus right to Caudate right	Feeder	4

$t = 2.6$

56 nodes, 95 edges, $p=0.001$

#	Node	Node network	#	Edge	Edge type	<i>t</i> -value
1	Precentral gyrus left	Core	1	Thalamus left to Cerebellum right	Core	2.6
2	Precentral gyrus right	Core	2	Inferior frontal gyrus (triangular) left to Postcentral gyrus right	Feeder	2.61
3	Superior frontal gyrus (dorsal) left	Core	3	Postcentral gyrus right to Temporal pole (superior) left	Peripheral	2.61
4	Orbitofrontal cortex (superior) left	Peripheral	4	Angular gyrus left to Cerebellum right	Feeder	2.61
5	Middle frontal gyrus left	Core	5	Olfactory right to Caudate right	Feeder	2.63
6	Middle frontal gyrus right	Core	6	Rectus gyrus left to Insula left	Feeder	2.64
7	Orbitofrontal cortex (medial) left	Peripheral	7	Rectus gyrus left to Angular gyrus left	Peripheral	2.65
8	Orbitofrontal cortex (medial) right	Peripheral	8	Precentral gyrus left to Supramarginal gyrus left	Feeder	2.66
9	Inferior frontal gyrus (opercular) left	Peripheral	9	Hippocampus left to Caudate right	Feeder	2.66
10	Inferior frontal gyrus (opercular) right	Peripheral	10	Middle frontal gyrus right to Anterior cingulate gyrus left	Core	2.68
11	Inferior frontal gyrus (triangular) left	Core	11	Hippocampus right to Cerebellum left	Feeder	2.68

12	Inferior frontal gyrus (triangular) right	Peripheral	12	Middle frontal gyrus right to Vermis	Core	2.71
13	Rolandic operculum left	Peripheral	13	Superior frontal gyrus (dorsal) left to Postcentral gyrus left	Feeder	2.72
14	Supplementary motor area left	Peripheral	14	Supplementary motor area left to Supramarginal gyrus left	Peripheral	2.72
15	Supplementary motor area right	Peripheral	15	Middle frontal gyrus right to Orbitofrontal cortex (medial) right	Feeder	2.73
16	Olfactory right	Peripheral	16	Rolandic operculum left to Rectus gyrus left	Peripheral	2.73
17	Superior frontal gyrus (medial) left	Core	17	Middle frontal gyrus right to Postcentral gyrus left	Feeder	2.73
18	Rectus gyrus left	Peripheral	18	Inferior frontal gyrus (opercular) right to Hippocampus right	Peripheral	2.74
19	Insula left	Core	19	Superior frontal gyrus (dorsal) left to Supramarginal gyrus left	Feeder	2.74
20	Anterior cingulate gyrus left	Core	20	Postcentral gyrus right to Supramarginal gyrus left	Peripheral	2.75
21	Median cingulate and paracingulate gyrus left	Core	21	Superior occipital gyrus left to Paracentral lobule right	Peripheral	2.76
22	Hippocampus left	Peripheral	22	Inferior frontal gyrus (triangular) right to Hippocampus right	Peripheral	2.77
23	Hippocampus right	Peripheral	23	Hippocampus right to Thalamus right	Feeder	2.77
24	Amygdala left	Peripheral	24	Middle occipital gyrus left to Cerebellum right	Core	2.77
25	Amygdala	Peripheral	25	Postcentral gyrus right to	Feeder	2.79

	right			Putamen left		
26	Cuneus right	Peripheral	26	Precentral gyrus left to Cerebellum right	Core	2.79
27	Superior occipital gyrus left	Peripheral	27	Inferior frontal gyrus (opercular) right to Postcentral gyrus right	Peripheral	2.8
28	Superior occipital gyrus right	Peripheral	28	Hippocampus right to Cerebellum right	Feeder	2.82
29	Middle occipital gyrus left	Core	29	Rolandic operculum left to Supplementary motor area right	Peripheral	2.83
30	Middle occipital gyrus right	Peripheral	30	Middle frontal gyrus right to Hippocampus right	Feeder	2.83
31	Inferior occipital gyrus left	Peripheral	31	Caudate left to Caudate right	Core	2.83
32	Postcentral gyrus left	Peripheral	32	Supplementary motor area left to Cerebellum right	Feeder	2.83
33	Postcentral gyrus right	Peripheral	33	Orbitofrontal cortex (medial) right to Caudate right	Feeder	2.84
34	Superior parietal gyrus left	Peripheral	34	Inferior parietal lobule right to Vermis	Feeder	2.84
35	Inferior parietal lobule left	Core	35	Middle frontal gyrus right to Inferior frontal gyrus (triangular) left	Core	2.85
36	Inferior parietal lobule right	Peripheral	36	Hippocampus left to Postcentral gyrus left	Peripheral	2.85
37	Supramarginal gyrus left	Peripheral	37	Hippocampus left to Inferior parietal lobule left	Feeder	2.85
38	Supramarginal gyrus right	Peripheral	38	Precentral gyrus left to Precuneus left	Core	2.85
39	Angular gyrus left	Peripheral	39	Supplementary motor area left to Hippocampus left	Peripheral	2.86
40	Angular gyrus	Core	40	Precentral gyrus right to	Core	2.86

	right			Cerebellum right		
41	Precuneus left	Core	41	Middle frontal gyrus right to Orbitofrontal cortex (medial) left	Feeder	2.87
42	Paracentral lobule right	Peripheral	42	Hippocampus left to Superior occipital gyrus left	Peripheral	2.87
43	Caudate left	Core	43	Amygdala right to Inferior parietal lobule right	Peripheral	2.89
44	Caudate right	Core	44	Putamen left to Vermis	Core	2.9
45	Putamen left	Core	45	Rolandic operculum left to Supplementary motor area left	Peripheral	2.91
46	Putamen right	Core	46	Superior frontal gyrus (dorsal) left to Middle frontal gyrus right	Core	2.92
47	Thalamus left	Core	47	Amygdala right to Angular gyrus right	Feeder	2.92
48	Thalamus right	Core	48	Orbitofrontal cortex (superior) left to Middle frontal gyrus right	Feeder	2.97
49	Heschl gyrus left	Peripheral	49	Inferior frontal gyrus (triangular) right to Postcentral gyrus right	Peripheral	2.98
50	Temporal pole (superior) left	Peripheral	50	Postcentral gyrus right to Cerebellum left	Feeder	2.98
51	Middle temporal gyrus left	Core	51	Cuneus right to Middle occipital gyrus right	Peripheral	2.99
52	Inferior temporal gyrus left	Peripheral	52	Hippocampus right to Superior occipital gyrus right	Peripheral	3
53	Inferior temporal gyrus right	Core	53	Superior occipital gyrus left to Postcentral gyrus left	Peripheral	3
54	Cerebellum left	Core	54	Thalamus right to Vermis	Core	3
55	Cerebellum right	Core	55	Inferior frontal gyrus (opercular) left to Postcentral	Peripheral	3.02

				gyrus right		
56	Vermis	Core	56	Hippocampus left to Angular gyrus left	Peripheral	3.05
			57	Rectus gyrus left to Heschl gyrus left	Peripheral	3.05
			58	Supplementary motor area left to Postcentral gyrus left	Peripheral	3.06
			59	Hippocampus right to Putamen right	Feeder	3.06
			60	Hippocampus right to Supramarginal gyrus right	Peripheral	3.07
			61	Middle frontal gyrus right to Caudate right	Core	3.07
			62	Median cingulate and paracingulate gyrus left to Postcentral gyrus left	Feeder	3.08
			63	Hippocampus left to Middle occipital gyrus left	Feeder	3.11
			64	Precentral gyrus right to Hippocampus right	Feeder	3.12
			65	Caudate right to Inferior temporal gyrus right	Core	3.13
			66	Precentral gyrus right to Cerebellum left	Core	3.13
			67	Middle frontal gyrus left to Middle frontal gyrus right	Core	3.14
			68	Orbitofrontal cortex (superior) left to Orbitofrontal cortex (medial) left	Peripheral	3.14
			69	Middle occipital gyrus left to Middle temporal gyrus left	Core	3.15
			70	Middle occipital gyrus left to Inferior occipital gyrus left	Feeder	3.17
			71	Hippocampus left to Superior parietal gyrus left	Peripheral	3.17

			72	Inferior occipital gyrus left to Middle temporal gyrus left	Feeder	3.29
			73	Hippocampus right to Inferior parietal lobule right	Peripheral	3.31
			74	Hippocampus left to Amygdala left	Peripheral	3.34
			75	Hippocampus left to Cerebellum left	Feeder	3.36
			76	Hippocampus right to Middle occipital gyrus right	Peripheral	3.4
			77	Postcentral gyrus left to Cerebellum right	Feeder	3.43
			78	Inferior frontal gyrus (triangular) left to Rolandic operculum left	Feeder	3.44
			79	Inferior frontal gyrus (opercular) left to Inferior frontal gyrus (triangular) left	Feeder	3.46
			80	Rectus gyrus left to Supramarginal gyrus left	Peripheral	3.47
			81	Rolandic operculum left to Superior frontal gyrus (medial) left	Feeder	3.49
			82	Thalamus right to Cerebellum left	Core	3.51
			83	Putamen right to Thalamus right	Core	3.52
			84	Thalamus right to Inferior temporal gyrus right	Core	3.52
			85	Hippocampus right to Angular gyrus right	Feeder	3.58
			86	Precentral gyrus right to Vermis	Core	3.7
			87	Superior frontal gyrus (dorsal) left to Rolandic operculum left	Feeder	3.71
			88	Inferior occipital gyrus left to	Peripheral	3.72

				Inferior temporal gyrus left		
			89	Hippocampus right to Postcentral gyrus left	Peripheral	3.77
			90	Putamen left to Thalamus left	Core	3.77
			91	Caudate right to Putamen left	Core	3.81
			92	Cerebellum left to Cerebellum right	Core	3.81
			93	Hippocampus left to Vermis	Feeder	3.93
			94	Hippocampus left to Cerebellum right	Feeder	3.97
			95	Hippocampus right to Caudate right	Feeder	4

$t = 2.7$

52 nodes, 84 edges, $p=0.05$

#	Node	Node network	#	Edge	Edge type	t-value
1	Precentral gyrus left	Core	1	Middle frontal gyrus right to Vermis	Core	2.71
2	Precentral gyrus right	Core	2	Superior frontal gyrus (dorsal) left to Postcentral gyrus right	Feeder	2.72
3	Superior frontal gyrus (dorsal) left	Core	3	Supplementary motor area left to Supramarginal gyrus left	Peripheral	2.72
4	Orbitofrontal cortex (superior) left	Periphery	4	Middle frontal gyrus right to Orbitofrontal cortex (medial) right	Feeder	2.73
5	Middle frontal gyrus left	Core	5	Rolandic operculum left to Rectus gyrus left	Peripheral	2.73
6	Middle frontal gyrus right	Core	6	Middle frontal gyrus right to Postcentral gyrus right	Feeder	2.73
7	Orbitofrontal cortex (medial) left	Periphery	7	Inferior frontal gyrus (opercular) right to Hippocampus right	Peripheral	2.74
8	Orbitofrontal cortex (medial) right	Periphery	8	Superior frontal gyrus (dorsal) left to Supramarginal gyrus left	Feeder	2.74
9	Inferior frontal gyrus (opercular) left	Periphery	9	Postcentral gyrus right to Supramarginal gyrus left	Peripheral	2.75
10	Inferior frontal gyrus (opercular) right	Periphery	10	Superior occipital gyrus left to Paracentral lobule right	Peripheral	2.76
11	Inferior frontal gyrus (triangular) left	Core	11	Inferior frontal gyrus (triangular) right to Hippocampus right	Peripheral	2.77
12	Inferior frontal gyrus (triangular) right	Periphery	12	Hippocampus right to Thalamus right	Feeder	2.77

13	Rolandic operculum left	Periphery	13	Middle occipital gyrus left to Cerebellum right	Core	2.77
14	Supplementary motor area left	Peripheral	14	Postcentral gyrus right to Putamen left	Feeder	2.79
15	Supplementary motor area right	Peripheral	15	Precentral gyrus left to Cerebellum right	Core	2.79
16	Superior frontal gyrus (medial) left	Core	16	Inferior frontal gyrus (opercular) right to Postcentral gyrus right	Peripheral	2.8
17	Rectus gyrus left	Peripheral	17	Hippocampus right to Cerebellum right	Feeder	2.82
18	Median cingulate and paracingulate gyrus left	Core	18	Rolandic operculum left to Supplementary motor area right	Peripheral	2.83
19	Hippocampus left	Peripheral	19	Middle frontal gyrus right to Hippocampus right	Feeder	2.83
20	Hippocampus right	Peripheral	20	Caudate left to Caudate right	Core	2.83
21	Amygdala left	Peripheral	21	Supplementary motor area left to Cerebellum right	Feeder	2.83
22	Amygdala right	Peripheral	22	Orbitofrontal cortex (medial) right to Caudate right	Feeder	2.84
23	Cuneus right	Peripheral	23	Inferior parietal lobule right to Vermis	Feeder	2.84
24	Superior occipital gyrus left	Peripheral	24	Middle frontal gyrus right to Inferior frontal gyrus (triangular) left	Core	2.85
25	Superior occipital gyrus right	Peripheral	25	Hippocampus left to Postcentral gyrus left	Peripheral	2.85
26	Middle occipital gyrus left	Core	26	Hippocampus left to Inferior parietal lobule left	Feeder	2.85
27	Middle occipital gyrus right	Peripheral	27	Precentral gyrus left to Precuneus left	Core	2.85

28	Inferior occipital gyrus left	Peripheral	28	Supplementary motor area left to Hippocampus left	Peripheral	2.86
29	Postcentral gyrus left	Peripheral	29	Precentral gyrus right to Cerebellum right	Core	2.86
30	Postcentral gyrus right	Peripheral	30	Middle frontal gyrus right to Orbitofrontal cortex (medial) left	Feeder	2.87
31	Superior parietal gyrus left	Peripheral	31	Hippocampus left to Superior occipital gyrus left	Peripheral	2.87
32	Inferior parietal lobule left	Core	32	Amygdala right to Inferior parietal lobule right	Peripheral	2.89
33	Inferior parietal lobule right	Peripheral	33	Putamen left to Vermis	Core	2.9
34	Supramarginal gyrus left	Peripheral	34	Rolandic operculum left to Supplementary motor area left	Peripheral	2.91
35	Supramarginal gyrus right	Peripheral	35	Superior frontal gyrus (dorsal) left to Middle frontal gyrus right	Core	2.92
36	Angular gyrus left	Peripheral	36	Amygdala right to Angular gyrus right	Feeder	2.92
37	Angular gyrus right	Core	37	Orbitofrontal cortex (superior) left to Middle frontal gyrus right	Feeder	2.97
38	Precuneus left	Core	38	Inferior frontal gyrus (triangular) right to Postcentral gyrus right	Peripheral	2.98
39	Paracentral lobule right	Peripheral	39	Postcentral gyrus right to Cerebellum left	Feeder	2.98
40	Caudate left	Core	40	Cuneus right to Middle occipital gyrus right	Peripheral	2.99
41	Caudate right	Core	41	Hippocampus right to Superior occipital gyrus right	Peripheral	3
42	Putamen left	Core	42	Superior occipital gyrus left to Postcentral gyrus right	Peripheral	3

43	Putamen right	Core	43	Thalamus right to Vermis	Core	3
44	Thalamus left	Core	44	Inferior frontal gyrus (opercular) left to Postcentral gyrus right	Peripheral	3.02
45	Thalamus right	Core	45	Hippocampus left to Angular gyrus left	Peripheral	3.05
46	Heschl gyrus left	Peripheral	46	Rectus gyrus left to Heschl gyrus left	Peripheral	3.05
47	Middle temporal gyrus left	Core	47	Supplementary motor area left to Postcentral gyrus right	Peripheral	3.06
48	Inferior temporal gyrus left	Peripheral	48	Hippocampus right to Putamen right	Feeder	3.06
49	Inferior temporal gyrus right	Core	49	Hippocampus right to Supramarginal gyrus right	Peripheral	3.07
50	Cerebellum left	Core	50	Middle frontal gyrus right to Caudate right	Core	3.07
51	Cerebellum right	Core	51	Median cingulate and paracingulate gyrus left to Postcentral gyrus right	Feeder	3.08
52	Vermis	Core	52	Hippocampus left to Middle occipital gyrus left	Feeder	3.11
			53	Precentral gyrus right to Hippocampus right	Feeder	3.12
			54	Caudate right to Inferior temporal gyrus right	Core	3.13
			55	Precentral gyrus right to Cerebellum left	Core	3.13
			56	Middle frontal gyrus left to Middle frontal gyrus right	Core	3.14
			57	Orbitofrontal cortex (superior) left to Orbitofrontal cortex (medial) left	Peripheral	3.14
			58	Middle occipital gyrus left to Middle temporal gyrus left	Core	3.15

			59	Middle occipital gyrus left to Inferior occipital gyrus left	Feeder	3.17
			60	Hippocampus left to Superior parietal gyrus left	Peripheral	3.17
			61	Inferior occipital gyrus left to Middle temporal gyrus left	Feeder	3.29
			62	Hippocampus right to Inferior parietal lobule right	Peripheral	3.31
			63	Hippocampus left to Amygdala left	Peripheral	3.34
			64	Hippocampus left to Cerebellum left	Feeder	3.36
			65	Hippocampus right to Middle occipital gyrus right	Peripheral	3.4
			66	Postcentral gyrus left to Cerebellum right	Feeder	3.43
			67	Inferior frontal gyrus (triangular) left to Rolandic operculum left	Feeder	3.44
			68	Inferior frontal gyrus (opercular) left to Inferior frontal gyrus (triangular) left	Feeder	3.46
			69	Rectus gyrus left to Supramarginal gyrus left	Peripheral	3.47
			70	Rolandic operculum left to Superior frontal gyrus (medial) left	Feeder	3.49
			71	Thalamus right to Cerebellum left	Core	3.51
			72	Putamen right to Thalamus right	Core	3.52
			73	Thalamus right to Inferior temporal gyrus right	Core	3.52
			74	Hippocampus right to Angular gyrus right	Feeder	3.58
			75	Precentral gyrus right to Vermis	Core	3.7

			76	Superior frontal gyrus (dorsal) left to Rolandic operculum left	Feeder	3.71
			77	Inferior occipital gyrus left to Inferior temporal gyrus left	Peripheral	3.72
			78	Hippocampus right to Postcentral gyrus right	Peripheral	3.77
			79	Putamen left to Thalamus left	Core	3.77
			80	Caudate right to Putamen left	Core	3.81
			81	Cerebellum left to Cerebellum right	Core	3.81
			82	Hippocampus left to Vermis	Feeder	3.93
			83	Hippocampus left to Cerebellum right	Feeder	3.97
			84	Hippocampus right to Caudate right	Feeder	4

$t = 2.8$

46 nodes, 66 edges, $p < 0.001$

#	Node	Node network	#	Edge	Edge type	t-value
1	Precentral gyrus right	Core	1	Inferior frontal gyrus (opercular) right to Postcentral gyrus right	Peripheral	2.8
2	Superior frontal gyrus (dorsal) left	Core	2	Hippocampus right to Cerebellum right	Feeder	2.82
3	Orbitofrontal cortex (superior) left	Peripheral	3	Rolandic operculum left to Supplementary motor area right	Peripheral	2.83
4	Middle frontal gyrus left	Core	4	Middle frontal gyrus right to Hippocampus right	Feeder	2.83
5	Middle frontal gyrus right	Core	5	Caudate left to Caudate right	Core	2.83
6	Orbitofrontal cortex (medial) left	Peripheral	6	Supplementary motor area left to Cerebellum right	Feeder	2.83
7	Orbitofrontal cortex (medial) right	Peripheral	7	Orbitofrontal cortex (medial) right to Caudate right	Feeder	2.84
8	Inferior frontal gyrus (opercular) left	Peripheral	8	Inferior parietal lobule right to Vermis	Feeder	2.84
9	Inferior frontal gyrus (opercular) right	Peripheral	9	Middle frontal gyrus right to Inferior frontal gyrus (triangular) left	Core	2.85
10	Inferior frontal gyrus (triangular) left	Core	10	Hippocampus left to Postcentral gyrus left	Peripheral	2.85
11	Inferior frontal gyrus (triangular) right	Peripheral	11	Hippocampus left to Inferior parietal lobule left	Feeder	2.85
12	Rolandic operculum left	Peripheral	12	Supplementary motor area left to Hippocampus left	Peripheral	2.86

13	Supplementary motor area left	Peripheral	13	Precentral gyrus right to Cerebellum right	Core	2.86
14	Supplementary motor area right	Peripheral	14	Middle frontal gyrus right to Orbitofrontal cortex (medial) left	Feeder	2.87
15	Superior frontal gyrus (medial) left	Core	15	Hippocampus left to Superior occipital gyrus left	Peripheral	2.87
16	Median cingulate and paracingulate gyrus left	Core	16	Amygdala right to Inferior parietal lobule right	Peripheral	2.89
17	Hippocampus left	Peripheral	17	Putamen left to Vermis	Core	2.9
18	Hippocampus right	Peripheral	18	Rolandic operculum left to Supplementary motor area left	Peripheral	2.91
19	Amygdala left	Peripheral	19	Superior frontal gyrus (dorsal) left to Middle frontal gyrus right	Core	2.92
20	Amygdala right	Peripheral	20	Amygdala right to Angular gyrus right	Feeder	2.92
21	Cuneus right	Peripheral	21	Orbitofrontal cortex (superior) left to Middle frontal gyrus right	Feeder	2.97
22	Superior occipital gyrus left	Peripheral	22	Inferior frontal gyrus (triangular) right to Postcentral gyrus right	Peripheral	2.98
23	Superior occipital gyrus right	Peripheral	23	Postcentral gyrus right to Cerebellum left	Feeder	2.98
24	Middle occipital gyrus left	Core	24	Cuneus right to Middle occipital gyrus right	Peripheral	2.99
25	Middle occipital gyrus right	Peripheral	25	Hippocampus right to Superior occipital gyrus right	Peripheral	3
26	Inferior occipital gyrus	Peripheral	26	Superior occipital gyrus left to Postcentral gyrus right	Peripheral	3

	left					
27	Postcentral gyrus left	Peripheral	27	Thalamus right to Vermis	Core	3
28	Postcentral gyrus right	Peripheral	28	Inferior frontal gyrus (opercular) left to Postcentral gyrus right	Peripheral	3.02
29	Superior parietal gyrus left	Peripheral	29	Hippocampus left to Angular gyrus left	Peripheral	3.05
30	Inferior parietal lobule left	Core	30	Supplementary motor area left to Postcentral gyrus right	Peripheral	3.06
31	Inferior parietal lobule right	Peripheral	31	Hippocampus right to Putamen right	Feeder	3.06
32	Supramarginal gyrus right	Peripheral	32	Hippocampus right to Supramarginal gyrus right	Peripheral	3.07
33	Angular gyrus left	Peripheral	33	Middle frontal gyrus right to Caudate right	Core	3.07
34	Angular gyrus right	Core	34	Median cingulate and paracingulate gyrus left to Postcentral gyrus right	Feeder	3.08
35	Caudate left	Core	35	Hippocampus left to Middle occipital gyrus left	Feeder	3.11
36	Caudate right	Core	36	Precentral gyrus right to Hippocampus right	Feeder	3.12
37	Putamen left	Core	37	Caudate right to Inferior temporal gyrus right	Core	3.13
38	Putamen right	Core	38	Precentral gyrus right to Cerebellum left	Core	3.13
39	Thalamus left	Core	39	Middle frontal gyrus left to Middle frontal gyrus right	Core	3.14
40	Thalamus right	Core	40	Orbitofrontal cortex (superior) left to Orbitofrontal cortex (medial) left	Peripheral	3.14
41	Middle temporal gyrus	Core	41	Middle occipital gyrus left to Middle temporal gyrus left	Core	3.15

	left					
42	Inferior temporal gyrus left	Peripheral	42	Middle occipital gyrus left to Inferior occipital gyrus left	Feeder	3.17
43	Inferior temporal gyrus right	Core	43	Hippocampus left to Superior parietal gyrus left	Peripheral	3.17
44	Cerebellum left	Core	44	Inferior occipital gyrus left to Middle temporal gyrus left	Feeder	3.29
45	Cerebellum right	Core	45	Hippocampus right to Inferior parietal lobule right	Peripheral	3.31
46	Vermis	Core	46	Hippocampus left to Amygdala left	Peripheral	3.34
			47	Hippocampus left to Cerebellum left	Feeder	3.36
			48	Hippocampus right to Middle occipital gyrus right	Peripheral	3.4
			49	Postcentral gyrus left to Cerebellum right	Feeder	3.43
			50	Inferior frontal gyrus (triangular) left to Rolandic operculum left	Feeder	3.44
			51	Inferior frontal gyrus (opercular) left to Inferior frontal gyrus (triangular) left	Feeder	3.46
			52	Rolandic operculum left to Superior frontal gyrus (medial) left	Feeder	3.49
			53	Thalamus right to Cerebellum left	Core	3.51
			54	Putamen right to Thalamus right	Core	3.52
			55	Thalamus right to Inferior temporal gyrus right	Core	3.52
			56	Hippocampus right to Angular gyrus right	Feeder	3.58
			57	Precentral gyrus right to	Core	3.7

				Vermis		
			58	Superior frontal gyrus (dorsal) left to Rolandic operculum left	Feeder	3.71
			59	Inferior occipital gyrus left to Inferior temporal gyrus left	Peripheral	3.72
			60	Hippocampus right to Postcentral gyrus right	Peripheral	3.77
			61	Putamen left to Thalamus left	Core	3.77
			62	Caudate right to Putamen left	Core	3.81
			63	Cerebellum left to Cerebellum right	Core	3.81
			64	Hippocampus left to Vermis	Feeder	3.93
			65	Hippocampus left to Cerebellum right	Feeder	3.97
			66	Hippocampus right to Caudate right	Feeder	4

$t = 2.9$

41 nodes, 50 edges, $p < 0.001$

#	Node	Node network	#	Edge	Edge type	t-value
1	Precentral gyrus right	Core	1	Putamen left to Vermis	Core	2.9
2	Superior frontal gyrus (dorsal) left	Core	2	Rolandic operculum left to Supplementary motor area left	Peripheral	2.91
3	Orbitofrontal cortex (superior) left	Peripheral	3	Superior frontal gyrus (dorsal) left to Middle frontal gyrus right	Core	2.92
4	Middle frontal gyrus left	Core	4	Amygdala right to Angular gyrus right	Feeder	2.92
5	Middle frontal gyrus right	Core	5	Orbitofrontal cortex (superior) left to Middle frontal gyrus right	Feeder	2.97
6	Orbitofrontal cortex (medial) left	Peripheral	6	Inferior frontal gyrus (triangular) right to Postcentral gyrus right	Peripheral	2.98
7	Inferior frontal gyrus (opercular) left	Peripheral	7	Postcentral gyrus right to Cerebellum left	Feeder	2.98
8	Inferior frontal gyrus (triangular) left	Core	8	Cuneus right to Middle occipital gyrus right	Peripheral	2.99
9	Inferior frontal gyrus (triangular) right	Peripheral	9	Hippocampus right to Superior occipital gyrus right	Peripheral	3
10	Rolandic operculum left	Peripheral	10	Superior occipital gyrus left to Postcentral gyrus right	Peripheral	3
11	Supplementary motor area left	Peripheral	11	Thalamus right to Vermis	Core	3
12	Superior frontal gyrus (medial) left	Core	12	Inferior frontal gyrus (opercular) left to Postcentral gyrus right	Peripheral	3.02
13	Median cingulate and	Core	13	Hippocampus left to Angular gyrus left	Peripheral	3.05

	paracingulate gyrus left					
14	Hippocampus left	Peripheral	14	Supplementary motor area left to Postcentral gyrus right	Peripheral	3.06
15	Hippocampus right	Peripheral	15	Hippocampus right to Putamen right	Feeder	3.06
16	Amygdala left	Peripheral	16	Hippocampus right to Supramarginal gyrus right	Peripheral	3.07
17	Amygdala right	Peripheral	17	Middle frontal gyrus right to Caudate right	Core	3.07
18	Cuneus right	Peripheral	18	Median cingulate and paracingulate gyrus left to Postcentral gyrus right	Feeder	3.08
19	Superior occipital gyrus left	Peripheral	19	Hippocampus left to Middle occipital gyrus left	Feeder	3.11
20	Superior occipital gyrus right	Peripheral	20	Precentral gyrus right to Hippocampus right	Feeder	3.12
21	Middle occipital gyrus left	Core	21	Caudate right to Inferior temporal gyrus right	Core	3.13
22	Middle occipital gyrus right	Peripheral	22	Precentral gyrus right to Cerebellum left	Core	3.13
23	Inferior occipital gyrus left	Peripheral	23	Middle frontal gyrus left to Middle frontal gyrus right	Core	3.14
24	Postcentral gyrus left	Peripheral	24	Orbitofrontal cortex (superior) left to Orbitofrontal cortex (medial) left	Peripheral	3.14
25	Postcentral gyrus right	Peripheral	25	Middle occipital gyrus left to Middle temporal gyrus left	Core	3.15
26	Superior parietal gyrus left	Peripheral	26	Middle occipital gyrus left to Inferior occipital gyrus left	Feeder	3.17
27	Inferior parietal lobule	Peripheral	27	Hippocampus left to Superior parietal gyrus left	Peripheral	3.17

	right					
28	Supramarginal gyrus right	Peripheral	28	Inferior occipital gyrus left to Middle temporal gyrus left	Feeder	3.29
29	Angular gyrus left	Peripheral	29	Hippocampus right to Inferior parietal lobule right	Peripheral	3.31
30	Angular gyrus right	Core	30	Hippocampus right to Amygdala left	Peripheral	3.34
31	Caudate right	Core	31	Hippocampus left to Cerebellum left	Feeder	3.36
32	Putamen left	Core	32	Hippocampus right to Middle occipital gyrus right	Peripheral	3.4
33	Putamen right	Core	33	Postcentral gyrus left to Cerebellum right	Feeder	3.43
34	Thalamus left	Core	34	Inferior frontal gyrus (triangular) left to Rolandic operculum left	Feeder	3.44
35	Thalamus right	Core	35	Inferior frontal gyrus (opercular) left to Inferior frontal gyrus (triangular) left	Feeder	3.46
36	Middle temporal gyrus left	Core	36	Rolandic operculum left to Superior frontal gyrus (medial) left	Feeder	3.49
37	Inferior temporal gyrus left	Peripheral	37	Thalamus right to Cerebellum left	Core	3.51
38	Inferior temporal gyrus right	Core	38	Putamen right to Thalamus right	Core	3.52
39	Cerebellum left	Core	39	Thalamus right to Inferior temporal gyrus right	Core	3.52
40	Cerebellum right	Core	40	Hippocampus right to Angular gyrus right	Feeder	3.58
41	Vermis	Core	41	Precentral gyrus right to Vermis	Core	3.7
			42	Superior frontal gyrus (dorsal) left to Rolandic operculum left	Feeder	3.71

			43	Inferior occipital gyrus left to Inferior temporal gyrus left	Peripheral	3.72
			44	Hippocampus right to Postcentral gyrus right	Peripheral	3.77
			45	Putamen left to Thalamus left	Core	3.77
			46	Caudate right to Putamen left	Core	3.81
			47	Cerebellum left to Cerebellum right	Core	3.81
			48	Hippocampus left to Vermis	Feeder	3.93
			49	Hippocampus left to Cerebellum right	Feeder	3.97
			50	Hippocampus right to Caudate right	Feeder	4

$t = 3.0$

35 nodes, 39 edges, $p=0.001$

#	Node	Node network	#	Edge	Edge type	t-value
1	Precentral gyrus right	Core	1	Superior occipital gyrus left to Postcentral gyrus right	Peripheral	3
2	Superior frontal gyrus (dorsal) left	Core	2	Inferior frontal gyrus (opercular) left to Postcentral gyrus right	Peripheral	3.02
3	Middle frontal gyrus left	Core	3	Hippocampus left to Angular gyrus left	Peripheral	3.05
4	Middle frontal gyrus right	Core	4	Supplementary motor area left to Postcentral gyrus right	Peripheral	3.06
5	Inferior frontal gyrus (opercular) left	Peripheral	5	Hippocampus right to Caudate right	Feeder	3.06
6	Inferior frontal gyrus (triangular) left	Core	6	Hippocampus right to Supramarginal gyrus right	Peripheral	3.07
7	Rolandic operculum left	Peripheral	7	Middle frontal gyrus right to Caudate right	Core	3.07
8	Supplementary motor area left	Peripheral	8	Median cingulate and paracingulate gyrus left to Postcentral gyrus right	Feeder	3.08
9	Superior frontal gyrus (medial) left	Core	9	Hippocampus left to Middle occipital gyrus left	Feeder	3.11
10	Median cingulate and paracingulate gyrus left	Core	10	Precentral gyrus right to Hippocampus right	Feeder	3.12
11	Hippocampus left	Peripheral	11	Caudate right to Inferior temporal gyrus right	Core	3.13
12	Hippocampus right	Peripheral	12	Precentral gyrus right to Cerebellum left	Core	3.13
13	Amygdala left	Peripheral	13	Middle frontal gyrus left to Middle frontal gyrus right	Core	3.14
14	Superior occipital gyrus	Peripheral	14	Middle occipital gyrus left to Middle temporal gyrus left	Core	3.15

	left					
15	Middle occipital gyrus left	Core	15	Middle occipital gyrus left to Inferior occipital gyrus left	Feeder	3.17
16	Middle occipital gyrus right	Peripheral	16	Hippocampus left to Superior parietal gyrus left	Peripheral	3.17
17	Inferior occipital gyrus left	Peripheral	17	Inferior occipital gyrus left to Middle temporal gyrus left	Feeder	3.29
18	Postcentral gyrus left	Peripheral	18	Hippocampus right to Inferior parietal lobule right	Peripheral	3.31
19	Postcentral gyrus right	Peripheral	19	Hippocampus left to Amygdala left	Peripheral	3.34
20	Superior parietal gyrus left	Peripheral	20	Hippocampus left to Cerebellum left	Feeder	3.36
21	Inferior parietal lobule right	Peripheral	21	Hippocampus right to Middle occipital gyrus right	Peripheral	3.4
22	Supramarginal gyrus right	Peripheral	22	Postcentral gyrus left to Cerebellum right	Feeder	3.43
23	Angular gyrus left	Peripheral	23	Inferior frontal gyrus (triangular) left to Rolandic operculum left	Feeder	3.44
24	Angular gyrus right	Core	24	Inferior frontal gyrus (opercular) left to Inferior frontal gyrus (triangular) left	Feeder	3.46
25	Caudate right	Core	25	Rolandic operculum left to Superior frontal gyrus (medial) left	Feeder	3.49
26	Putamen left	Core	26	Thalamus right to Cerebellum left	Core	3.51
27	Putamen right	Core	27	Putamen right to Thalamus right	Core	3.52
28	Thalamus left	Core	28	Thalamus right to Inferior temporal gyrus right	Core	3.52
29	Thalamus	Core	29	Hippocampus right to	Feeder	3.58

	right			Angular gyrus right		
30	Middle temporal gyrus left	Core	30	Precentral gyrus right to Vermis	Core	3.7
31	Inferior temporal gyrus left	Peripheral	31	Superior frontal gyrus (dorsal) left to Rolandic operculum left	Feeder	3.71
32	Inferior temporal gyrus right	Core	32	Inferior occipital gyrus left to Inferior temporal gyrus left	Peripheral	3.72
33	Cerebellum left	Core	33	Hippocampus right to Postcentral gyrus right	Peripheral	3.77
34	Cerebellum right	Core	34	Putamen left to Thalamus left	Core	3.77
35	Vermis	Core	35	Caudate right to Putamen left	Core	3.81
			36	Cerebellum left to Cerebellum right	Core	3.81
			37	Hippocampus left to Vermis	Feeder	3.93
			38	Hippocampus left to Cerebellum right	Feeder	3.97
			39	Hippocampus right to Caudate right	Feeder	4

$t = 3.2$

Network 1 – 10 nodes, 10 edges, $p=0.009$

#	Node	Node network	#	Edge	Edge type	<i>t</i> -value
1	Precentral gyrus right	Core	1	Hippocampus left to Amygdala left	Peripheral	3.34
2	Hippocampus left	Peripheral	2	Hippocampus left to Cerebellum left	Feeder	3.36
3	Amygdala left	Peripheral	3	Postcentral gyrus left to Cerebellum right	Feeder	3.43
4	Postcentral gyrus left	Peripheral	4	Thalamus right to Cerebellum left	Core	3.51
5	Putamen right	Core	5	Putamen right to Thalamus right	Core	3.52
6	Thalamus right	Core	6	Thalamus right to Inferior temporal gyrus right	Core	3.52
7	Inferior temporal gyrus right	Core	7	Precentral gyrus right to Vermis	Core	3.7
8	Cerebellum left	Core	8	Cerebellum left to Cerebellum right	Core	3.81
9	Cerebellum right	Core	9	Hippocampus left to Vermis	Feeder	3.93
10	Vermis	Core	10	Hippocampus left to Cerebellum right	Feeder	3.97

Network 2 – 8 nodes, 7 edges, $p=0.022$

#	Node	Node network	#	Edge	Edge type	<i>t</i> -value
1	Hippocampus right	Peripheral	1	Hippocampus right to Inferior parietal lobule right	Peripheral	3.31
2	Middle occipital gyrus right	Peripheral	2	Hippocampus right to Middle occipital gyrus right	Peripheral	3.4
3	Postcentral gyrus right	Peripheral	3	Hippocampus right to Angular gyrus right	Feeder	3.58
4	Inferior parietal lobule right	Peripheral	4	Hippocampus right to Postcentral gyrus right	Peripheral	3.77

5	Angular gyrus right	Core	5	Putamen left to Thalamus left	Core	3.77
6	Caudate right	Core	6	Caudate right to Putamen left	Core	3.81
7	Putamen left	Core	7	Hippocampus right to Caudate right	Feeder	4
8	Thalamus left	Core				

$t = 3.3$

Network 1 – 10 nodes, 10 edges, $p=0.005$

#	Node	Node network	#	Edge	Edge type	<i>t</i> -value
1	Precentral gyrus right	Core	1	Hippocampus left to Amygdala left	Peripheral	3.34
2	Hippocampus left	Peripheral	2	Hippocampus left to Cerebellum left	Feeder	3.36
3	Amygdala left	Peripheral	3	Postcentral gyrus left to Cerebellum right	Feeder	3.43
4	Postcentral gyrus left	Peripheral	4	Thalamus right to Cerebellum left	Core	3.51
5	Putamen right	Core	5	Putamen right to Thalamus right	Core	3.52
6	Thalamus right	Core	6	Thalamus right to Inferior temporal gyrus right	Core	3.52
7	Inferior temporal gyrus right	Core	7	Precentral gyrus right to Vermis	Core	3.7
8	Cerebellum left	Core	8	Cerebellum left to Cerebellum right	Core	3.81
9	Cerebellum right	Core	9	Hippocampus left to Vermis	Feeder	3.93
10	Vermis	Core	10	Hippocampus left to Cerebellum right	Feeder	3.97

Network 2 – 5 nodes, 4 edges, $p=0.046$

#	Node	Node network	#	Edge	Edge type	<i>t</i> -value
1	Superior frontal gyrus (dorsal) left	Core	1	Inferior frontal gyrus (triangular) left to Rolandic operculum left	Feeder	3.44
2	Inferior frontal gyrus (opercular) left	Peripheral	2	Inferior frontal gyrus (opercular) left to Inferior frontal gyrus (triangular) left	Feeder	3.46
3	Inferior frontal gyrus (triangular) left	Core	3	Rolandic operculum left to Superior frontal gyrus (medial) left	Feeder	3.49

4	Rolandic operculum left	Peripheral	4	Superior frontal gyrus (dorsal) left to Rolandic operculum left	Feeder	3.71
5	Superior frontal gyrus (medial) left	Core				

Network 3 – 8 nodes, 7 edges, $p=0.0012$

#	Node	Node network	#	Edge	Edge type	<i>t</i> -value
1	Hippocampus right	Peripheral	1	Hippocampus right to Inferior parietal lobule right	Peripheral	3.31
2	Middle occipital gyrus right	Peripheral	2	Hippocampus right to Middle occipital gyrus right	Peripheral	3.4
3	Postcentral gyrus right	Peripheral	3	Hippocampus right to Angular gyrus right	Feeder	3.58
4	Inferior parietal lobule right	Peripheral	4	Hippocampus right to Postcentral gyrus right	Peripheral	3.77
5	Angular gyrus right	Core	5	Putamen left to Thalamus left	Core	3.77
6	Caudate right	Core	6	Caudate right to Putamen left	Core	3.81
7	Putamen left	Core	7	Hippocampus right to Caudate right	Feeder	4
8	Thalamus left	Core				

$t = 3.4$

Network 1 – 9 nodes, 8 edges, $p=0.004$

#	Node	Node network	#	Edge	Edge type	<i>t</i> -value
1	Precentral gyrus right	Core	1	Postcentral gyrus left to Cerebellum right	Feeder	3.43
2	Hippocampus left	Peripheral	2	Thalamus right to Cerebellum left	Core	3.51
3	Postcentral gyrus left	Peripheral	3	Putamen right to Thalamus right	Core	3.52
4	Putamen right	Core	4	Thalamus right to Inferior temporal gyrus right	Core	3.52
5	Thalamus right	Core	5	Precentral gyrus right to Vermis	Core	3.7
6	Inferior temporal gyrus right	Core	6	Cerebellum left to Cerebellum right	Core	3.81
7	Cerebellum left	Core	7	Hippocampus left to Vermis	Feeder	3.93
8	Cerebellum right	Core	8	Hippocampus left to Cerebellum right	Feeder	3.97
9	Vermis	Core				

Network 2 – 5 nodes, 4 edges, $p=0.027$

#	Node	Node network	#	Edge	Edge type	<i>t</i> -value
1	Superior frontal gyrus (dorsal) left	Core	1	Inferior frontal gyrus (triangular) left to Rolandic operculum left	Feeder	3.44
2	Inferior frontal gyrus (opercular) left	Peripheral	2	Inferior frontal gyrus (opercular) left to Inferior frontal gyrus (triangular) left	Feeder	3.46
3	Inferior frontal gyrus (triangular) left	Core	3	Rolandic operculum left to Superior frontal gyrus (medial) left	Feeder	3.49
4	Rolandic operculum left	Peripheral	4	Superior frontal gyrus (dorsal) left to Rolandic operculum left	Feeder	3.71

5	Superior frontal gyrus (medial) left	Core				
---	--------------------------------------	------	--	--	--	--

Network 3 –6 nodes, 5 edges, p=0.0014

#	Node	Node network	#	Edge	Edge type	t-value
1	Hippocampus right	Peripheral	1	Hippocampus right to Angular gyrus right	Feeder	3.58
2	Postcentral gyrus right	Peripheral	2	Hippocampus right to Postcentral gyrus right	Peripheral	3.77
3	Angular gyrus right	Core	3	Putamen left to Thalamus left	Core	3.77
4	Caudate right	Core	4	Caudate right to Putamen left	Core	3.81
5	Putamen left	Core	5	Hippocampus right to Caudate right	Feeder	4
6	Thalamus left	Core				

$t = 3.5$

Network 1 – 8 nodes, 7 edges, $p=0.003$

#	Node	Node network	#	Edge	Edge type	<i>t</i> -value
1	Precentral gyrus right	Core	1	Thalamus right to Cerebellum left	Core	3.51
2	Hippocampus left	Peripheral	2	Putamen right to Thalamus right	Core	3.52
3	Putamen right	Core	3	Thalamus right to Inferior temporal gyrus right	Core	3.52
4	Thalamus right	Core	4	Precentral gyrus right to Vermis	Core	3.7
5	Inferior temporal gyrus right	Core	5	Cerebellum left to Cerebellum right	Core	3.81
6	Cerebellum left	Core	6	Hippocampus left to Vermis	Feeder	3.93
7	Cerebellum right	Core	7	Hippocampus left to Cerebellum right	Feeder	3.97
8	Vermis	Core				

Network 2 – 6 nodes, 5 edges, $p=0.008$

#	Node	Node network	#	Edge	Edge type	<i>t</i> -value
1	Hippocampus right	Peripheral	1	Hippocampus right to Angular gyrus right	Feeder	3.58
2	Postcentral gyrus right	Peripheral	2	Hippocampus right to Postcentral gyrus right	Peripheral	3.77
3	Angular gyrus right	Core	3	Putamen left to Thalamus left	Core	3.77
4	Caudate right	Core	4	Caudate right to Putamen left	Core	3.81
5	Putamen left	Core	5	Hippocampus right to Caudate right	Feeder	4.00
6	Thalamus left	Core				

Supplementary results 2

Supplementary Table 2. Subnetwork with reduced structural connectivity in CHD neonates after removing the outlier, its respective matched control and CHD infant. From the 29 nodes with reduced structural connectivity in infants with CHD, 18 were core nodes (out of a total of 34 core nodes, 52.9%), while 11 were peripheral nodes (out of a total of 59 peripheral nodes, 18.6%). Of the 33 edges with reduced connectivity in CHD, 12 (36.36%) were core, 15 (45.45%) were feeders and 6 (18.18%) were peripheral.

#	Node	Node network	#	Edge	Edge type	t-value
1	Superior frontal gyrus (dorsal) left	Core	1	Superior occipital gyrus left to Postcentral gyrus right	Peripheral	3.11
2	Middle frontal gyrus right	Core	2	Rolandic operculum left to Superior frontal gyrus (medial) left	Feeder	3.12
3	Orbitofrontal cortex (superior) left	Peripheral	3	Inferior frontal gyrus (opercular) left to Postcentral gyrus right	Peripheral	3.12
4	Middle frontal gyrus left	Core	4	Inferior parietal lobule right to Vermis	Core	3.13
5	Inferior frontal gyrus (opercular) left	Peripheral	5	Superior frontal gyrus (dorsal) left to Middle frontal gyrus right	Core	3.14
6	Inferior frontal gyrus (triangular) left	Core	6	Hippocampus left to Superior parietal gyrus left	Peripheral	3.15
7	Rolandic operculum left	Peripheral	7	Inferior frontal gyrus (triangular) left to Rolandic operculum left	Feeder	3.16
8	Superior frontal gyrus (medial) left	Core	8	Orbitofrontal cortex (superior) left to Middle frontal gyrus right	Feeder	3.17
9	Precentral gyrus right	Core	9	Hippocampus right to Thalamus right	Feeder	3.17
10	Hippocampus right	Peripheral	10	Supplementary motor area left to Postcentral gyrus right	Peripheral	3.18
11	Middle occipital gyrus right	Peripheral	11	Precentral gyrus right to Cerebellum left	Core	3.19

12	Postcentral gyrus right	Peripheral	12	Hippocampus left to Cerebellum left	Feeder	3.21
13	Supplementary motor area left	Peripheral	13	Inferior frontal gyrus (opercular) left to Inferior frontal gyrus (triangular) left	Feeder	3.23
14	Median cingulate and paracingulate gyrus left	Core	14	Caudate right to Inferior temporal gyrus right	Core	3.25
15	Superior occipital gyrus left	Peripheral	15	Precentral gyrus right to Hippocampus right	Feeder	3.28
16	Hippocampus left	Peripheral	16	Hippocampus right to Inferior parietal lobule right	Feeder	3.33
17	Superior parietal gyrus left	Peripheral	17	Hippocampus right to Middle occipital gyrus right	Peripheral	3.34
18	Inferior parietal lobule right	Core	18	Thalamus right to Cerebellum left	Core	3.35
19	Angular gyrus right	Core	19	Median cingulate and paracingulate gyrus left to Postcentral gyrus right	Feeder	3.42
20	Caudate right	Core	20	Putamen right to Thalamus right	Core	3.43
21	Putamen left	Core	21	Middle frontal gyrus left to Middle frontal gyrus right	Core	3.44
22	Thalamus left	Core	22	Hippocampus right to Angular gyrus right	Feeder	3.46
23	Thalamus right	Core	23	Superior frontal gyrus (dorsal) left to Rolandic operculum left	Feeder	3.48
24	Putamen right	Core	24	Postcentral gyrus left to Cerebellum right	Feeder	3.51
25	Inferior temporal gyrus right	Core	25	Caudate right to Putamen left	Core	3.57
26	Cerebellum left	Core	26	Cerebellum left to Cerebellum right	Core	3.63

27	Postcentral gyrus left	Peripheral	27	Thalamus right to Inferior temporal gyrus right	Core	3.64
28	Cerebellum right	Core	28	Hippocampus right to Postcentral gyrus right	Peripheral	3.78
29	Vermis	Core	29	Hippocampus left to Cerebellum right	Feeder	3.83
			30	Putamen left to Thalamus left	Core	3.85
			31	Hippocampus left to Vermis	Feeder	3.90
			32	Precentral gyrus right to Vermis	Core	3.99
			33	Hippocampus right to Caudate right	Feeder	4.18

Appendix B
Supplementary material of : Metastable neural dynamics in the neonate brain

1. Supplementary results: Bonferroni corrected pairwise comparisons of the metastability of the resting-state networks in neonates

Supplementary table 6.1. Bonferroni corrected pairwise comparisons of the metastability of the resting-state networks in neonates				
Pairs of networks	Mean difference in metastability	95% CI (lower bound)	95% CI (upper bound)	p-value
Temporoparietal-Medial motor	-0.03	-0.04	-0.02	<0.0001
Auditory left-Medial motor	0.02	0.01	0.03	<0.0001
Auditory right-Medial motor	0.01	0.00	0.02	<0.0001
Visual association left-Medial motor	0.01	0.00	0.02	0.0001
Visual 2-Medial motor	0.01	0.00	0.02	0.0005
Posterior parietal-Medial motor	0.02	0.01	0.03	<0.0001
Visual 1-Medial motor	0.01	0.01	0.02	<0.0001
Thalamus-Medial motor	0.04	0.03	0.05	<0.0001
Temporoparietal-Visual association right	-0.04	-0.05	-0.03	<0.0001
Auditory left-Visual association right	0.01	0.00	0.02	0.0061
Ventral frontal-Visual association right	-0.01	-0.02	-0.01	<0.0001
Somatosensory right-Visual association right	-0.01	-0.02	-0.01	<0.0001
Posterior parietal-Visual association right	0.01	0.00	0.02	0.0028

Parietal-Visual association right	-0.01	-0.02	0.00	0.0220
Thalamus-Visual association right	0.03	0.03	0.04	<0.0001
Auditory left-Temporoparietal	0.05	0.04	0.06	<0.0001
Prefrontal-Temporoparietal	0.04	0.03	0.04	<0.0001
Auditory right-Temporoparietal	0.04	0.04	0.05	<0.0001
Visual association left-Temporoparietal	0.04	0.03	0.05	<0.0001
Ventral frontal-Temporoparietal	0.02	0.02	0.03	<0.0001
Visual 2-Temporoparietal	0.04	0.03	0.05	<0.0001
Lateral motor-Temporoparietal	0.04	0.03	0.05	<0.0001
Somatosensory right-Temporoparietal	0.02	0.02	0.03	<0.0001
Premotor-Temporoparietal	0.04	0.03	0.04	<0.0001
Posterior parietal-Temporoparietal	0.05	0.04	0.06	<0.0001
Somatosensory left-Temporoparietal	0.04	0.03	0.04	<0.0001
Visual 1-Temporoparietal	0.05	0.04	0.05	<0.0001
Parietal-Temporoparietal	0.03	0.02	0.04	<0.0001
Dorsal frontal-Temporoparietal	0.03	0.02	0.04	<0.0001
Thalamus-Temporoparietal	0.07	0.06	0.08	<0.0001
Prefrontal-Auditory left	-0.01	-0.02	-0.01	<0.0001
Ventral frontal-Auditory left	-0.03	-0.03	-0.02	<0.0001
Lateral motor-Auditory left	-0.01	-0.02	0.00	0.0013

Somatosensory right-Auditory left	-0.03	-0.03	-0.02	<0.0001
Premotor-Auditory left	-0.01	-0.02	-0.01	<0.0001
Somatosensory left-Auditory left	-0.01	-0.02	-0.01	<0.0001
Parietal-Auditory left	-0.02	-0.03	-0.01	<0.0001
Dorsal frontal-Auditory left	-0.02	-0.03	-0.01	<0.0001
Auditory right-Prefrontal	0.01	0.00	0.02	0.0257
Ventral frontal-Prefrontal	-0.01	-0.02	0.00	0.0040
Somatosensory right-Prefrontal	-0.01	-0.02	0.00	0.0053
Posterior parietal-Prefrontal	0.02	0.01	0.02	<0.0001
Visual 1-Prefrontal	0.01	0.00	0.02	0.0079
Thalamus-Prefrontal	0.04	0.03	0.05	<0.0001
Ventral frontal-Auditory right	-0.02	-0.03	-0.01	<0.0001
Somatosensory right-Auditory right	-0.02	-0.03	-0.01	<0.0001
Premotor-Auditory right	-0.01	-0.02	0.00	0.0447
Somatosensory left-Auditory right	-0.01	-0.02	0.00	0.0359
Parietal-Auditory right	-0.01	-0.02	-0.01	<0.0001
Dorsal frontal-Auditory right	-0.01	-0.02	0.00	0.0024
Thalamus-Auditory right	0.03	0.02	0.04	<0.0001
Ventral frontal-Visual association left	-0.02	-0.03	-0.01	<0.0001
Somatosensory right-Visual association left	-0.02	-0.03	-0.01	<0.0001

Parietal-Visual association left	-0.01	-0.02	0.00	<0.0001
Dorsal frontal-Visual association left	-0.01	-0.02	0.00	0.0101
Thalamus-Visual association left	0.03	0.02	0.04	<0.0001
Visual 2-Ventral frontal	0.02	0.01	0.03	<0.0001
Lateral motor-Ventral frontal	0.01	0.01	0.02	<0.0001
Premotor-Ventral frontal	0.01	0.00	0.02	0.0021
Posterior parietal-Ventral frontal	0.03	0.02	0.03	<0.0001
Somatosensory left-Ventral frontal	0.01	0.00	0.02	0.0027
Visual 1-Ventral frontal	0.02	0.01	0.03	<0.0001
Dorsal frontal-Ventral frontal	0.01	0.00	0.02	0.0406
Thalamus-Ventral frontal	0.05	0.04	0.06	<0.0001
Somatosensory right-Visual 2	-0.02	-0.03	-0.01	<0.0001
Parietal-Visual 2	-0.01	-0.02	0.00	<0.0001
Dorsal frontal-Visual 2	-0.01	-0.02	0.00	0.0351
Thalamus-Visual 2	0.03	0.02	0.04	<0.0001
Somatosensory right-Lateral motor	-0.01	-0.02	0.00	<0.0001
Posterior parietal-Lateral motor	0.01	0.00	0.02	0.0006
Thalamus-Lateral motor	0.03	0.03	0.04	<0.0001
Premotor-Somatosensory right	0.01	0.00	0.02	0.0028
Posterior parietal-Somatosensory right	0.03	0.02	0.03	<0.0001

Somatosensory left-Somatosensory right	0.01	0.00	0.02	0.0036
Visual 1-Somatosensory right	0.02	0.01	0.03	<0.0001
Thalamus-Somatosensory right	0.05	0.04	0.06	<0.0001
Posterior parietal-Premotor	0.01	0.01	0.02	<0.0001
Visual 1-Premotor	0.01	0.00	0.02	0.0144
Thalamus-Premotor	0.04	0.03	0.05	<0.0001
Somatosensory left-Posterior parietal	-0.01	-0.02	-0.01	<0.0001
Parietal-Posterior parietal	-0.02	-0.03	-0.01	<0.0001
Dorsal frontal-Posterior parietal	-0.02	-0.03	-0.01	<0.0001
Thalamus-Posterior parietal	0.02	0.01	0.03	<0.0001
Visual 1-Somatosensory left	0.01	0.00	0.02	0.0114
Thalamus-Somatosensory left	0.04	0.03	0.05	<0.0001
Parietal-Visual 1	-0.02	-0.02	-0.01	<0.0001
Dorsal frontal-Visual 1	-0.01	-0.02	0.00	0.0006
Thalamus-Visual 1	0.03	0.02	0.04	<0.0001
Thalamus-Parietal	0.04	0.03	0.05	<0.0001
Thalamus-Dorsal frontal	0.04	0.03	0.05	<0.0001

2. Supplementary results: Bonferroni corrected pairwise comparisons of the synchrony of the resting-state networks in neonates

Supplementary table 6.2. Bonferroni corrected pairwise comparisons of the synchrony of the resting-state networks in neonates				
Pairs of networks	Mean difference in synchrony	95% CI (lower bound)	95% CI (upper bound)	p-value
Visual association right-Medial motor	-0.09	-0.12	-0.05	<0.0001
Temporoparietal-Medial motor	-0.36	-0.39	-0.32	<0.0001
Auditory left-Medial motor	-0.14	-0.17	-0.10	<0.0001
Prefrontal-Medial motor	-0.22	-0.25	-0.18	<0.0001
Auditory right-Medial motor	-0.17	-0.20	-0.13	<0.0001
Visual association left-Medial motor	-0.19	-0.23	-0.16	<0.0001
Ventral frontal-Medial motor	-0.30	-0.33	-0.26	<0.0001
Premotor-Medial motor	-0.05	-0.09	-0.02	<0.0001
Posterior parietal-Medial motor	-0.08	-0.11	-0.05	<0.0001
Somatosensory left-Medial motor	0.08	0.05	0.12	<0.0001
Visual 1-Medial motor	-0.05	-0.08	-0.02	<0.0001
Dorsal frontal-Medial motor	-0.14	-0.17	-0.11	<0.0001
Thalamus-Medial motor	-0.10	-0.13	-0.07	<0.0001

Temporoparietal-Visual association right	-0.27	-0.30	-0.24	<0.0001
Auditory left-Visual association right	-0.05	-0.08	-0.02	<0.0001
Prefrontal-Visual association right	-0.13	-0.16	-0.10	<0.0001
Auditory right-Visual association right	-0.08	-0.11	-0.05	<0.0001
Visual association left-Visual association right	-0.11	-0.14	-0.07	<0.0001
Ventral frontal-Visual association right	-0.21	-0.24	-0.18	<0.0001
Visual 2-Visual association right	0.11	0.07	0.14	<0.0001
Lateral motor-Visual association right	0.08	0.05	0.12	<0.0001
Somatosensory right-Visual association right	0.11	0.08	0.15	<0.0001
Premotor-Visual association right	0.03	0.00	0.07	0.0379
Somatosensory left-Visual association right	0.17	0.14	0.20	<0.0001
Visual 1-Visual association right	0.04	0.00	0.07	0.0103
Parietal-Visual association right	0.10	0.07	0.14	<0.0001
Dorsal frontal-Visual association right	-0.05	-0.09	-0.02	<0.0001
Auditory left-Temporoparietal	0.22	0.19	0.25	<0.0001
Prefrontal-Temporoparietal	0.14	0.11	0.17	<0.0001
Auditory right-Temporoparietal	0.19	0.16	0.22	<0.0001
Visual association left-Temporoparietal	0.16	0.13	0.20	<0.0001
Ventral frontal-Temporoparietal	0.06	0.03	0.10	<0.0001
Visual 2-Temporoparietal	0.38	0.34	0.41	<0.0001

Lateral motor-Temporoparietal	0.36	0.32	0.39	<0.0001
Somatosensory right-Temporoparietal	0.39	0.35	0.42	<0.0001
Premotor-Temporoparietal	0.31	0.27	0.34	<0.0001
Posterior parietal-Temporoparietal	0.28	0.24	0.31	<0.0001
Somatosensory left-Temporoparietal	0.44	0.41	0.47	<0.0001
Visual 1-Temporoparietal	0.31	0.27	0.34	<0.0001
Parietal-Temporoparietal	0.37	0.34	0.41	<0.0001
Dorsal frontal-Temporoparietal	0.22	0.19	0.25	<0.0001
Thalamus-Temporoparietal	0.26	0.22	0.29	<0.0001
Prefrontal-Auditory left	-0.08	-0.11	-0.05	<0.0001
Visual association left-Auditory left	-0.06	-0.09	-0.02	<0.0001
Ventral frontal-Auditory left	-0.16	-0.19	-0.13	<0.0001
Visual 2-Auditory left	0.16	0.12	0.19	<0.0001
Lateral motor-Auditory left	0.13	0.10	0.17	<0.0001
Somatosensory right-Auditory left	0.17	0.13	0.20	<0.0001
Premotor-Auditory left	0.08	0.05	0.12	<0.0001
Posterior parietal-Auditory left	0.06	0.02	0.09	<0.0001
Somatosensory left-Auditory left	0.22	0.19	0.25	<0.0001
Visual 1-Auditory left	0.09	0.05	0.12	<0.0001
Parietal-Auditory left	0.15	0.12	0.19	<0.0001

Thalamus-Auditory left	0.04	0.00	0.07	0.0086
Auditory right-Prefrontal	0.05	0.02	0.08	<0.0001
Ventral frontal-Prefrontal	-0.08	-0.11	-0.05	<0.0001
Visual 2-Prefrontal	0.24	0.20	0.27	<0.0001
Lateral motor-Prefrontal	0.21	0.18	0.25	<0.0001
Somatosensory right-Prefrontal	0.24	0.21	0.28	<0.0001
Premotor-Prefrontal	0.16	0.13	0.20	<0.0001
Posterior parietal-Prefrontal	0.13	0.10	0.17	<0.0001
Somatosensory left-Prefrontal	0.30	0.27	0.33	<0.0001
Visual 1-Prefrontal	0.17	0.13	0.20	<0.0001
Parietal-Prefrontal	0.23	0.20	0.27	<0.0001
Dorsal frontal-Prefrontal	0.08	0.04	0.11	<0.0001
Thalamus-Prefrontal	0.12	0.08	0.15	<0.0001
Ventral frontal-Auditory right	-0.13	-0.16	-0.10	<0.0001
Visual 2-Auditory right	0.19	0.15	0.22	<0.0001
Lateral motor-Auditory right	0.16	0.13	0.20	<0.0001
Somatosensory right-Auditory right	0.19	0.16	0.23	<0.0001
Premotor-Auditory right	0.11	0.08	0.15	<0.0001
Posterior parietal-Auditory right	0.08	0.05	0.12	<0.0001
Somatosensory left-Auditory right	0.25	0.22	0.28	<0.0001

Visual 1-Auditory right	0.12	0.08	0.15	<0.0001
Parietal-Auditory right	0.18	0.15	0.22	<0.0001
Thalamus-Auditory right	0.07	0.03	0.10	<0.0001
Ventral frontal-Visual association left	-0.10	-0.14	-0.07	<0.0001
Visual 2-Visual association left	0.21	0.18	0.25	<0.0001
Lateral motor-Visual association left	0.19	0.16	0.22	<0.0001
Somatosensory right-Visual association left	0.22	0.19	0.25	<0.0001
Premotor-Visual association left	0.14	0.11	0.17	<0.0001
Posterior parietal-Visual association left	0.11	0.08	0.14	<0.0001
Somatosensory left-Visual association left	0.28	0.24	0.31	<0.0001
Visual 1-Visual association left	0.14	0.11	0.18	<0.0001
Parietal-Visual association left	0.21	0.18	0.24	<0.0001
Dorsal frontal-Visual association left	0.05	0.02	0.09	<0.0001
Thalamus-Visual association left	0.09	0.06	0.13	<0.0001
Visual 2-Ventral frontal	0.31	0.28	0.35	<0.0001
Lateral motor-Ventral frontal	0.29	0.26	0.33	<0.0001
Somatosensory right-Ventral frontal	0.32	0.29	0.36	<0.0001
Premotor-Ventral frontal	0.24	0.21	0.28	<0.0001
Posterior parietal-Ventral frontal	0.21	0.18	0.25	<0.0001
Somatosensory left-Ventral frontal	0.38	0.35	0.41	<0.0001

Visual 1-Ventral frontal	0.25	0.21	0.28	<0.0001
Parietal-Ventral frontal	0.31	0.28	0.35	<0.0001
Dorsal frontal-Ventral frontal	0.16	0.12	0.19	<0.0001
Thalamus-Ventral frontal	0.20	0.16	0.23	<0.0001
Premotor-Visual 2	-0.07	-0.10	-0.04	<0.0001
Posterior parietal-Visual 2	-0.10	-0.13	-0.07	<0.0001
Somatosensory left-Visual 2	0.06	0.03	0.10	<0.0001
Visual 1-Visual 2	-0.07	-0.10	-0.04	<0.0001
Dorsal frontal-Visual 2	-0.16	-0.19	-0.12	<0.0001
Thalamus-Visual 2	-0.12	-0.15	-0.09	<0.0001
Premotor-Lateral motor	-0.05	-0.08	-0.02	<0.0001
Posterior parietal-Lateral motor	-0.08	-0.11	-0.05	<0.0001
Somatosensory left-Lateral motor	0.09	0.05	0.12	<0.0001
Visual 1-Lateral motor	-0.05	-0.08	-0.01	0.0001
Dorsal frontal-Lateral motor	-0.14	-0.17	-0.10	<0.0001
Thalamus-Lateral motor	-0.10	-0.13	-0.06	<0.0001
Premotor-Somatosensory right	-0.08	-0.11	-0.05	<0.0001
Posterior parietal-Somatosensory right	-0.11	-0.14	-0.08	<0.0001
Somatosensory left-Somatosensory right	0.05	0.02	0.09	<0.0001
Visual 1-Somatosensory right	-0.08	-0.11	-0.04	<0.0001

Dorsal frontal-Somatosensory right	-0.17	-0.20	-0.13	<0.0001
Thalamus-Somatosensory right	-0.13	-0.16	-0.09	<0.0001
Somatosensory left-Premotor	0.14	0.10	0.17	<0.0001
Parietal-Premotor	0.07	0.04	0.10	<0.0001
Dorsal frontal-Premotor	-0.09	-0.12	-0.05	<0.0001
Thalamus-Premotor	-0.05	-0.08	-0.01	0.0001
Somatosensory left-Posterior parietal	0.16	0.13	0.20	<0.0001
Parietal-Posterior parietal	0.10	0.07	0.13	<0.0001
Dorsal frontal-Posterior parietal	-0.06	-0.09	-0.02	<0.0001
Visual 1-Somatosensory left	-0.13	-0.17	-0.10	<0.0001
Parietal-Somatosensory left	-0.07	-0.10	-0.03	<0.0001
Dorsal frontal-Somatosensory left	-0.22	-0.26	-0.19	<0.0001
Thalamus-Somatosensory left	-0.18	-0.22	-0.15	<0.0001
Parietal-Visual 1	0.07	0.03	0.10	<0.0001
Dorsal frontal-Visual 1	-0.09	-0.12	-0.06	<0.0001
Thalamus-Visual 1	-0.05	-0.08	-0.02	<0.0001
Dorsal frontal-Parietal	-0.16	-0.19	-0.12	<0.0001
Thalamus-Parietal	-0.12	-0.15	-0.08	<0.0001

